AERO-ACOUSTIC TESTS OF DUCT-BURNING TURBOFAN EXHAUST NOZZLES

By: Hilary Kozlowski
Allan B. Packman

Pratt & Whitney Aircraft Division
United Technologies Corporation

Advanced Information Copy

prepared for

NATIONAL AERONAUTICS AND SPACE ADMINISTRATION

NASA Lewis Research Center
Contract NAS3-17866

TABLE OF CONTENTS

TABLE OF CONTENTS (Cont'd)

1.0 SUMMARY

The acoustic and aerodynamic characteristics of several exhaust systems suitable for duct burning turbofan (DBTF) engines were established in this program. Scale models representing unsuppressed and suppressed coannular exhaust systems were evaluated statically under varying exhaust conditions. Ejectors with both hardwall and acoustically treated inserts were also evaluated in the program.

The unsuppressed coannular configurations were found to be as much as 11 PNdB quieter than current predictions when scaled to 1.27m (50 in.) equivalent diameter size. At conditions typical of engines being considered under the Advanced Supersonic Technology (AST) program, reductions of approximately 8 PNdB were observed. The reductions for a specific engine are a function of the exact combination of stream temperatures and velocities. The noise power levels and perceived noise levels, scaled to full size, were found to collapse to single lines when correlated with fan stream velocity and temperature, fan to primary velocity ratio (V_f/V_p) area ratio (A_f/A_p). Spectral characteristics and velocity profile measurements in the jet plume indicate that the noise suppression (when $V_f/V_p > 1$) is due to more rapid mixing of the coannular jet compared to standard circular jets.

The mechanically suppressed configurations produced as much as 18 PNdB reduction below current predictions for an unsuppressed nozzle (4 PNdB of this is due to a treated ejector). At typical AST engine conditions, reductions of approximately 15 PNdB were observed. Relative to the unsuppressed configurations, the suppressed nozzles provided noise reductions over a wider range of conditions.

Additional correlations of the data from both suppressed and unsuppressed configurations showed that the noise was a function of exhaust system geometry and also that it was related to the maximum velocities existing in the jet plume downstream of the nozzle exit.

The measured force data indicated that the basic suppressor configurations yielding the most noise suppression had the highest thrust losses. The impact of adding an ejector was highly dependent on the suppressor design since the match between the suppressor and ejector is critical. Similarly, the impact of adding acoustical treatment in the ejector was also very dependent on the size of the suppressor.

The overall impact of these results on recent AST studies has been significant in terms of engine sizing and vehicle characteristics.

The suppressed configurations consisted of multi-element suppressor units applied to the fan stream only, since the DBTF fan stream is the dominant noise source. Three concepts were evaluated: a multi-tube unit having 44 tubes, an 18 lobe convoluted design and a finger type employing 32 segments. The total jet area of the models was equivalent to a 0.127 m (5 in.) diameter convergent nozzle, or approximately one-tenth of the full scale size being studied under AST programs. The area ratio between the fan and primary stream was varied from 0.75 to 1.2 in some configurations, with the total area maintained constant.

A total of 417 test conditions were evaluated. The fan stream pressure ratio was varied from 1.3 to 4.1 and the primary stream pressure ratio from 1.53 to 2.5. The temperature in both streams was varied independently from 395°K to 1090°K. The resultant data is presented in the Comprehensive Data Report, CR 134910.

2.0 INTRODUCTION

2.1 BACKGROUND

Prior to this program, extensive propulsion system studies, conducted as part of the NASA sponsored Advanced Supersonic Technology (AST) effort, identified the duct burning turbofan (DBTF) as a promising cycle in terms of both system economics and low noise generation. The DBTF engine cycle can be matched to provide a high velocity duct (fan) stream surrounding a low velocity core (primary) stream. This type of cycle requires that only the fan stream be suppressed to provide reduction in jet noise. However, very little experimental substantiation existed for this type of exhaust system.

The noise characteristics of conventional coannular exhaust systems, whereby the fan exhaust is of lower velocity than the primary stream exhaust, have been extensively investigated during the past few years. The work of Williams (Ref. 1) first pointed out that the noise of a coannular jet was related to fan to primary stream velocity ratio and showed that the noise of a coannular jet was less than the noise of the primary jet under isolated conditions for a large range of fan to primary velocity ratios less than one. The basic results of Williams were extended by Eldred (Ref. 2) to include coannular jets having a heated stream and included the effects of fan to primary stream exhaust area ratio. Analytical models developed in References 1 and 2 showed that the gross results of the coannular jet could be related to the aerodynamic characteristics of the jet exhaust plume. For example, high frequencies were shown to be reduced due to the relative velocity effect of the fan exhaust surrounding the primary stream, and low frequency characteristics were ascribed to the presence of a merged jet resulting from the mixing of the fan and primary jets downstream of the nozzle. The experimental investigations of Olsen (Ref. 3) and Bielak (Ref. 4) confirmed the results of Williams and Eldred, and the SAE Subcommittee on Jet Noise has developed a coannular jet noise prediction procedure drawing upon some of the results from References 1 - 4, and additional coannular jet noise data produced during recent experimental testing. Predictions from the SAE procedure have shown very reasonable agreement with model and full-scale engine noise data, but is limited to subsonic flow conditions where the fan exit velocity is less than the primary velocity. The recently published prediction procedure of Stone (Ref. 5) includes the effects of supersonic jets, but is limited to V_f/V_p ratios less than 1.0. The work of Dosanjh (Ref. 6) focused on the noise of coaxial and triaxial cold supersonic jets. Results from his investigation have shown that the jet noise could be minimized for certain combinations of pressure ratios between the coaxial and triaxial jets, including cases where the inner stream velocity was less than the velocity of the outer stream. However, due to the cold jets, Dosanjh's results relate to the shock noise component of jet noise, and are not directly applicable to the noise of the hot jet exhausts existing on a duct burning turbofan engine.

Thus, a large effort has been expended on investigations of coannular jet noise, but the results of these studies cannot be used to assess the noise generated by the hot coannular jet exhaust of a DBTF engine having a fan to primary velocity ratio greater than one.

2.2 PROGRAM DESCRIPTION

The program described herein was conducted to establish the aero-acoustic performance characteristics of unsuppressed and fan stream suppressed coannular nozzles over a large range of operating conditions, in particular at conditions where the fan to primary stream velocity ratio was greater than one.

During the design phase of the program, two basic coannular nozzles were designed to simulate nozzles that could exist on a full size DBTF engine. These nozzles were designed to achieve fan to primary area ratios of 0.75 and 1.2 in order to investigate the aero-acoustic effects of area ratio over a range considered practical for DBTF operation in a supersonic transport.

Three multi-element nozzle suppressors were designed to produce various amounts of noise suppression in the fan jet of the 0.75 area ratio nozzle. These configurations, in order of increasing predicted suppression, were convoluted, finger and multi-tube. Hardwall and acoustically treated flight type ejector shrouds were designed to investigate the effects of an ejector on the noise of the basic nozzle configurations. In addition, a convoluted suppressor configuration, with and without ejectors, was designed at an area ratio of 1.2 to determine the effect of area ratio on a typical suppressor configuration. All nozzle models had the same equivalent exit diameter (0.127m), which was one-tenth of the full size diameter (1.27m). The studies leading to the design of all the configurations are documented in Reference 7.

All of the configurations were fabricated and tested statically at the Pratt & Whitney Aircraft Outdoor Jet Noise Test Facility located in West Palm Beach, Florida. This test facility produces two independently controlled flows with properties typical of the primary and fan flow streams of a DBTF. A total of 417 test points were run on 17 separate nozzle configurations, including a single stream convergent nozzle used to provide reference noise levels. The pressure ratio in the fan stream was varied from 1.3 to 4.1 and in the primary stream from 1.53 to 2.5. Total temperature was varied from 395°K to 1090°K in both streams. Far field noise signals were measured at 9 angles, ranging from 60° to 165° relative to the upstream jet axis. Pressure, temperature, weight flows, and thrust were measured for all test points. Exit pressure and temperature profiles were measured for selected test points. Section 3.0 contains detailed descriptions of the test facility and models tested. All data obtained during the testing is contained in the Comprehensive Data Report (Ref. 8), while the major results of the program are contained in this report.

3.0 APPARATUS

The experimental apparatus used in this program is described herein. This includes the test facility, along with supplementary hardware and instrumentation, as well as the model nozzle configuration evaluated in the program.

3.1 TEST FACILITY

The facility used in this program (shown in Figure 3-1) is the P&WA Jet Noise Test Facility located in West Palm Beach, Florida. The details of the test facility are shown schematically in Figure 3-2.

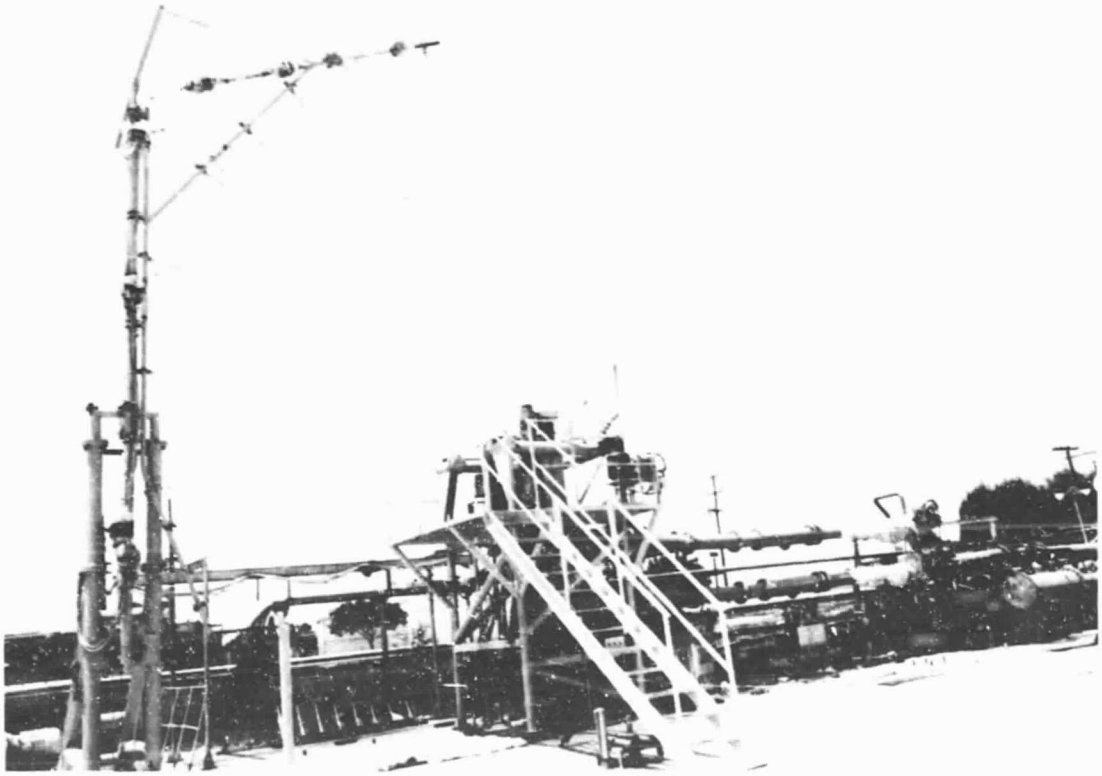

Figure 3-1 Pratt & Whitney Aircraft (P&WA) Outdoor Jet Noise Test Facility

The airflow to the test model is supplied by bleed flow from a JT3C "slave" engine and passes through a 0.25m (10 in) diameter underground pipe surfacing near the test stand. The flow enters the test rig at the pivot point, where teflon seals prevent leakage while allowing the rig to pivot freely in the vertical plane. The flow is then divided into two 0.20m (8 in) diameter pipes. The flow in each pipe is independently controlled by motor-operated wafer valves in each line. Flow rates are measured independently in each pipe by flow-measuring venturies which have been accurately calibrated at the Colorado Engineering Experimentation Station, Inc. Temperatures are set by separate heater/burner systems in each line. The burners are JP-fueled, and are capable of temperatures up to 1922°K (3000°F). The fuel flow

into the system is established by calibrated digital fuel meters. Both flow lines are then turned 90° through water cooled sections, and formed to provide coannular flows to the test model. The flow then passes through a transition section into the instrumentation section and test model. The assembly is suspended from two cables, on opposite sides of the vertical centerline, which are in series with load cells and connected to the rigid supporting framework. The load cell axes are coplanar with the vertical flow axis. An array of microphones is positioned at a 4.57m (15 ft) radial distance from the nozzle exit, in the plane of the nozzle centerline.

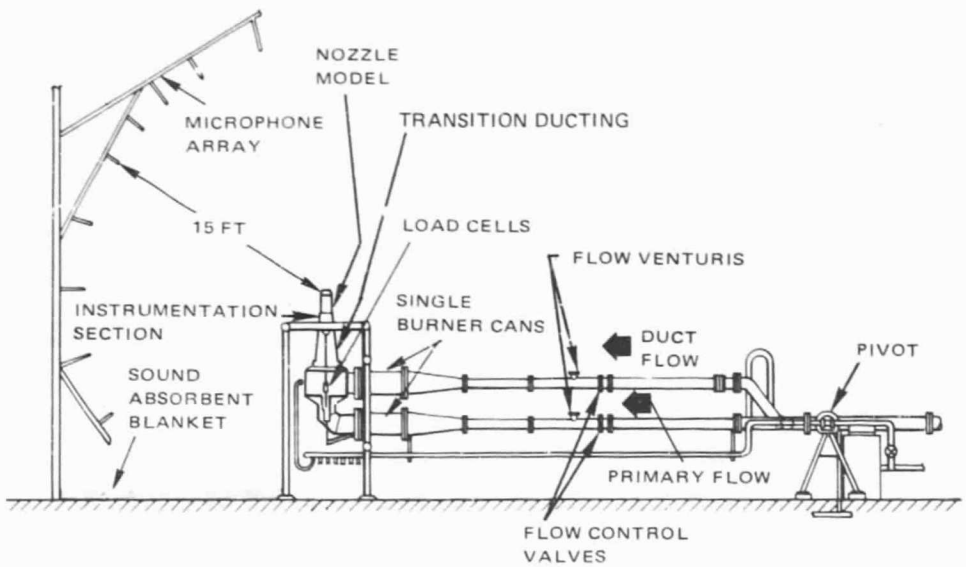

Figure 3-2 Schematic of P&WA outdoor Jet Noise Test Facility

This facility allows free field jet noise measurements since the nozzle is situated 4.2m (14 ft) above the ground in a vertical orientation and thus essentially eliminates spectral distortion from ground reflections. The possibility of small amounts of signal enhancement at high frequencies, at the more forward-angle microphones, was eliminated by the use of acoustically absorbing fiberglass matting 0.1m (4 in) thick, positioned on the ground underneath the microphones. Figure 3-3 shows the model test rig assembly installed on an 0.71m (28-in) diameter flange near the top of the test stand. The assembly was made long enough to insure that no obstruction existed between the nozzle exit and the microphone array, whose lowest point lies 30° below the plane of the nozzle exit.

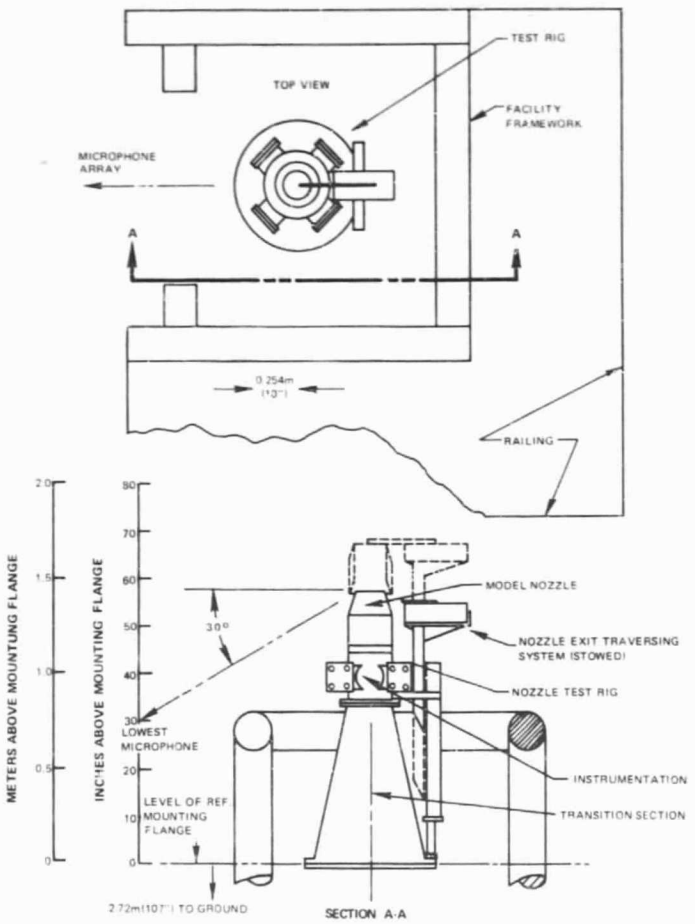

Figure 3-3 Details of Test Model Installation

The components of the test rig assembly are shown in detail in Figure 3-4 and described in the following sections. All of the hardware was made from AMS 5512 material. The relative position of the various components are indicated by station numbers which equal the distance from the reference mounting flange (STA 0).

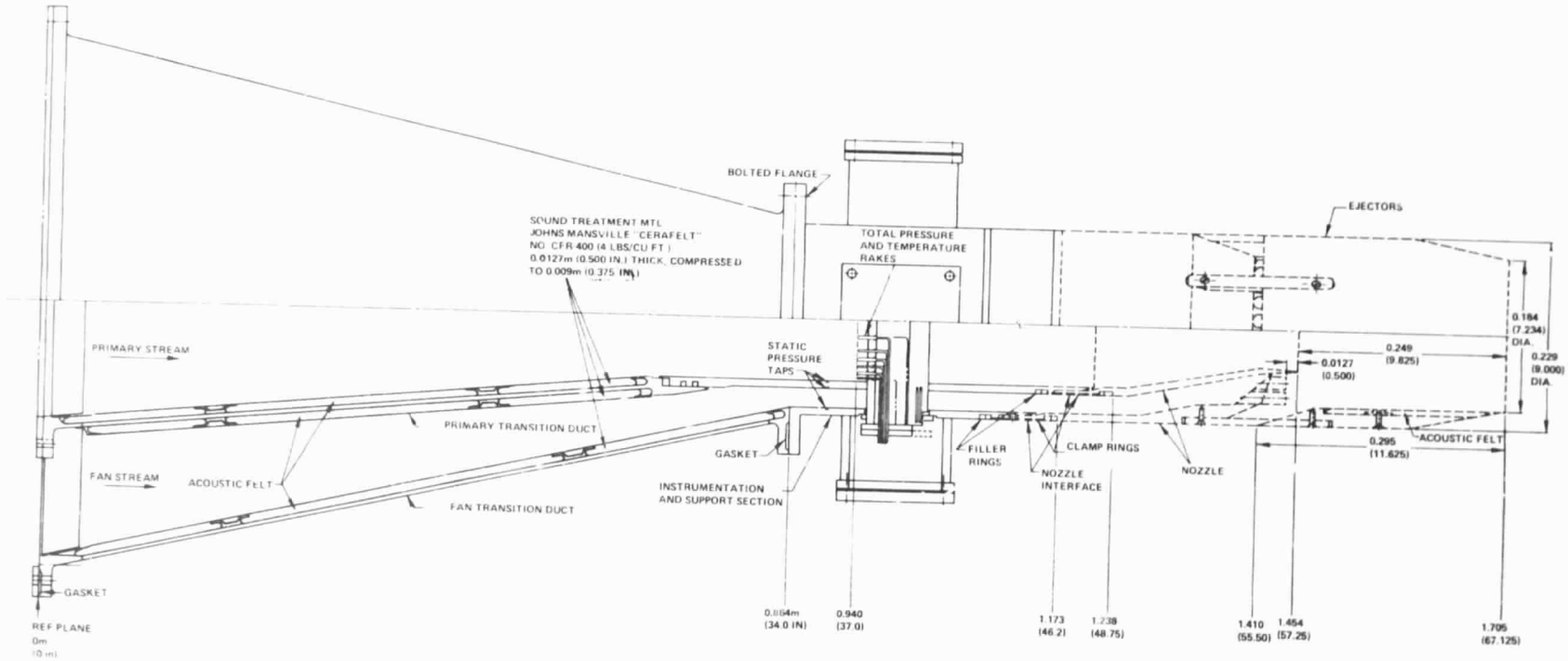

Figure 3-4 *Details of Transition and Instrumentation Sections Shown With Multi-Tube Suppressor and Treated Ejector Mounted*

3.1.1 Transition Ducting

The transition ducting mates the model test hardware to the existing rig and serves as a muffler. It consists of a set of conical approach ducts. The duct walls are lined with acoustic blankets made of "Cerafelt" to damp out any extraneous noise from within the basic test stand. Cerafelt is a lightweight, refractory-fiber insulation notable for its excellent thermal and chemical stability. Made predominately of alumina and silica, it combines lightness, heat resistance, low conductivity, and high sound-absorption qualities. Available in various densities and thicknesses, the particular type selected in the muffler is 0.0127m (½ in) thick and has a density of 64.07 kg/m^3 (4 lbs./ft^3). These values were chosen to provide sound attenuation over a wide frequency range for the operating conditions encountered during the tests. The attenuation (or transmission loss) through the muffler was on the order of 20 dB. The sound treatment material is contained by a perforated facing sheet having 30 percent porosity, with 0.0014m (0.056 inch) diameter holes, which does not interfere with the sound absorbing capabilities of the absorber material. Thermal expansion of the facing sheet is allowed for by the provision of sliding joints at the upstream end of each sheet.

The outer duct forms the main support for the model test rig. It is bolted to the instrumentation assembly section and takes the blow-off load at the large flange which interfaces with the test facility. Leakage is prevented between the streams by means of a slip joint with piston rings. The joint takes no axial load but is instead permitted to slide, allowing for axial growth due to temperature variation.

3.1.2 Instrumentation and Support Section

This section of the test rig serves a dual purpose. It maintains the concentricity of the assembly and contains all of the necessary instrumentation to define the properties of the flow entering the nozzles.

The major portions of the instrumentation duct are shown in Figure 3-5. A single strut, having an 18 percent NACA series 400 airfoil cross-section, passes through the primary duct and is welded in place at the primary duct walls. The same strut passes freely through the fan duct walls where clearance is provided to allow for relative growth due to temperature differentials in the two streams. Two short struts, welded to the outer diameter of the primary tube and positioned 90° to the primary strut, also pass freely through the fan duct wall. When operating with a thermal gradient, the fan duct is allowed to change in diameter relative to the primary duct without distorting the duct shape and without any significant variation in concentricity. Outer seal housings were built around the floating struts to prevent leakage from the fan stream.

Instrumentation for the measurement of total pressure and total temperature were installed within the struts. The probes are made up of removable rakes which are held in place at the ends of the struts. The rakes may therefore be installed or removed after rig assembly without having direct access to the primary or secondary flow passages.

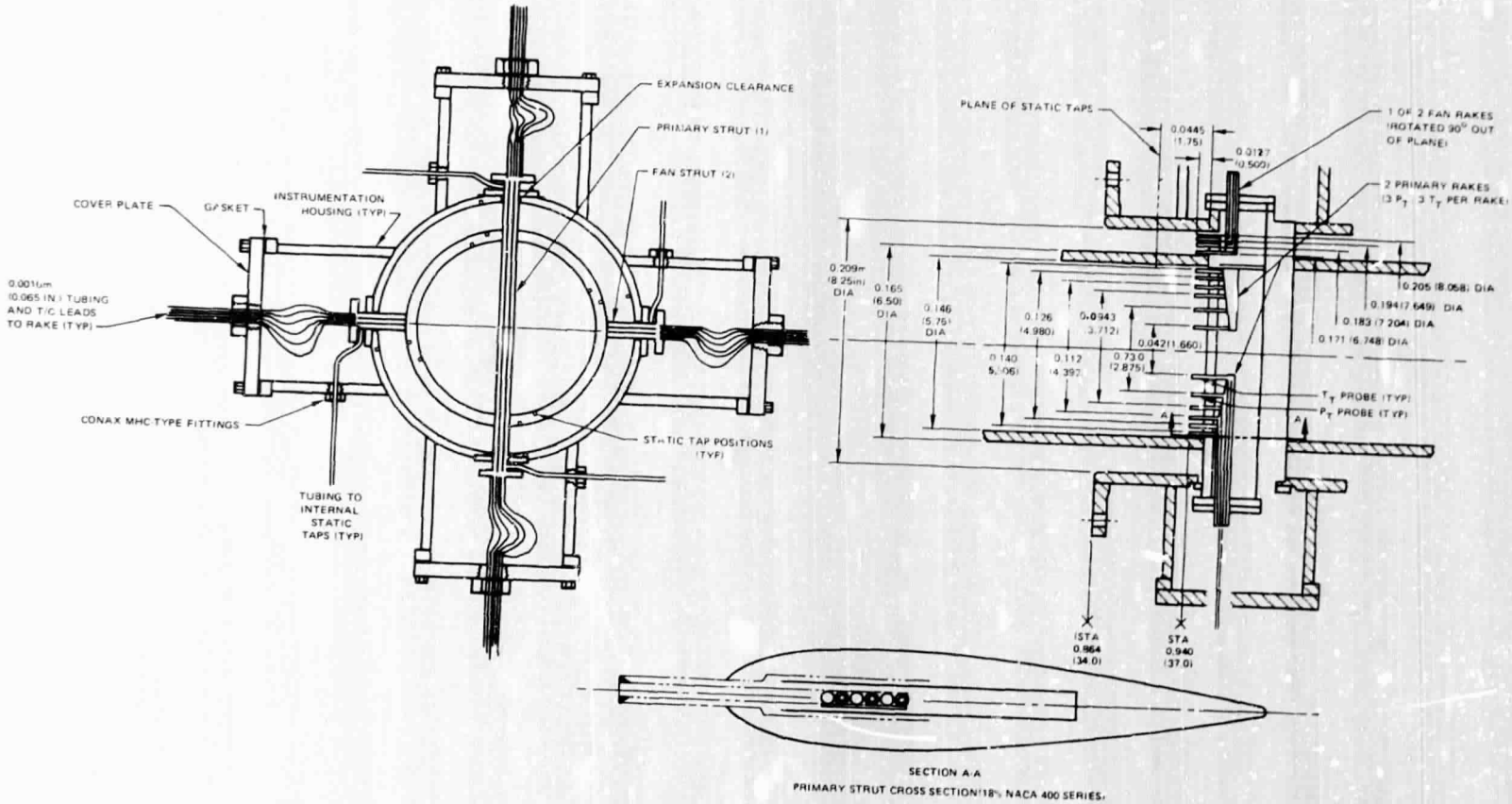

Figure 3-5 Details of Instrumentation and Support Section

Two diametrically opposed rakes are used in each stream to establish the total pressures and temperatures. The probes (P_t and T_t) are arranged radially in each duct such that the probes represent equal areas. An arithmetic average of the probe readings is then equal to the area-averaged value. The pressure and temperature probes are both included in each rake so that the flow is sampled across the entire duct to determine an average of each property.

Static pressure taps were installed on the walls of the instrumentation section to define the endpoints of the total pressure profiles across the passages. A total of 12 static taps were installed; 4 on each wall at 90° intervals (4 primary taps, 8 fan taps). The taps were positioned upstream and to the side of the struts to insure that the pressure readings are not influenced by the blockage of struts or rakes.

In addition to supplementing the total pressure profile data, the static pressure readings provide an alternate means of determining the total pressure; the continuity averaging process. In this process, the total pressure is calculated on the basis of the static pressure, the duct area and the measured flow rate.

3.1.3 Exit Plane Instrumentation/Traverse Rig

The mechanism used to traverse the ejector exit plane for flow properties is shown in Figure 3-6. The purpose of the traverse rig is to establish the static pressure, total pressure, and total temperature of the flow along a radial line at the exit plane of the ejector.

During selected nozzle tests, the exit plane traverse was accomplished immediately after thrust and acoustic data were taken. This procedure calls for a traversing system that is not in view of the microphone array while acoustic data are taken. A vertical traverse unit is used to move the horizontal (i.e., exit plane) probe traverse system into its operating position, where the probe is driven along a radial line at the exit of the ejector. When exit plane data are not being taken, the traversing system is stowed in a position upstream of the nozzle exit, on the side of the nozzle opposite the microphone array.

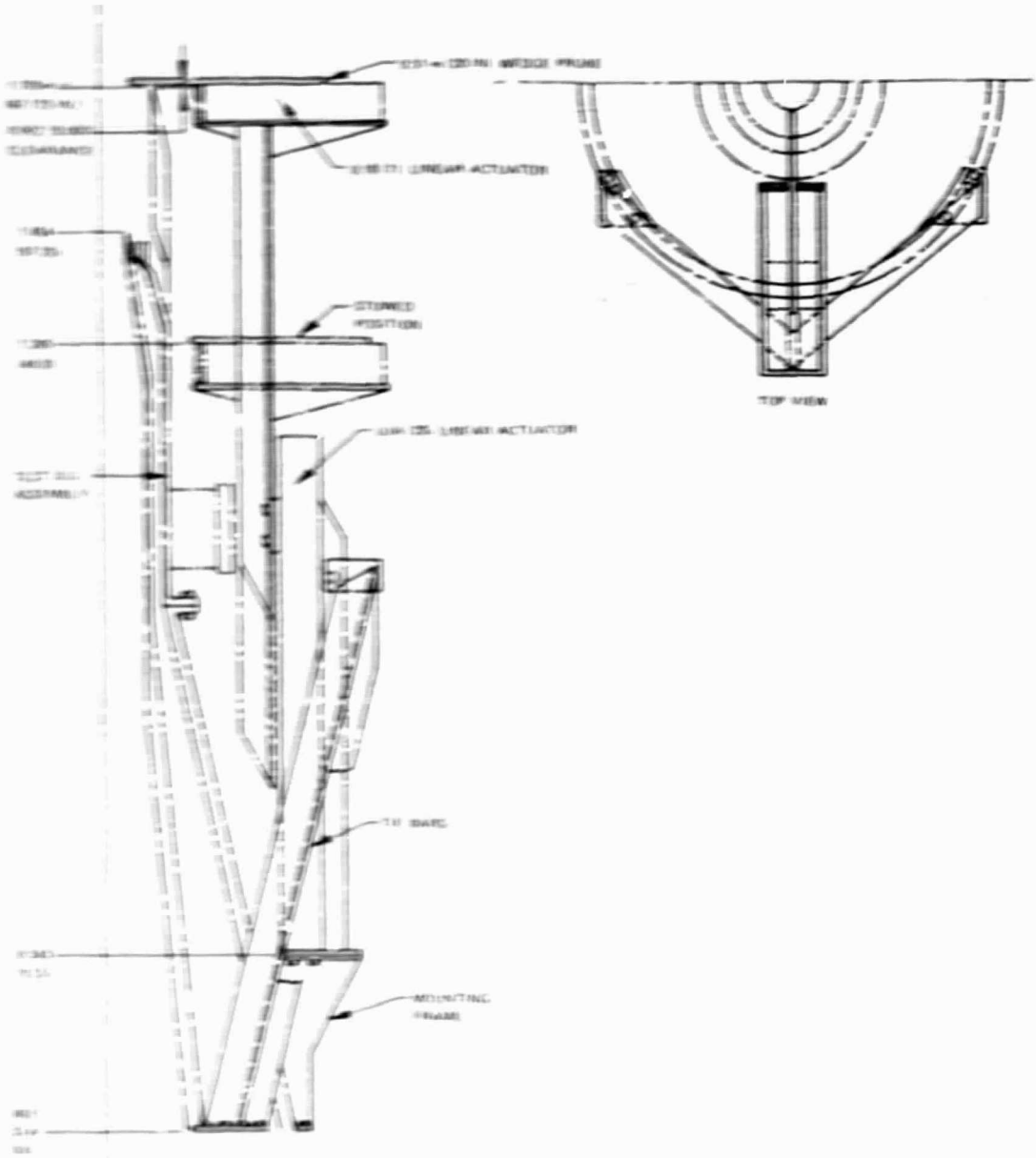

Figure 3-6 Details of Exit Plane Instrumentation Traversing System

The flow properties were measured with the probe shown in Figure 3-7. The static pressures were measured with two orifices (a and b), one on each side of the 20° wedge. The total pressure was measured at point c, at the front edge of the wedge. The total temperature was determined by means of a thermocouple that is exposed to flow through ports at the rear of the wedge, at points d and e. The flow exits at the base of the wedge through port f, which controls the flow past the thermocouple head. This port was sized to establish the best balance between conductive and convective heat transfer.

The probe was calibrated for pressure and temperature measurement over the range of flow parameters in the ejector nozzle flow.

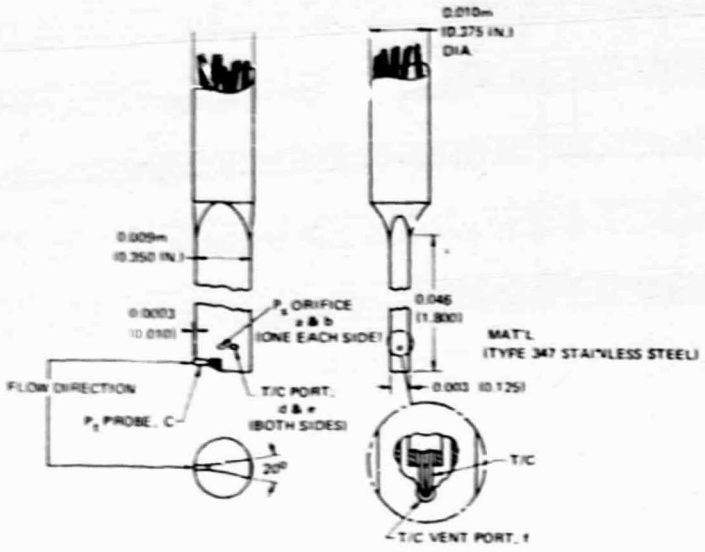

Figure 3-7 Details of Traverse Probe

3.1.4 Acoustic Instrumentation

Laboratory calibrated Bruell and Kjaer 0.006m (0.25 in) (No. 4135) microphones were employed without protective grids or wind screens. They were positioned in a polar array containing nine microphones at 60°, 75°, 90°, 105°, 120°, 130°, 140°, 150°, and 165° relative to the upstream jet axis at a distance of 4.6m (15 ft) from the exit of the nozzle. The signals from each microphone were recorded by a Honeywell 7600 series FM tape recorder, in a double extended bandwidth mode operating at 3.05 m/sec (120 in/sec). The frequency response in this operating mode was 80 kHz.

3.2 NOZZLE CONFIGURATIONS

A total of seventeen different configurations were evaluated during this program. All were fabricated from AMS 5512 material. The pertinent geometric variables of the basic configurations (without ejectors) are presented in Table 3-I. These variables include fan stream exit area (A_f), primary stream exit area (A_p), total exit area (A_t), equivalent diameter (D_{eq}) based on total exit area, and the diameter encompassing the fan nozzle and primary nozzle assembly (D_{per}), which represents the outer perimeter of the total basic nozzle unit.

TABLE 3-I

PERTINENT GEOMETRIC VARIABLES OF THE BASIC NOZZLE CONFIGURATIONS

Configuration	A_f m^2 (in^2)	A_p m^2 (in^2)	A_f/A_p	A_t m^2 (in^2)	D_{eq} m (in)	D_{per} m (in)
Reference Convergent Nozzle	—	—	—	.0126 (19.6)	.127 (5.0)	.127 (5.0)
Unsuppressed Coannular Nozzle	.0054 (8.40)	.0072 (11.20)	0.75	.0126 (19.6)	.127 (5.0)	.135 (5.32)
Unsuppressed Coannular Nozzle	.0069 (10.69)	.0057 (8.91)	1.2	.0126 (19.6)	.127 (5.0)	.135 (5.32)
Multi-Tube Suppressor Nozzle	.0054 (8.40)	.0072 (11.20)	0.75	.0126 (19.6)	.127 (5.0)	.178 (7.00)
Convoluted Suppressor Nozzle	.0054 (8.40)	.0072 (11.20)	0.75	.0126 (19.6)	.127 (5.0)	.161 (6.34)
Convoluted Suppressor Nozzle	.0069 (10.69)	.0057 (8.91)	1.2	.0126 (19.6)	.127 (5.0)	.165 (6.49)
Finger Suppressor Nozzle	.0054 (8.40)	.0072 (11.20)	0.75	.0126 (19.6)	.127 (5.0)	.169 (6.66)

Detailed descriptions of all of the test models are presented in the following sections.

3.2.1 Reference Convergent Nozzle

The single stream reference nozzle is a low angle conical convergent nozzle shown in Figure 3-8. In order to adapt this nozzle to the coannular ducting of the test rig, a primary duct fairing was made to blend the two streams, maintaining a constant fan/engine area ratio to the mixing plane. The end piece is tapered to a minimum thickness to prevent an undesirable wake. When testing this nozzle, the same flow properties were established in both segments, therefore, the flow at the nozzle exit is uniform.

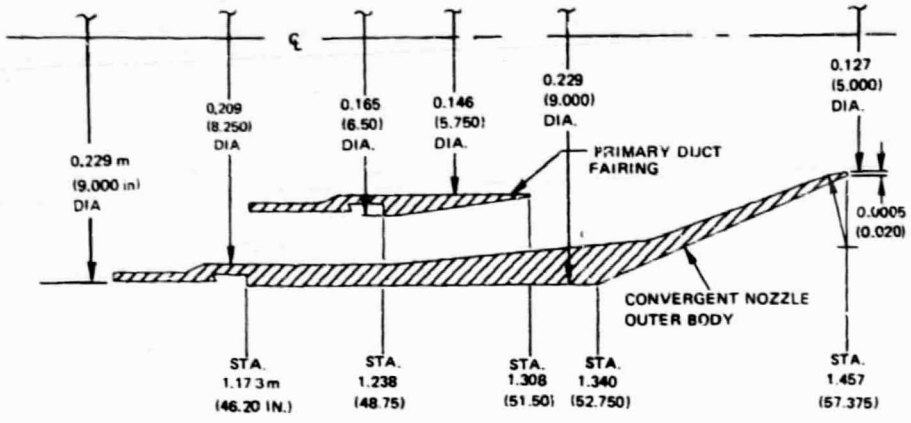

Figure 3-8 Details of Reference Convergent Nozzle

3.2.2 Unsuppressed Coannular Nozzles

Two unsuppressed coannular nozzles were built. The first with a fan to primary area ratio of 0.75 is illustrated in Figure 3-9, while the second configuration, having an area ratio of 1.2 is illustrated in Figure 3-10. The primary nozzle for both configurations is a convergent-divergent design (with an exit to throat area ratio of 1.1). This type of nozzle design has been employed during many of the SCAR studies where high Mach number operation is the key design point. The axial spacing between the primary and fan stream exits is also consistent with these requirements.

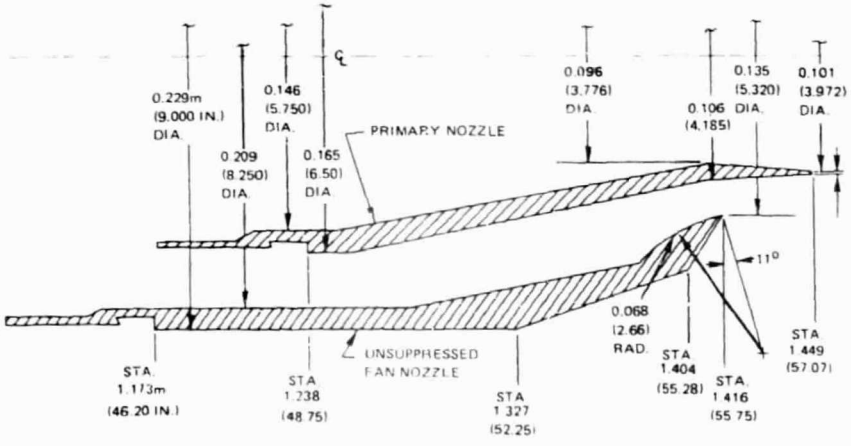

Figure 3-9 Details of Unsuppressed Coannular Nozzle, 0.75 Area Ratio

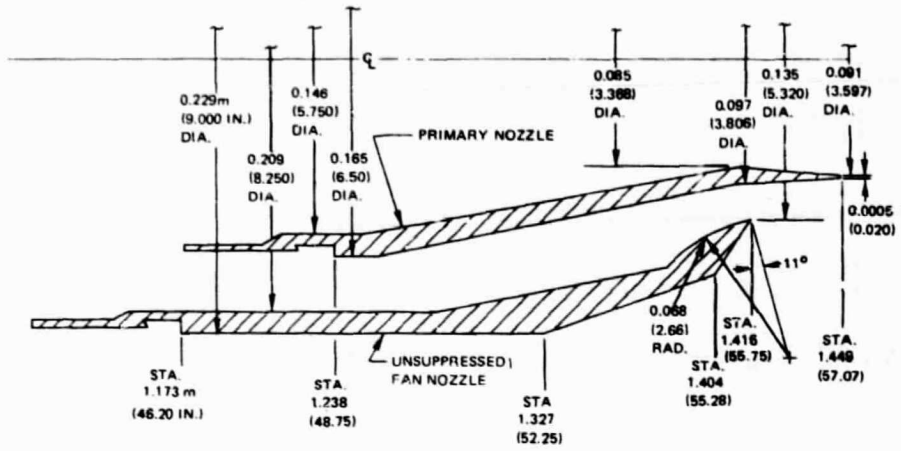

Figure 3-10 Details of Unsuppressed Coannular Nozzle, 1.2 Area Ratio

3.2.3 Multi-Tube Suppressor Nozzle

This configuration consists of 44 identical tubes arranged in two circumferential rows which form the throat of the fan nozzle (See Figure 3-11). Each tube is a convergent nozzle having a 15 percent diameter convergence (area convergence ratio of 1.32), with a convergence half-angle of 15°. The primary nozzle is the same as that used with the corresponding unsuppressed coannular nozzle.

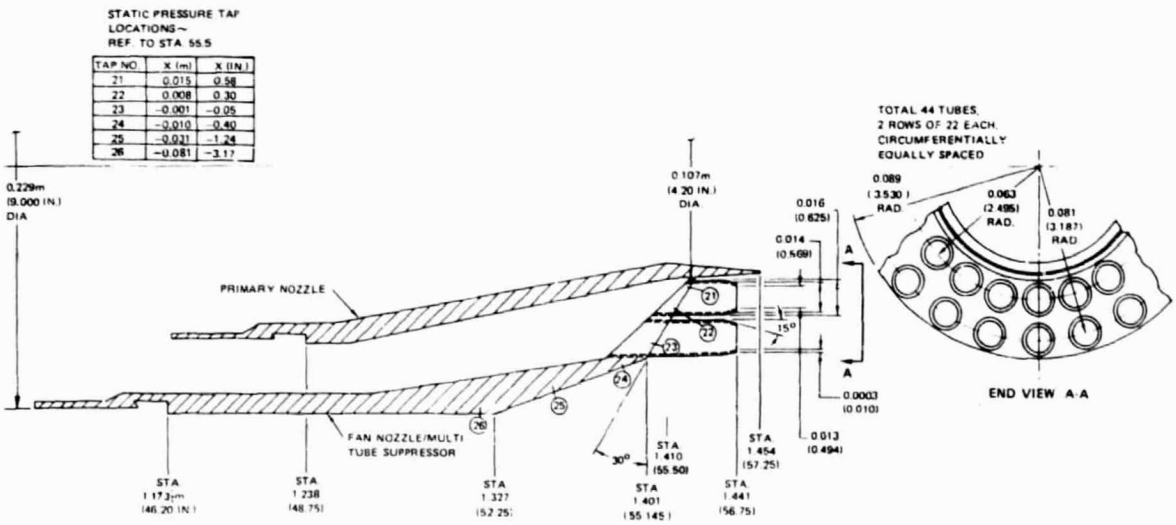

Figure 3-11 Details of Multi-Tube Suppressor Nozzle, 0.75 Area Ratio

The tubes are fixed in a conical ring which is an integral part of the fan nozzle body. The external lines of this conical ring are identical to those of the coannular unsuppressed nozzle. The upstream ends of the tubes are blended with the internal surface of the conical ring. The downstream ends are at the same axial station, upstream of the primary nozzle exit.

The conical ring, to which the tubes are attached, comes into near-contact with the external surface of the primary nozzle. A radial clearance of about 0.0006m (0.025 inch) is provided to allow for differential thermal expansion.

Six static pressure taps were placed on the external surface of the suppressor to monitor the external flow characteristics and to aid in analyzing performance and acoustic data. The tap locations are referenced to station 55.5 which corresponds to the position of the ejector leading edge when an ejector is employed. The taps are aligned axially, in the space between the radial segments of tubes; three at the base of the tube assembly and three along the approach to the tubes.

3.2.4 Convoluted Suppressor Nozzles

The first convoluted suppressor consists of 18 equally spaced lobes which form the fan stream throat area (see Figure 3-12). This configuration has a fan to primary area ratio of 0.75. Each of the internal lobes were machined to a constant width, continuing upstream from the exit (along the inner slope shown in the side view in Figure 3-12) blending with the cylindrical duct upstream of the convergence. The external lobes were likewise machined along their inner slope, blending with the external surface of the fan duct. The result is a three-dimensional convoluted approach to the fan exit by which the fan flow and ambient air (or external flow) are mixed.

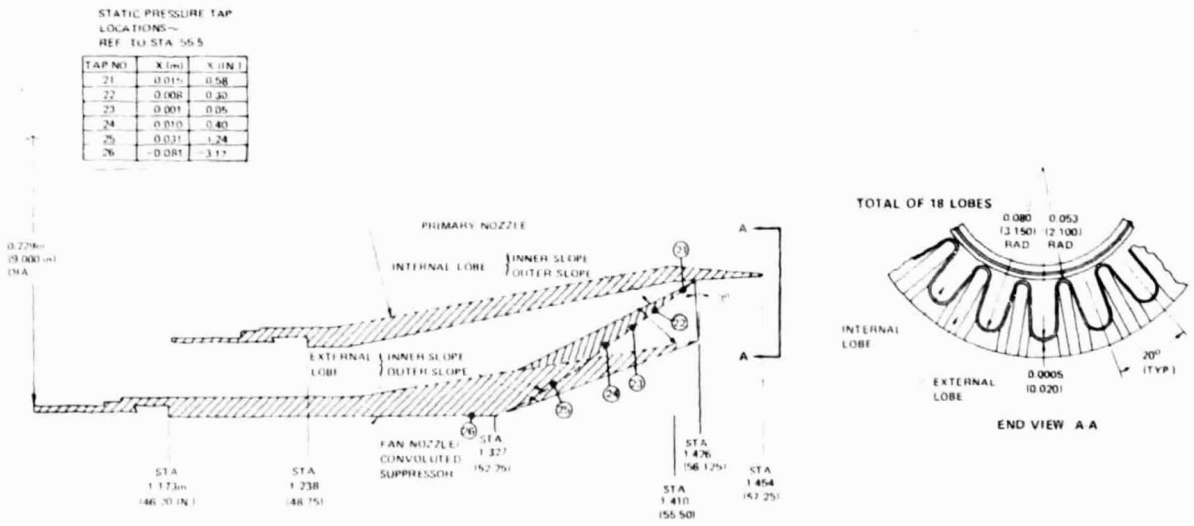

Figure 3-12 Details of Convoluted Suppressor Nozzle, 0.75 Area Ratio

The axial positions of the taps on this convoluted suppressor are the same as those of the tubular suppressor arranged along the inner slope of an external flow convolute (see Figure 3-11).

A second convoluted suppressor, of similar design to the first, but with a fan to primary area ratio of 1.2 is illustrated in Figure 3-13.

The primary nozzles used with the convoluted suppressors are the same as those used with the unsuppressed coannular nozzles of the same fan to primary area ratio.

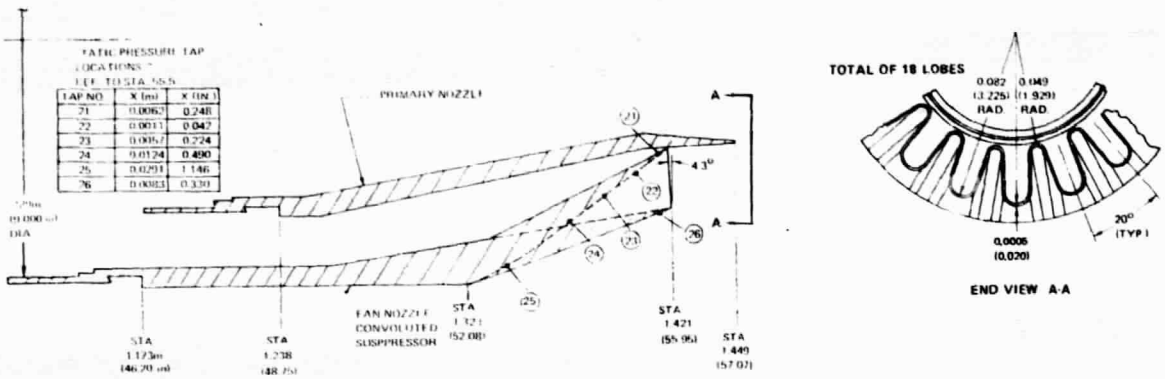

Figure 3-13 Details of Convoluted Suppressor Nozzle, 1.2 Area Ratio

3.2.5 Finger Suppressor Nozzle

The finger suppressor is composed of 32 equally spaced radial projections which subdivide the fan nozzle exit into an equal number of individual rectangular nozzles (Figure 3-14). As in the other suppressor designs, the external lines approaching the plane of the fingers are identical to those of the unsuppressed coannular nozzle.

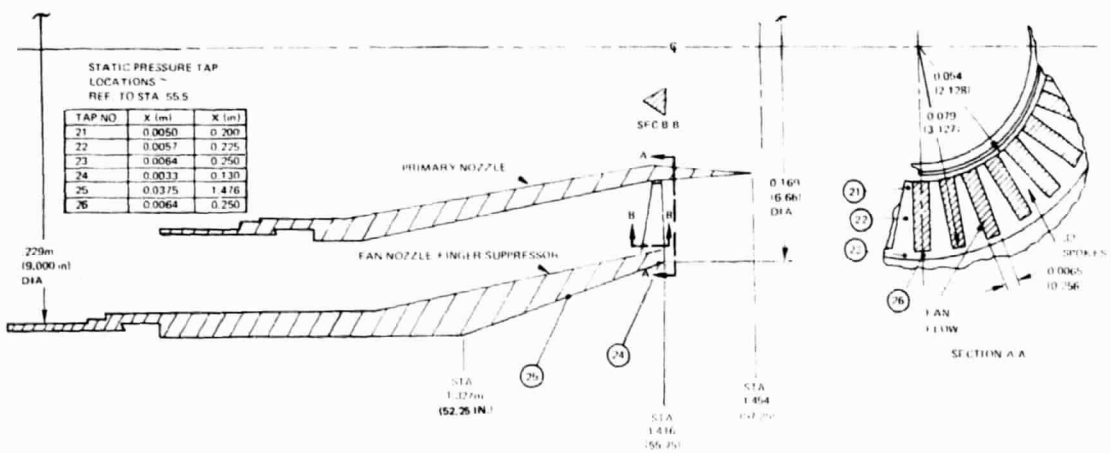

Figure 3-14 Details of Finger Suppressor Nozzle, 0.75 Area Ratio

The fingers have a triangular cross-section (as shown in Figure 3-14, Section B-B); the apex being at the upstream side to smooth the approach to the exit plane. The downstream side is flat, representing the portion of the finger that would be flush with the inner wall of the fan duct when the suppressor is stowed. The primary nozzle was the same as that used for the 0.75 area ratio unsuppressed coannular nozzle.

As with the other suppressors, pressure taps were placed on the downstream surface of the fingers and on other portions of the suppressor where non-ambient pressure levels were expected in order to monitor the flow characteristics and to aid in interpreting the data.

3.2.6 Ejectors

The ejector geometry is based on the configurations used for recent SCAR studies and, as such, represents a flight-type, high Mach number design. The same ejector length/diameter ratios are maintained. The relation between the ejector and the primary/fan nozzle system was established on the basis of supersonic cruise requirements. The ejector inlet and exit areas however, were sized to produce high performance at static conditions for the 0.75 area ratio unsuppressed coannular nozzle. However, the same ejectors were used with all configurations.

Two ejector configurations were tested; a hardwall version and one with internal sound treatment. A basic ejector shell could accept a hardwall or an acoustically treated insert. Each of the two ejectors were interchangeable with the suppressor configurations. The hardwall ejector is shown in Figure 3-15, mated with the convoluted suppressor. The treated ejector is shown in Figure 3-16, mated with the tubular suppressor. In all configurations, the leading edge of the ejector is at station 55.5.

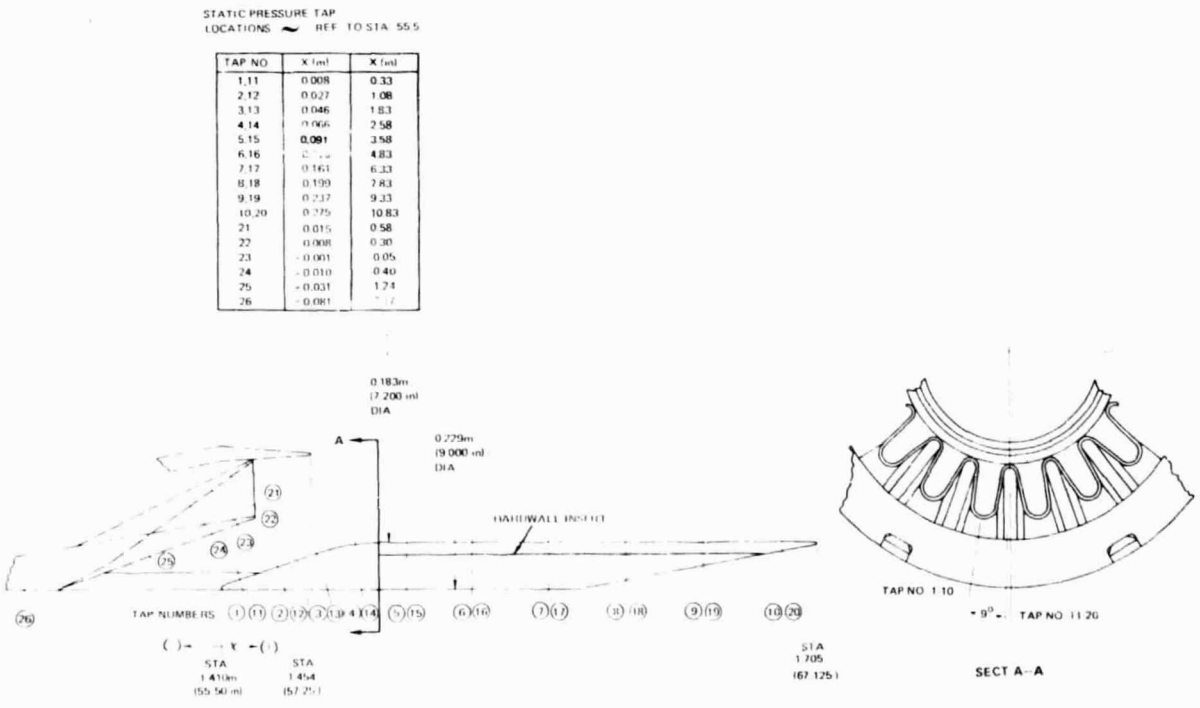

Figure 3-15 Details of Hardwall Ejector Mounted to the 0.75 Area Ratio Convoluted Suppressor

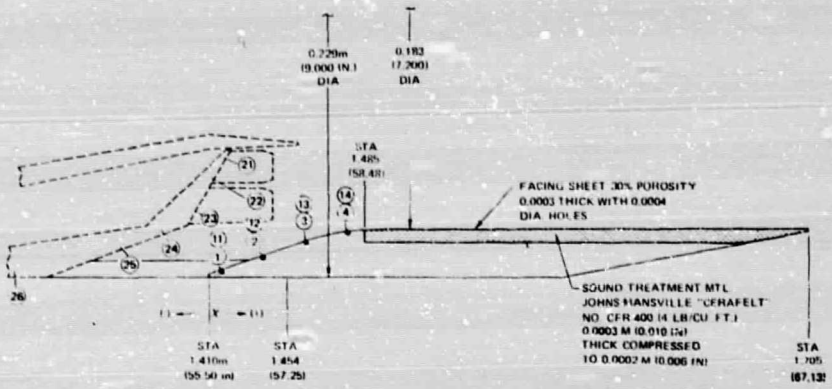

Figure 3-16 Details of Acoustically Treated Ejector Mounted to the 0.75 Area Ratio Multi-Tube Suppressor

The hardwall ejector contained the instrumentation required to establish the internal axial static pressure gradient along the full length of the ejector wall. The instrumentation in the cylindrical portion of the ejector was contained within the hardwall insert. This instrumentation was eliminated when the hardwall insert was replaced with the acoustically treated insert. However, the upstream static taps remained in place for both configurations. The pressure taps were placed in two axial rows at circumferential positions that correspond to the extremes of the suppressor. For example, when the ejector is assembled with the convoluted suppressor, one of the rows of taps is aligned with an internal (fan stream) lobe and the other is aligned with an external lobe. When the ejector is combined with the tubular suppressor, one row of taps is aligned with the tubes; the other with the spaces between the tubes. The two rows of pressure taps are placed 9° apart circumferentially. This relative location accommodates all suppressor installations. The taps were located circumferentially about mid-way between the ejector struts to avoid the local flow interference in the vicinity of the struts.

The internal wall of the treated ejector is fitted with an insert containing a 0.0064m (¼ in) thickness of compressed "Cerafelt", used to absorb flow-generated sound. The insert has a face sheet porosity of 30 percent made with holes of 0.0004m (0.016 in) diameter.

The relation of the ejector to the unsuppressed and suppressed coannular configurations is illustrated in Figure 3-17. The axial spacing (ΔX) between the fan nozzle exit and the leading edge of the ejector is indicated along with the ratio of the ejector diameter to the diameter of the circle enclosing the basic nozzle/suppressor exit (D_{ejec}/D_{per}).

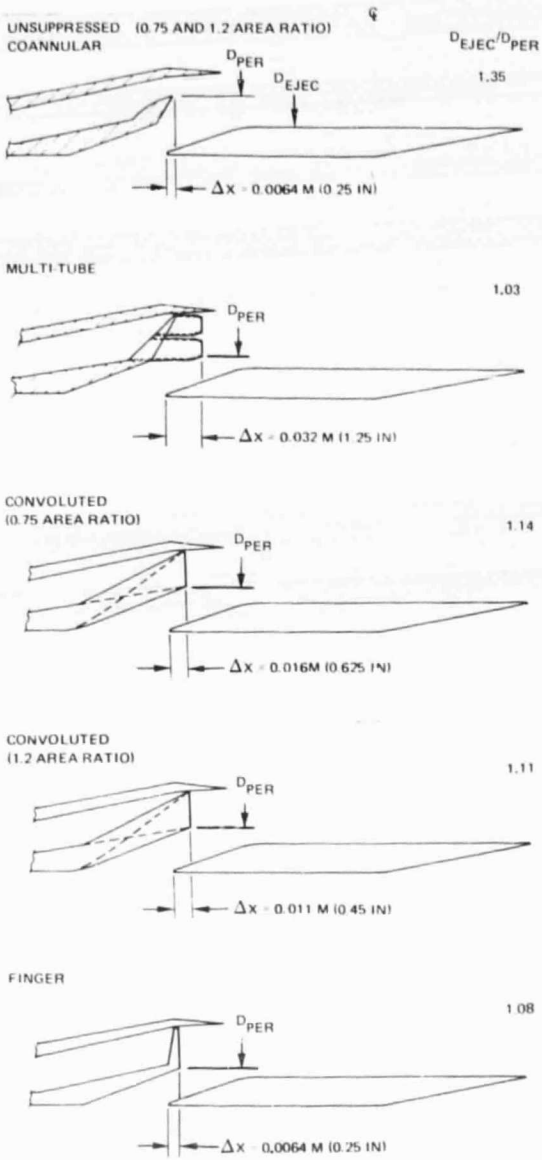

Figure 3-17 Ejector Size and Placement Relative to All the Tested Nozzle Configurations

4.0 DATA

The types of data produced from the experimental testing are described in this section, along with the test procedure and a matrix showing the conditions at which each of the model configurations was tested. Various acoustic and aerodynamic parameters were obtained from the testing of the 17 different configurations over a matrix at pressure ratios and temperatures. Data covered a total of 417 operating points. Acoustic data from this program is documented in model size as well as scaled to represent a full size AST powerplant.

The model scale data is based on the 0.127m (5in) equivalent diameter size models tested. The acoustic parameters are:

- One-third octave band sound pressure level spectra at 4.6m (15 ft) radius from 60° to 165° relative to the upstream jet axis, corrected to theoretical day conditions. "Theoretical day" is a hypothetical day with atmospheric conditions producing zero atmospheric attenuation of noise. The noise levels thus were corrected for the full amount of atmospheric absorbtion occuring during each test point acquisition time period.

- Overall sound pressure level at 4.6m (15 ft) for the same angles as spectra.

- One-third octave band power spectra for 0.127m (5 in) equivalent diameter models.

- Overall sound power level.

The following acoustic parameters are scaled 10X to a 1.27m (50 in) size to represent a full size AST powerplant:

- One-third octave band sound pressure level spectra at 45.7m (150 ft) radius from 60° to 165° relative to the upstream jet axis.

- Overall sound pressure level at 45.7m (150 ft) radius from 60° to 165° relative to the upstream jet axis.

- One-third octave band power spectra.

- Overall sound power level.

- Perceived noise levels calculated at various sideline distances including 648.6m sideline at zero altitude from 60° to 165° relative to the upstream jet axis.

The aerodynamic parameters are:

- Nozzle thrust coefficient.

- Nozzle flow coefficient for each stream.

- Static pressure distribution along the internal surface of the ejector and the external surface of the suppressed nozzle.

- Temperature and velocity profiles in the plane of the ejector exit, whether or not the ejector was in place.

The actual test procedure used to obtain data was as follows:

1) The slave J57 engine used to provide the model airflow was started and allowed to run for ½ hr. in order to warm the ductwork and expell any foreign matter in the piping.

2) The acoustic and thrust measuring systems were checked and calibrated.

3) Wind velocities were monitored. Normally, acoustic measurements were made with wind velocities under 8 mps; however, on occasion, slightly higher wind velocities were allowed, but only if all microphones exhibited normal behavior.

4) Pressures and temperatures were set in each stream and allowed to stabilize.

5) Pressure, temperature and thrust levels were read under steady state operating conditions and entered on computer coding sheets for subsequent computerized data reduction.

6) Acoustic data was recorded simultaneously for all 9 channels on a 14 channel tape recorder for subsequent processing.

7) On-line one-third octave band analysis was performed on signals from selected microphones (i.e., angles) to ensure satisfactory operation.

The above test procedure was followed in the testing of all configurations ensuring consistency in the results obtained during the program.

Samples of all of the full scale acoustic and aerodynamic parameters are presented in this report for each configuration, illustrating the major findings of the program. In addition, a tabulation of acoustic power level and perceived noise levels, at all measurement angles, for all test points, is included in Appendix I.

Due to the large amount of data involved, the complete results of the testing have been compiled separately in the Comprehensive Data Report (CDR), NASA CR-134910 (Ref 8). This report includes both the model scale and full size data.

Table 4-I lists the nozzle operating conditions for each test point. In this table, nominal values of the stream temperatures and pressures are listed.

The detailed data reduction procedures and sample data outputs are presented in Sections 4.1 and 4.2. A discussion of data validity based on the acoustic measurements taken with a convergent nozzle is presented in Section 4.3. The method used to synthesize the jet noise of a coannular nozzle is presented in Section 4.4 for reference purposes.

TABLE 4-I

TEST MATRIX

P_{tp}/P_a	T_{tp} (°K)	T_{tf} (°K)	P_{tf}/P_a 1.3	1.8	2.5	3.2	4.1
0.75 Area Ratio Unsuppressed Coannular							
1.53	395	395	X(1)	X	X	X	
		700	X	X	X	X	
		895	X	X	X	X	
		1089		X	X	X	X
	700	395	X	X	X	X	
		700	X	X	X	X	
		895	X	X	X	X	
		1089		X	X		X
	811	395	X	X	X	X	
		700	X	X	X	X	
		895	X	X	X	X	
		1089		X	X	X	X
	1089	395	X	X	X	X	
		700	X	X	X	X	
		895	X	X	X	X	
		1089		X	X	X	X
2.0	811	700	X	X		X	X
2.0	811	1089		X	X		X
2.5	811	700	X	X		X	
2.5	811	1089		X	X		X
0.75 Area Ratio Unsuppressed Coannular With Hardwall Ejector							
1.53	811	700	X	X		X	
		1089		X	X	X	X
0.75 Area Ratio Unsuppressed Coannular With Treated Ejector							
1.53	811	700	X	X		X	
		1089		X	X	X	X
1.2 Area Ratio Unsuppressed Coannular							
1.53	395	700	X	X	X	X	
		1089		X	X		X
	811	700	X	X	X	X	
		1089		X	X		X

(1) P_{TF}/P_a = 1.15

TABLE 4-I (Cont'd)

P_{tp}/P_a	T_{tp} (°K)	T_{tf} (°K)	P_{tf}/P_a				
			1.3	1.8	2.5	3.2	4.1
Multitube Suppressor							
1.53	395	395	X	X		X	
		700	X	X	X	X	
		895	X	X	X	X	
		1089		X	X		X
	811	395	X	X		X	
		700	X	X	X	X	
		895	X	X	X	X	
		1089		X	X		X
2.0	811	700	X	X		X	
2.0	811	1089		X	X		X
2.5	811	700	X	X		X	
	811	1089		X	X		X
Multitube Suppressor With Hardwall Ejector							
1.53	395	395	X	X		X	
		700	X	X	X	X	
		895	X	X	X	X	
		1089		X	X		X
1.53	811	395	X	X		X	
		700	X	X	X	X	
		895	X	X	X	X	
		1089		X	X		X
Multitube Suppressor With Treated Ejector							
1.53	395	395	X	X		X	
		700	X	X	X	X	
		895	X	X	X	X	
		1089		X	X		X
	811	395	X	X		X	
		700	X	X	X	X	
		895	X	X	X	X	
		1089		X	X		X
2.0	811	700	X	X		X	
2.0	811	1089		X	X		X
2.5	811	700	X	X		X	
2.5	811	1089		X	X		X

TABLE 4.1 (Cont'd)

P_{tp}/P_a	T_{tp} (°K)	T_{tf} (°K)	P_{tf}/P_a				
			1.3	1.8	2.5	3.2	4.1
Finger Suppressor							
1.53	395	700	X	X	X	X	
		1089		X	X		X
	811	700	X	X	X	X	
		1089		X	X		X
Finger Suppressor With Hardwall Ejector							
1.53	811	700	X	X	X	X	
		1089		X	X		X
Finger Suppressor With Treated Ejector							
1.53	395	700	X	X	X	X	
		1089		X	X		X
	811	700	X	X	X	X	
		1089		X	X		X
0.75 Area Ratio Convoluted Suppressor							
1.53	395	395	X	X		X	
		700	X	X	X	X	
		895	X	X	X	X	
		1089		X	X		X
	811	395	X	X		X	
		700	X	X	X	X	
		895	X	X	X	X	
		1089		X	X		X
2.0	811	700	X	X		X	
2.0	811	1089		X	X		X
2.5	811	700	X	X		X	
2.5	811	1089		X	X		X
0.75 Area Ratio Convoluted Suppressor With Hardwall Ejector							
1.53	395	395	X	X		X	
		700	X	X	X	X	
		895	X	X	X	X	
		1089		X	X		X
	811	395	X	X		X	
		700	X	X	X	X	
		895	X	X	X	X	
		1089		X	X		X

TABLE 4-I (Concluded)

P_{tp}/P_a	T_{tp} (°K)	T_{tf} (°K)	P_{tf}/P_a				
			1.3	1.8	2.5	3.2	4.1
0.75 Area Ratio Convoluted Suppressor With Treated Ejector							
1.53	395	395	X	X		X	
		700	X	X	X	X	
		895	X	X	X	X	
		1089		X	X		X
	811	395	X	X		X	
		700	X	X	X	X	
		895	X	X	X	X	
		1089		X	X		X
1.2 Area Ratio Convoluted Suppressor							
1.53	395	700	X	X	X	X	
		1089		X	X		X
	811	700	X	X	X	X	
		1089		X	X		X
1.2 Area Ratio Convoluted Suppressor With Hardware Ejector							
1.53	395	700	X	X	X	X	
		1089		X	X		X
	811	700	X	X	X	X	
		1089		X	X		X
1.2 Area Ratio Convoluted Suppressor With Treated Ejector							
1.53	395	700	X	X	X	X	
		1089		X	X		X
	811	700	X	X	X	X	
		1089		X	X		X

Convergent Nozzle

T_t (°K)	P_t/P_a							
	1.15	1.3	1.53	1.8	2.0	2.5	2.65	3.2
395	X	X	X	X		X	X	
700		X	X	X		X		X
811			X		X	X		
895	X	X	X	X		X		X
1089		X	X	X		X		X

4.1 AERODYNAMIC DATA REDUCTION

The measured aerodynamic properties are divided into three categories:

(a) Thrust Coefficients and Flow Coefficients
(b) Surface Static Pressures
(c) Exit Profiles

The basic aerodynamic performance characteristics are presented in category (a) along with the flow properties in each stream. The static pressures (b) provide the axial pressure distributions useful in diagnosing the performance of the nozzles. The exit profiles (c) include the temperature and velocity surveys measured in the nozzle plume.

These data are based on pressure, temperature and thrust measurements made while maintaining steady-state model flow conditions during each test point. The pressure data were established by means of U-tube manometers, Heise gauges and a pressure transducer system. The temperatures were measured with the use of Brown potentiometers. The thrust measurements were based on the output of two Baldwin-Lima-Hamilton load cells (5000 lb. capacity),whose accuracy was rated at ±0.02% of full rated load.

The reduction of the basic data to the final aerodynamic parameters is described in detail in following sections.

4.1.1 Thrust Coefficients and Flow Coefficients

The thrust coefficient of a nozzle is a function of the thrust produced by the nozzle (F) and the ideal thrust which is available (F_i) based on the properties of the flow entering the nozzle. The nozzle thrust coefficient, C_v, is defined as:

$$C_V = \frac{F}{F_{i_t}}$$

The nozzle thrust is measured with two load cells positioned between the floating thrust bed and the stationary platform. The Nozzle thrust (F) is established as follows:

$$F = F_t - F_o + \Delta F_1 + \Delta F_2 + \Delta F_3 \qquad \text{(N, lbs)}$$

where:

F_t	=	Total load cell output
F_o	=	"No-flow" load cell output; the initial load cell readings taken after the stand is brought up to operating temperature.
ΔF_1, ΔF_2	=	Stand tare forces associated with variations due to thermal growth of the metric components.
ΔF_3	=	Corrections for variations in the air weight within the metric portion of the stand. The volume of the metric portion of the flow system is large enough to experience some variations in air weight within the operating range of temperature and pressure.

The total ideal thrust (F_{i_t}) is defined as:

$$F_{i_t} = F_{i_{Primary}} + F_{i_{Fan}} \qquad (N, lbf)$$

The ideal thrust (F_i) of each stream is calculated by the equation:

$$F_i = P_t A^* \sqrt{\frac{2\gamma^2}{\gamma-1}\left(\frac{2}{\gamma+1}\right)^{\frac{\gamma+1}{\gamma-1}}\left[1-\left(\frac{P_a}{P_t}\right)^{\frac{\gamma-1}{\gamma}}\right]}$$

where:

P_t = Total pressure at instrumentation station (N/m^2, psia)

P_a = ambient pressure (N/m^2, psia)

$$A^* = \frac{W_t}{P_t}\sqrt{\frac{T_t \mathscr{R}}{g_c \gamma}}\left(1+\frac{\gamma-1}{2}\right)^{\frac{\gamma+1}{2(\gamma-1)}}$$

and

W_t	=	Total Mass Flow = $W + W_{fuel}$ (kg/sec, lbm/sec)
W	=	Air flow rate, measured at the upstream venturis (kg/sec, lbm/sec)
W_{fuel}	=	Fuel flow, measured by digital fuel meters (kg/sec, lbm/sec)
T_t	=	Total temperature at instrumentation station (°K, °R)
γ	=	Specific heat ratio
$\mathscr{R}$	=	Gas constant = (88.51 Nm/kg °K, 53.3 lbf ft/lbm °R)
g_c	=	Conversion factor = (1.0 kg m/N sec^2, 32.174 lbm ft/lbf sec^2)

The nozzle flow coefficient for each stream is calculated by the equation:

$$C_d = \frac{W_t}{W_i}$$

where:

$$W_i = \frac{P_t A}{\sqrt{T_t}} M \sqrt{\frac{\gamma g_c}{\mathscr{R}}}\left(1+\frac{\gamma-1}{2}M^2\right)^{-\frac{(\gamma+1)}{2(\gamma-1)}} \quad ; M \leqslant 1.0$$

(kg/sec, lbm/sec)

A = Nozzle exit area in each stream (m^2, in^2)

The exit areas were determined by measurement at ambient temperature and corrected for the effect of the elevated testing temperature.

M = Fully Expanded Mach Number = $\sqrt{\frac{2}{\gamma - 1}\left((P_t/P_a)^{\frac{\gamma - 1}{\gamma}} - 1\right)}$

The thrust coefficients and flow coefficients for all the test configurations are included in Section B of Volume II of the CDR. A sample of the data available in the CDR is presented in Figure 4.1-1a for Configuration (3) which is the multi-tube suppressor nozzle. The thrust and flow coefficient are tabulated along with the flow properties of each stream (Pressure ratio, P_t/P_a, temperature T_t, and ideal jet velocity V).

4.1.2 Surface Static Pressures

Static pressures (P) were measured along the external surface of the suppressors and along the internal surface of the ejectors. The pressures are ratioed to ambient pressure (P_a) and tabulated in the CDR where they are identified by pressure orifice number (TAP) and axial location, X/L, where:

X = position of pressure orifices relative to station 55.5 (which corresponds to leading edge of the ejector)

L = Ejector length = 0.295M (11.63 in.)

All of the static pressure data is presented in Section B, Volume II of the CDR. A sample of the data is presented in Figure 4.1-1b for Configuration (4) which is the multi-tube suppressor with the hardwall ejector.

4.1.3 Exit Profiles

Temperature and velocity profiles were obtained in the plane of the ejector exit. All configurations (with or without an ejector) were traversed along a radial line in the same plane. The suppressor nozzles were oriented circumferentially such that the probe was midway between extreme points of the suppressor geometry. When an ejector was used, it was oriented circumferentially such that the traverse probe was midway between the support struts. The probe readings therefore reflect an average of the circumferential distribution.

The probe simultaneously measured a static pressure (P_s), a total pressure (P_t) and a total temperature (T_t) at a given radial position (R). The velocity (V) was then calculated by the following equation:

$$V = \sqrt{\left(\frac{\gamma g_c \mathcal{R} T_t M^2}{1 + \frac{\gamma - 1}{2} M^2} \right)} \qquad \text{(m/sec, ft/sec)}$$

where:

$$M = \sqrt{\frac{2}{\gamma - 1} \left((P_t / P_s)^{\frac{\gamma - 1}{\gamma}} - 1 \right)}$$

All of the resultant traverse data is included in Section B, Volume II of the CDR. A sample of the data is illustrated in Figure 4.1-1c. It is presented at each radial position (R), non-dimensionalized to the exit radius of the ejector (R_{exit}).

a) Thrust coefficients and Flow Coefficients

CONFIG NO.	TEST PT.	PTP/PA	TTP (DEGF)	VP (FPS)	PTF/PA	TTF(DEGF)	VF(FPS)	CV	CDP	CDF
3.0	205.03	2.00	952.	1755.	1.78	1463.	1889.	0.939	0.988	0.923
3.0	206.01	2.48	999.	2015.	3.21	824.	2103.	0.958	0.985	0.941
3.0	206.02	2.51	987.	2018.	1.80	813.	1543.	0.944	0.999	0.921
3.0	206.03	2.49	990.	2013.	1.29	807.	1031.	0.938	1.000	0.906
3.0	207.01	2.49	995.	2016.	4.08	1509.	2841.	0.949	0.995	0.951
3.0	207.02	2.53	984.	2021.	2.55	1501.	2374.	0.948	0.986	0.918
3.0	207.03	2.50	984.	2011.	1.79	1491.	1904.	0.953	0.997	0.908

b) Surface Static Pressures

CONFIG. (4) MULTI-TUBE W/HARD EJECTOR — TEST POINT NO. = 60.010

TAP	1	2	3	4	5	6	7	8	9	10	11	12	13
X/L	.028	.093	.157	.222	.308	.416	.545	.674	.803	.932	.028	.093	.157
P/PA	0.826	0.826	0.864	0.854	0.888	0.957	0.990	0.993	0.994	0.990	0.810	0.830	0.870
TAP	14	15	16	17	18	19	20	21	22	23	24	25	26
X/L	.222	.308	.416	.545	.674	.803	.932	.050	.026	-.004	- .034	-.107	-.273
P/PA	0.850	0.881	0.950	0.991	1.000	0.999	1.000	0.783	0.866	0.841	0.931	0.991	0.998

c) Exit Profiles

CONFIGURATION (3) MULTI-TUBE — TEST POINT NO. = 55.010

R/REXIT	0.0	0.139	0.278	0.417	0.556	0.694	0.833	0.972	1.111	1.250
TTEXIT	931.	930.	939.	917.	890.	753.	569.	402.	270.	190.
VEXIT	909.	953.	974.	957.	1017.	990.	729.	413.	188.	73.

Figure 4.1-1 Sample of the Aerodynamic Data Contained in the Comprehensive Data Report NASA CR134910

4.2 ACOUSTIC DATA REDUCTION

The measured acoustic signals recorded by the nine microphone array at 4.6m (15 ft) radius were corrected, analyzed and converted to full size engine data (10X model size) by the procedure illustrated in Figure 4.2-1. This figure also indicates the data outputs available for both the 0.127m (5 in) equivalent diameter model size and the 1.27m (50 in.) full size scaled engine data. All of the data is available in the companion Comprehensive Data Report, NASA CR-134910 (Ref. 8).

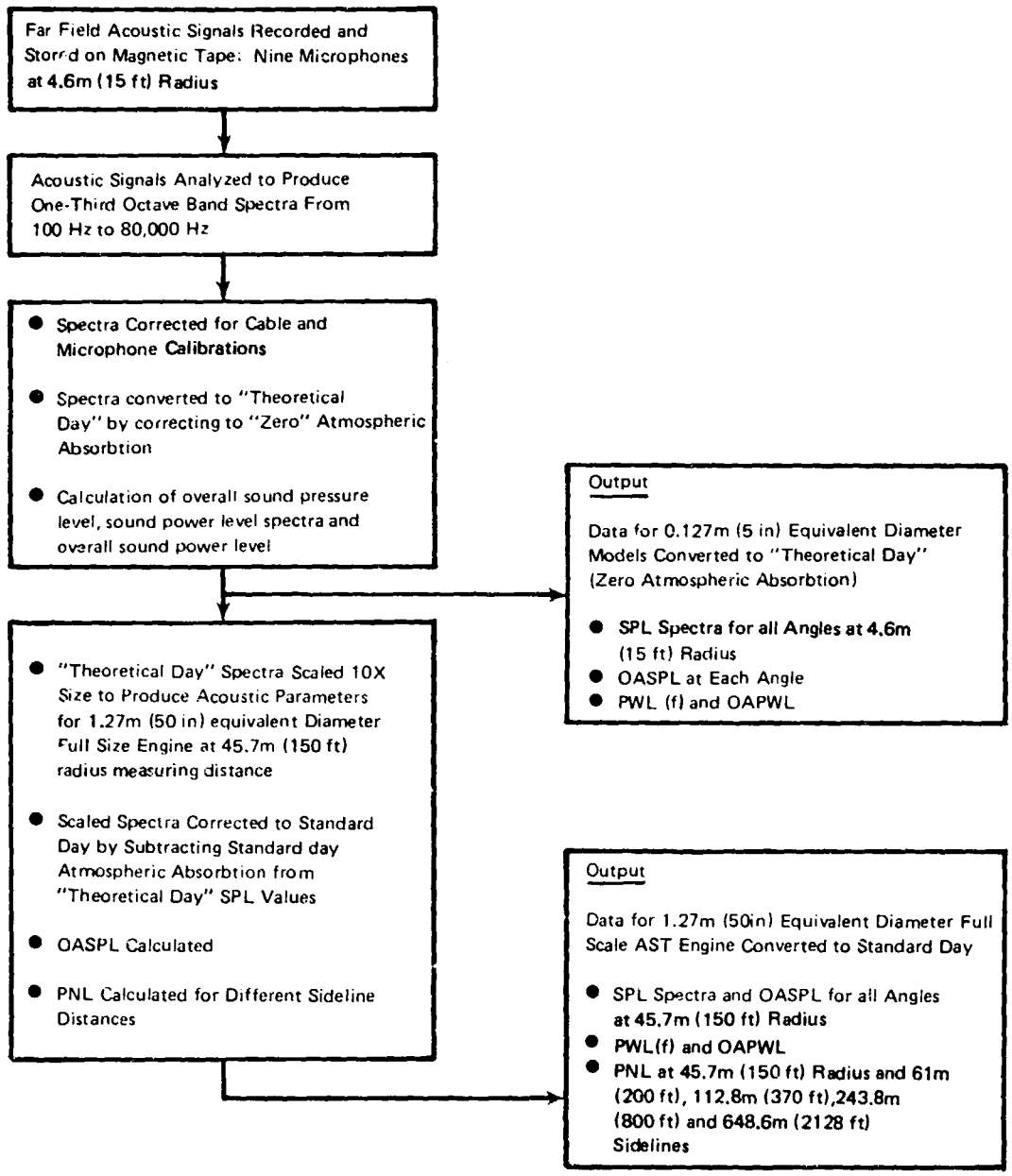

Figure 4.2-1 Acoustic Data Reduction Procedure

The tape recorded far field signals from the nine microphones were reduced to one-third octave band sound pressure levels by analog/digital analysis equipment. This analysis was performed on a General Radio No. 1921 Analyzer.

The one-third octave band as-measured model size sound pressure levels, analyzed in the GR 1921 Spectrum Analyzer from 100 Hz to 80,000 Hz, were corrected for calibrated cable and microphone response. The data were then transformed into "theoretical day" data by applying the values of atmospheric absorption defined in reference 9. This procedure entails adding a ΔSPL as a function of frequency, relative humidity, and ambient temperature to the measured SPL levels. The ΔSPL corrections represent an estimate of the absolute sound absorption for noise in each of the one-third octave bands. The resulting "theoretical day" data represents the noise that would be measured at the microphone if no noise were lost through atmospheric absorption. Typical values of atmospheric absorption calculated by the method of reference 9 for the 15 ft measuring distance used in this program are illustrated in Table 4-II.

TABLE 4-II
ATMOSPHERIC ABSORBTION ESTIMATES
FOR A TYPICAL DATA POINT

4.57m (15 ft) Radius
Temperature –307°K (93°F)
Relative Humidity –49%

Freq (KHz)	Δ SPL	Freq (KHz)	Δ SPL	Freq (KHz)	Δ SPL
0.050	0.0	0.80	0.0	12.5	0.5
0.063	0.0	1.00	0.0	16.0	0.6
0.080	0.0	1.25	0.0	20.0	0.9
0.100	0.0	1.60	0.1	25.0	1.4
0.125	0.0	2.00	0.1	31.5	1.9
0.160	0.0	2.50	0.1	40.0	2.8
0.200	0.0	3.15	0.1	50.0	4.4
0.250	0.0	4.00	0.1	63.0	6.4
0.315	0.0	5.00	0.2	80.0	9.6
0.400	0.0	6.30	0.2	100.0	14.4
0.500	0.0	8.00	0.3		
0.630	0.0	10.00	0.3		

The corrections at the very high frequencies, i.e., above 40K Hz, become quite large. At 80K Hz, the correction of 9.6 dB represents a loss of nearly 90% of the noise that would have radiated to the microphone if no atmospheric absorption were present. The formulae used in Reference 9 have been verified as accurate only for sound frequencies below 10,000 Hz. However, since a more accurate method of estimating atmospheric absorption is not presently available, the formulae of Reference 9 were used directly to calculate the values of

atmospheric absorption for frequencies up to 80,000 Hz required for the scale model data. The "theoretical day" SPL's were integrated over the measured frequency range to obtain overall sound pressure levels (OASPL).

The theoretical day model scale data from all test points are compiled on computer output sheets in the Comprehensive Data Report (Ref. 8). Table 4-III is a sample data page. At the top of the page are listed the pertinent ambient and nozzle operating parameters in both U.S. customary units as well as the International System of Units (S.I.).

The left hand column lists the ambient temperature (TEMP), pressure (PRES), and relative humidity (REL H). Wind direction (WIND D) and wind velocity (WIND V) were also monitored but not included in the data sheets. A tabulation of wind velocities is included in the Comprehensive Data Report.

The center columns list the full scale primary and fan stream exhaust nozzle areas (AREA) as equal to zero to indicate that the noise data are in model scale form. In the same columns are found the stream total to ambient pressure ratio (P.R.), stream temperature (TEMP), and stream density (RHO), and the ideally expanded velocity (VEL).

The right hand columns list the full scale mass flow (MASS FLOW) as equal to zero to indicate that the noise data are in scale model form. Also listed in this column are the model size ideal thrusts (THRUST, IDL), exhaust nozzle areas (AREA MOD), and mass flows (W MODEL).

Below the parameter listing are the tabulated, model scale one-third octave band sound pressure levels at a 4.57 m (15 ft.) polar distance under free field measurement conditions during a "theoretical day." The center frequencies of the 30 measured one-third octave bands from 100 Hz to 80 K Hz are listed in the left hand column. The one-third octave band sound pressure levels for each microphone measuring angle, 60°, 75°, 90°, 105°, 120°, 130°, 140°. 150°, and 165°, at each one-third octave band are listed in the appropriate columns.

The one-third octave band power levels (referenced to 10^{-12} watts) are listed at the extreme right hand side of the page.

Below the one-third octave band sound pressure and sound power levels are listed the 4.57 m (15 ft.) radius overall sound pressure level (OSPL) for each angle and the overall sound power level (OAPWL).

The theoretical day noise data were also scaled to represent a full size SCAR engine having linear dimensions corresponding to a 1.27 m (50 in.) equivalent nozzle diameter (ten times the model size). Thus, the measured SPL levels were increased by 20 log 10 or 20 dB and measured frequencies were reduced by a factor of 10 to produce full scale engine noise characteristics.

The full scale SPL levels were extrapolated to 45.7 m radius for a standard FAA day by applying the spherical divergence law, Δ dB = 20 log r_2/r_1 and the atmospheric attenuation corrections of SAE ARP 866. Overall sound pressure levels (OASPL) were determined by integrating the SPL values from 50 Hz to 8000 Hz.

TABLE 4-III
SAMPLE OF ACOUSTIC DATA
(Model Size; Theoretical Day)

STAND X033 RIG ID 4 TEST DATE 07/11/74 SCALE RATIO 10.0/1 RUN NUMBER 60.01

					PRIMARY	FAN		PRIMARY	FAN			PRIMARY	FAN		PRIMARY	FAN
TEMP	93.0(F)	33.9(C)	AREA	SQFT	0.0	0.0	SQM	0.0	0.0	MASS FLOW	LB/S	0.0	0.0	KG/S	0.0	0.0
PRES	25.001N	0.858AR	P.R.		1.54	2.50		1.54	2.50	THRUST,IDL	LB	159.4	282.9	N	709.1	1258.3
WIND	D		TEMP	(R)	753.2	1971.0	(K)	418.4	1095.0	THRUST,MEA	LB		0.0	N		0.0
WIND	V 0KPH	0.0M/S	RHO	LB/FT3	0.060	0.025	KG/M3	0.959	0.405	AREA (MOD)	SQFT	0.08	0.06	SQM	0.007	0.005
REL	H 49.0%		VEL	FPS	1026.0	2358.0	M/S	312.7	718.7	W (MODEL)	LB/S	5.0	3.9	KG/S	2.3	1.8

1/3 OCTAVE BAND MODEL JET NOISE DATA 15.0FT RADIUS THEORETICAL DAY SPL - (MODEL)

BAND CENTER FREQ (KHZ)	MICROPHONE ANGLES IN DEGREES 60	75	90	105	120	130	140	150	165	POWER 1E-12W
.050	0.0	0.0	0.0	0.0	0.0	0.0	0.0	0.0	0.0	22.6
.063	0.0	0.0	0.0	0.0	0.0	0.0	0.0	0.0	0.0	22.6
.080	0.0	0.0	0.0	0.0	0.0	0.0	0.0	0.0	0.0	22.6
.100	80.8	79.8	81.4	82.9	85.3	87.1	91.3	95.4	101.4	112.3
.125	81.3	84.0	82.7	84.6	87.3	89.7	94.1	98.3	104.0	114.9
.160	79.8	83.5	84.9	86.9	89.5	91.7	95.7	100.3	106.1	116.9
.200	84.7	85.4	86.7	88.5	92.2	94.5	98.5	103.3	108.8	119.7
.250	83.7	86.3	87.3	90.4	92.8	96.3	100.5	105.1	109.5	121.0
.315	87.8	86.9	90.0	93.0	94.8	97.3	102.6	106.7	110.0	122.3
.400	88.0	87.0	91.3	92.3	96.0	99.1	102.6	106.4	108.2	121.9
.500	89.4	88.5	91.9	94.2	97.7	100.0	103.8	106.5	105.9	122.1
.630	90.6	92.0	92.7	95.0	98.3	100.4	104.3	106.5	104.0	122.3
.800	91.5	91.3	93.8	96.1	99.8	102.3	104.8	106.0	101.8	122.6
1.00	91.1	90.4	94.8	96.5	99.8	101.5	104.3	104.7	99.3	122.0
1.25	92.4	94.4	95.5	97.5	100.7	102.4	104.4	103.9	97.9	122.4
1.60	92.3	91.7	94.9	96.2	101.3	102.6	103.6	102.8	96.3	122.0
2.00	92.8	92.6	95.4	96.0	101.7	102.6	103.1	101.9	95.1	121.9
2.50	93.1	92.8	95.5	98.4	101.8	101.8	101.8	100.6	93.7	121.5
3.15	93.5	92.8	95.8	98.7	103.1	101.4	101.3	99.6	92.8	121.8
4.00	94.2	93.4	96.9	99.9	104.3	101.1	100.5	98.5	91.7	122.3
5.00	95.0	94.6	97.8	101.3	105.8	101.6	100.1	97.6	90.7	123.3
6.30	95.7	95.7	99.1	102.8	107.5	102.6	99.8	97.1	90.3	124.6
8.00	96.3	96.7	100.6	104.6	108.9	103.5	100.3	96.6	89.7	125.9
10.0	95.6	97.7	101.9	106.8	109.5	104.6	101.6	96.9	89.6	127.2
12.5	97.4	97.3	102.7	107.7	109.2	104.7	101.1	96.3	89.5	127.4
16.0	97.2	100.5	103.0	107.9	108.6	104.5	100.6	95.7	89.6	127.4
20.0	95.9	103.1	102.3	107.9	107.2	103.4	99.4	95.5	88.8	127.0
25.0	95.3	101.5	102.6	109.2	107.2	104.4	100.7	96.0	89.6	127.5
31.5	94.3	101.8	101.4	107.4	105.2	103.2	99.4	95.2	88.5	126.1
40.0	93.9	102.6	101.2	106.4	105.1	103.4	99.3	95.6	89.6	125.8
50.0	92.4	102.7	101.2	105.4	103.8	103.4	100.0	96.6	90.7	125.1
63.0	89.7	103.2	100.1	104.0	103.8	103.5	100.5	98.2	92.3	124.8
80.0	88.1	105.9	99.4	104.4	104.6	104.9	101.3	100.8	91.9	126.0
100.	14.4	14.4	14.4	14.4	14.4	14.4	14.4	14.4	14.4	37.1
										DAPWL = 138.8
OSPL	107.9	113.0	113.2	118.0	119.1	116.8	116.3	116.8	117.3	

Perceived noise levels (PNdB) were computed according to SAE ARP 865 from the SPL spectra and extrapolated to various sideline distances at zero altitude.

Sound power level spectra and overall power level were determined individually for the model data and data scaled to full size by spatial integration over the nine microphone positions from the listed SPL and OASPL values assuming symmetry about the jet axis of the noise generation. Since the theoretical day model scale data represents the noise that would be measured if no atmospheric absorption were present, the power levels represent noise generation at the source. The full scale data, however, represents noise that would be measured on a standard FAA day. Thus the full scale power levels represent an integration of the far field noise levels on a standard FAA day, reflecting the common method for comparing full scale data. The actual power level calculations employed were:

$$PWL = 10 \log \left(\frac{W}{W_{ref}} \right) = \text{sound power level, in decibels}$$

where: $W = \sum_{i=1}^{n} \frac{P_i^2}{\rho_o C} \Delta A_i$ = the acoustic power, in watts

$W_{ref} = 10^{-12}$ watts = the reference power level

$P_i^2 = 10^{\left(\frac{SPL}{10}\right)} P_{ref}^2$ = mean square sound pressure

$P_{ref} = 20 \times 10^{-6}$ N/M^2 = reference acoustic pressure

ρ_o = atmospheric density

C = atmospheric speed of sound

n = number of microphones

ΔA_i = surface area of spherical segment associated with i^{th} microphone

- for the first microphone

$$\Delta A_1 = 2\pi r^2 \left[\cos \theta_1 - \cos \left(\frac{\theta_1 + \theta_2}{2} \right) \right]$$

- for intermediate microphones

$$\Delta A_i = 2\pi r^2 \left[\cos \left(\frac{\theta_{i-1} + \theta_i}{2} \right) - \cos \left(\frac{\theta_i + \theta_{i+1}}{2} \right) \right]$$

- for the last microphone

$$\Delta A_n = 2\pi r^2 \left[\cos\left(\frac{\theta_{n-1} + \theta_n}{2}\right) - \cos\theta_n\right]$$

where: r = distance of microphone from nozzle

As the characteristics of the test facility insure far field acoustic signals free from ground reflections, all acoustic values calculated from the measured data are also far field. The extrapolated values do not include extra ground attenuation. The acoustic data from all test points is compiled on computer output sheets in the Comprehensive Data Report (Ref. 8). Table 4-IV is a sample data page. At the top of the page are listed the pertinent ambient and nozzle operating parameters in U.S. customary units as well as the International System of Units (S.I.).

The left hand column lists the ambient temperature (TEMP), pressure (PRES), and relative humidity (REL H). Wind direction (WIND D) and wind velocity (WIND V) were also monitored but not included in the data sheets. A tabulation of wind velocities is included in the Comprehensive Data Report.

The center columns list the full scale primary and fan stream exhaust nozzle areas (AREA) as well as stream total to ambient pressure ratio, (P.R.), stream temperature (TEMP), and stream density (RHO). The ideally expanded velocity (VEL) is also presented.

The right hand columns list the full scale mass flow (MASS FLOW) and the full scale ideal thrusts (THRUST, IDL), model size exhaust nozzle areas (AREA MOD), and mass flow (W MODEL) of the scale models used in the test.

Below the parameter listing are the tabulated, full scale one-third octave band sound pressure levels at a 45.7 m (150 ft.) polar distance under free field measurement conditions during a standard FAA day. The center frequencies of the 24 measured one-third octave bands from 50 Hz to 8000 Hz are listed in the left hand column. The one-third octave band sound pressure levels for each microphone measuring angle, 60°, 75°, 90°, 105°, 120°, 130°, 140°, 150°, and 165°, at each one-third octave band are listed in the appropriate columns.

The one-third octave band power levels (referenced to 10^{-12} watts) are listed at the extreme right hand side of the page.

Below the sound pressure level and sound power level spectra are listed the 45.7 m (150 ft.) radius overall sound pressure level (OSPL) for each angle and the overall sound power level (OAPWL). Perceived noise levels (PNL) are listed for each measuring angle at 45.7 m (150 ft.) radius, and at 60 m (200 ft.), 111m (370 ft.), 244 m (800 ft.), and 648.6 m (2128 ft.) sideline distances at the bottom of the data sheet.

TABLE 4-IV

SAMPLE OF ACOUSTIC DATA
(Scaled to a 1.27 m (50 in.) Equivalent Diameter Engine)

MULTI TUBE W/HOWLL EJECTOR .75 CONF 4 150.2049

STAND X033 RIG ID 4 TEST DATE 07/11/74 SCALE RATIO 10.0/1 RUN NUMBER 60.01

					PRIMARY	FAN		PRIMARY	FAN		PRIMARY	FAN		PRIMARY	FAN
TEMP	93.0(F)	33.9(C)	AREA	SQFT	7.78	5.83	SQM	0.723	0.542	MASS FLOW LB/S	500.3	386.3	KG/S	226.9	175.2
PRES	25.00 IN	0.85BAR	P.R.		1.54	2.50		1.54	2.50	THRUST,IDL LB	15941.2	28288.7	N	70909.8	125833.5
WIND D			TEMP	(R)	752.2	1971.0	(K)	418.4	1095.0	THRUST,MEA LB		0.0	N		0.0
WIND V	0 MPH	0.0M/S	RHO	LB/FT3	0.060	0.025	KG/M3	0.959	0.405	AREA (MOD) SQFT	0.09	0.06	SQM	0.007	0.005
REL H	49.0%		VEL	FPS	1026.0	2358.0	M/S	312.7	719.7	W (MODEL) LB/S	5.0	3.9	KG/S	2.3	1.8

EAA DAY 1/3 OCTAVE BAND ENGINE JET NOISE DATA 150.0FT RADIUS (SCALED ENGINE)

BAND CENTER FREQ (KHZ)	MICROPHONE ANGLES IN DEGREES 60	75	90	105	120	130	140	150	165	POWER 1E-12W
.050	89.4	88.5	91.9	94.2	97.7	100.0	103.8	106.5	105.9	142.1
.063	90.6	92.0	92.7	95.0	98.3	100.4	104.3	106.5	104.0	142.2
.080	91.5	91.3	93.8	96.1	99.8	102.3	104.8	106.0	101.8	142.6
.100	91.1	90.4	94.8	98.5	99.8	101.5	104.3	104.7	99.3	142.0
.125	92.4	94.4	95.5	97.5	100.7	102.4	104.4	103.9	97.9	142.4
.160	92.2	91.6	94.8	98.1	101.2	102.5	103.5	102.7	96.2	142.0
.200	92.7	92.5	95.3	97.9	101.6	102.5	103.0	101.8	95.0	141.9
.250	93.0	92.7	95.4	98.3	101.7	101.7	101.7	100.5	93.6	141.4
.315	93.4	92.7	95.7	98.6	103.0	101.3	101.2	99.5	92.7	141.7
.400	94.1	93.3	96.8	99.8	104.2	101.0	100.4	98.4	91.6	142.2
.500	94.8	94.4	97.6	101.1	105.6	101.4	99.9	97.4	90.5	143.1
.630	95.5	95.5	98.9	102.6	107.3	102.4	99.6	96.9	90.1	144.5
.800	96.0	96.4	100.3	104.3	108.6	103.2	100.0	96.3	89.4	145.7
1.00	96.4	97.5	101.7	106.6	109.3	104.4	101.4	96.7	89.4	146.9
1.25	97.0	96.9	102.3	107.3	108.8	104.3	100.7	95.9	89.1	147.0
1.60	96.8	100.1	102.6	107.5	108.7	104.1	100.2	95.3	89.2	147.0
2.00	95.4	102.6	101.8	107.4	106.7	102.9	98.9	95.0	88.3	146.5
2.50	95.6	100.8	101.9	108.5	106.5	103.7	100.0	95.3	88.9	146.9
3.15	93.5	101.0	100.6	106.6	104.4	102.4	98.6	94.4	87.7	145.2
4.00	92.8	101.5	100.1	105.3	104.0	102.3	98.2	94.5	88.5	144.6
5.00	91.1	101.4	99.9	104.1	102.5	102.1	98.7	95.3	89.4	143.8
6.30	88.0	101.5	98.4	102.3	102.1	101.8	98.8	96.5	90.6	143.1
8.00	85.8	103.6	97.1	102.1	102.3	102.6	99.0	98.5	99.6	143.7
10.0	11.3	11.3	11.3	11.3	11.3	11.3	11.3	11.3	11.3	54.0
									OAPWL =	157.9
OSPL	107.4	111.9	112.5	117.3	118.6	116.1	115.3	114.7	110.7	
PNL	119.1	124.9	125.1	130.3	130.2	127.9	125.3	122.3	116.3	
200. SIDELINE										
PNL	115.1	121.8	122.4	127.3	126.2	122.6	118.4	113.8	99.6	
370. SIDELINE										
PNL	108.9	115.4	116.3	121.2	120.0	116.4	112.0	106.2	92.0	
800. SIDELINE										
PNL	100.2	106.4	107.7	112.5	111.3	107.4	102.9	96.7	81.6	
2120. SIDELINE										
PNL	86.8	92.5	94.1	98.6	97.9	93.2	89.1	83.8	67.5	

4.3 ACOUSTIC DATA VALIDITY/REFERENCE CONVERGENT NOZZLE

In this section, the validity of the testing, measurement, recording, and data reduction techniques used during the program is established. This was accomplished by comparing the jet noise characteristics measured for the reference convergent nozzle with values predicted using two new prediction methods. One method, described in Reference 10, is based on the work of the SAE Subcommittee on Jet Noise and is intended to replace the original SAE Jet Noise Procedures of Reference 11. Predictions using this method have shown reasonable agreement with measured full scale engine data, especially at the angle of peak sideline noise which is normally located at 130 - 135°. The second method, described in Reference 5, is part of a new procedure developed by J. Stone at NASA Lewis Research Center. Neither prediction method has, as of yet, been accepted as a standard. Therefore, both methods were used to predict the levels of the jet noise of the convergent reference nozzle. A comparison of the measured OASPL data and the two prediction procedures is shown in Figure 4.3-1 for the 90° angle. The measured results agree well with the two prediction methods. A comparison of the OASPL directivities is shown in Figure 4.3-2. At the lower of the two jet velocities, the data and values predicted by both methods agree over all angles. At the higher jet velocity, the measured noise agrees well with the Stone method at all angles, while the SAE procedure underpredicts the levels at angles aft of 130°. Comparisons of the one-third octave band SPL spectra at 90°, 130°, and 150° are shown in Figure 4.3-3 for the two values of velocity. At the lower velocity (Figure 4.3-3a), the data agrees well with the SAE predictions at all angles. The agreement with the Stone method is almost as good at 90° and 130°. At 150°, the Stone method overpredicts the levels at the high frequencies, but agrees with the data in terms of peak SPL. At the higher jet velocity (Figure 4.3-3b), the data agrees well with both prediction methods at 90° and 130°. At 150°, the data agrees much better with the Stone method than with the SAE method. Similar results were obtained at other high velocity, high temperature conditions. The results of these tests indicate that the Stone method appears to predict the noise of high velocity, high temperature jets more accurately than does the SAE procedure. Based on these comparisons, the noise data for the reference convergent nozzle at subsonic operating conditions is considered valid.

The measured data for the reference convergent nozzle scaled to a nozzle diameter of 1.27 meter (i.e., 10 X model size) is shown in Figure 4.3-4 for all conditions tested. In this figure, the overall noise power level (PWL) is shown as a function of ideally expanded jet velocity, along lines of constant total temperature. Subsonic nozzle conditions ($P_t/P_a < 1.89$) are shown as open symbols, and supersonic nozzle conditions ($P_t/P_a > 1.89$) are shown as solid symbols. At the present time, no reliable method to predict supersonic jet noise is available so the noise levels are not compared with predicted values. However, the consistent data trend at both subsonic and supersonic conditions suggest that equally valid data were obtained for all operating conditions. Since the same testing and data reduction procedures were used for the entire program, all the data obtained are considered valid.

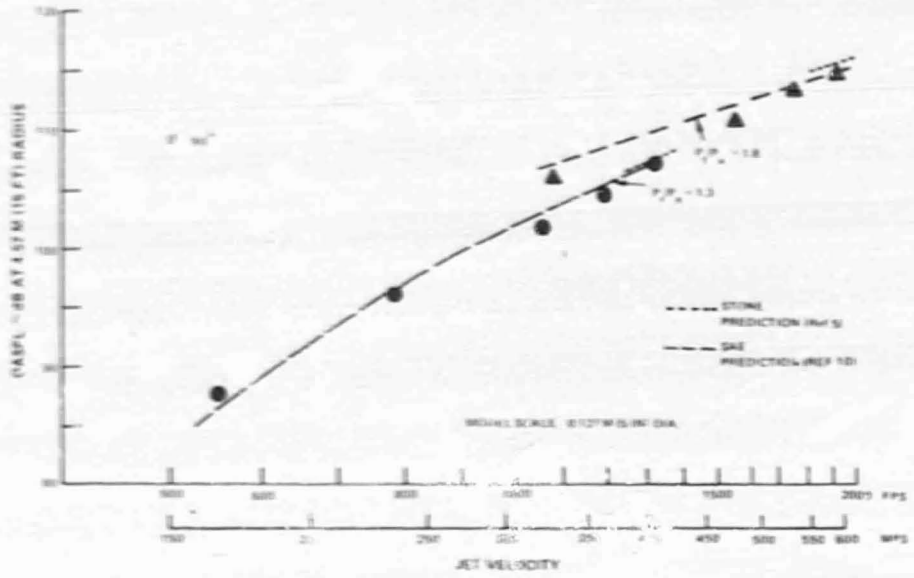

Figure 4.3-1 Convergent Nozzle Data Compared to Two Predictive Procedures

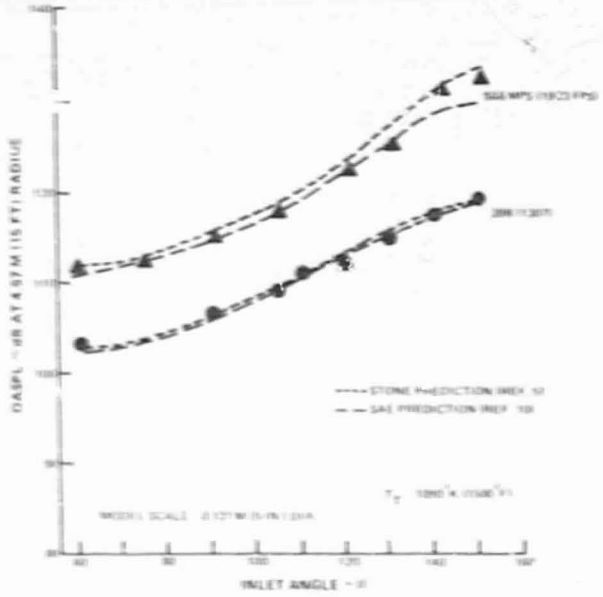

Figure 4.3-2 Convergent Nozzle Directivity Compared to Two Prediction Procedures

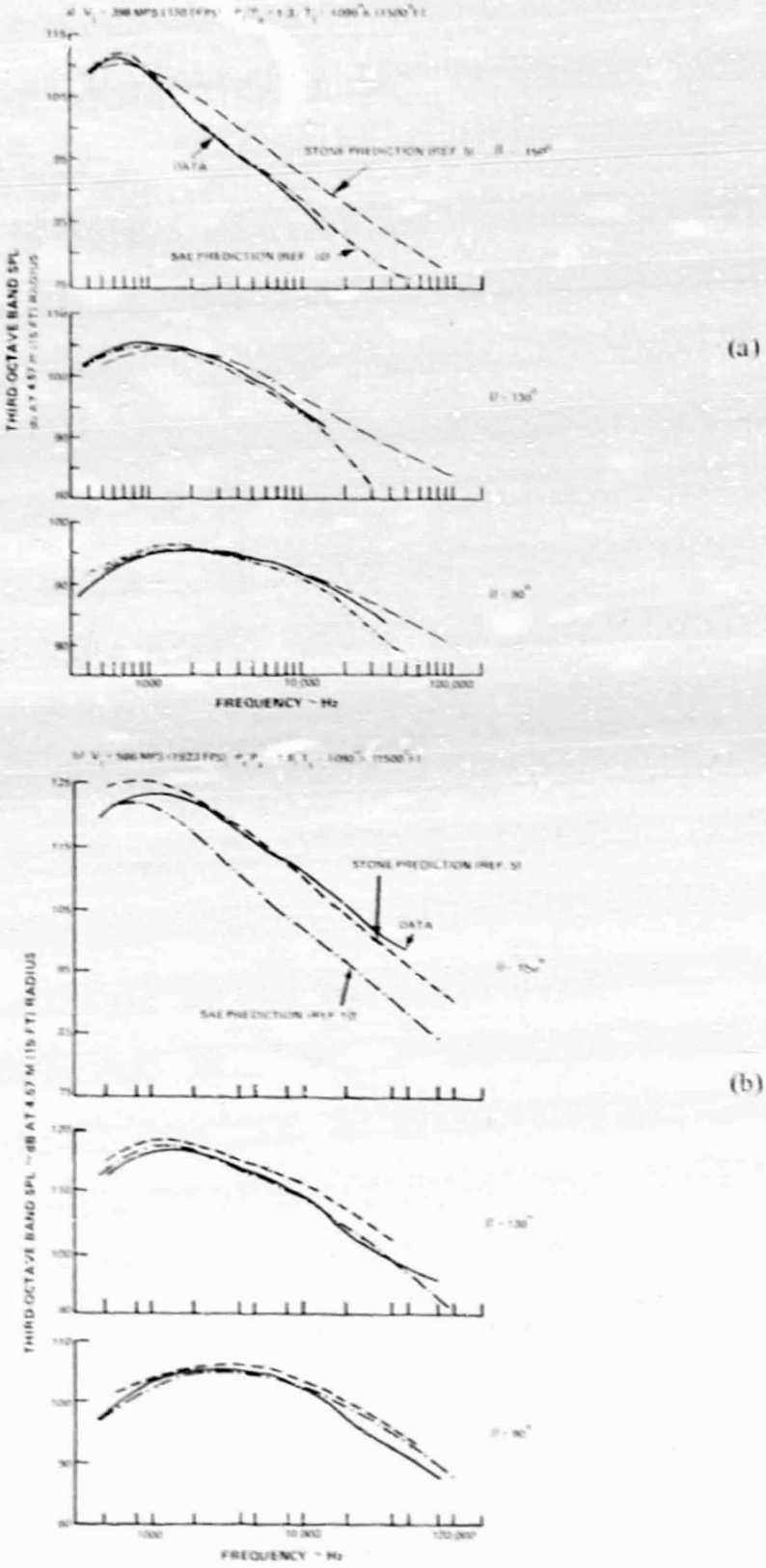

Figure 4.3-3 Convergent Nozzle Spectral Data Compared to Two Prediction Procedures. Data Presented In Model Size, 0.127m (5.0 in) Diameter

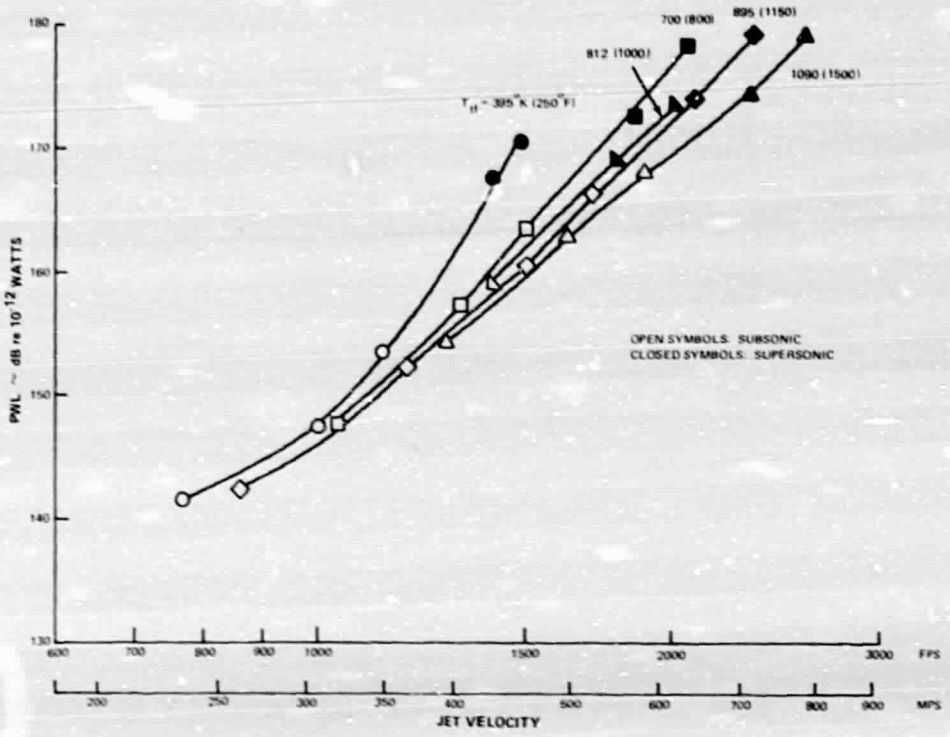

Figure 4.3-4 Convergent Nozzle Sound Power Level for all Data Points Scaled to 1.27m (50 in.) Diameter (10X Model Size)

4.4 COANNULAR NOISE SYNTHESIS

At the onset of the SCAR studies, no procedure was available that would provide accurate estimates of jet noise from turbofan exhausts having jet velocities in the fan stream higher than in the primary stream. Existing jet prediction methods are applicable only to single jets and conventional turbofan exhausts (i.e., $V_f < V_p$).

In order to support the SCAR cycle studies, a simple prediction procedure was developed to provide estimates of jet noise from turbofan exhausts having fan jet velocities higher than the primary stream. This procedure therefore provided a base to which the reference coannular nozzle noise data could be compared.

This procedure, based in part on the original SAE ARP 876 (Ref. 11) and NASA TMX 71618 (Ref. 5) predicts the sound power level from a coannular nozzle to be equal to the sum of the sound power levels from two independent, single jets whose areas are the same as the fan and primary nozzle areas, as shown in Figure 4.4-1. The operating conditions of the individual jets are taken to be equal to the fan and primary conditions of the coannular nozzle. To allow accurate prediction on this basis, the reference convergent nozzle was tested at all of the primary and fan conditions of the coannular nozzle test matrix. The convergent nozzle test data was scaled in level to the appropriate exhaust areas, and scaled for frequency to the equivalent circular diameters of the primary and fan nozzle areas, respectively. The scaled data was then added logarithmically as shown in Figure 4.4-1. Typical power level predictions based on this synthesized model are shown in Figure 4.4-2 for the 0.75 area ratio model.

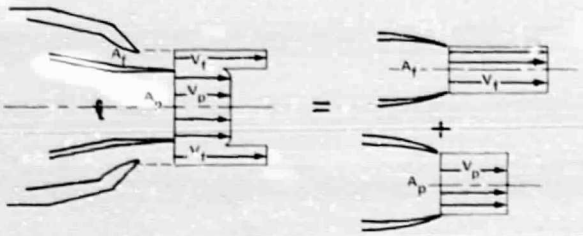

- SYNTHESIZED NOISE OF COANNULAR NOZZLE = SUM OF NOISE FROM INDEPENDENT CIRCULAR JETS AT PRIMARY AND FAN STREAM CONDITIONS
- $(\text{POWER LEVEL})_{SYN.} = 10 \log \left[\text{LOG}^{-1} \left(\frac{PWL}{10} \right)_p + \text{LOG}^{-1} \left(\frac{PWL}{10} \right)_f \right]$
- $\text{PERCEIVED NOISE LEVEL (PNL)} = 10 \log \left[\text{LOG}^{-1} \left(\frac{PNL}{10} \right)_p + \text{LOG}^{-1} \left(\frac{PNL}{10} \right)_f \right]$

Figure 4.4-1 Coannular Jet Noise Synthesis Procedure

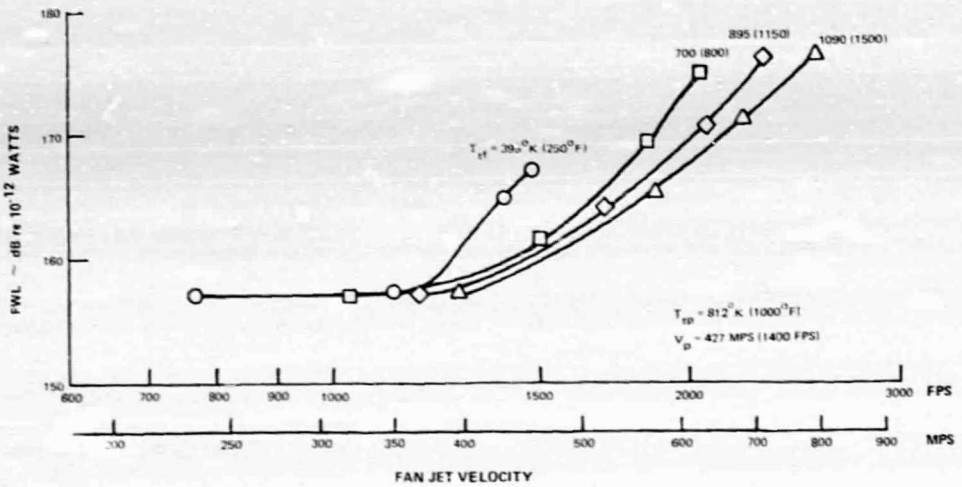

Figure 4.4-2 Synthesized Coannular Jet Noise Power Levels, 0.75 Area Ratio, Scaled to 1.27m (50 in.) Equivalent Diameter

The predicted values of perceived noise levels (PNL) were synthesized in a similar manner (see Fig. 4.4.1), i.e., the PNL's of the scaled convergent nozzle data were added logarithmically to obtain a synthesized PNL. The PNL values obtained in this manner are very close to the values that would be determined by summing the one-third octave band noise spectra of the convergent nozzle scaled to the fan and primary nozzle sizes and then computing PNL from the resulting summed spectra because the primary and fan streams were close in exit area and in equivalent circular diameter. Power level and perceived noise level predictions based on this synthesis procedure can be obtained for both the 0.75 and 1.2 area ratio coannular nozzles at any of the nozzle operating conditions by applying the method illustrated in Figure 4.4-1 to the convergent nozzle data contained in Appendix A.

5.0 RESULTS AND DISCUSSION

The acoustic and aerodynamic results obtained during the program are presented in this section, along with a discussion of the potential impact these results have on AST engine cycle studies. The results are generally presented over a partial range of conditions which illustrate the important characteristics and conclusions. The complete acoustic and aerodynamic data (model size and scaled 10X to engine size) are contained in the Comprehensive Data Report, NASA CR-134910.

5.1 ACOUSTIC RESULTS

The tests of the various suppressed and unsuppressed nozzle configurations produced a large amount of acoustic data which characterizes the noise emission of the models over a wide range of operating conditions. In the following sections, a description of the important noise features of the various configurations is presented. The noise characteristics of the models tested are presented in terms of peak perceived noise level, perceived noise level directivity, one-third octave band sound pressure and power spectra, and overall power level; as necessary to describe and document the noise of the various nozzle configurations both on an absolute basis and relative to each other and to the reference configurations. Appendix I contains a complete listing of acoustic power and perceived noise level directivity for all testing conditions. The following topics are discussed: unsuppressed coannular nozzles, fan stream suppressors, effect of ejectors and data correlations. All of the noise data are scaled to a 1.27 m equivalent nozzle diameter (10 times the model linear size) and extrapolated to 648.6 m sideline distance to typify an AST propulsion system at a sideline take-off condition.

5.1.1 Unsuppressed Coannular Nozzles

The measured acoustic data from the 0.75 and 1.2 area ratio unsuppressed coannular nozzles serve a dual purpose. First, it provides a base of new information characterizing the basic noise emission of a DBTF exhaust system. Secondly, it provides reference noise characteristics with which to compare the results obtained from the various fan stream suppressor configurations.

5.1.1.1 Measured Characteristics

Since the fan stream jet tends to control the total measured jet noise for most of the test range, ideally expanded fan jet velocity was selected as the main parameter for presentation of the acoustic data. The perceived noise level (PNL) at the angle of peak noise level is shown in Figure 5.1-1 as a function of ideally expanded fan jet velocity, for fixed values of fan stream total temperature, and fixed primary jet total temperature and velocity. This is typical of the data obtained at the various primary operating conditions, showing the influence of the fan jet velocity and temperature on the measured noise. The data are well behaved, as evidenced by the smooth shape of the curves fit through the data points. It should be noted that the curves tend to converge to a single curve as the fan jet velocity decreases to levels below that of the primary jet velocity. This behavior indicates that the controlling noise mechanism transfers from the fan jet to the primary jet. Figure 5.1-2 shows the effect of primary stream velocity on the peak PNL for three values of fan velocity.

At the lowest fan velocity, an increase in primary velocity causes a rapid increase in noise, indicating little influence of the fan stream on the noise. At the two higher fan velocities, the effect of increasing primary velocity is less significant, especially at primary velocities below 400 mps. A point of interest in this figure is that the noise at the highest fan velocity (853 mps) is affected by primary velocity in the range of 400 - 550 mps. Since the noise at $V_f = 314$ mps is completely dominated by the primary jet, it could be considered a floor level primary stream jet noise. As this primary stream noise is 10 dB or more below the noise levels at $V_f = 853$ mps for V_p below 550 mps, the primary jet noise would not be expected to cause changes in the noise at the high fan velocity if the streams generated noise independently as assumed in the synthesis. A conceptual model of noise generation for coannular jets having $V_f > V_p$ shows that this behavior is related to the unique mixing of the primary and fan jets associated with the inverted velocity profile jet exhaust. A detailed description of the conceptual model is presented in Section 5.1.1.2.

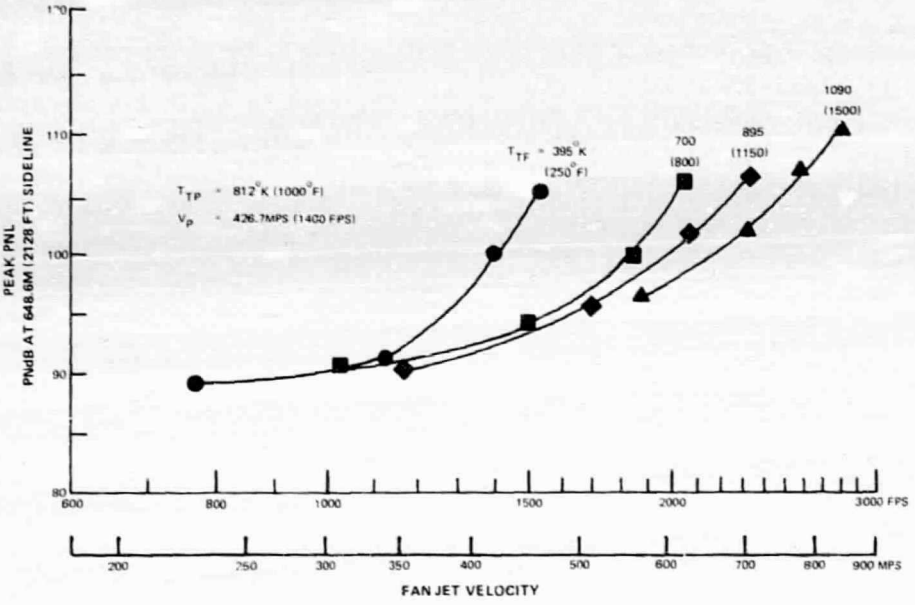

Figure 5.1-1 Effect of Fan Stream Velocity on Perceived Noise Levels – Coannular Unsuppressed Nozzle, 0.75 Area Ratio, Scaled to 1.27m (50 in.) Equivalent Diameter

The directivity characteristics of the data are illustrated in Figure 5.1-3, which shows PNL as a function of measuring angle for a series of fan jet velocities. The noise level varies continuously with angle at all velocities, and the directivity shapes are the same for all velocities at angles aft of 90°. The slight change in directivity shape at angles forward of 90° at the two higher velocities compared to the two lower velocities is due to the presence of shock noise at the supersonic pressure ratios ($P_t/P_a > 1.89$).

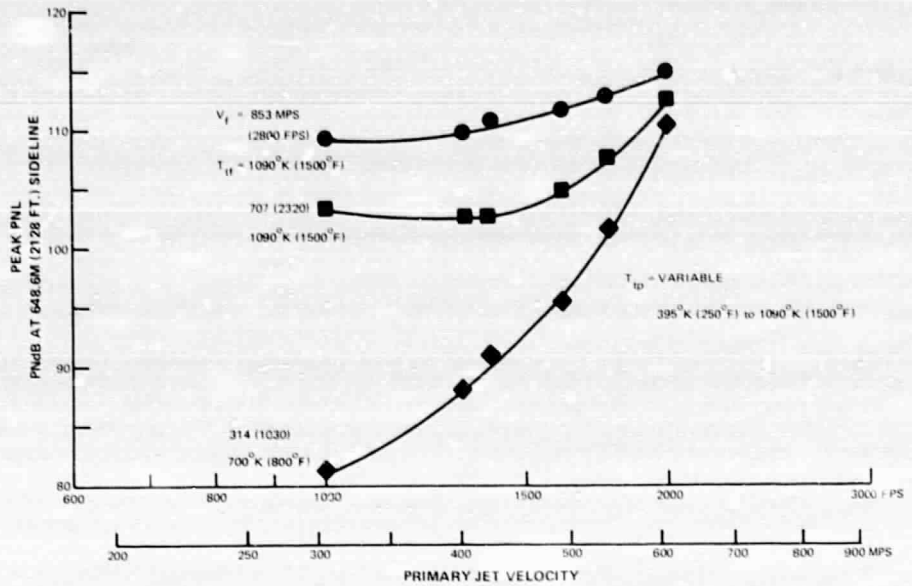

Figure 5.1-2 Effect of Primary Stream Velocity on Perceived Noise Levels – Coannular Unsuppressed Nozzle, 0.75 Area Ratio, Scaled to 1.27m (50 in.) Equivalent Diameter

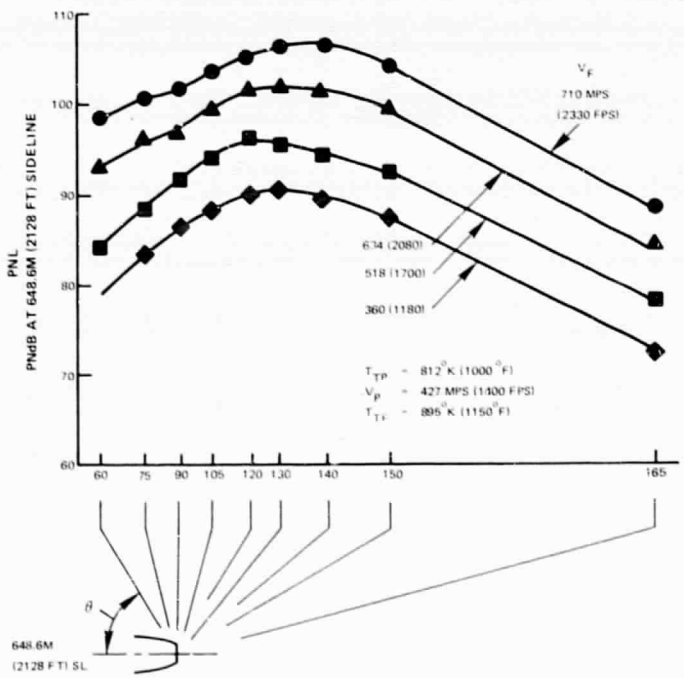

Figure 5.1-3 Directivity – Coannular Unsuppressed Nozzle, 0.75 Area Ratio, Scaled to 1.27m (50 in.) Equivalent Diameter

One-third octave band spectra at the 140° angle (the angle at which jet noise normally is a maximum) are shown in Figure 5.1-4 for six different combinations of primary and fan velocities. These spectra show some of the unique noise characteristics of coannular nozzles operating with velocity ratios (V_f/V_p) less than 1.0 and greater than 1.0. Curves A, B, and C show the effect of increasing primary velocity for a relatively low fan velocity. The spectra are similar to those generated by standard turbofan exhaust jets ($V_f < V_p$), and the noise level increases with increases in primary velocity. Curves D, E, and F show the effect of increasing primary velocity for a high fan velocity. First, comparing Curve D to Curve A (constant primary velocity), it is seen that the noise spectrum undergoes a radical change as the fan velocity increases. The spectrum in D is much higher in level, and more significantly, has a shape differing considerably from the spectrum in A. The "spike" in the spectrum is a shock screech tone possibly due to the underexpanded supersonic fan flow. Such tones are normally present in model tests at these conditions but not present in full scale engine noise spectra because of the physical non-uniformities that exist in full scale engines. By fairing a smooth curve through the spectrum to edit out the extraneous shock tone, the peak frequency of the broadband noise is seen to occur at 500-600 Hz. This peak frequency is characteristic of a jet with a smaller diameter than that of a circular nozzle having either the fan or primary nozzle area. This feature is true of all operating conditions where the fan jet velocity is much larger than the primary jet velocity. Its presence can be explained by the annular shape of the fan exhaust which produces a jet with a much smaller characteristic dimension than an equivalent circular jet (i.e., annular height rather than equivalent diameter). Further, this implies that the noise of the annular fan jet is dominated by the mixing process occurring in the nozzle flow field where the fan jet is still annular rather than after it mixes with the primary stream to form a single jet further downstream. As shown by comparing curves D and E, an increase in primary jet velocity caused an increase in the low frequency end of the spectrum with little change at the higher frequencies. This implies that the annular fan jet noise generation is relatively unchanged, but the contribution from the downstream jet resulting from mixing of the fan and primary jets is increased because of an increase in the mixed velocity.

At a still higher primary velocity (Curve F), the spectrum remained similar to a single jet at high velocity. The noise at high frequencies from the annular fan jet is no longer present as a specific peak since it has now merged with the primary flow to produce a spectrum characteristic of a single jet.

The spectral characteristics of the data, when the fan to primary area ratio is increased to 1.2, is shown in Figure 5.1-5. These spectra follow the same basic trends observed with the lower area ratio nozzle. A direct spectral comparison of the two area ratios is shown in Figure 5.1-6. This comparison shows two effects. First, the 1.2 area ratio produces slightly higher broad-band noise levels due to the larger fan area. Secondly, a shock screech tone present in the 0.75 area ratio model is not present in the larger area ratio spectra. This difference in shock tone behavior is typical of the intermittent nature of shock screech tones. It should again be noted that shock screech tones are not normally present in full scale engine noise spectra. The spectral characteristics of the noise from the unsuppressed coannular nozzle, for conditions where the fan jet is of much higher velocity than the primary jet, become extremely important for understanding large differences between measured and predicted jet noise levels for the duct burning turbofan (DBTF) type of nozzle.

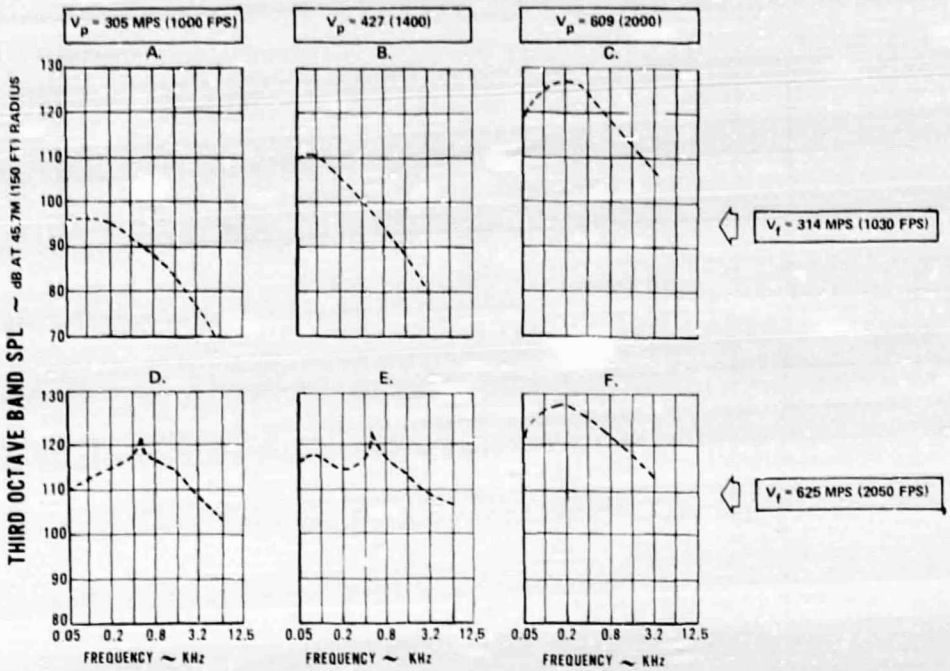

Figure 5.1-4 Effect of Primary and Fan Stream Velocities on SPL Spectra, at 140° From Inlet – Coannular Unsuppressed Nozzle, 0.75 Area Ratio, Scaled to 1.27m (50 in.) Equivalent Diameter

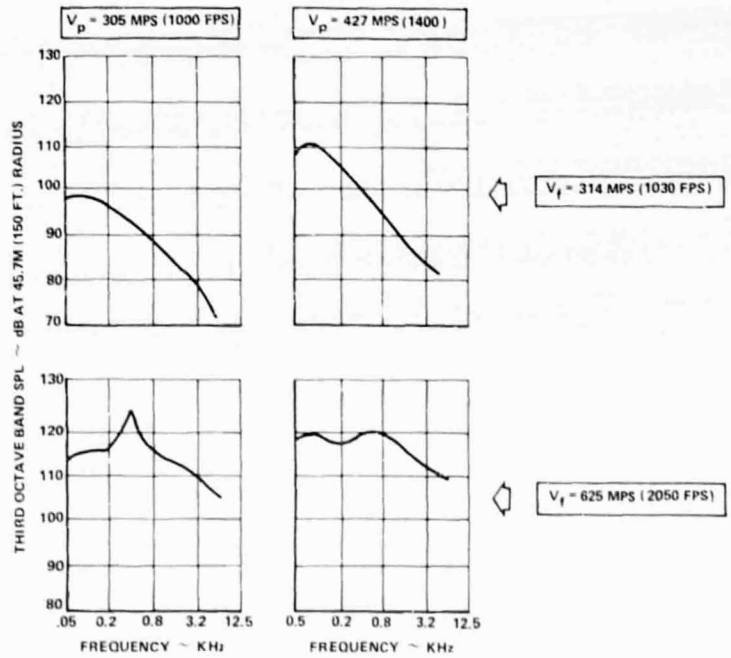

Figure 5.1-5 Effect of Primary and Fan Stream Velocities on SPL Spectra, at 140° From Inlet – Coannular Unsuppressed Nozzle, 1.2 Area Ratio, Scaled to 1.27m (50 in.) Equivalent Diameter

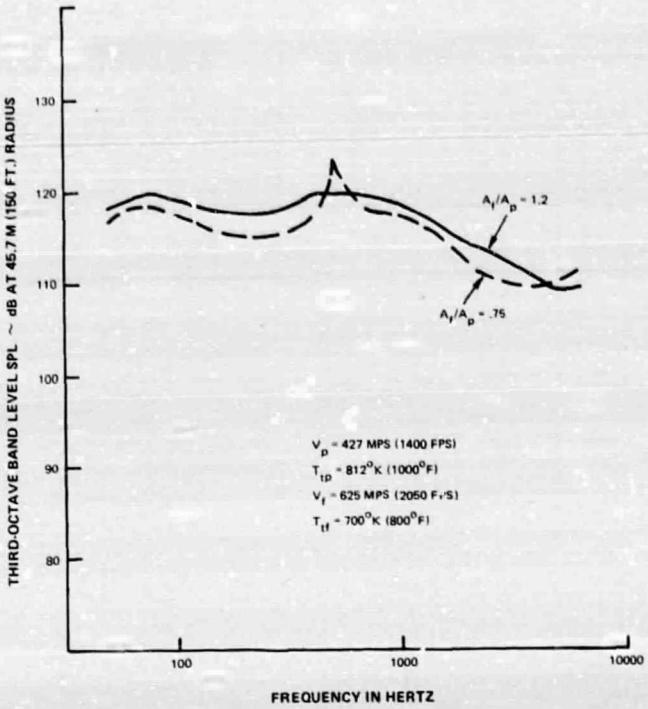

Figure 5.1-6 Spectral Comparison of Coannular Unsuppressed Nozzles, at 140° From Inlet, Scaled to 1.27m (50 in.) Equivalent Diameter

The unsuppressed coannular nozzle was also tested to investigate the possibility of temperature shielding on the jet noise of a DBTF exhaust. The temperature shielding concept employs a low velocity hot annulus of flow surrounding a higher velocity cooler central jet. To accomplish this, nozzle operating conditions were selected to produce a cold supersonic primary stream and a hot subsonic fan stream for a controlled experiment in which the fan jet noise would be substantially lower than the noise from the primary (or central) jet.

Results of the temperature shielding tests are presented in Figure 5.1-7a illustrating the OASPL directivity at a constant primary jet velocity (593 mps) and fan velocity (366 mps) for a range of fan temperatures (395°K to 1090°K). If a temperature-shielding effect were present, the noise at the aft angles should decrease with increasing fan temperature. However, the reverse is seen to be true. The hotter fan temperatures result in slightly higher noise levels than observed with cooler fan stream conditions over the range of surveyed angles. The spectral comparison presented in Figure 5.1-7b further illustrates this magnification effect. While the broadband portion of the spectra is essentially unchanged, indicating that a temperature shielding effect is not present, the shock tone from the primary jet is seen to vary considerably with fan temperature and is the basic cause of the OASPL increasing with temperature. These test results indicate that the temperature of the secondary stream has an important effect on the shock noise of the primary stream, but is ineffective in reducing the jet mixing noise generated by a central jet.

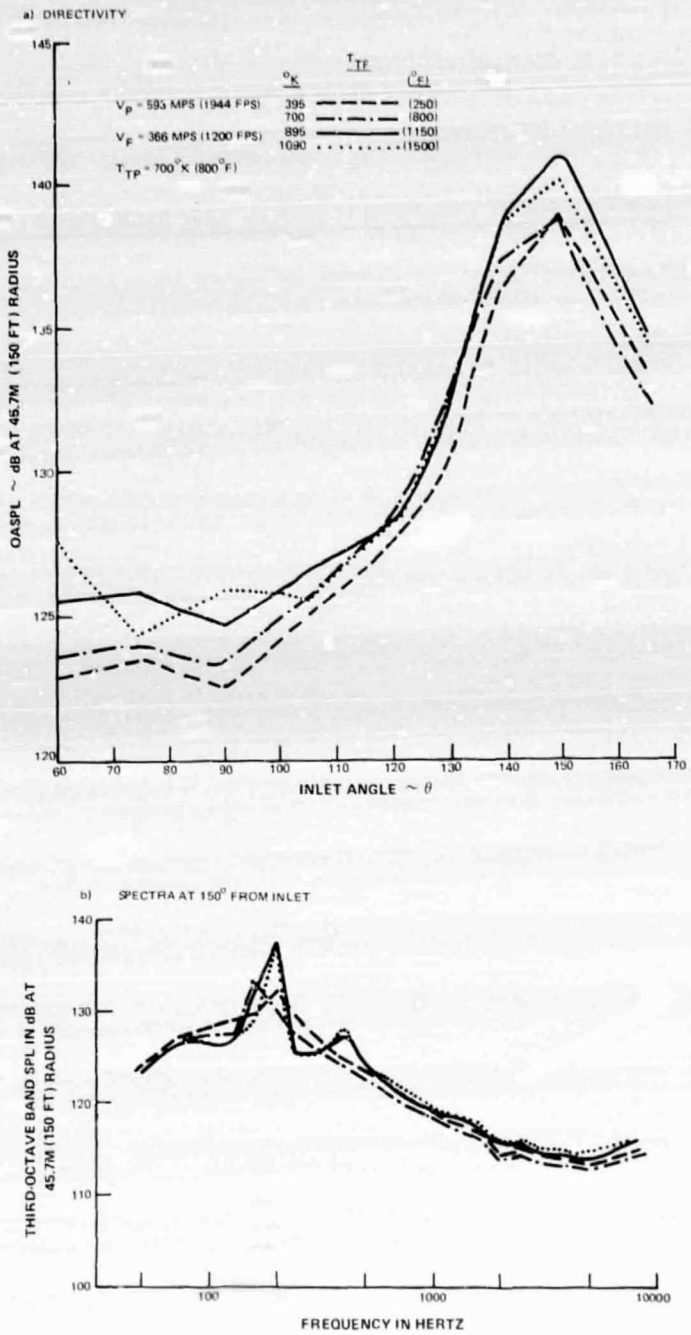

Figure 5.1-7 Effect of Fan Stream Temperature on Primary Stream Jet Noise (for Fan Velocity Lower Than Primary Velocity) – Coannular Unsuppressed Nozzle, 0.75 Area Ratio, Scaled to 1.27m (50 in.) Equivalent Diameter

5.1.1.2 Measured Versus Synthesis

In order to assess the effects of the interaction of the coannular flows on noise generation, the measured noise characteristics are compared to those obtained by the synthesis described in Section 4.4. A comparison of the measured and synthesized power levels for the 0.75 area ratio unsuppressed coannular nozzle is presented in Figure 5.1-8a. The differe.. between the measured and synthesized power levels is shown as a function of fan jet velocity and temperature. A most important feature of DBTF type unsuppressed coannular nozzle jet noise is illustrated in this plot; the measured levels are substantially lower (up to 8 dB) than the predictions based on the synthesized model. Suppression was observed to exist at all primary stream conditions with the level of suppression decreasing at the higher values of primary velocity. Appendix I contains the data necessary to compare measured and synthesized levels at other operating conditions. This suppression effect enhances the potential of the DBTF cycle for SST application, since actual noise levels are substantially lower than those based on earlier prediction methods.

A similar comparison of synthesized and measured power levels was made for the 1.2 area ratio unsuppressed coannular nozzle as illustrated in Figure 5.1.8b. Comparisons of measured and sythesized spectra produced results similar to the 0.75 area ratio case, although the larger area ratio nozzle produced slightly less suppression relative to the synthesis. In a later section of this report (5.1.4), the noise power level data from all operating conditions at which both the unsuppressed coannular nozzles were tested are seen to correlate well after applying normalizing factors related to fan stream temperature, fan to primary velocity ratio and exhaust nozzle area ratio.

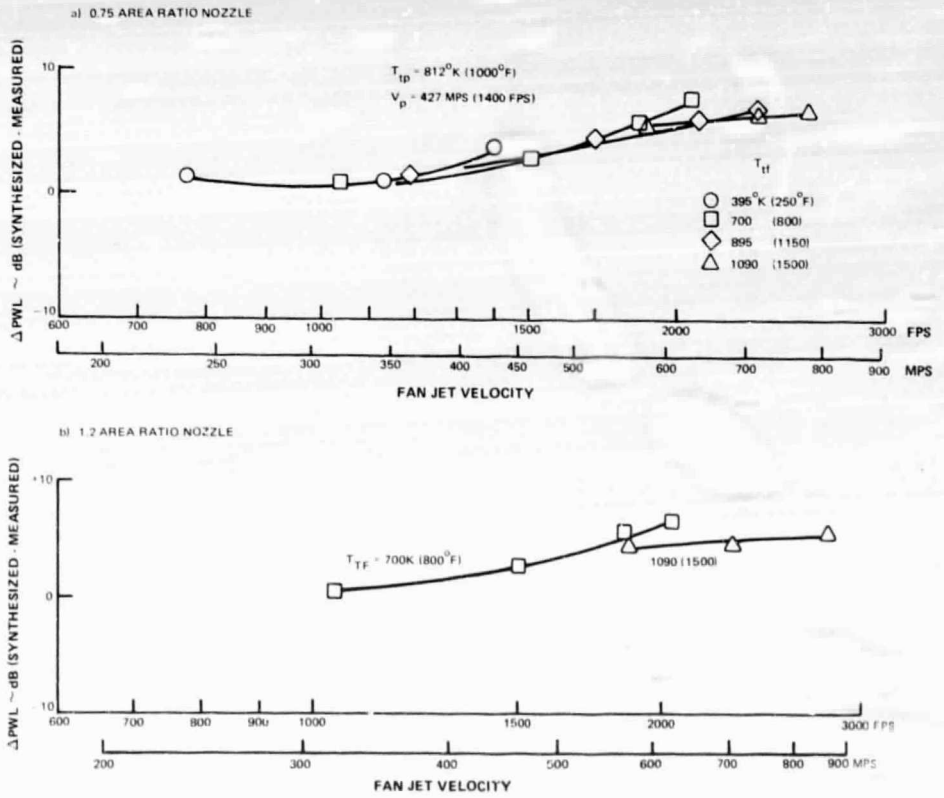

Figure 5.1-8 PWL Reduction of Coannular Unsuppressed Nozzles When Compared to Synthesized Values, Scaled to 1.27m (50 in.) Equivalent Diameter

Noise power level represents the total noise generated, but for evaluating its impact on aircraft mission studies, the perceived noise level (PNL) is the widely accepted unit. Therefore, the difference in measured and synthesized coannular noise levels for both area ratio nozzles is presented as a ΔPNL at the respective angles for peak noise on a 648.6m sideline in Figure 5.1-9. Although some change in curve shape is seen relative to the previous PWL comparisons (Figure 5.1-8), the major trends remain the same. Measured PNL reductions of up to 9 PNdB occur compared to the coannular synthesis. Similar comparisons for other operating conditions can be obtained from the data contained in Appendix I.

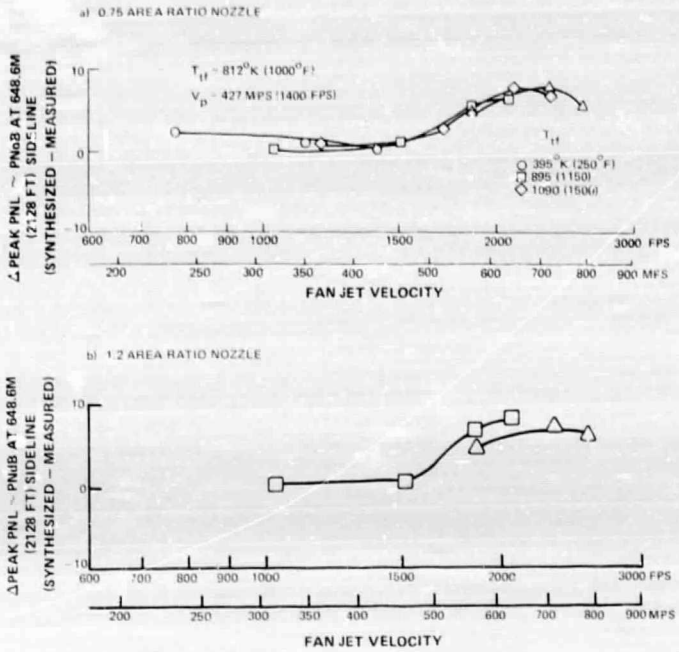

Figure 5.1-9 PNL Reduction of Coannular Unsuppressed Nozzles When Compared to Synthesized Values, Scaled to 1.27m (50 in.) Equivalent Diameter

The synthesized and measured PNL directivities are shown in Figure 5.1-10 for supersonic and subsonic fan jet velocities. In both cases, the actual measurements are less than the predicted value for all angles, although in the subsonic fan velocity case, the reductions are much larger in the aft angles. This observation is true for all cases tested. The data contained in the appendix can be used to construct the comparisons at any operating conditions tested. The reason for the different behavior at subsonic and supersonic fan stream conditions can be explained with the aide of the spectral comparisons of Figure 5.1-11. The subsonic case (V_f = 457 mps) shows large reductions in the measured low frequency noise of the coannular nozzle relative to the synthesis at 140°; while at 90° and 60°, the measured spectra show small reductions at low frequencies, with the higher frequencies at about the same level. Since the PNL's at 90° and 60° are controlled by the high frequencies, the resulting PNL differences are slight. However, at the supersonic fan velocities (V_f = 564 and 625 mps), the results are substantially different. At 90° and 60°, the measured low frequency noise is significantly lower than the synthesis. This result is due to a reduction in the shock noise which dominates

at the side and forward angles. At 140°, large reductions in low frequency noise similar to the subsonic case are present. Since at this angle, mixing noise dominates over shock noise, the agreement between the subsonic and supersonic cases is not unexpected. The spectral results shown here were repeated at the other operating points where $V_f > V_p$.

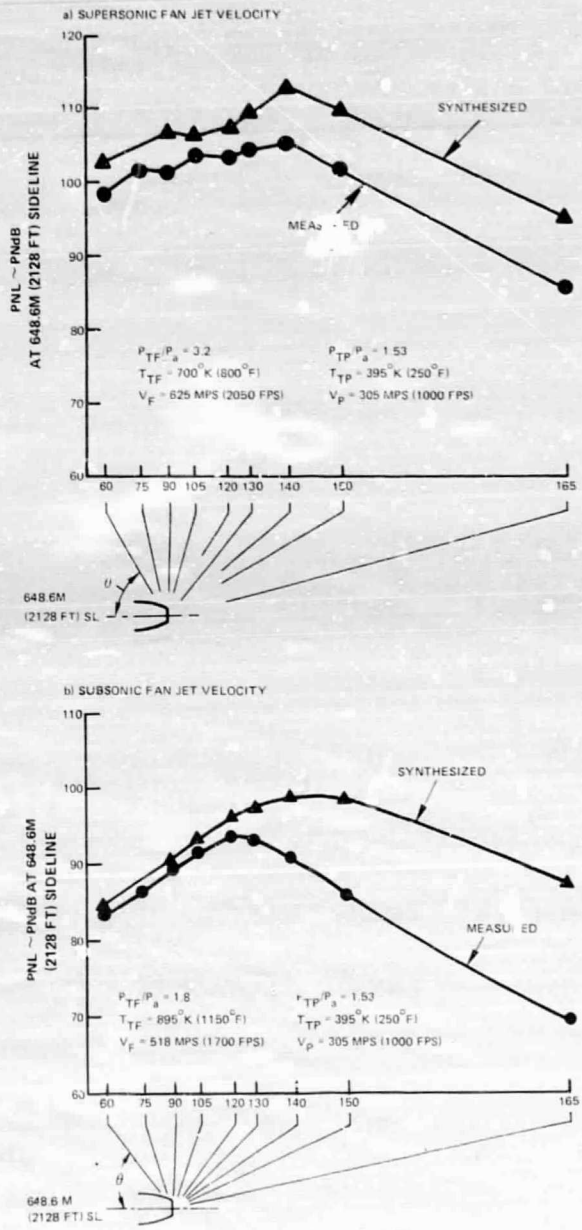

Figure 5.1-10 Comparison of Synthesized and Measured PNL Directivity For Coannular Unsuppressed Nozzle, 0.75 Area Nozzle, Scaled to 1.27m (50 in.) Equivalent Diameter

The spectra shown are scaled to a full size engine having linear dimensions 10 times the model size. The model data at frequencies below 500 Hz (below 50 Hz full-scale) is not presented in the spectral plots of Figure 5.1-11 since 50 Hz is the lowest frequency of interest in aircraft noise measurements. In order to compare the behavior of the spectra at very low frequencies, the measured model acoustic-power spectrum is compared to a synthesized model spectrum in Figure 5.1-12. From this comparison, it can be seen that the measured and synthesized spectra agree at the very low frequencies. Thus, it appears that the synthesis method provides a reasonable prediction of the coannular noise for $V_f/V_p > 1$ only at very low and very high frequencies, and significantly overestimates the noise in the middle frequency range.

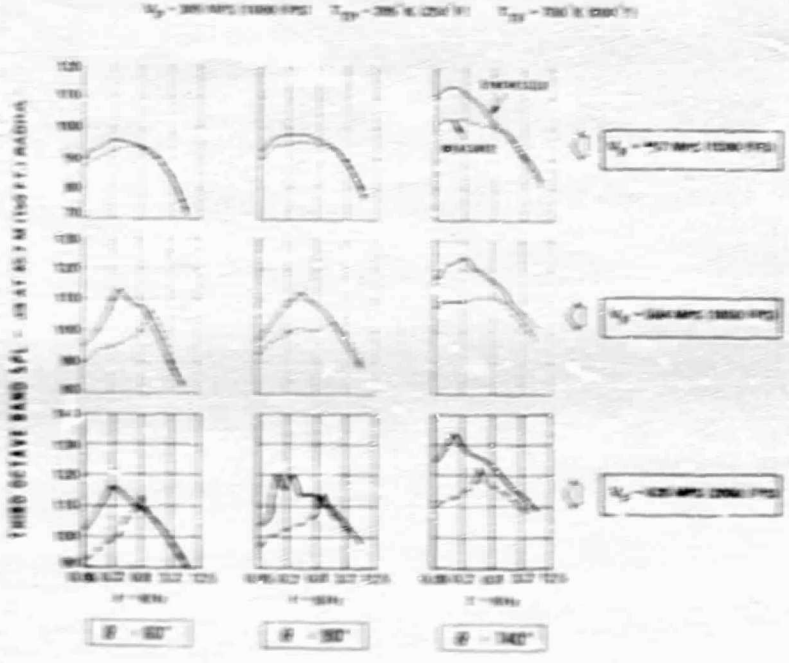

Figure 5.1-11 Comparison of Synthesized and Measured Spectra for Coannular Unsuppressed Nozzle, 0.75 Area Ratio, Scaled to 1.27m (50 in.) Equivalent Diameter

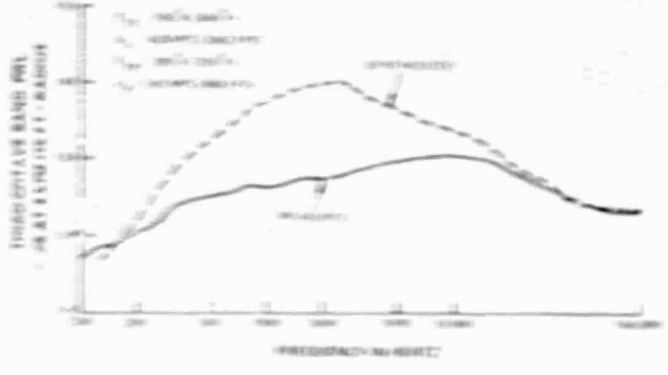

Figure 5.1-12 Comparison of Synthesized and Measured Spectra For Coannular Unsuppressed Nozzle Model, 0.75 Area Ratio

The measured coannular nozzle noise characteristics can also be related to the noise that would be generated if the fan and primary streams were fully mixed prior to leaving the engine. To make this comparison, values of fully mixed velocity and temperature were calculated from the conditions of the primary and fan stream. The noise power level for this ideally mixed jet was determined from the measured convergent nozzle data. Figure 5.1-13 illustrates the results of the PWL spectra comparison. As shown, the mixed jet is considerably noisier in the frequency range up to 500 Hz, and slightly quieter at the higher frequencies. The spectral shapes of the mixed and unmixed cases are quite different.

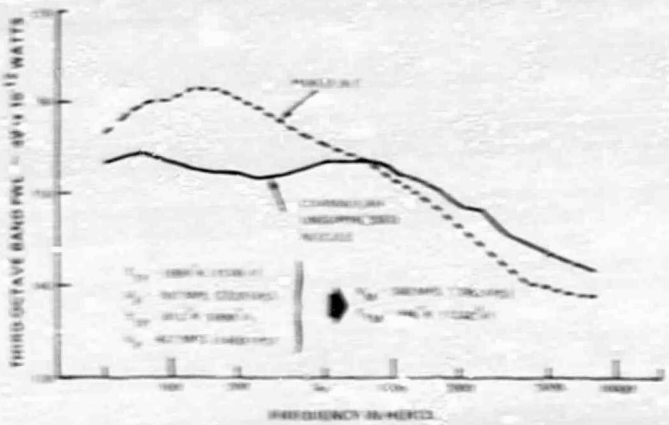

Figure 5.1-13 Comparison of Coannular Unsuppressed Nozzle (0.75 Area Ratio) Noise With Noise From Fully Mixed Jet, Scaled to 1.27m (50 in.) Equivalent Diameter

A comparison of peak perceived noise level (PNL) of the measured coannular nozzle and fully mixed jet is shown in Figure 5-1-14. At a high fan stream temperature (Figure 5.1-14a), the unsuppressed coannular nozzle is significantly quieter than the mixed jet at all fan velocities. At this temperature, the fan jet velocity is always much greater than that of the primary jet. At a low fan stream temperature (Figure 5.1-14b), the coannular nozzle noise levels are lower than the mixed jet at the high fan jet velocities. At low fan velocities, the noise levels of the coannular and single jet are equal where the fan velocity is equal to or lower than the primary velocity.

Comparisons of the unsuppressed coannular nozzle noise characteristics with the synthesis, and also with a fully mixed jet, suggest that the coannular nozzle, having $V_f > V_p$, behaves in the following manner. The high velocity annular fan jet, upon exiting from the fan nozzle, begins mixing with the outside ambient air and with the low velocity primary jet. The noise generation in this initial region is dominated by the outer annular fan exhaust shear layer mixing with the ambient air, (due to the larger velocity difference present across the outer shear layer as compared to the inner shear layer). Since the coannular nozzle outer diameter is only slightly larger than the equivalent circular jet, the high frequency noise should behave approximately the same in both cases. The large low frequency noise reduction is ascribed to the rapid mixing and velocity decay of the annulus caused by the mixing in both the outer and inner shear layers. The rapid mixing causes a reduction, compared to a single jet, in the velocity of each flow volume contributing to the noise at a particular frequency in the spectrum.

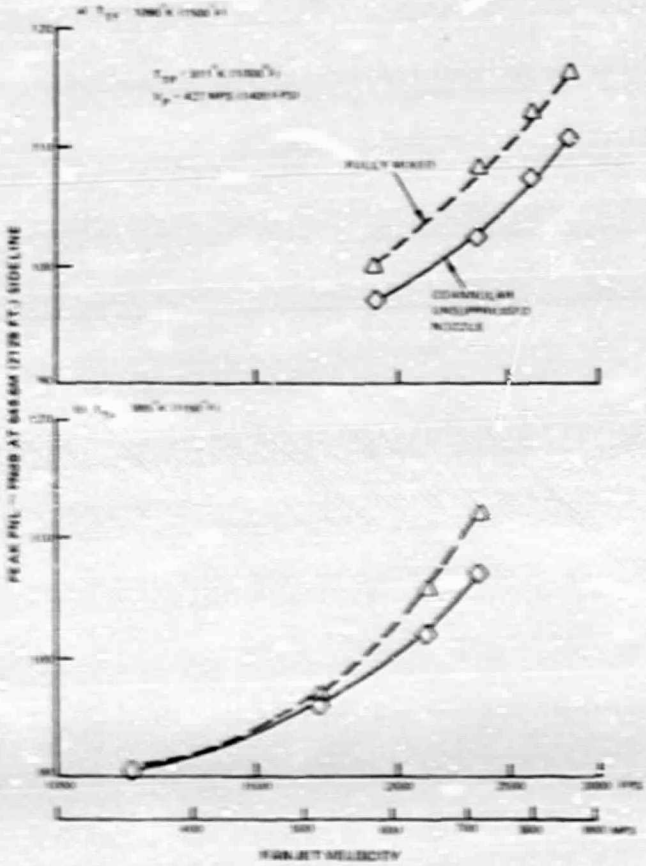

Figure 5.1-14 Comparison of Perceived Noise Levels For Coannular Unsuppressed Nozzle (0.75 Area Ratio) and Fully Mixed Jet, Scaled to 1.27m (50 in.) Equivalent Diameter

It is precisely this low frequency noise reduction that causes the spectrum to peak at the higher frequency associated with a characteristic dimension related to the fan annulus height rather than to the larger dimension corresponding to either the fan or primary jet diameters. Figure 5.1-15 helps to illustrate this point. Pressure and temperature profiles were measured downstream of the coannular nozzle with calibrated probes. The velocity profile was calculated from the measurements and compared with the initial profile at the nozzle exit. Note that a large reduction (20%) in fan jet peak velocity has occurred. Also shown is a typical velocity profile from single jet data, measured at a comparable downstream axial station. The peak velocity shows no reduction from its initial value. These velocity measurements in the flow identify more rapid mixing and velocity decay of the annular fan jet compared to the equivalent circular jet. The result of this enhanced velocity decay is that the DBTF cycle, with the fan jet velocity higher than that of the primary jet, possesses inherent noise benefits due to the annular nature of the fan exhaust.

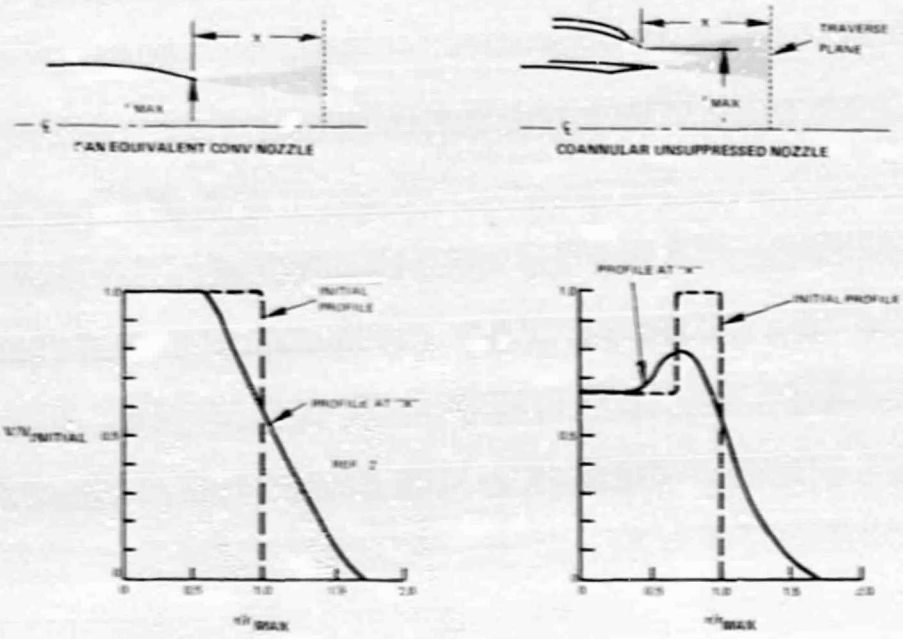

Figure 5.1.2.5 Comparison of Mixing in Circular and Coannular Jets

A lower limit of noise that could be produced by the coannular nozzle with $V_f > V_p$ can also be identified from the conceptual model of coannular jet behavior. This lower noise limit is based on the fact that the jet resulting from the mixing of the fan and primary streams has a level of velocity between the original primary and fan exit velocities. Since the fan jet decays axially, the primary stream must actually increase in velocity via a momentum exchange with the fan stream. Thus, the final mixed jet has both a velocity and a cross sectional area greater than the primary jet at the nozzle exit. This implies that the noise produced by the coannular nozzle can never be lower than the noise that would be produced by the primary jet alone.

5.1.2 Fan Stream Suppressors

In the previous section (5.1.1.2), it was shown that the unsuppressed coannular nozzle was significantly quieter than predictions based on the synthesized model. In this section, data are presented showing that additional noise reductions can be obtained by the use of various fan stream suppressors with and without a flight type ejector.

The fan stream suppressors tested were selected to be representative of suppressor types that could be used on an advanced supersonic transport. The design process led to the selection of three basic suppressor types: multi-tube, convoluted and finger. The multi-tube and convoluted designs were selected to achieve high and moderate degrees of suppression, respectively, while the finger type represented a mechanically simple concept providing a degree of suppression between the other two. All of the configurations were sized with a fan to primary area ratio of 0.75 with the exception of the convoluted suppressor which was also sized to have a fan to primary area ratio of 1.2.

5.1.2.1 Multi-Tube Suppresor Nozzle

The reductions in the perceived noise level produced by the multi-tube suppressor relative to the measured unsuppressed coannular nozzle noise levels and to the synthesized levels are shown in Figure 5.1-16 for the full range of fan jet conditions and a representative primary velocity. Data for other primary velocities are contained in the appendix. The following trends can be derived from this data:

- Suppression increases with fan velocity at constant fan temperature
- Suppression decreases with increasing fan temperature at constant velocity
- Maximum suppression obtained for a hot fan stream temperature was 7 PNdB relative to the reference coannular nozzle, and up to 14 PNdB relative to the synthesized levels.

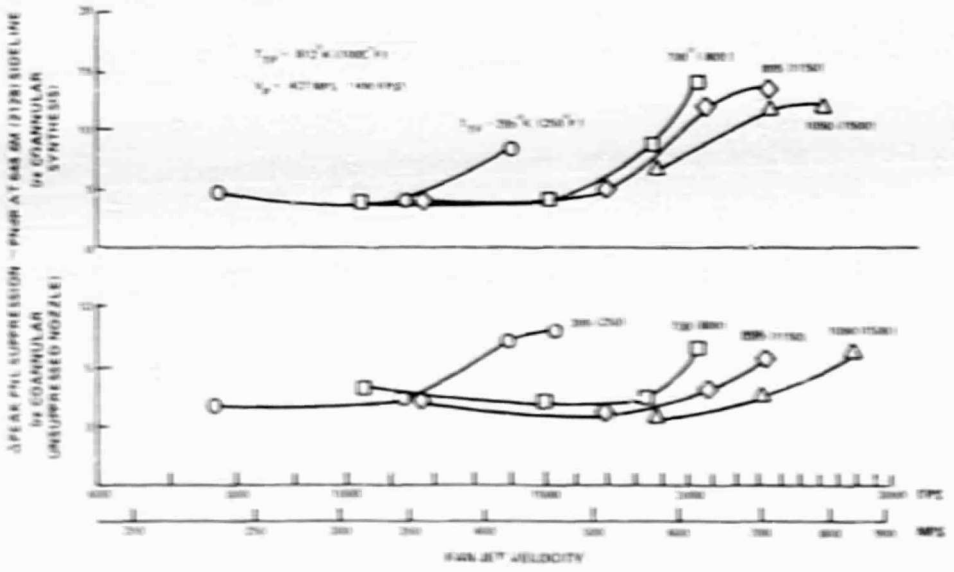

Figure 5.1-16 Peak PNL Reduction of Multi-Tube Suppressor, 0.75 Area Ratio, Scaled to 1.27m (50 in.) Equivalent Diameter

5.1.2.2 Finger Suppressor Nozzle

The suppression obtained by the use of the finger suppressor is shown in Figure 5.1-17. It is seen that the trends are similar to those for the multi-tube suppressor, except that the noise reductions are slightly lower.

5.1.2.3 Convoluted Suppressor Nozzle

The behavior of the convoluted suppressor is illustrated in Figure 5.1-18. The data behaves in a similar manner to the other suppressors, but as anticipated, the suppression is somewhat lower.

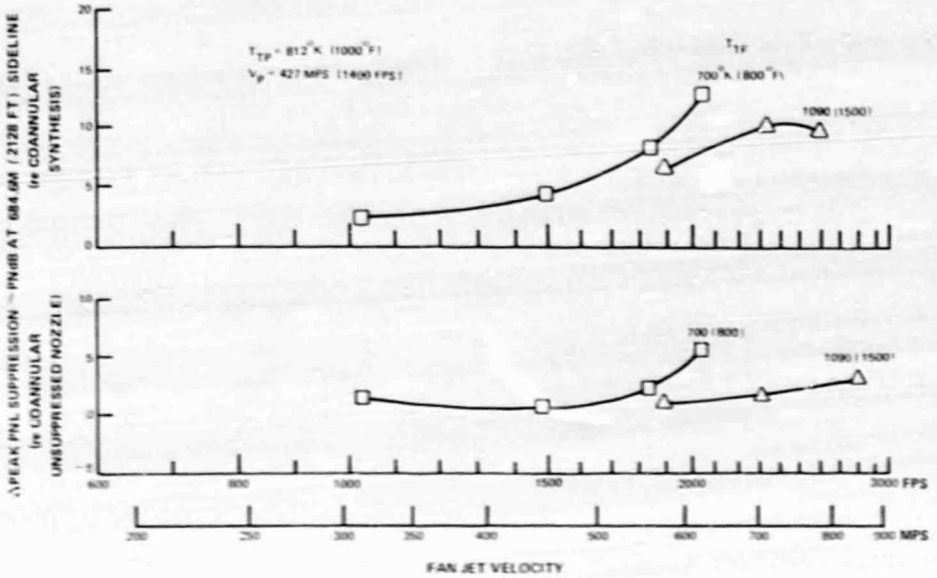

Figure 5.1-17 Peak PNL Reduction of Finger Suppressor, 0.75 Area Ratio, Scaled to 1.27m (50 in.) Equivalent Diameter

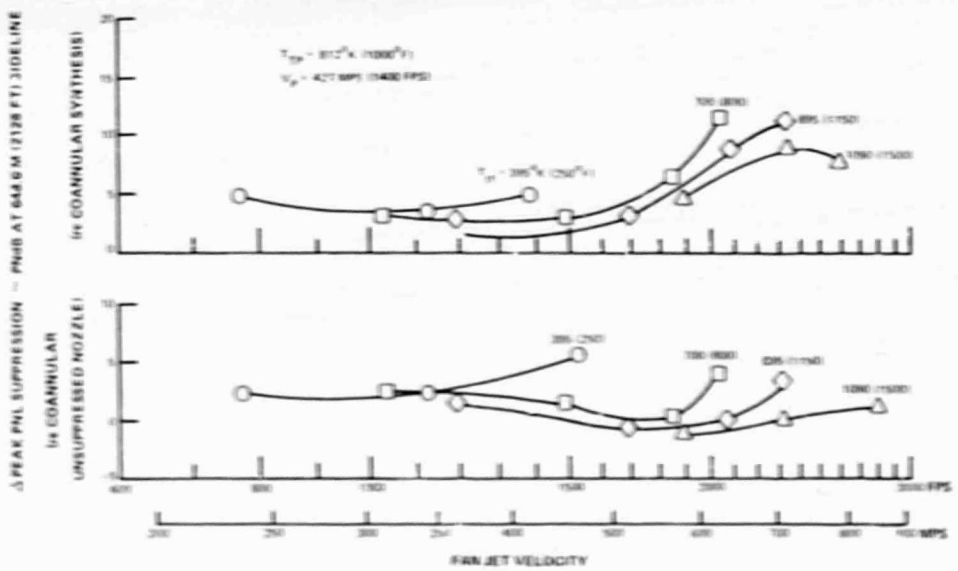

Figure 5.1-18 Peak PNL Reduction of Convoluted Suppressor, 0.75 Area Ratio, Scaled to 1.27m (50 in.) Equivalent Diameter

The effect of fan to primary nozzle area ratio on the noise characteristics of the convoluted suppressor is shown in Figures 5.1-19, 5.1-20 and 5.1-21. The peak PNL suppression of the two convoluted suppressors is presented in Figure 5.1-19, relative to their respective unsuppressed nozzles and also to the synthesis. As shown, the suppression of the two configurations is essentially the same over the range of test conditions. Thus, the suppression with the convoluted suppressor is insensitive to area ratio between 0.75 and 1.2. PNL directivities for one condition are shown in Figure 5.1-20. The directivity shapes follow the same general trend with the 1.2 area ratio levels being slightly higher because of the larger fan jet area. Spectral comparisons are shown in Figure 5.1-21 for two angles. At 140°, a slight shift of the high frequency peak (around 1000 Hz) to lower frequencies can be associated with the larger characteristic dimensions of the 1.2 area ratio convolute (i.e., the 1.2 fan exhaust is larger and contains the same number of convolutes). At 90°, this trend (around 1000 Hz) is also present. The spectra were not normalized to correct for the effect of different fan and primary areas existing on the 0.75 and 1.2 area ratio configurations as the conceptual model of noise generation presented earlier suggests that different corrections would be necessary to correct the noise at different frequencies.

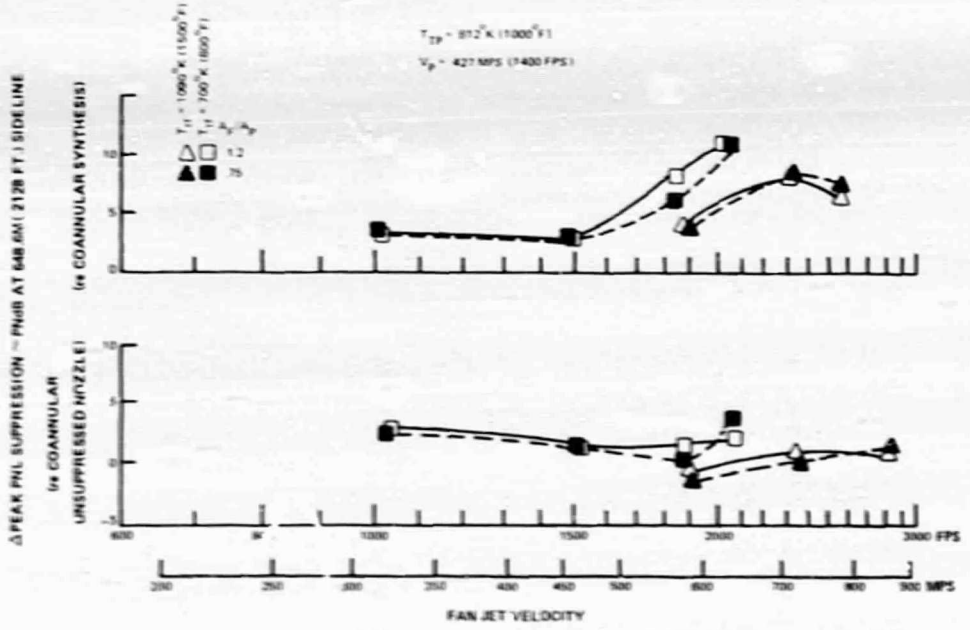

Figure 5.1-19 Comparison of Perceived Noise Level Reduction for Convoluted Suppressors, Scaled to 1.27m (50 in.) Equivalent Diameter

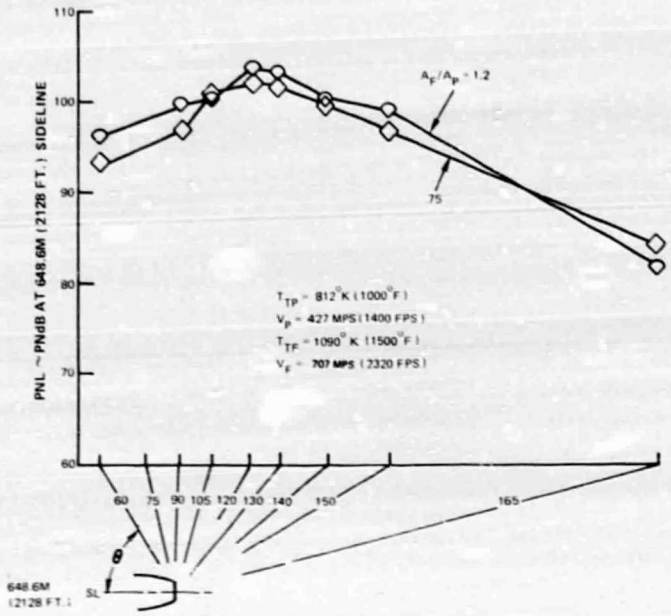

Figure 5.1-20 Comparison of PNL Directivity for Convoluted Suppressors, Scaled to 1.27m (50 in.) Equivalent Diameter

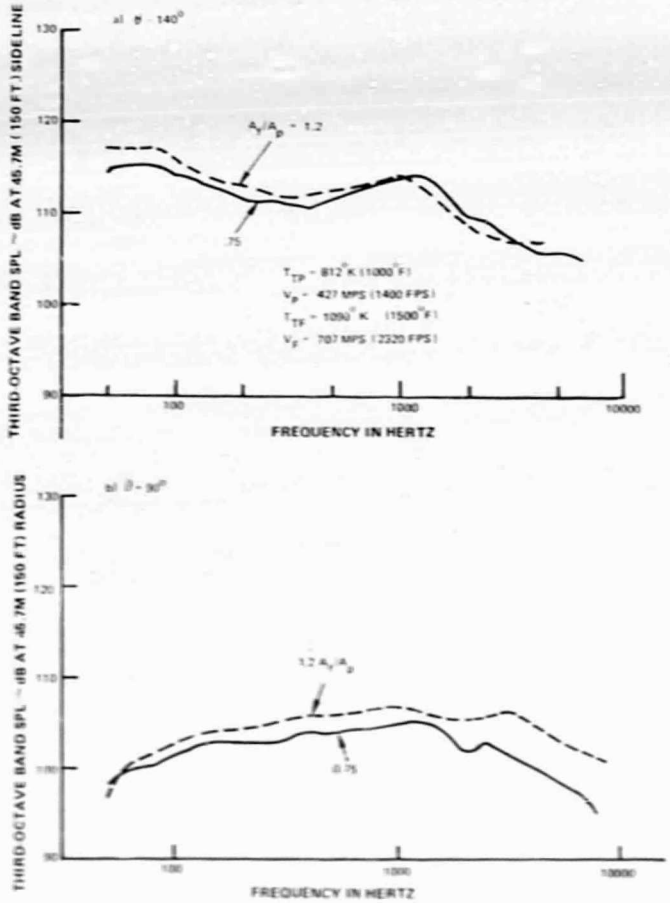

Figure 5.1-21 Comparison of SPL Spectra for Convoluted Suppressors, scaled to 1.27m (50 in.) Equivalent Diameter

5.1.2.4 Suppressor Comparisons

A direct comparison of the suppression obtained from the three suppressor configurations is shown in Figure 5.1-22 as a function of fan velocity for two fan temperatures. As illustrated, the three concepts represent different levels of suppression which must be weighed against the mechanical complexity of those designs.

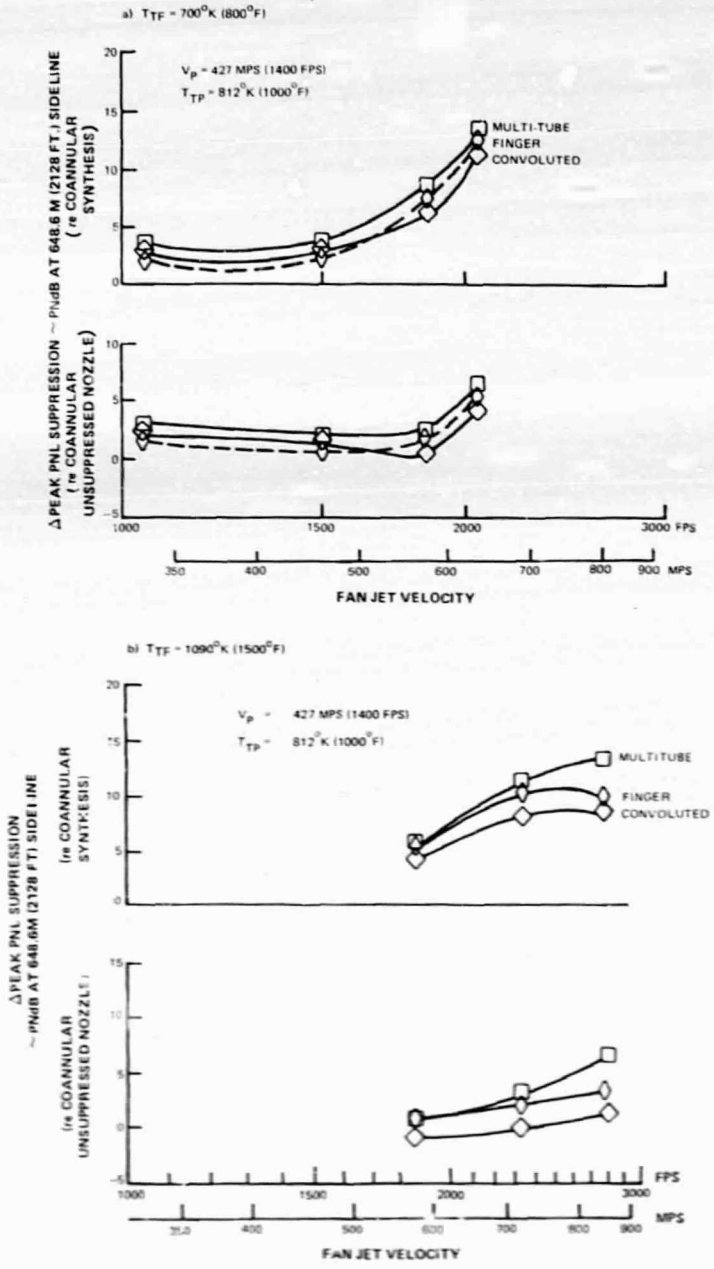

Figure 5.1-22 Comparison of Perceived Noise Levels for Multi-Tube, Finger and Convoluted Suppressors, 0.75 Area Ratio, Scaled to 1.27m (50 in.) Equivalent Diameter

The directivity patterns for the three suppressors are shown in Figure 5.1-23 for two different fan temperatures. The trend of increasing suppression from convoluted to finger to multi-tube, is seen to be reasonably consistent at all angles for both operating conditions, with the highest suppression occurring from 140 to 150° on a sideline basis.

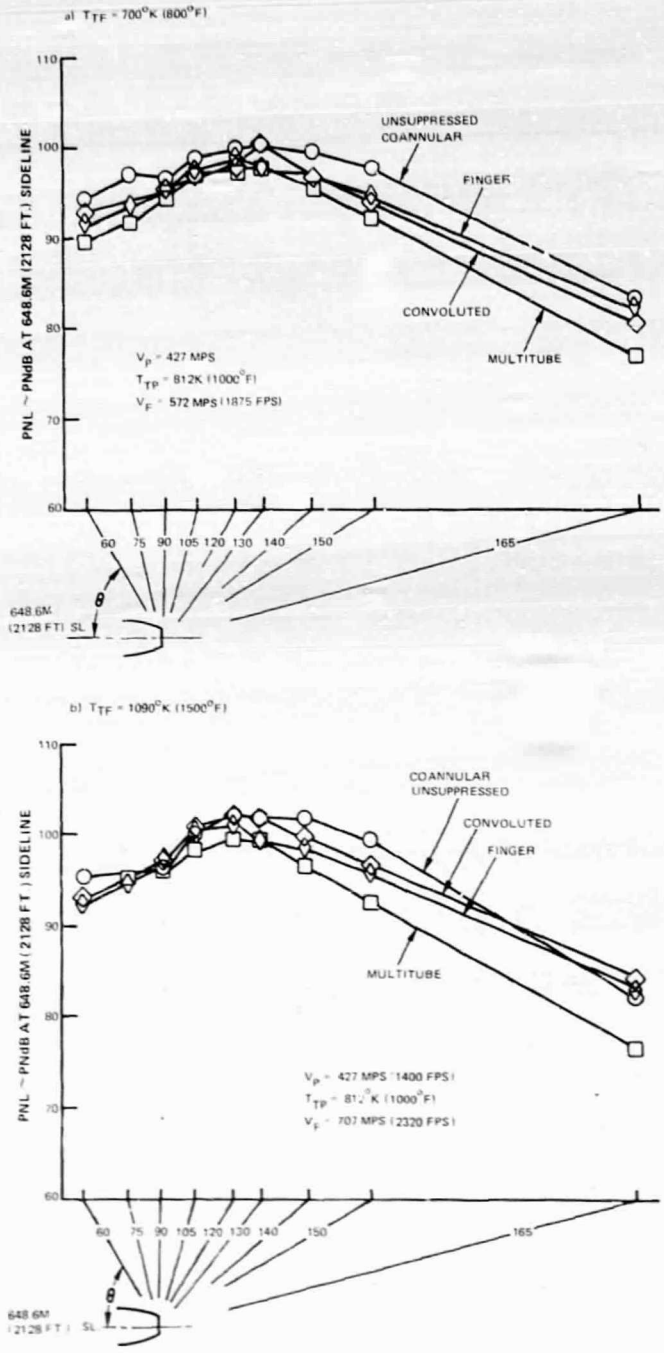

Figure 5.1-23 Comparison of PNL Directivity for Coannular Nozzles, 0.75 Area Ratio, Scaled to 1.27m (50 in.) Equivalent Diameter

The SPL spectral characteristics of the suppressors at angles of 90° and 140° at the two fan temperatures are shown in Figure 5.1-24. The previously observed trend of increasing suppression in going from convoluted to finger to multi-tube suppressors can now be interpreted in terms of measured spectral changes. The spectra at the 140° angle, in Figure 5.1-24b and d is used for the interpretation, since the low and high frequency components of the noise are separated in frequency. At mid frequencies, between 500 and 2000 Hz, the noise reductions are due to the improved mixing rates of the three suppressors causing more rapid velocity decay of the annular fan jet. The smaller reductions at lower frequencies result from the lower velocity annulus mixing with the low velocity primary jet and producing smaller reductions in the effective velocity of the downstream mixed single jet compared to the reductions in the annulus velocity. The small changes in peak frequency (near 1000 Hz) are related to the different characteristic dimensions of the suppressor elements (i.e., 18 convolutes, 32 fingers, 44 multi-tubes). The greater the number of elements, the smaller the characteristic dimension, and thus the higher the characteristic or peak frequency. The presence of double humps in the spectra at 140° compared to the broad simple spectra at 90° is similar to the results from turbojet suppressors, as in references 12 and 13.

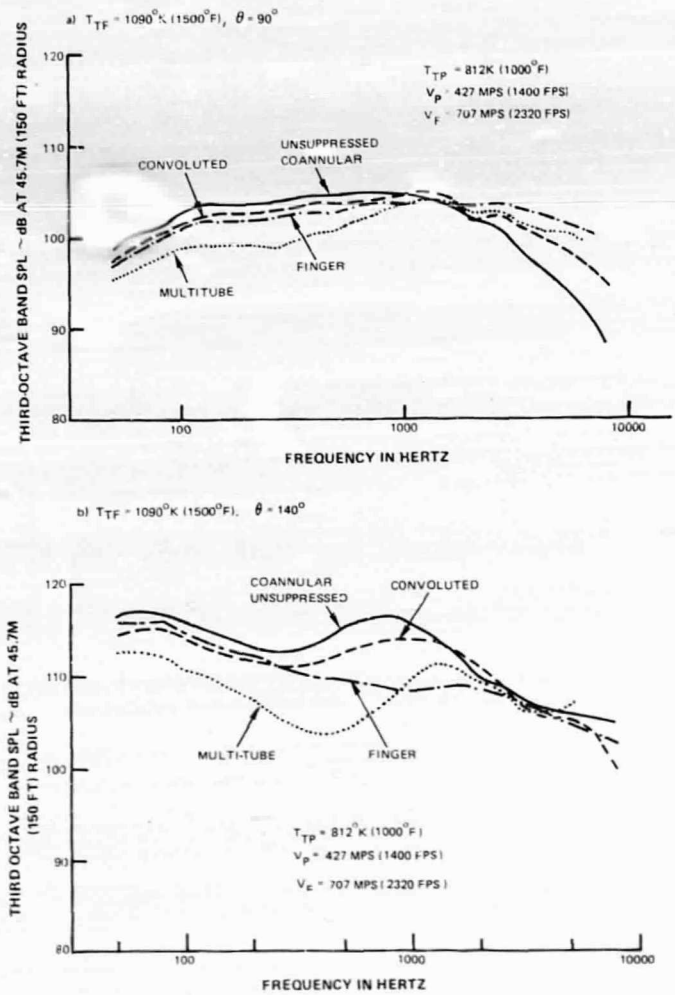

Figure 5.1-24 Spectral Comparison of Coannular Nozzles, 0.75 Area Ratio, Scaled to 1.27m (50 in.) Equivalent Diameter

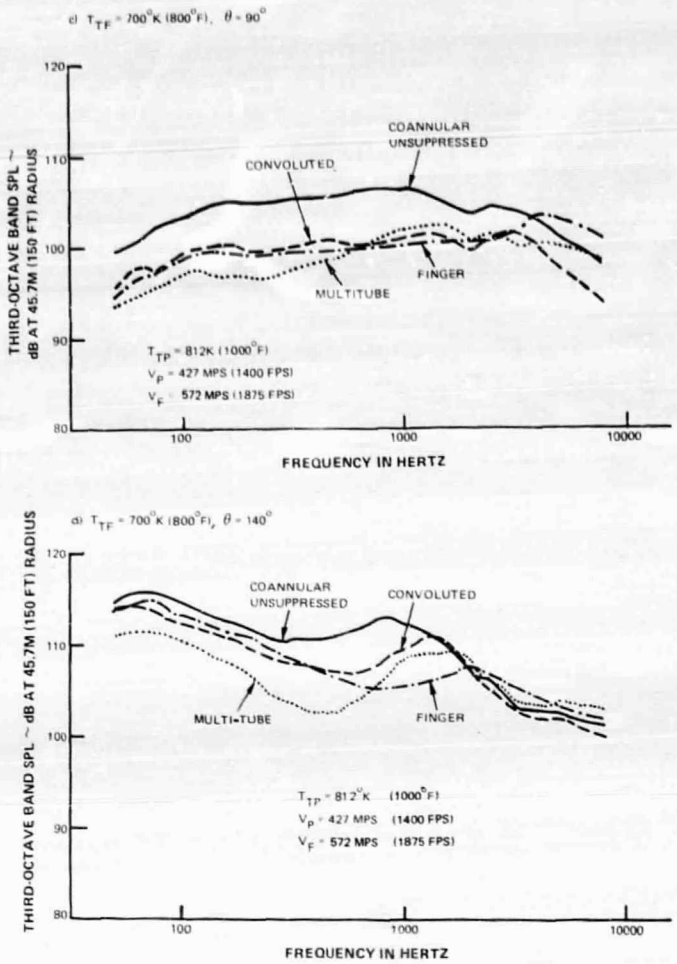

Figure 5.1-24 Spectral Comparison of Coannular Nozzles, 0.75 Area Ratio, Scaled to 1.27m (50 in.) Equivalent Diameter (Concluded)

Examining the effect of primary velocity on the absolute PNL noise levels and the Δ PNL suppression provides a better understanding of the relative importance of fan and primary velocities. Figure 5.1-25 shows the PNL level in terms of primary velocity for the multi-tube and finger suppressors. It is clearly shown that the noise level is essentially constant when V_p is low relative to V_f, and increases with increasing V_p as V_p approaches V_f. Similar characteristics are seen for the convoluted suppressor with both the 0.75 and 1.2 area ratio nozzles, as illustrated in Figure 5.1-26.

An interesting feature is noted in the noise characteristics of the 0.75 area ratio convoluted suppressor in Figure 5.1-26. The noise at V_f = 853 mps shows approximately a 2 PNdB increase when V_p increases from 425 to 520 mps, even though V_f is appreciably greater than V_p. The explanation for the higher observed noise levels is that the jet noise for co-annular nozzles having $V_f > V_p$ is composed of high frequency noise generated by the convoluted annular fan jet plus low frequency noise generated by the downstream merged jet. At V_f = 853 mps, the annular jet noise dominates at the lower V_p, as evidenced by the constant noise level at the two lower values of primary velocity. The increase in noise caused

by the still higher values of primary velocity is due to the merged jet noise becoming dominant over the annular jet noise. The increases in noise level can then be explained by the fact that the merged jet noise is dependent upon the merged jet velocity, which is higher than the primary jet velocity.

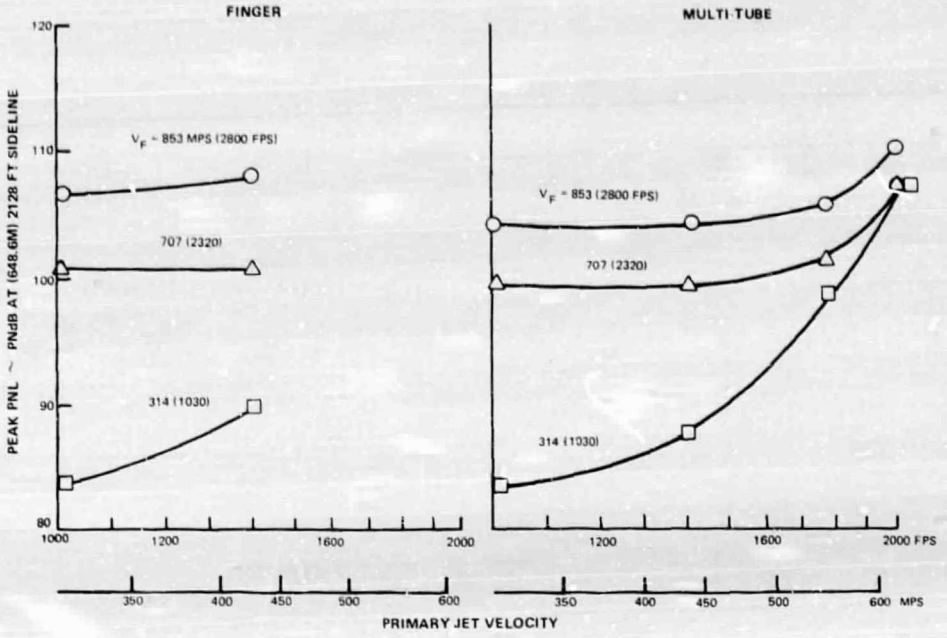

Figure 5.1-25 Effect of Primary Velocity on PNL of Finger and Multi-Tube Suppressors, 0.75 Area Ratio, Scaled to 1.27m (50 in.) Equivalent Diameter

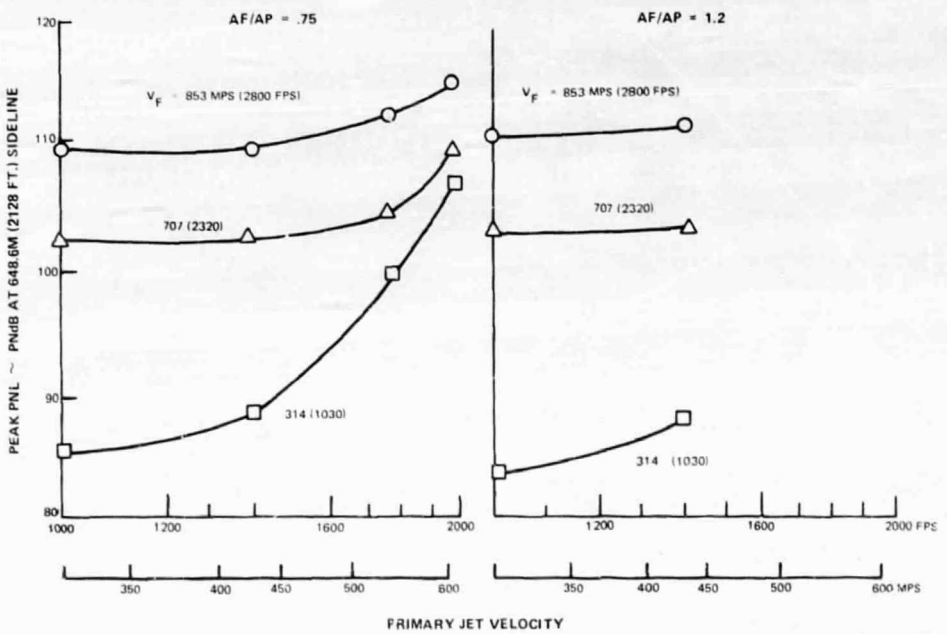

Figure 5.1-26 Effect of Primary Velocity on PNL of Convoluted Suppressors, Scaled to 1.27m (50 in.) Equivalent Diameter

5.1.3 Effect of Ejectors

Turbofan engines that power supersonic aircraft may incorporate ejectors in the exhaust system to provide high performance at all operating conditions. Thus, an important aspect of this program was to determine the effect of both hardwall and acoustically treated ejectors on the noise and performance characteristics of the various nozzle configurations. In this section, the effect of the ejectors on the noise characteristics is described.

5.1.3.1 Unsuppressed Coannular Nozzle With Ejectors

The effect of the hardwall and treated ejectors on the peak PNL of the 0.75 area ratio unsuppressed coannular nozzle is shown in Figure 5.1-27. A slight (< 1 dB) reduction was obtained by adding the hardwall ejector. The presence of acoustical treatment in the ejector produced a small amount of additional suppression. Across the test range, 2 PNdB or less total suppression was obtained. Since the unsuppressed coannular nozzle results described earlier indicated that the high frequency noise was generated in the fan annular exhaust near the nozzle exit and the low frequencies in the mixed jet downstream, some shielding suppression of the high frequency noise was expected by addition of the ejector, and further reduction is consistent with the addition of acoustic treatment. The effect of the ejectors on PNL directivity is shown in Figure 5.1-28. Little difference exists in the directivity shapes, although a slight reduction at 140-150° is seen for the ejectors cases. The spectral comparisons in Figure 5.1-29 show an interesting effect of the hardwall ejector. At 140°, a large reduction in the SPL at high frequencies is seen, while at 90°, the high frequency levels show a slight increase. The treated ejector provides a moderate reduction in high frequency at all angles. The power spectra comparison shown in Figure 5.1-30 illustrates that the hardwall ejector causes only minor changes to the noise generation while the addition of treatment reduces the noise at high frequencies.

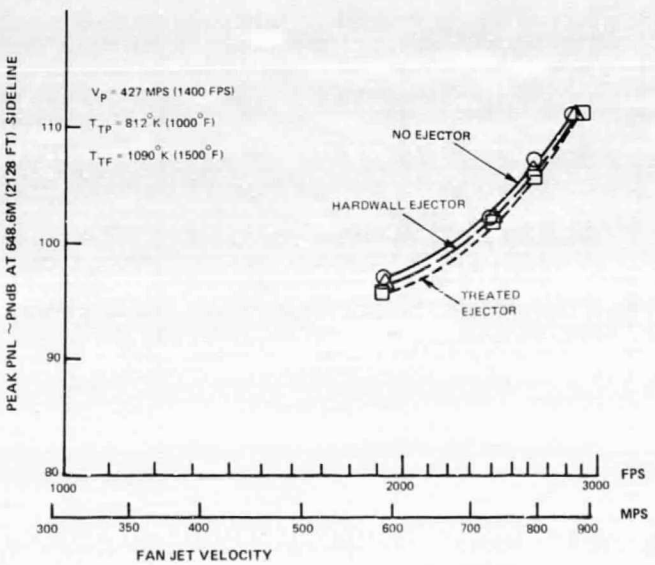

Figure 5.1-27 Effect of Hardwall and Treated Ejectors on Peak PNL of Coannular Unsuppressed Nozzle, 0.75 Area Ratio, Scaled to 1.27m (50 in.) Equivalent Diameter

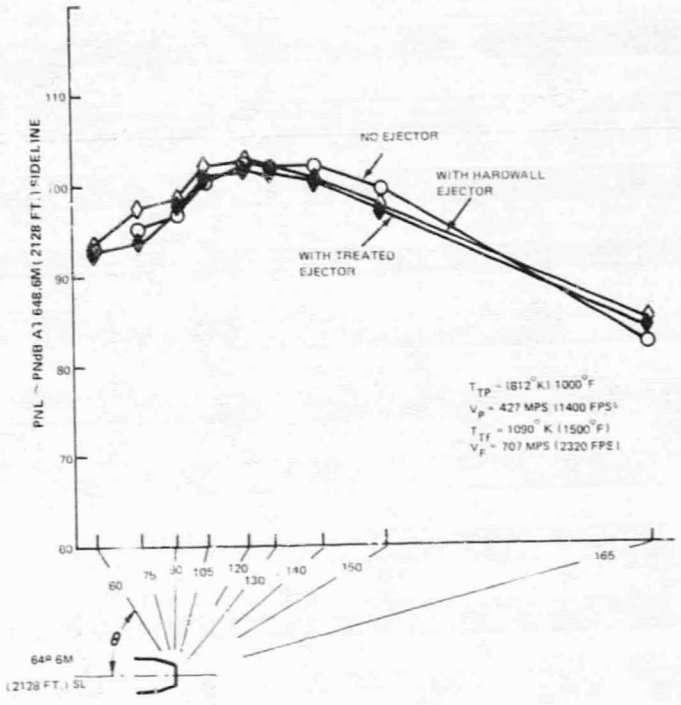

Figure 5.1-28 Effect of Hardwall and Treated Ejectors on PNL Directivity of Coannular Unsuppressed Nozzle, 0.75 Area Ratio, Scaled to 1.27m (50 in.) Equivalent Diameter

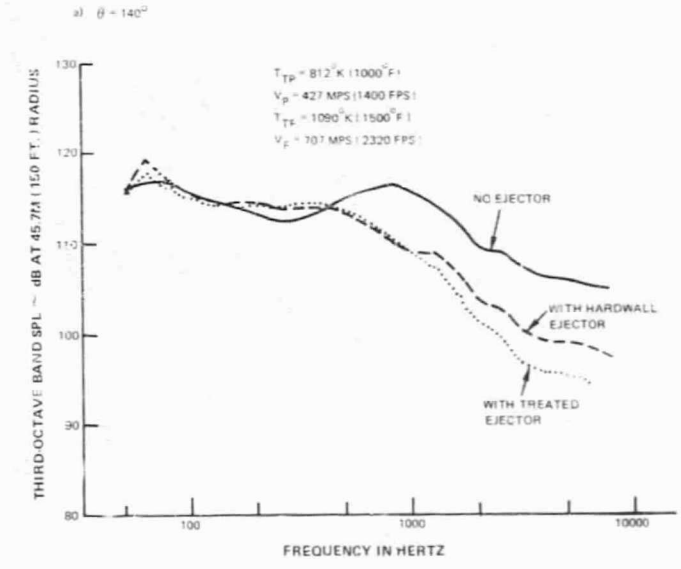

Figure 5.1-29 Effect of Hardwall and Treated Ejectors on SPL Spectra of Coannular Unsuppressed Nozzle, 0.75 Area Ratio, Scaled to 1.27m (50 in.) Equivalent Diameter

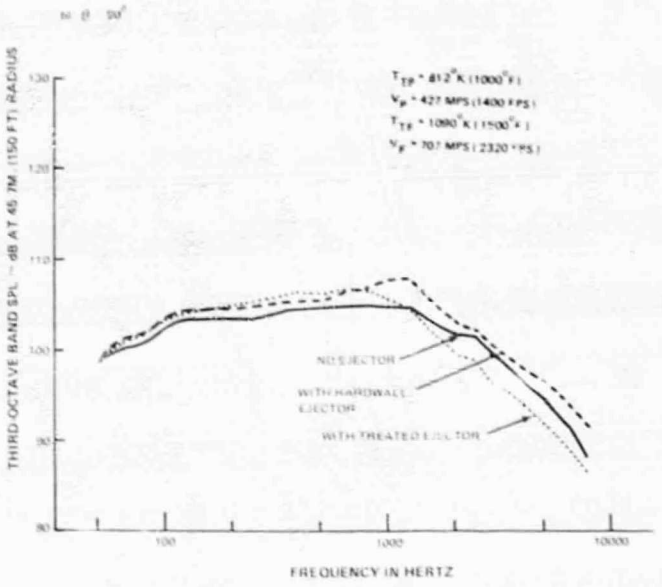

Figure 5.1-29 Effect of Hardwall and Treated Ejectors on SPL Spectra of Coannular Unsuppressed Nozzle, 0.75 Area Ratio, Scaled to 1.27m (50 in.) Equivalent Diameter (Concluded)

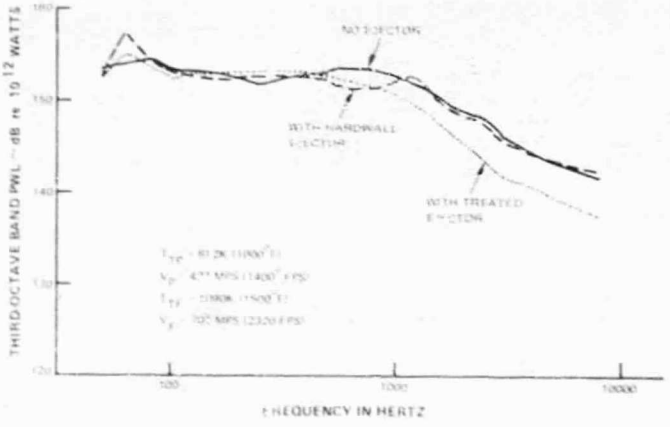

Figure 5.1-30 Effect of Hardwall and Treated Ejectors on PWL Spectra of Coannular Unsuppressed Nozzle, 0.75 Area Ratio, Scaled to 1.27m (50 in.) Equivalent Diameter

5.1.3.2 Multi-Tube Suppressor With Ejectors

The peak PNL of the multi-tube suppressor with and without an ejector is presented in Figure 5.1-31. The hardwall ejector provides a small reduction in peak PNL at most of the operating conditions while the addition of acoustic treatment causes more significant reductions (i.e., 4 PNdB at the lower fan velocities and 3 PNdB at higher fan velocities). Figure 5.1-32 displays the PNL directivity for two fan stream velocities. At the lower fan velocity (Fig. 5.1-32a), the hardwall ejector causes large reductions at aft angles and little change at the side and front angles. The treated ejector provides only slightly more reduction at aft angles, but more significant reductions at side and front angles. At the higher fan velocity (Fig. 5-1-32b) the noise reduction due to the ejectors is approximately the same at both front, side, and aft angles.

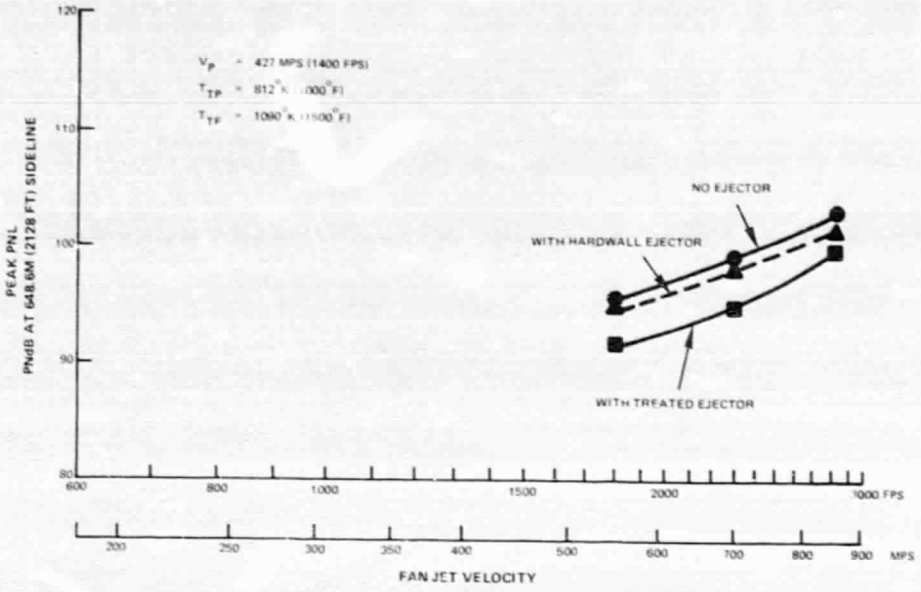

Figure 5.1-31 Effect of Hardwall and Treated Ejectors on Peak PNL of Multi-Tube Suppressor, 0.75 Area Ratio, Scaled to 1.27m (50 in.) Equivalent Diameter

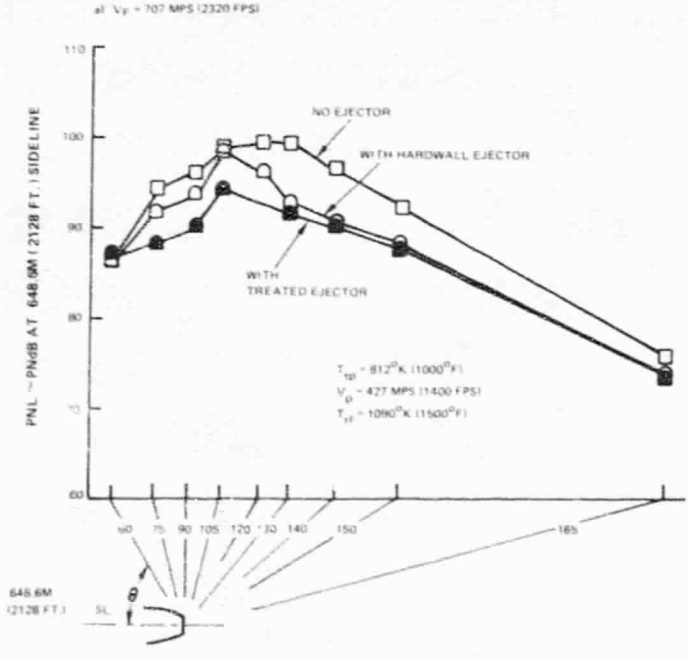

Figure 5.1-32 Effect of Hardwall and Treated Ejectors on PNL Directivity of Multi-Tube Suppressor, 0.75 Area Ratio, Scaled to 1.27m (50 in.) Equivalent Diameter

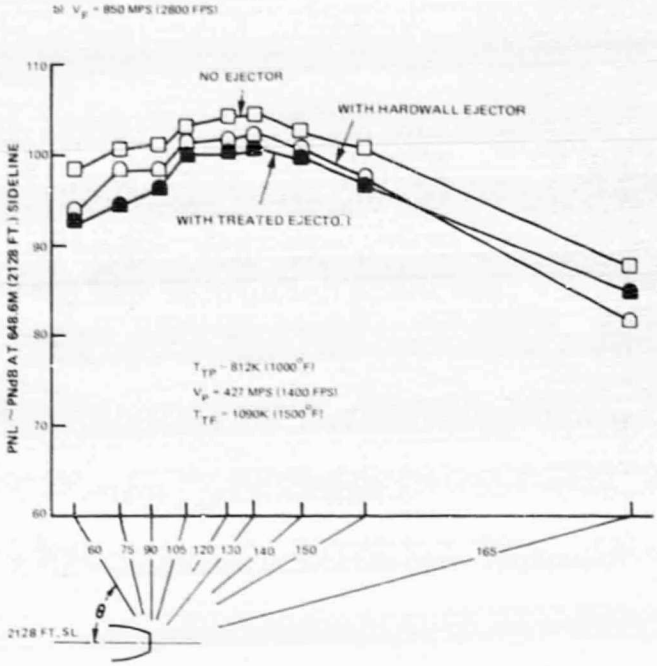

Figure 5.1-32 Effect of Hardwall and Treated Ejectors on PNL Directivity of Multi-Tube Suppressor, 0.75 Area Ratio, Scaled to 1.27m (50 in.) Equivalent Diameter (Concluded)

The corresponding spectral comparisons shown in Figures 5.1-33 are used to explain this behavior. One-third octave band SPL spectra at 90° and 140° and power spectra for the multi-tube nozzles are shown in Figure 5.1-33 for the lower fan velocity. At 90° (Figure 5.1-33a) the hardwall ejector causes a 2 dB reduction in the low and mid frequency range, and a 1 dB reduction at high frequencies. At 140° (Figure 5.1-33b), however, a large reduction in high frequency noise can be seen. The addition of treatment causes further reductions at high frequency at both angles, but no additional reductions at low frequency. The large angular variation in hardwall ejector attenuation is believed to be caused by refraction of the high frequency noise generated within the ejector and reflected from the ejector walls as it passes through the shear layer emanating from the ejector lip. This phenomenon is similar to the shear layer refraction present during open jet wind tunnel tests (Ref. 14). Similar directivity effects have also been observed in recent tests by the Boeing Company (Ref. 15). The low frequencies are unaffected since they are generated downstream of the ejector. To define the changes in radiated acoustic power caused by the ejector, the noise spectrum was integrated across all measuring angles to obtain the noise power spectrum shown in Figure 5.1-33c. The power spectra remove the refraction phenomenon, which is a directivity effect. This comparison clearly shows two effects. First, the hardwall ejector produces from 2 to 5 dB reduction across the spectra, which can be explained by source strength reduction due to the reduced relative velocity between the jet and the ejector induced flow. Secondly, the presence of the acoustical treatment causes no further reduction in the low frequency portion of the spectrum up to 400 Hz, but increasing amounts of suppression from 400 Hz to 10000 Hz. This is consistent with the design goal of the treatment, which was selected to provide broad band attenuation down to scaled frequencies of about 400 Hz.

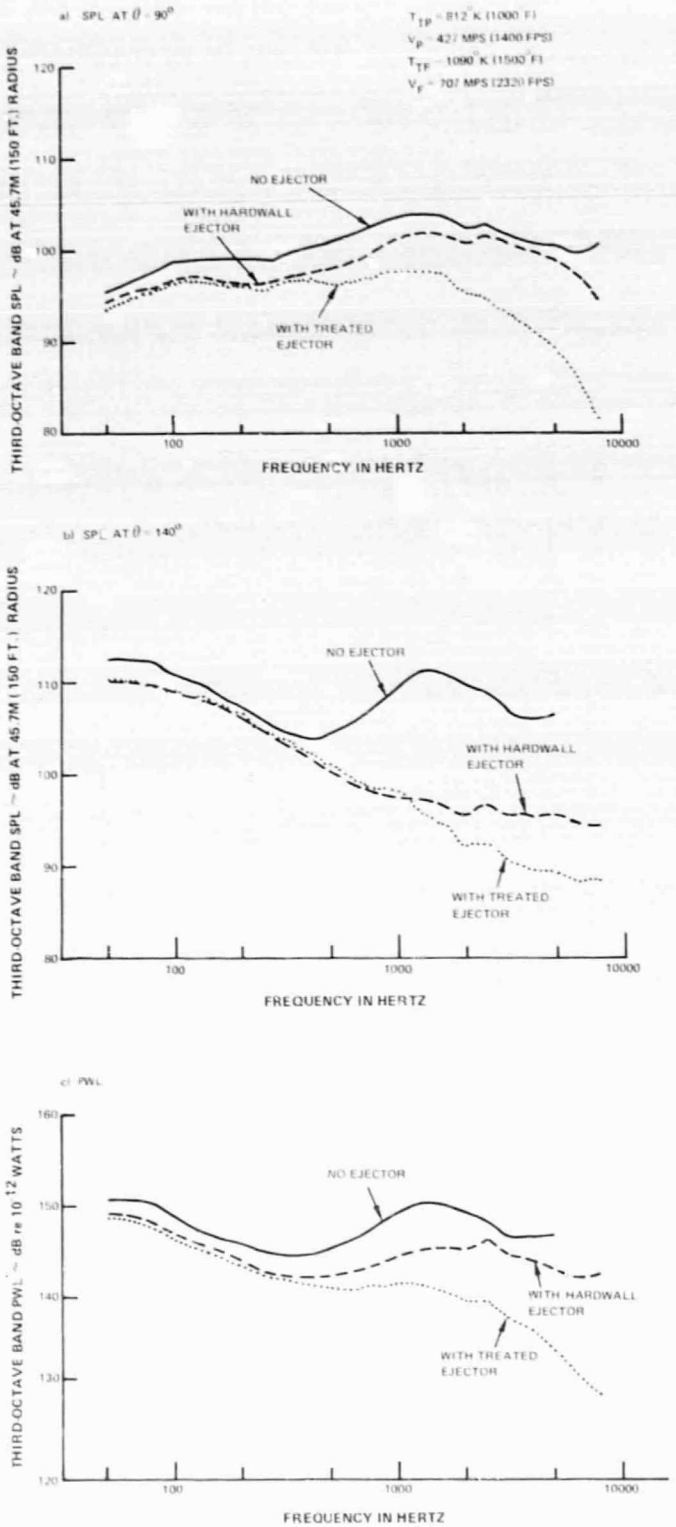

Figure 5.1-33 Effect of Hardwall and Treated Ejectors on Noise Spectra of Multi-Tube Suppressor at a Fan Velocity of 707 mps (2320 fps), 0.75 Area Ratio, Scaled to 1.27m (50 in.) Equivalent Diameter

Comparisons of the SPL spectra at 90° and 140°, and the power spectra, are shown for a fan velocity of 850 mps in Figure 5.1-34. The effect of the ejectors is similar to the effect in the previous case at the lower fan velocity. However, at the higher fan velocity, more noise exists in the low and mid frequency range (<500 Hz) relative to the noise at high frequencies. The ejector treatment (which attenuates only the high frequency noise generated by the annular fan jet close to the nozzle exit), therefore, is less efficient in reducing the noise.

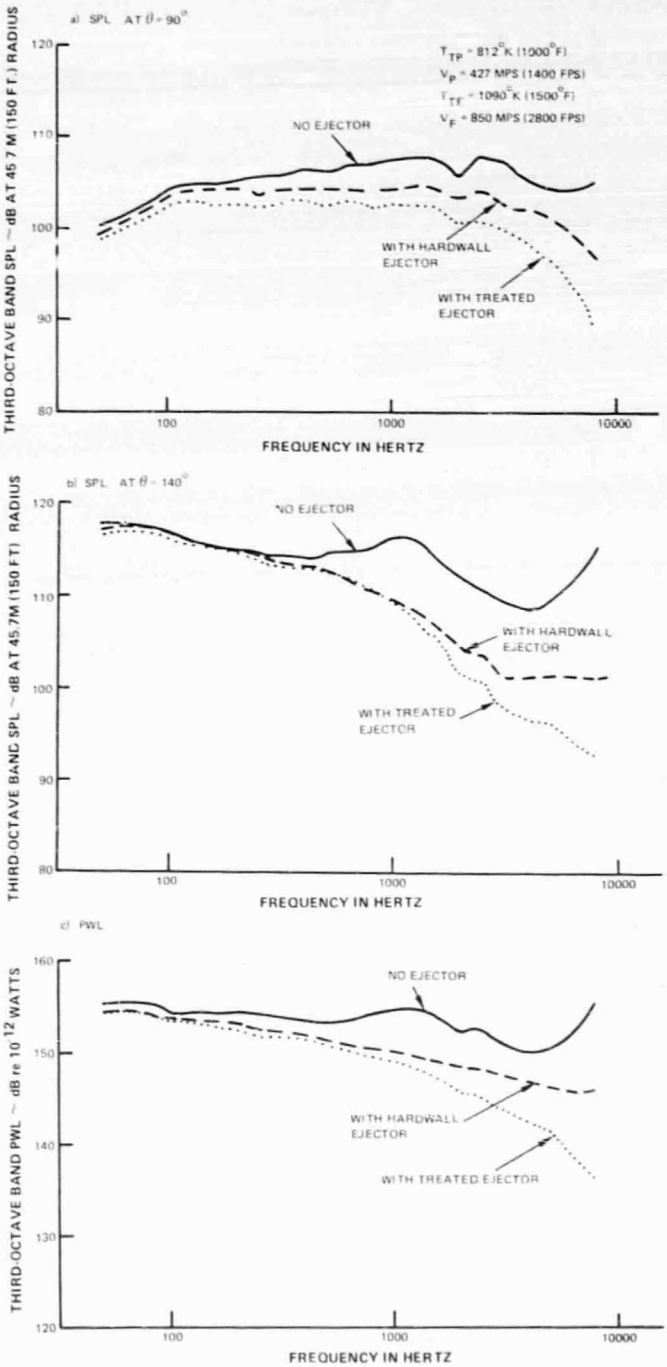

Figure 5.1-34 Effect of Hardwall and Treated Ejectors on Noise Spectra of Multi-Tube Suppressor at a Fan Velocity of 850 mps (2800 fps), 0.75 Area Ratio, Scaled to 1.27m (50 in.) Equivalent Diameter

5.1.3.3 Finger Suppressor With Ejectors

The effect of the ejectors on the noise reduction characteristics of the finger suppressors is essentially the same as for the multi-tube suppressor. The effect on peak PNL, shown in Figure 5.1-35, indicates a slight reduction due to the hardwall ejector (1 PNdB) while the addition of acoustical treatment produces a varying reduction ranging from 3 PNdB at low fan velocities to nearly zero at the higher velocities. The PNL directivity, as illustrated in Figure 5.1-36a, for a fan velocity of 707 mps shows reductions at aft angles for the hardwall ejector, and small additional suppressions at all angles due to the treatment. At V_F = 850 mps, Figure 5.1-36b, the hardwall ejector shows noise reductions similar to those at the lower fan velocity, but the treated ejector produces no further noise reduction.

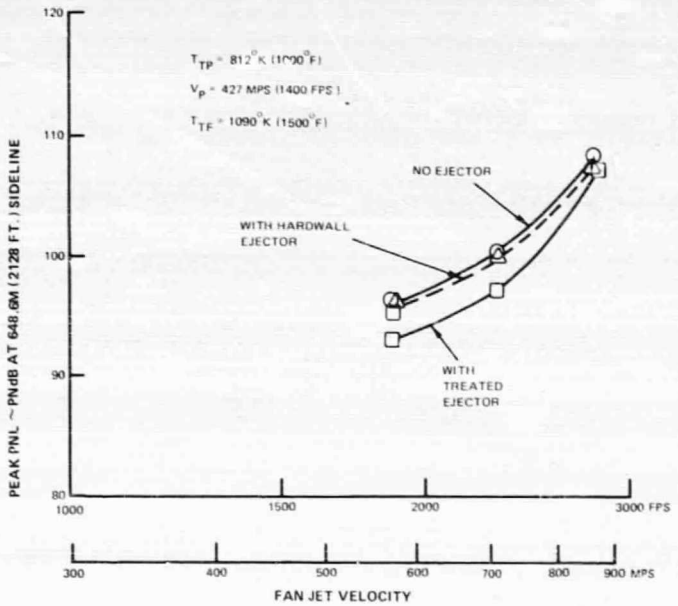

Figure 5.1-35 Effect of Hardwall and Treated Ejectors on Peak PNL of Finger Suppressor, 0.75 Area Ratio, Scaled to 1.27m (50 in.) Equivalent Diameter

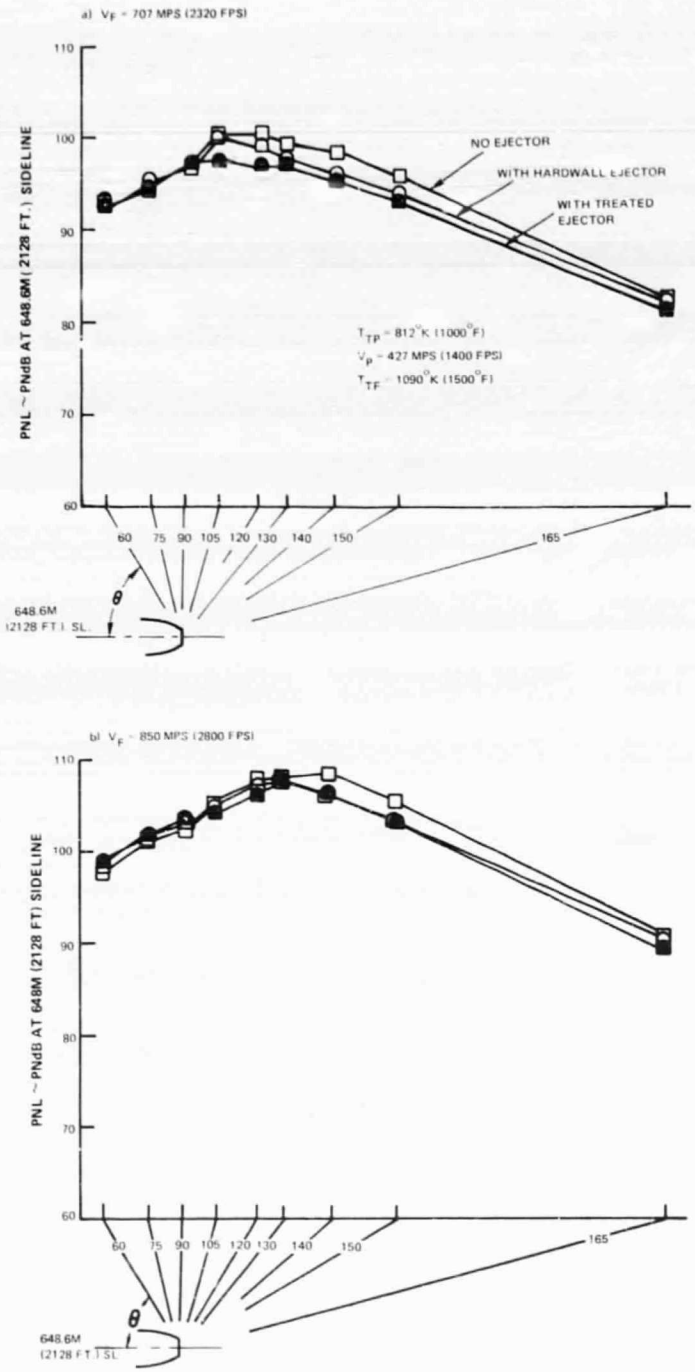

Figure 5.1-36 Effect of Hardwall and Treated Ejectors on PNL Directivity of Finger Suppressor, 0.75 Area Ratio, Scaled to 1.27m (50 in.) Equivalent Diameter

The SPL and power spectra comparisons at the lower fan velocity presented in Figure 5.1-37 show the same general characteristics as those exhibited by the multi-tube suppressor. In particular, a large reduction in the SPL at high frequencies at rear angles, caused by addition of the hardwall ejector, and consistent high frequency reductions at all angles due to the treatment. Comparisons of the SPL spectra at 90° and 140°, and the power spectra for V_F = 850 mps are presented in Figure 5.1-38. As was the case with the multi-tube suppressor, at this high fan velocity, the noise generated by the merged jet is much higher than for the lower fan velocity case and dominates the entire spectra. Thus, at the high fan velocity, the ejectors have negligible effect on the total noise. It is noted that the addition of treatment to the ejector provides no attenuation even at high frequencies. This result is different from the effect of the treated ejector on the noise of the multitube suppressor shown previously in Figure 5.1-34. The explanation for this different behavior lies in the amount of merged jet noise compared to the noise generated in the annular fan exhaust close to the nozzle exit illustrated in Figure 5.1-39.

The PWL spectra for the finger and multi-tube suppressors with hardwall ejectors at 707 mps, illustrated in Figure 5.1-39a, shows the merged jet noise spectra extrapolated to higher frequencies assuming a typical jet noise spectrum shape. The spectrum is therefore consistent with the noise that would be generated by a single jet exiting a circular nozzle at the merged jet condition. This "floor level" noise is below the SPL level of the high frequency noise actually generated by both suppressors. As the multi-tube case has a much lower merged jet noise, and therefore a lower "floor level" noise, the ejector treatment should provide more attenuation than for the finger suppressors as can be seen by comparing Figures 5.1-33 and 5.1-37. The effect of increasing the fan jet velocity to 850 mps is illustrated in Figure 5.1-39b. In this case, the merged jet spectrum extrapolation for the finger suppressor falls very close to the measured spectra, indicating that the merged jet noise dominates the noise over the entire frequency range. However, the same extrapolation of the merged jet noise of the multi-tube suppressor falls below the level of the suppressor generated noise. Thus, the application of the treatment would be expected to provide attenuation at the high frequencies for the multi-tube suppressor, but not for the finger suppressor.

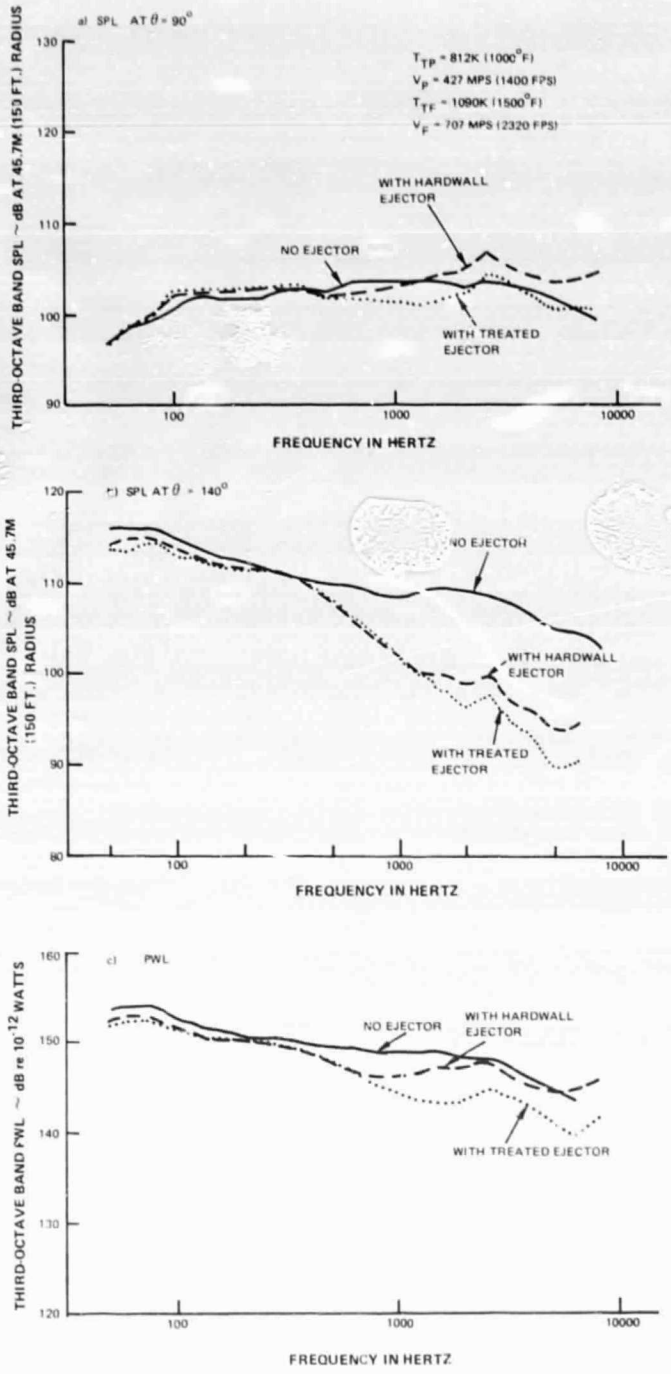

Figure 5.1-37 Effect of Hardwall and Treated Ejectors on Noise Spectra of Finger Suppressor at a Fan Velocity of 707 mps (2320 fps), 0.75 Area Ratio, Scaled to 1.27m (50 in.) Equivalent Diameter

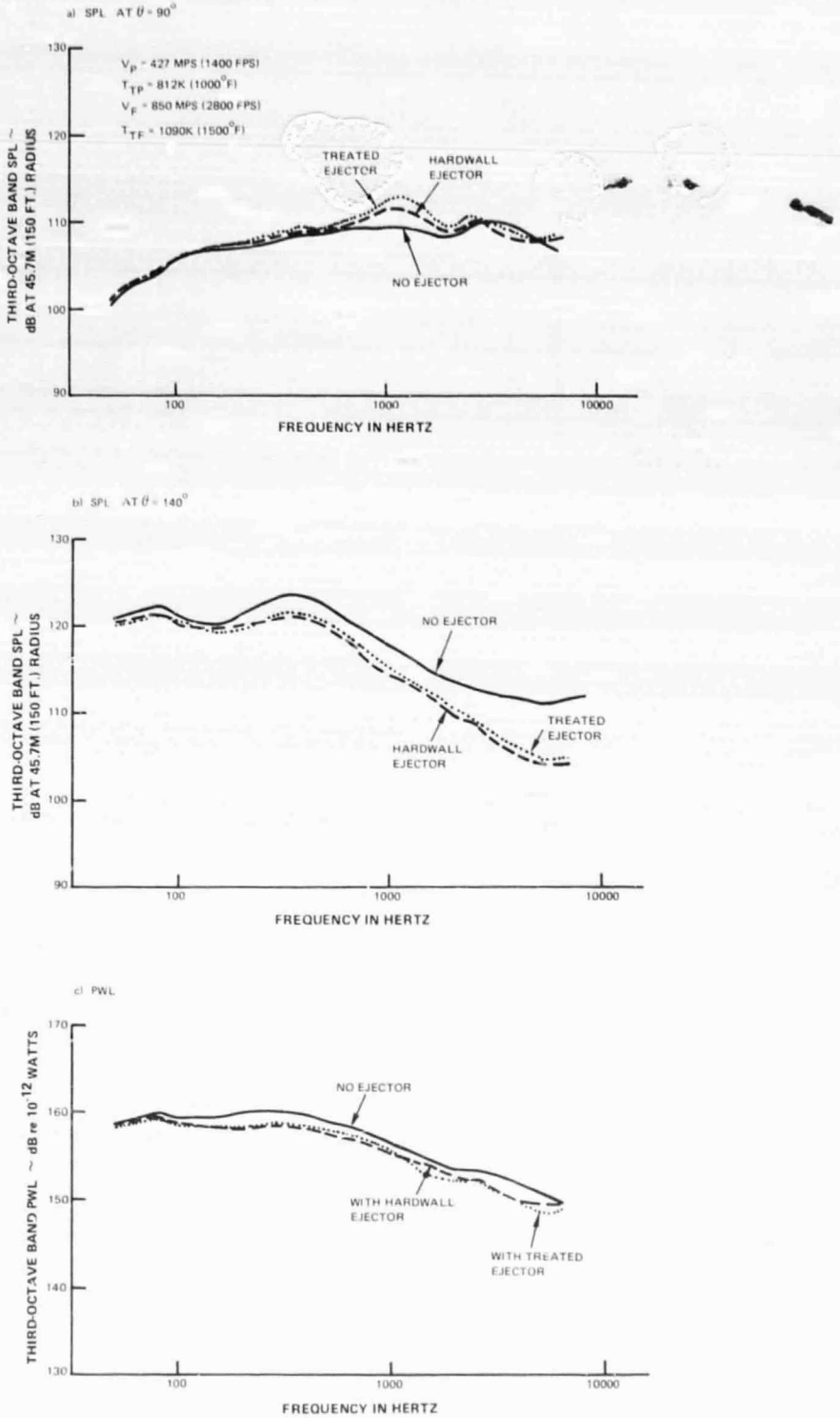

Figure 5.1-38 Effect of Hardwall and Treated Ejectors on Noise Spectra of Finger Suppressor at a Fan Velocity of 850 mps (2800 fps), 0.75 Area Ratio Scaled to 1.27m (50 in.) Equivalent Diameter

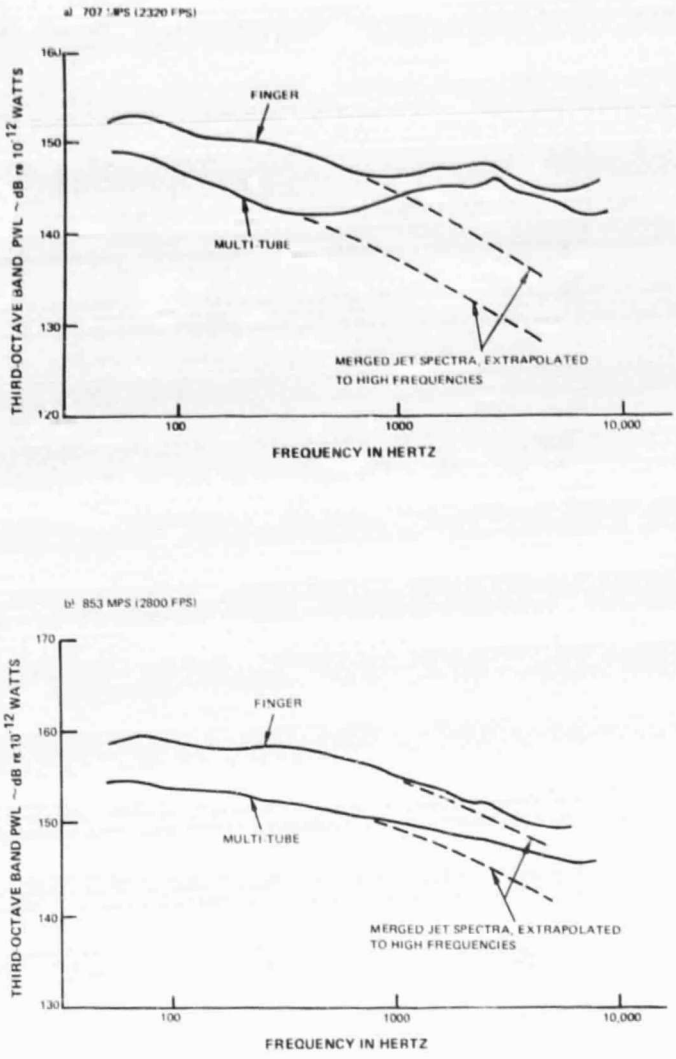

Figure 5.1-39 Noise Spectra of Finger and Multi-tube Suppressors With Hardwall Ejector, 0.75 Area Ratio Scaled to 1.27 m (50 in.) Equivalent Diameter

5.1.3.4 Convoluted Suppressors With Ejectors

The comparison of peak PNL for the 0.75 area ratio convoluted suppressor, with and without ejectors, is shown in Figure 5.1-40. As illustrated, the hardwall ejector provides approximately 1 PNdB reduction. The presence of the acoustically treated ejector provides an additional 4 PNdB reduction at low fan velocities and no reduction at the higher fan velocities. The PNL directivities at two fan velocities, shown in Figure 5.1-41, indicate a larger ejector impact at $\theta = 165°$ compared to the other suppressor configurations. However, at the peak PNL angle, the effect is comparable to that of the finger suppressor, but not as large as the multi-tube design. The PNL reduction due to the ejectors is negligible at side and forward angles at the fan velocity of 850 mps, similar to the results from the multi-tube and finger suppressors. SPL and power spectra comparisons are shown in Fig. 5.1-42 for a fan velocity of 707 mps. The hardwall ejector provides a large amount of suppression at high frequencies at $\theta = 140°$, but has little effect at $\theta = 90°$. The treated ejector provides high frequency suppression at both angles. The sound power spectra comparison in Figure 5.1-42c indicates a 1-3 dB reduction due to the hardwall ejector. The treated ejector provides up to 6 dB reduction at the higher frequencies. Comparisons of SPL spectra at 90° and 140° and power spectra for the higher fan velocity of 850 mps are shown in Figure 5.1-43. As was seen for the multi-tube and finger suppressors, the high levels of noise generated by the merged jet dominates the noise spectra at this high fan velocity, and the ejectors are ineffective in reducing the noise generated in the merged jet region. It is noted that no high frequency attenuation is present due to the treatment in the ejector for the 850 mps case. The explanation for this behavior is the same as for the finger suppressor discussed previously, i.e., the merged jet noise is dominant over the entire frequency spectrum.

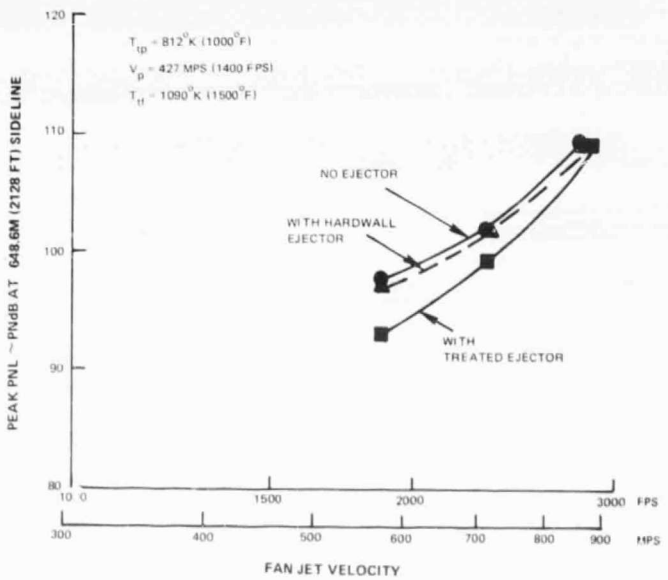

Figure 5.1-40 Effect of Hardwall and Treated Ejectors on Peak PNL of Convoluted Suppressor, 0.75 Area Ratio, Scaled to 1.27m (50 in.) Equivalent Diameter

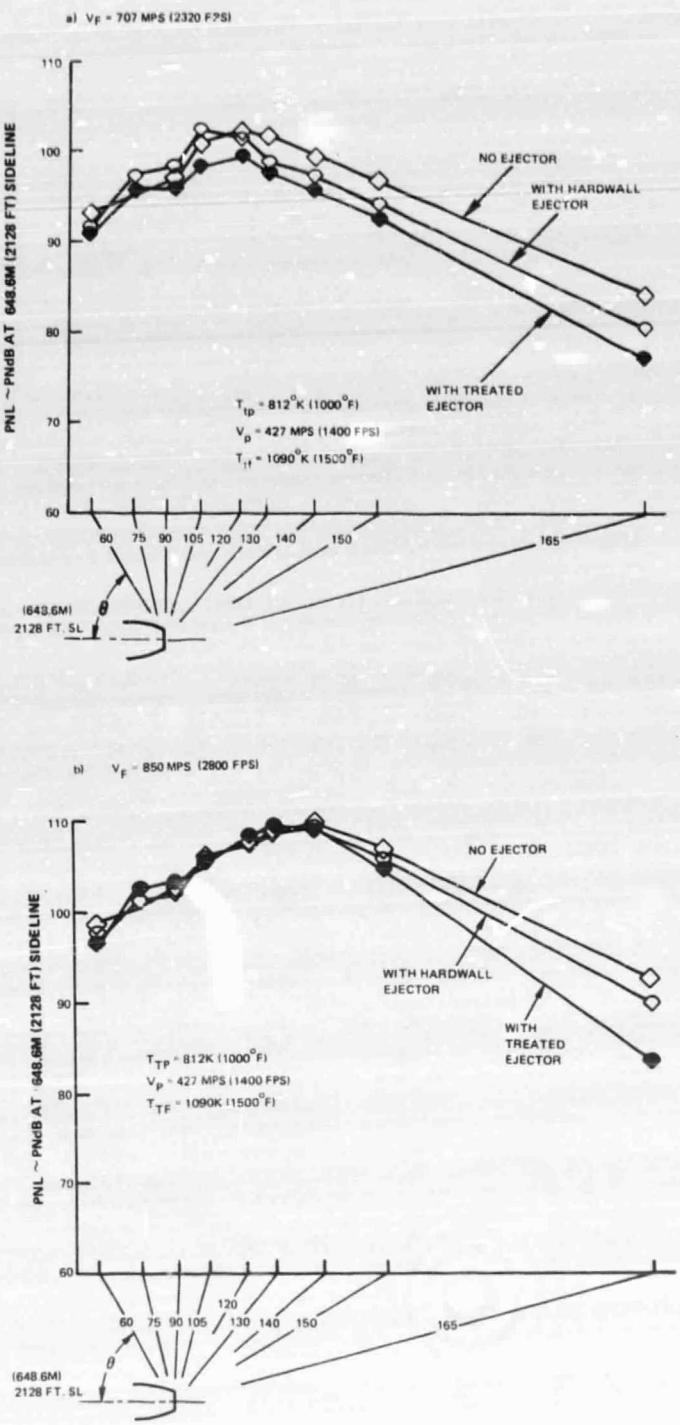

Figure 5.1-41 Effect of Hardwall and Treated Ejectors on PNL Directivity of Convoluted Suppressor, 0.75 Area Ratio, Scaled to 1.27m (50 in.) Equivalent Diameter

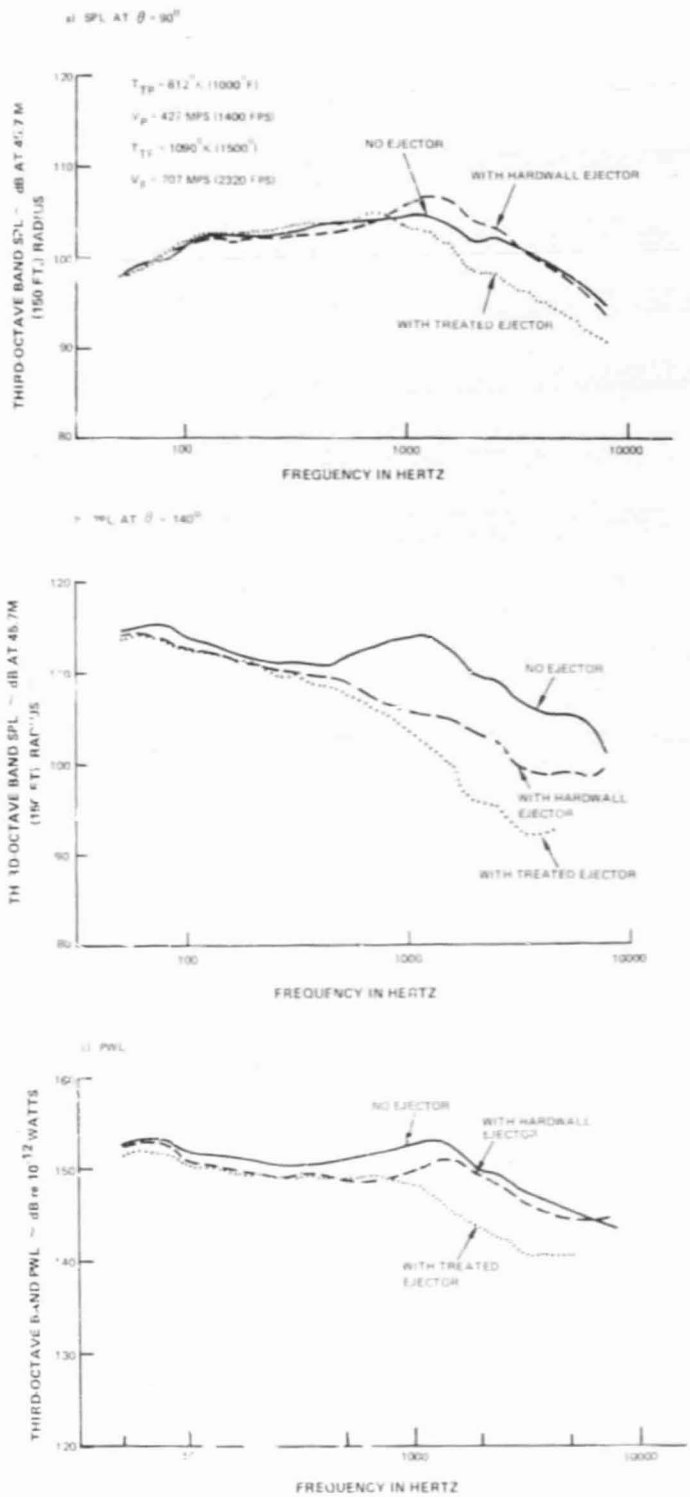

Figure 1-42 Effect of Hardwall and Treated Ejectors on Noise Spectra of Convoluted Suppressor at a Fan Velocity of 707 mps (2320 fps), 0.75 Area Ratio, Scaled to 1.27m (50 in.) Equivalent Diameter

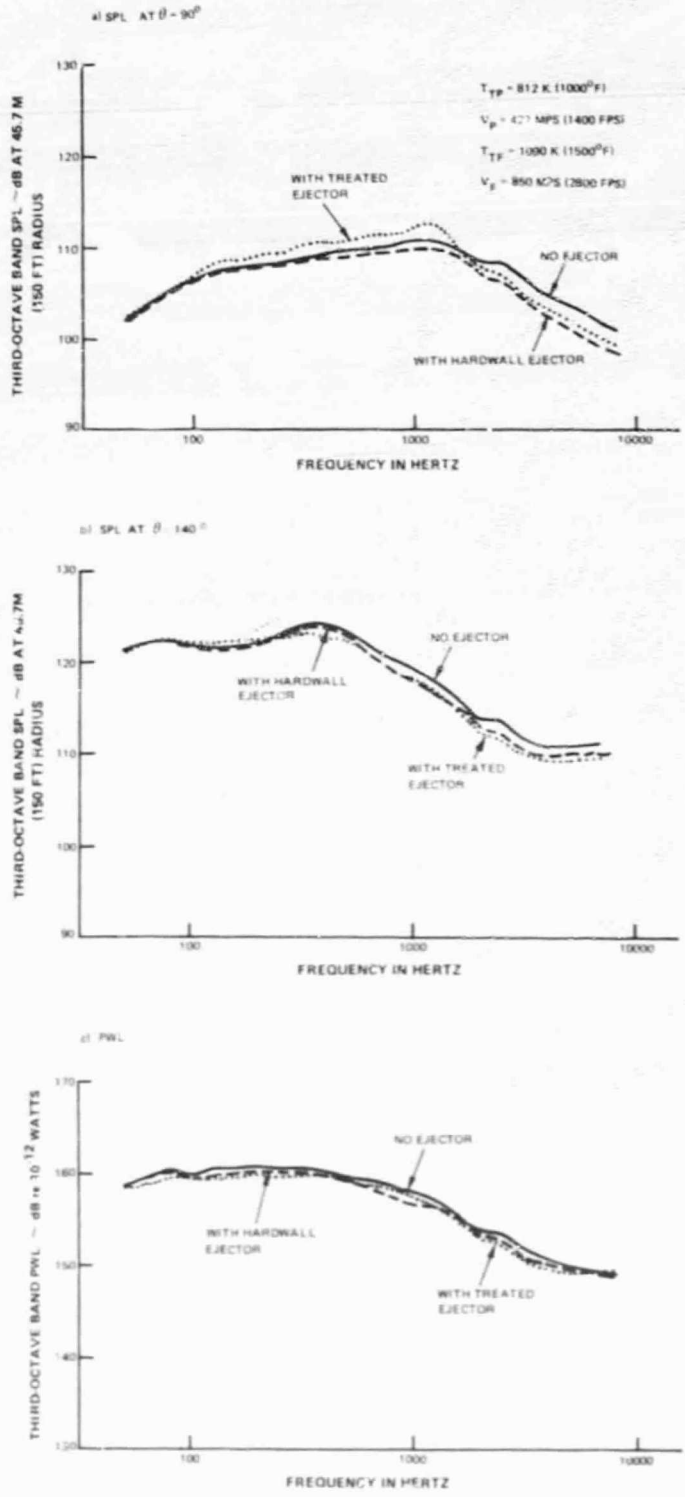

Figure 5.1-43 Effect of Hardwall and Treated Ejectors on Noise Spectra of Convoluted Suppressor at a Fan Velocity of 850 mps (2800 fps), 0.75 Area Ratio, Scaled to 1.27m (50 in.) Equivalent Diameter

The impact on peak PNL suppression of increasing the fan to primary area ratio of the convoluted suppressor from 0.75 to 1.2 is shown in Figure 5.1-44 for both the hardwall and treated ejectors. The suppression was essentially the same for the two different area ratios. The impact of the ejectors on the noise power spectra of the 1.2 area ratio convoluted suppressors is presented in Figure 5.1-45. The effect of the ejectors is seen to be similar to that of the 0.75 area ratio configuration illustrated in Figure 5.1-42. The hardwall ejector reduces the noise by varying amounts across the entire frequency range while the treated ejector results in additional suppression only at the higher frequencies. The reduction in noise power spectra. due to the ejectors relative to the convoluted suppressor noise with no ejector, is presented in Figure 5.1-46 for both area ratios. Except at the very high frequencies (above 4,000 Hz), the suppression spectra are quite similar for both the 0.75 and 1.2 area ratio models. Since the suppression spectra are approximately the same, it can inferred that the effect of ejectors on the suppression provided by the convoluted suppressor is essentially insensitive to nozzle area ratio changes from 0.75 to 1.2.

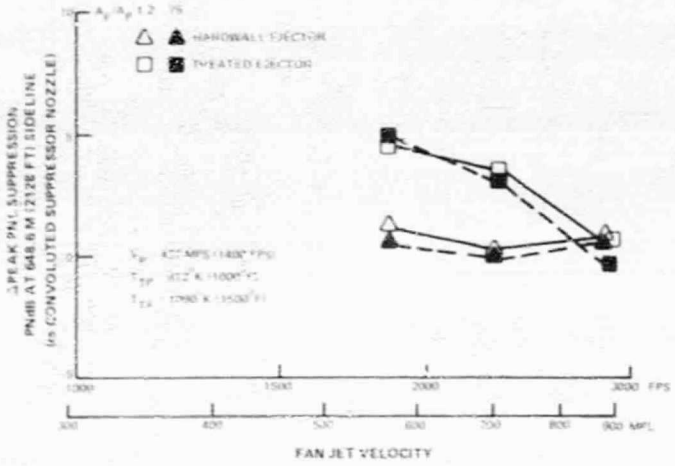

Figure 5.1-44 Effect of Hardwall and Treated Ejectors on Peak PNL Suppression of Convoluted Suppressors, Scaled to 1.27 m (50 in.) Equivalent Diameter

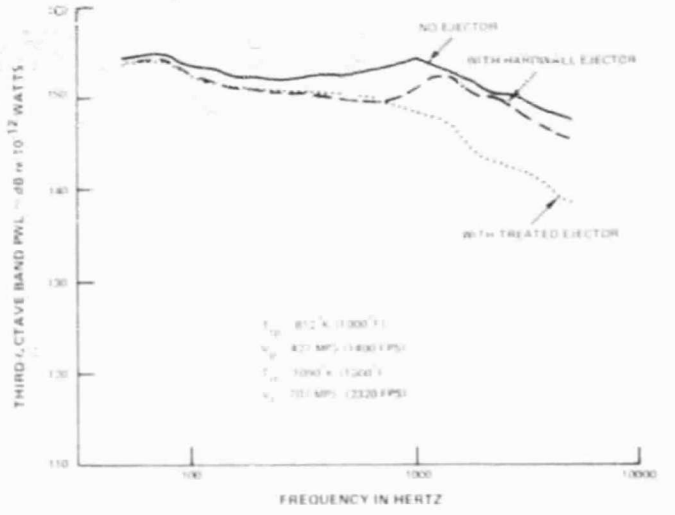

Figure 5.1-45 Effect of Hardwall and Treated Ejectors on PWL Spectra of Convoluted Suppressors, 1.2 Area Ratio, Scaled to 1.27m (50 in.) Equivalent Diameter

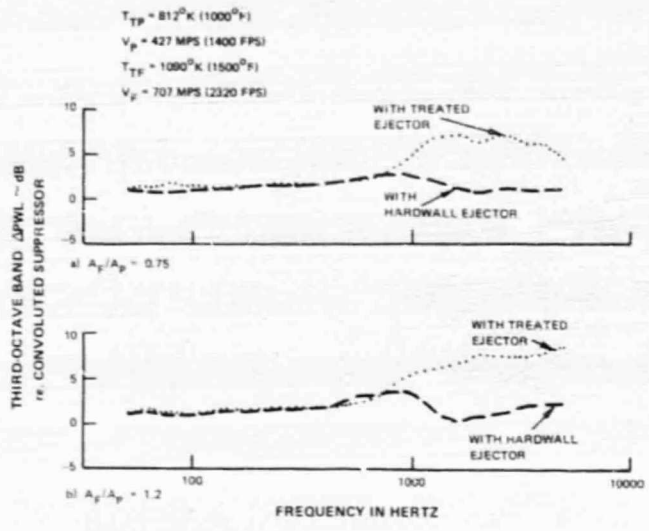

Figure 5.1-46 PWL Reduction of Convoluted Suppressors Due to Hardwall and Treated Ejectors, Scaled to 1.27m (50 in.) Equivalent Diameter

5.1.4 Data Correlations

Three special correlations developed using the jet noise power level data obtained during this program are presented in this section.

The correlations quantify the noise trends produced by the DBTF exhaust systems and focus on three topics:

- Acoustic power levels and perceived noise levels of the unsuppressed coannular nozzles defined in terms of fan to primary velocity and area ratios.
- Acoustic power level of all configurations in terms of suppressor geometric parameters.
- Acoustic power level of all configurations in terms of jet plume velocity profile measurements.

5.1.4.1 Correlation of Unsuppressed Coannular Nozzle Noise

Since the unsuppressed coannular nozzle produced significant noise reductions relative to the synthesis, it is desirable to correlate the results in a general manner that adequately describes the overall noise characteristics of the nozzle system. A general correlation of the unsuppressed coannular nozzle noise data is presented in this section. The results show that for $V_f/V_p > 1$, the noise power level, when corrected for fan stream temperature, can be represented as a function of fan stream velocity along a family of nearly straight lines of constant V_f/V_p. The effect of V_f/V_p and A_f/A_p are then accounted for by empirically derived normalizing factors.

The power level normalization factors were also used to coliapse the peak PNL data, the results being generally similar to those of the PWL correlation.

Figure 5.1-47 illustrates the power level along lines of constant fan stream temperature for all the values of primary stream velocity run during the tests of the unsuppressed coannular nozzle having $A_f/A_p = 0.75$ including V_p of 305, 402, 427, 500, 539 and 610 mps. The power levels stratify along constant fan stream temperature lines, especially at the higher values of fan velocity. This indicates that at the higher fan velocities, the fan flow is responsible for the dominant portion of the overall jet noise. Under these conditions, the use of a fan stream temperature (or density) normalizing parameter proved useful in collapsing the noise levels along a single line (i.e., removing the effect of fan temperature). The parameter used for this purpose is the fully expanded ratio of fan stream density to ambient density raised to an exponent which varies with jet velocity, where $\Delta PWL = 10 \log_{10} (\rho_f/\rho_a)^{\omega}$ is added to the noise level of a jet at elevated temperature to equal the noise level of an ambient temperature jet. Application of this parameter has been shown to provide an excellent collapse of subsonic jet mixing noise levels in Ref. 10. The exponent varies from -1 at low velocities to a value of +2 at high jet velocity as shown in Figure 5.1-48. This normalization applied to the convergent reference nozzle data produced an excellent collapse of the power level as shown in Figure 5.1-49. The curve shape closely simulates the results in Ref. 10 when the referenced data are converted to a power level basis. At low velocities the slope is approximately 8, then increases to 11.5 between 305 and 610 mps, and decreases at velocities above 610 mps. The 11.5 slope arises from the effects of convective amplification which becomes increasingly important above 305 mps. The only data points that do not collapse are for low temperature, supersonic velocity fan operating conditions that contain large amounts of shock screech energy. The otherwise excellent data collapse indicates that, on a power level basis, the jet noise is dominated by mixing noise rather than shock related noise sources. Applying the same normalizing factor based on fan jet density and velocity to the unsuppressed coannular nozzle noise levels results in the collapsed noise power curves in Figure 5.1-50, each curve representing a constant primary velocity. At $V_p = 305$ mps, the data collapses well over the entire velocity range, except for the two low temperature supersonic velocity fan points which contain shocks similar to those in the convergent nozzle data. Above 305 mps, the shape of the curve is similar to that of the convergent nozzle data (i.e., a reasonably straight line at velocities between 305 and 610 mps, and decreasing slope between 305 and above 620 mps). The slope of 8.5 in the mid-velocity range is less than that of the convergent nozzle data and is due to the jet noise from the primary stream becoming increasingly important at decreasing fan velocities. At $V_p = 402$ mps, the slope is 7, indicating a further contribution of the primary jet to the total jet noise. At $V_p = 427$ mps, the slope is 6.3, and it is seen that the normalization does not work at $V_f < V_p$ due to the high contribution of the primary jet to the total jet noise. At a velocity of 500 mps, the influence of the primary stream on the noise tends to obscure the slope in the 305-610 mps V_p range, and at $V_p = 539$ and 610 mps, the density normalization, for the limited data region tested, does not collapse the data due to the high contribution of primary jet noise. However, extrapolation of the data curves to higher fan velocity indicates a collapse at large V_f. Figure 5.1-50 shows the normalized power level curves for all primary velocities where the shaded regions represent the uncertainty in the density normalized curves due to non-collapse of the data. The correlation was established to represent the data at values of $V_f/V_p > 1.0$. The uncertainty exists for only a limited region of the correlation where the primary velocity is over 500 mps. The large uncertainty is ± 1.5 dB.

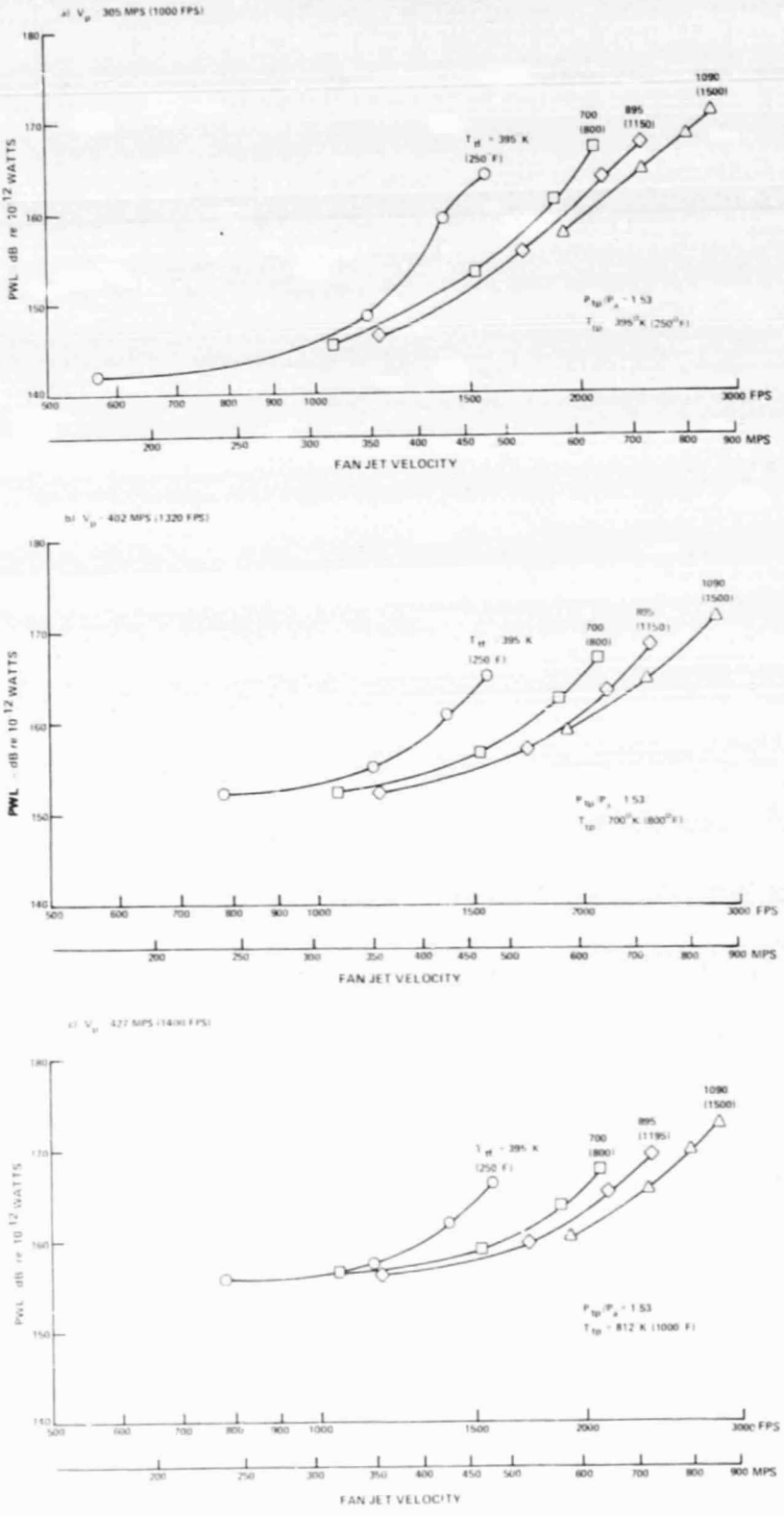

Figure 5.1-46 Effect of Fan Stream Temperature on PWL of Coannular Unsuppressed Nozzle, 0.75 Area Ratio, Scaled to 1.27m (50 in.) Equivalent Diameter

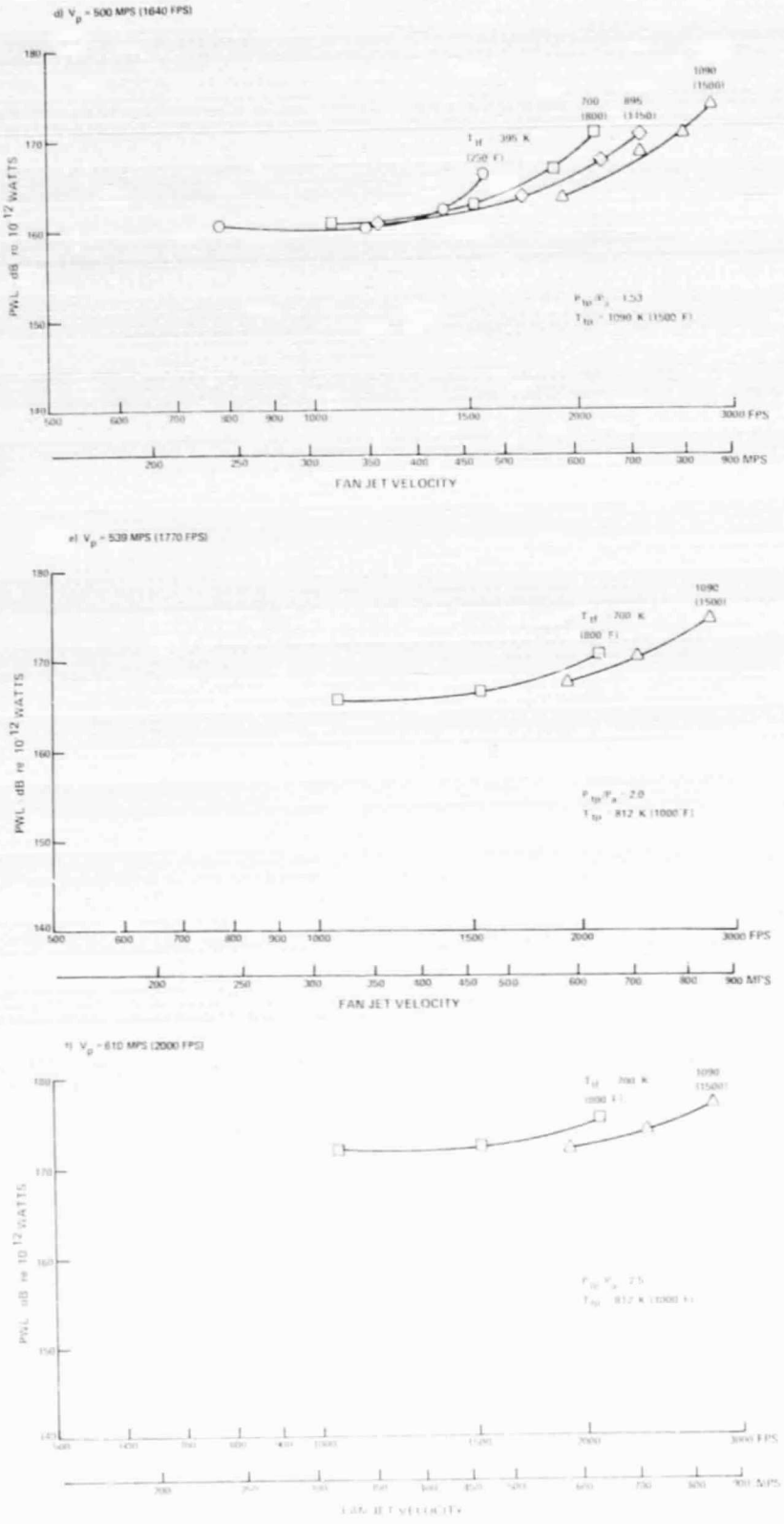

Figure 5.1-47 Effect of Fan Stream Temperature on PWL of Coannular Unsuppressed Nozzle, 0.75 Area Ratio, Scaled to 1.27m (50 in.) Equivalent Diameter (Concluded)

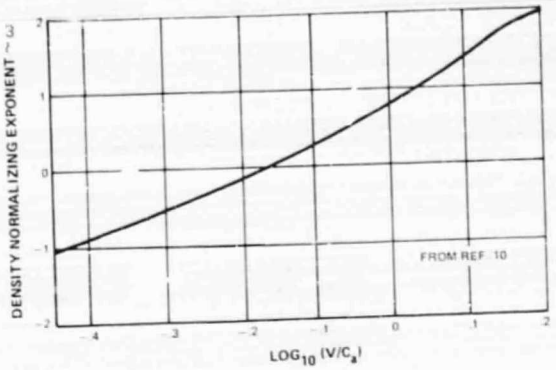

Figure 5.1-48 Density Normalizing Exponent

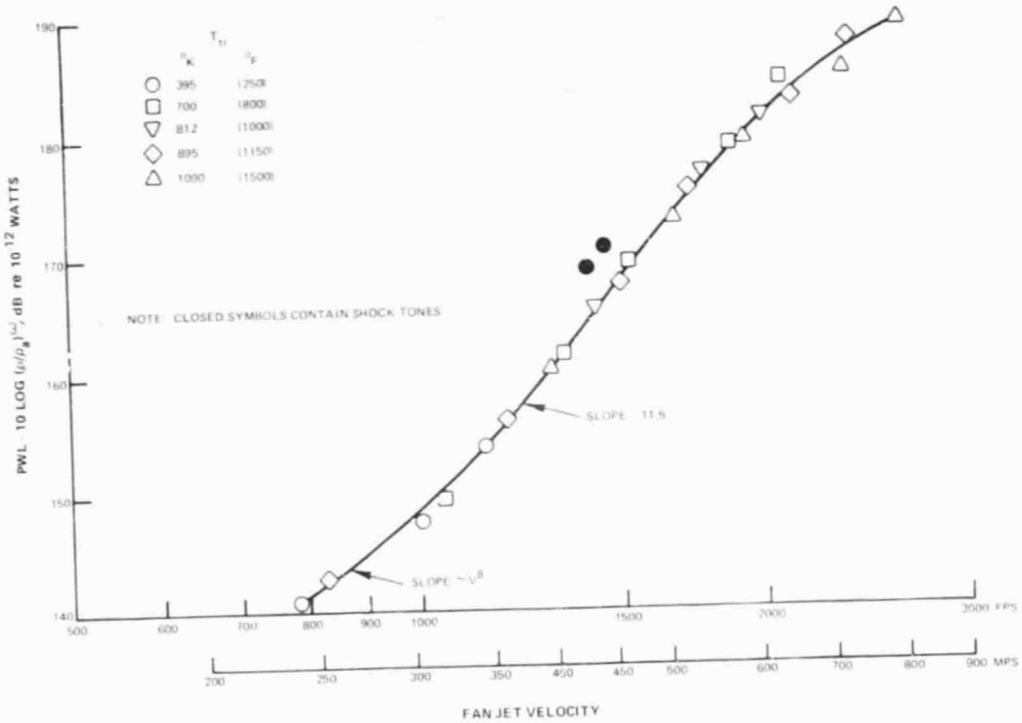

Figure 5.1-49 PWL of Convergent Nozzle Normalized for Jet Temperature, Scaled to 1.27m (50 in.) Equivalent Diameter

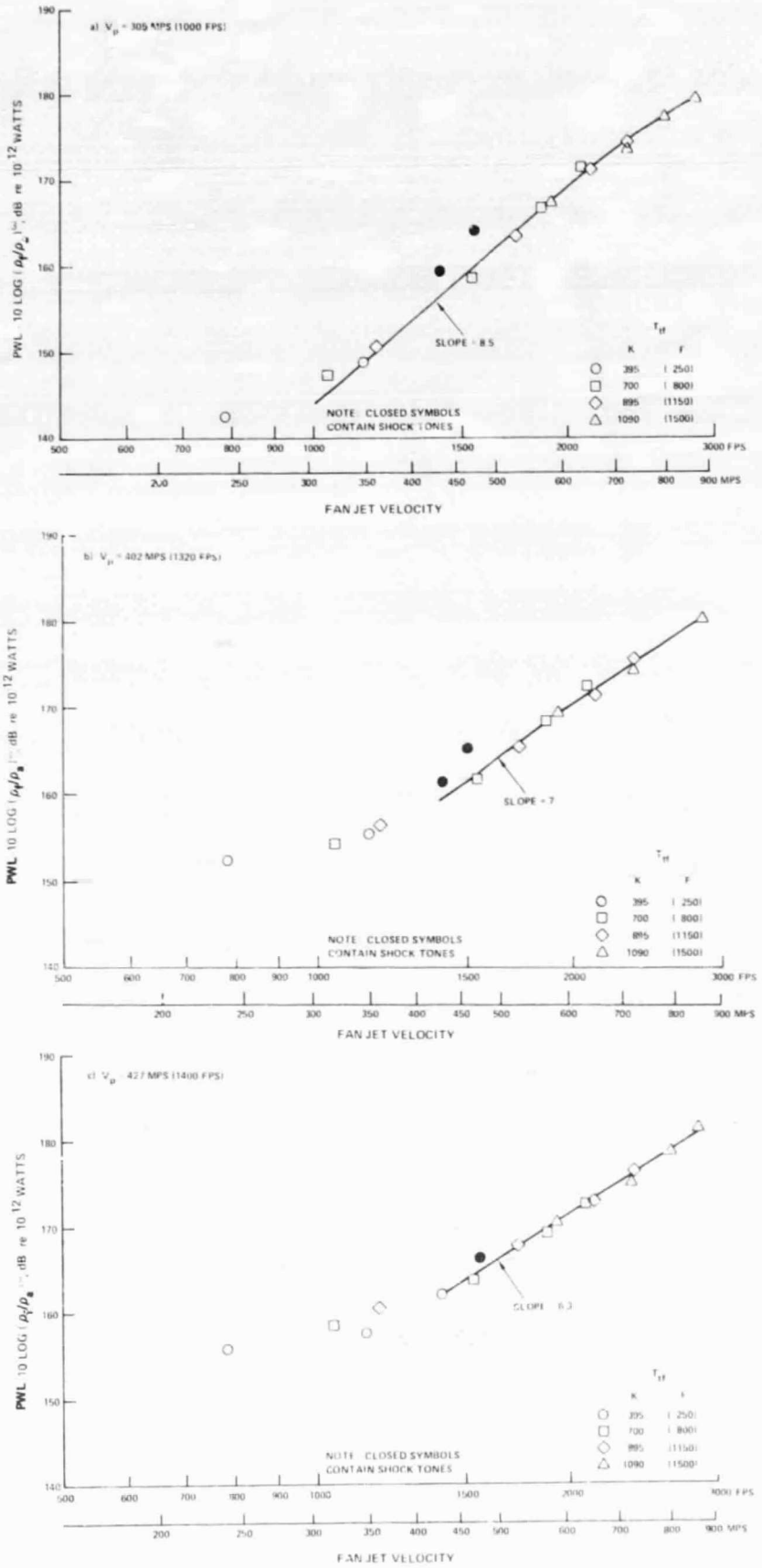

Figure 5.1-50 PWL of Coannular Unsuppressed Nozzle Normalized for Fan Jet Temperature, 0.75 Area Ratio, Scaled to 1.27m (50 in.) Equivalent Diameter

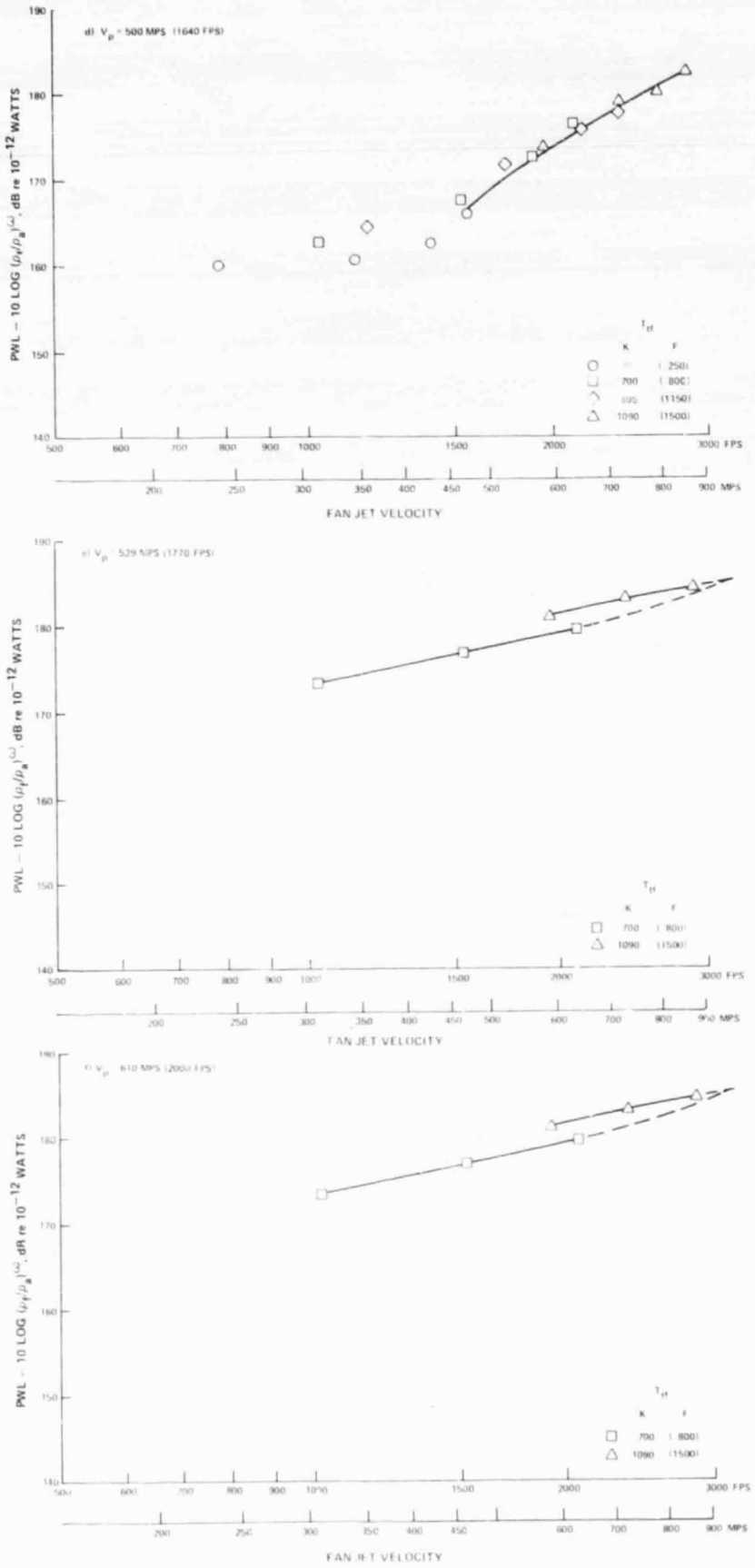

Figure 5.1-50 PWL of Coannular Unsuppressed Nozzle Normalized for Fan Jet Temperature, 0.75 Area Ratio, Scaled to 1.27m (50 in.) Equivalent Diameter (Concluded)

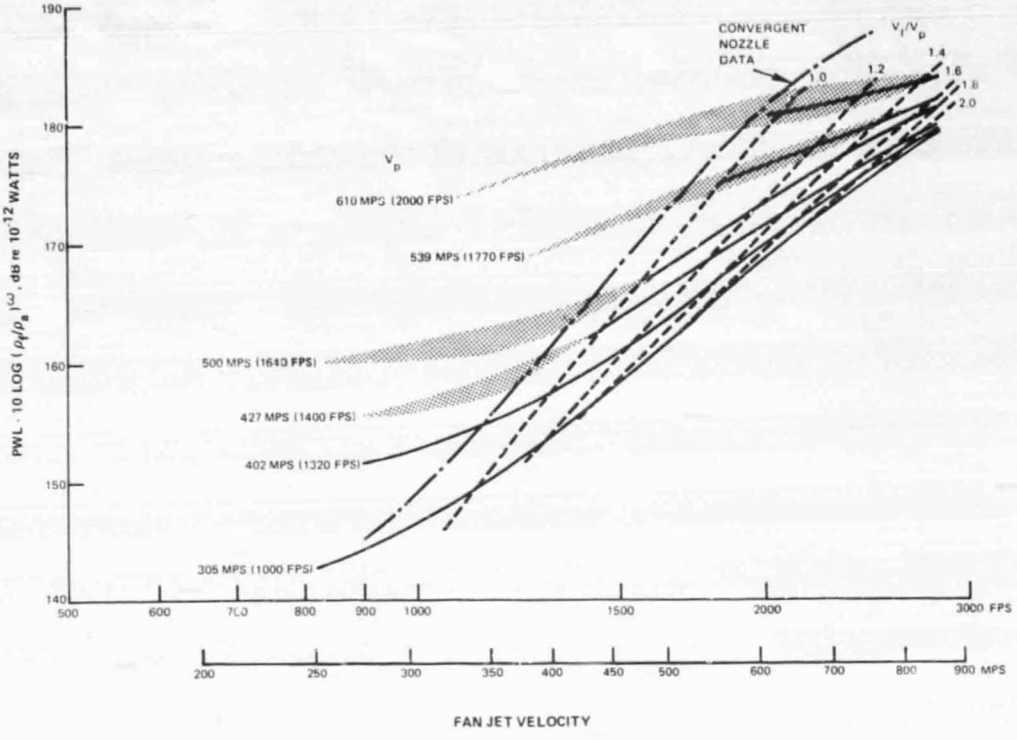

Figure 5.1-51 Composite Map of Density Normalized PWL of Coannular Unsuppressed Nozzle at All Tested Primary Velocities, 0.75 Area Ratio, Scaled to 1.27m (50 in.) Equivalent Diameter

To further enhance the data correlation, the effect of velocity ratio, V_f/V_p, was established. This was accomplished by locating points on each constant primary velocity line (on Figure 5.1-51) corresponding to V_f/V_p of 1.0, 1.2 . . . .2.8. The lines best fitting these points are shown as dashed lines in Figure 5.1-50 and by themselves in Figure 5.1-52 for more clarity.

Also shown on Figure 5.1-51 is the normalized power level curve from the convergent nozzle data. This line represents the ideal noise power level of a coannular nozzle having equal fan and primary velocities. Note that it lies from 2 to 5 dB above the coannular nozzle line having V_f/V_p = 1.0, thus indicating that the coannular nozzle under the conditions of equal primary and fan velocities produces less noise than a single jet. Two major factors may contribute to this result. The first factor is the differences in geometry. The presence of the primary stream tailpipe that separates the fan and primary streams can produce significant differences in the exit velocity profile compared to the convergent nozzle. In particular, an intermediate shear layer caused by the boundary layer growth inside of the primary nozzle and the fan nozzle inner diameter surface is present and could affect the actual mixing process. In addition the two streams exhaust to ambient at different axial locations, and this will also affect the mixing process relative to a single jet. The second factor is that the normalization for density was based strictly on the fan stream conditions. No adjustments could be made to correct for different primary stream densities as data were not obtained that would allow definition of the effect of this parameter.

In any event, the correlation of the coannular nozzle noise levels clearly shows that at all fan velocities, an increase of V_f/V_p causes substantial noise reductions up to $V_f/V_p = 2.0$. Increases of V_f/V_p above 2.0 causes only small additional noise reductions.

Using the results in this form enables determination of the noise reduction due to the inverted profile effect (i.e., $V_f > V_p$), knowing only the fan velocity and the fan to primary velocity ratio (for a configuration having $A_f/A_p = 0.75$). Since the V_f/V_p lines of Figure 5.1-52 are well behaved, the data correlation has been extended one additional step, which is the determination of the normalizing factor necessary to collapse all of the data to a single line. It was postulated that a data collapse could be accomplished by using only V_f/V_p as a parameter. Figure 5.1-53 shows plots of ΔPWL vs 10 log V_f/V_p for four different fan velocities, in order to determine the behavior over a wide range of fan velocity. These ΔPWL were determined by subtracting the PWL at each value of V_f/V_p from the PWL value at $V_f/V_p = 1.0$. These data collapsed reasonably well. The correlating parameter of ΔPWL based on the mean line through the points is 10 log $(V_f/V_p)^m$ as shown in Figure 5.1-54, where

$$m = \frac{\Delta \text{ PWL (Rel. to } V_f/V_p = 1)}{10 \log (V_f/V_p)} = -3.75 \left(\frac{1}{1 + 0.0127 X^5} \right)^{1/5}$$

Application of this parameter results in the final normalized power level curves shown in Figure 5.1-55. The maximum deviation of ± 1 dB from a mean line representing the curves indicates that the normalizing parameter adequately describes the effect of the fan to primary velocity ratio for this configuration having $A_f/A_p = 0.75$. An important observation that can be made from this correlation, and in particular from the expression for m shown above, is that negligible additional suppression (<½ dB) is gained for V_f/V_p greater than 2.0. This indicates that if the primary stream were turned off, i.e., $V_f/V_p = \infty$, the suppression would be approximately the same as for $V_f/V_p = 2.0$. In other words, a single jet exiting as an annulus surrounding a zero length plug centerbody would be expected to produce approximately the same suppression as a coannular flow of $V_f/V_p = 2.0$ if the annulus in each case is similar, and if the single jet were provided with a small amount of leakage flow to prevent a severe overexpansion shock system and its associated shock noise.

The same formula for m determined for the 0.75 area ratio nozzle was applied to the data produced by the second unsuppressed coannular nozzle, having $A_f/A_p = 1.2$. The normalized power level curves showed reasonable collapse as shown in Figure 5.1-56. A comparison of the normalized curves for the 0.75 and 1.2 area ratio unsuppressed coannular nozzle configurations shows that the noise of the 1.2 configuration is 2-3 dB higher. It also shows that the normalization tends to over-compensate the noise of the 1.2 area ratio nozzle at the higher ratios of V_f/V_p, implying that the inverted profile effect is less as A_f/A_p increases from 0.75 to 1.2.

The apparent effect of A_f/A_p was determined by using Δ PWL = 10 $\log_{10} (A_f/A_p)^n$, where for simplicity and due to the limited data, the area ratio and velocity ratio are considered to act independently. The value of n required to collapse the two sets of data was found to be equal to 1.0. The final data normalization using mean lines for both sets of data is illustrated in Figure 5.1-57.

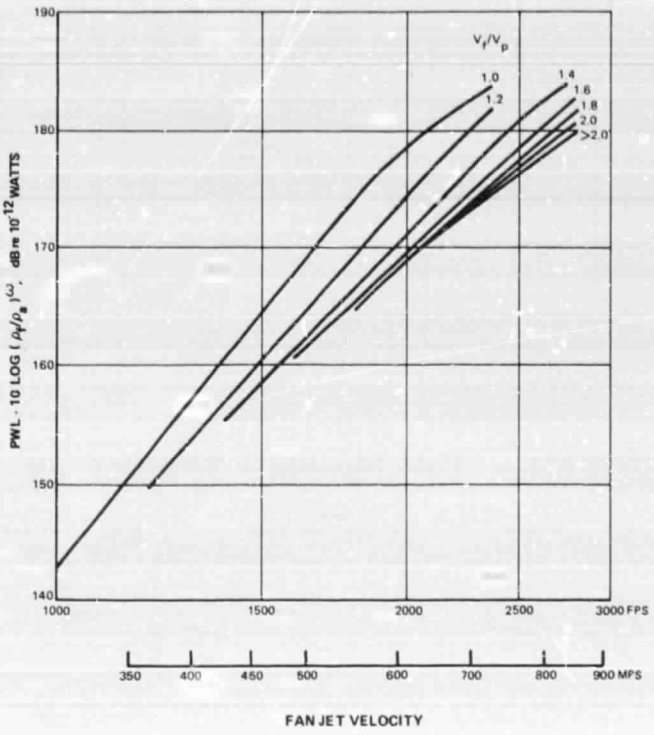

Figure 5.1-52 Effect of Fan to Primary Velocity Ratio on Normalized PWL of Coannular Unsuppressed Nozzle, 0.75 Area Ratio, Scaled to 1.27m (50 in.) Equivalent Diameter

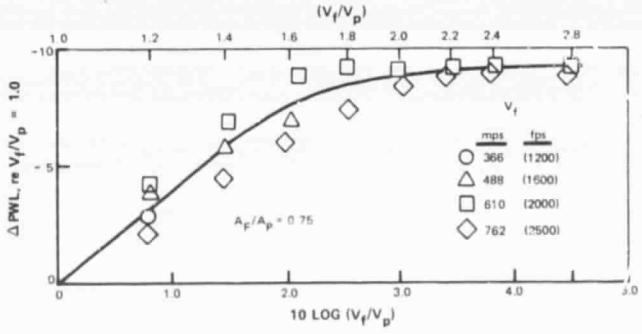

Figure 5.1-53 Decrease in PWL of Coannular Unsuppressed Nozzle Due to Fan to Primary Velocity Ratio Relative to Velocity Ratio of One. 0.75 Area Ratio, Scaled to 1.27 m (50 in.) Equivalent Diameter.

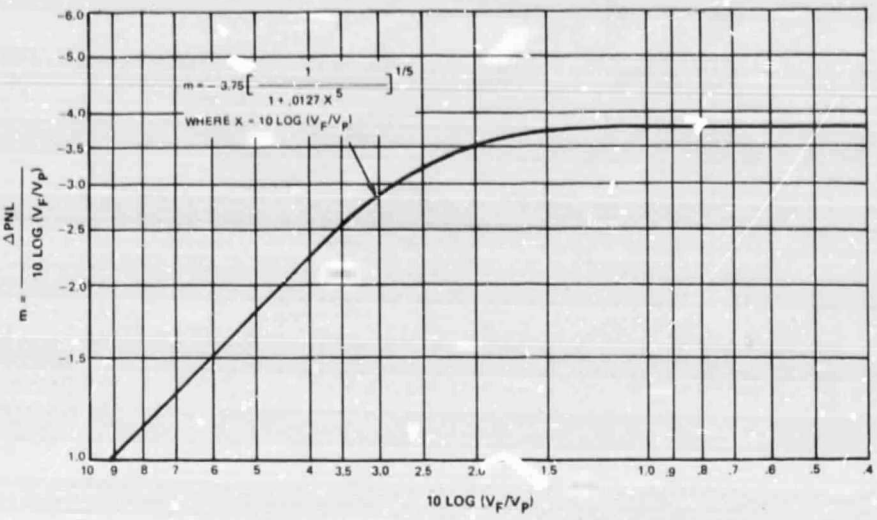

Figure 5.1-54 Exponent to Normalize Effect of Fan to Primary Velocity Ratio for PWL of Coannular Unsuppressed Nozzle

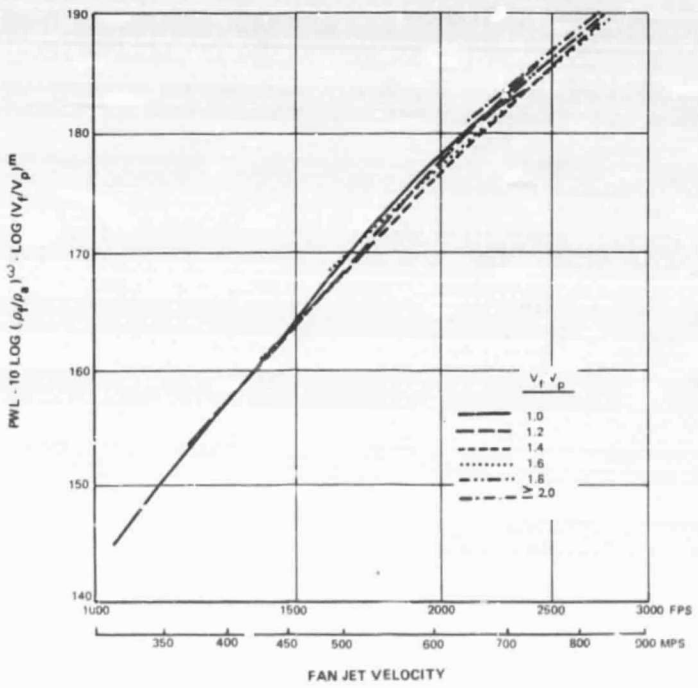

Figure 5.1-55 Normalized PWL of Coannular Unsuppressed Nozzle, 0.75 Area Ratio, Scaled to 1.27m (50 in.) Equivalent Diameter

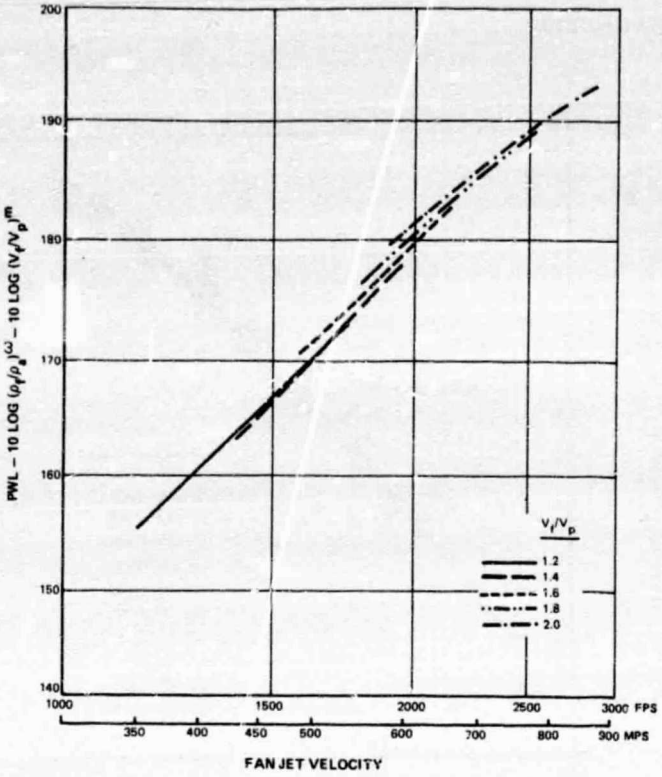

Figure 5.1-56 Normalized PWL of Coannular Unsuppressed Nozzle, 1.2 Area Ratio, Scaled to 1.27m (50 in.) Equivalent Diameter

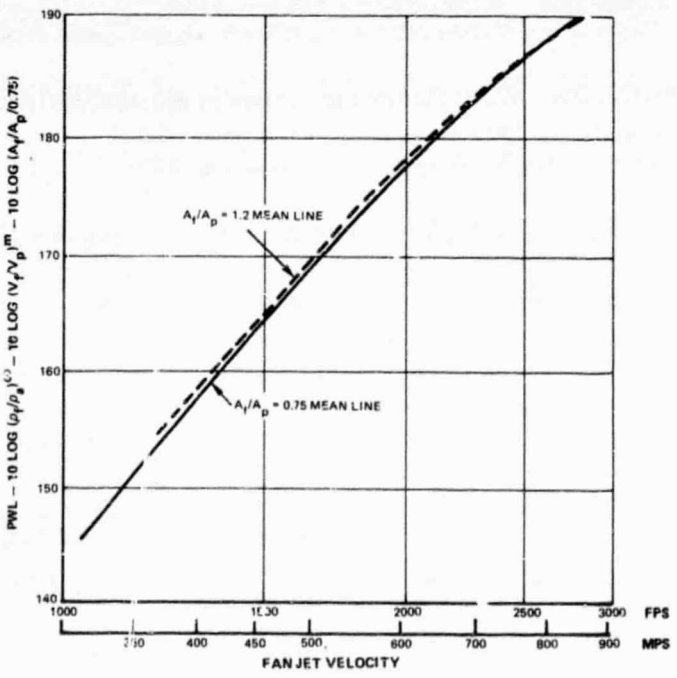

Figure 5.1-57 Normalized PWL of All Coannular Unsuppressed Nozzles, Scaled to 1.27m (50 in.) Equivalent Diameter

C-2

Figure 5.1-58 shows all the measured PWL data for the V_f/V_p operating conditions normalized by the resulting procedure.

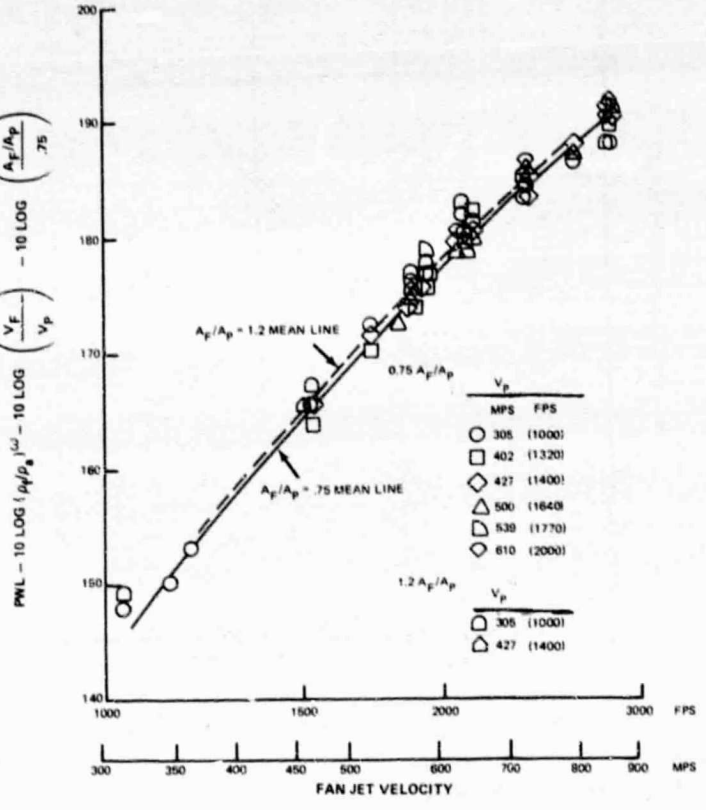

Figure 5.1-58 Comparison of normalized PWL Test Data and Correlation Curves for Coannular Unsuppressed Nozzles, Scaled to 1.27m (50 in.) Equivalent Diameter

The same numerical values of correlating parameters used to correlate the power level data were used to normalize the perceived noise level data results shown in Figure 5.1-59. The data spread is similar to that of the power level normalization.

This correlation procedure produced a reasonable collapse of the noise levels of the inverted velocity profile coannular nozzles. However, for airplane mission studies, a prediction procedure is required which includes the estimation of SPL spectral characteristics at all angles. This more sophisticated prediction requirement is needed in order to allow EPNL calculations for flyover conditions. In order to develop a prediction procedure of this type, consideration of the noise generation process is necessary. The total noise spectrum is comprised of low frequency noise related to the properties of a downstream merged jet, and high frequency noise related to the properties of the annular fan stream close to the nozzle. The use of simple parameters based on ideally expanded properties of each stream at the nozzle exit to correlate a noise level representing the sum of the noise from the two sources is considered to be too simple a basis for providing an accurate method to normalize the data. Preliminary correlations based on dividing the measured SPL spectra into separate high and low frequency noise components indicate that a satisfactory prediction procedure could be developed by correlating the low frequency and high frequency noise individually against parameters better representing the noise generation in the two separate regions.

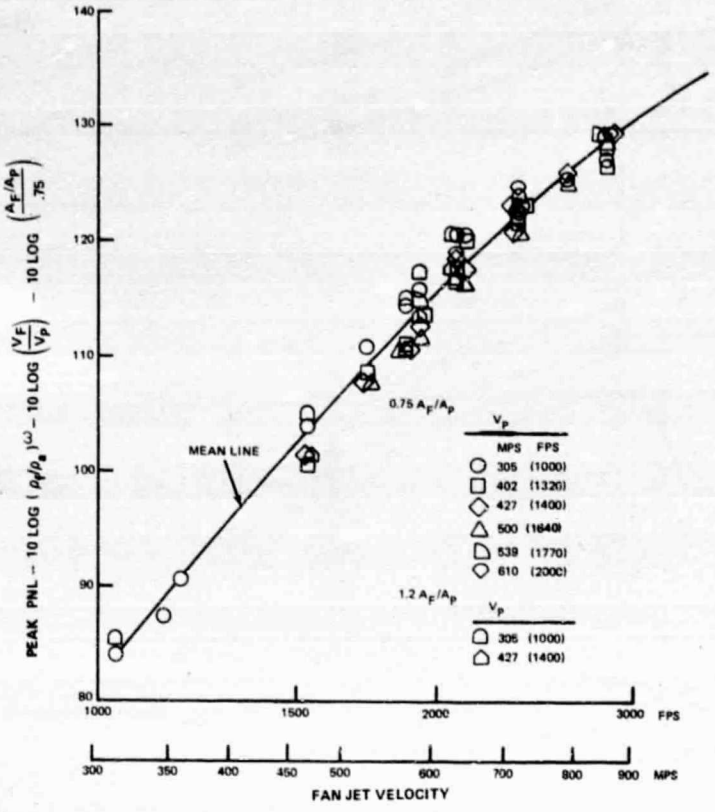

Figure 5.1-59 Comparison of Normalized Peak PNL Test Data and Correlation Curve for Coannular Unsuppressed Nozzles, Scaled to 1.27 m (50 in.) Equivalent Diameter

5.1.4.2 Suppressor Geometry Correlation

This correlation is shown in Figure 5.1-60 for a variety of flow combinations. The geometric parameter selected is the projected area ratio, defined as the total area enclosed by a circle surrounding the outermost perimeter of the fan nozzle (Suppressor Projected Area), divided by the actual fan exhaust flow area (Flow Area). When the fan velocity is substantially higher than the primary velocity, this parameter represents a rough measure of the cross sectional area available for the high velocity fan flow to mix with both the ambient and low velocity primary exhaust flows and thus to decay to lower velocities downstream. This parameter is analogous to the suppressor area ratio parameter used to correlate noise suppression of turbojet suppressors (Ref. 16). The noise levels for the projected area ratio of 1.0, (i.e., the single jet) was obtained by scaling the reference convergent nozzle noise levels to a single jet having the same area as the fan area of the coannular nozzle. The correlation between noise power and the area ratio parameter suggests that the suppressor-like behavior of the unsuppressed coannular nozzle, when compared to a convergent nozzle, is related to the ratio of the fan area to total area, and that this is the parameter which controls the subsequent mixing with both the lower velocity primary exhaust and the ambient air.

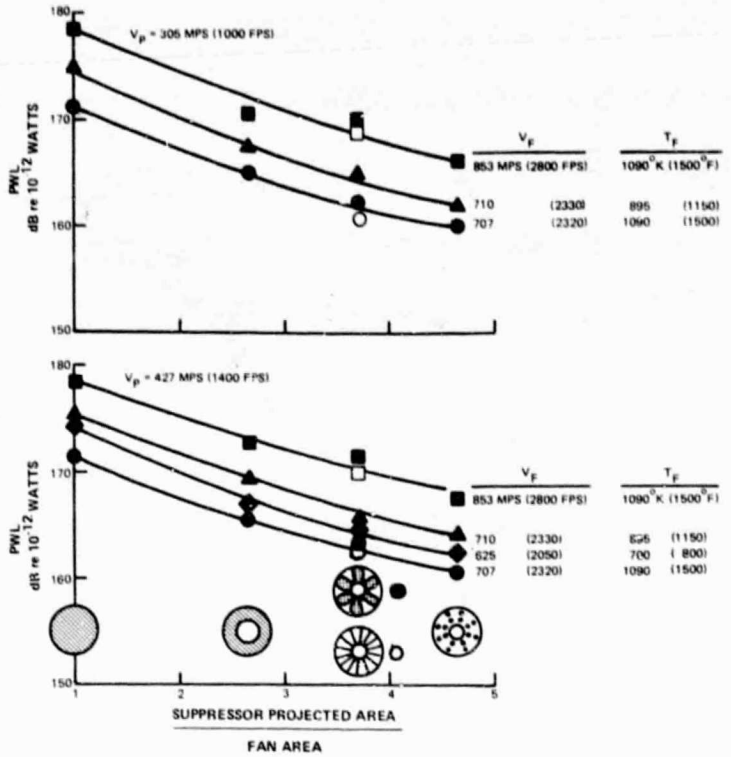

Figure 5.1-60 Correlation of PWL and Projected Area Ratio for Coannular Nozzles, 0.75 Area Ratio, Scaled to 1.27m (50 in.) Equivalent Diameter

Based on this limited correlation, an inference could be made relating to the possibility of obtaining the inherent coannular nozzle noise reductions for $V_f/V_p > 1$ exhaust profiles through the use of a large centerbody plug in place of a low velocity primary stream. Data contained in Ref. 12 indicates that a single stream annular nozzle with no centerbody generally produces noise reduction consistent with the coannular nozzle having large V_f/V_p. However, results of Ref. 13 showed that a single stream annular nozzle surrounding a large, long plug centerbody produced only a moderate amount of suppression compared to the coannular noise reductions obtained during this program. Consideration of the flow aerodynamics would explain these results. Whereas the coannular jet provides for mixing of the high velocity fan flow jet with the ambient air on the jet outer diameter and with low velocity primary flow on the jet inner diameter, the presence of a large centerbody plug in place of the low velocity inner flow would severely reduce the mixing on the jet inner diameter. Thus, the coannular noise/geometry correlation presented in this section would be optimistic if used to predict the suppression of an annular jet surrounding a large, long plug centerbody.

5.1.4.3 Velocity Profile Correlation

The third correlation was developed to relate the noise to the jet plume characteristics of the various configurations. The measurements of velocity profiles at the axial position of the ejector exit plane (whether or not an ejector was used), shown in Figure 5.1-61 for a typical operating point, were used in conjunction with the measured noise power levels to derive a correlation between the noise and the flowfield characteristics of the various configurations. The basis for this correlation is the work of Chen (Ref. 17) in which he demonstrated that jet noise can be approximated by a spatial integration across the jet volume of

a large number of radiating noise elements (or turbulent eddies). Each of the elements generates noise approximately as the eighth power of the local mean velocity. The approach used in this program was to determine the maximum velocity behind both the primary and fan stream nozzle at the ejector exit plane station, and add these values logarithmically with an appropriate area weighting factor relating to the fan to primary stream area ratio. The velocity profiles were highly dependent upon the nozzle configuration at each operating condition, as would be expected due to the large influence of nozzle suppressor geometry upon the mixing and subsequent velocity decay of the jet exhausts. This is illustrated by the profiles presented in Figure 5.1-61. The correlation of noise level with the velocity parameter for all points at which profile measurements were made is shown in Figure 5.1-62. The maximum deviation from the mean line was 3 dB; however, 2/3 of the data falls within 1 dB. Extended studies in this area may prove useful in supplementing the understanding of suppressor nozzle behavior.

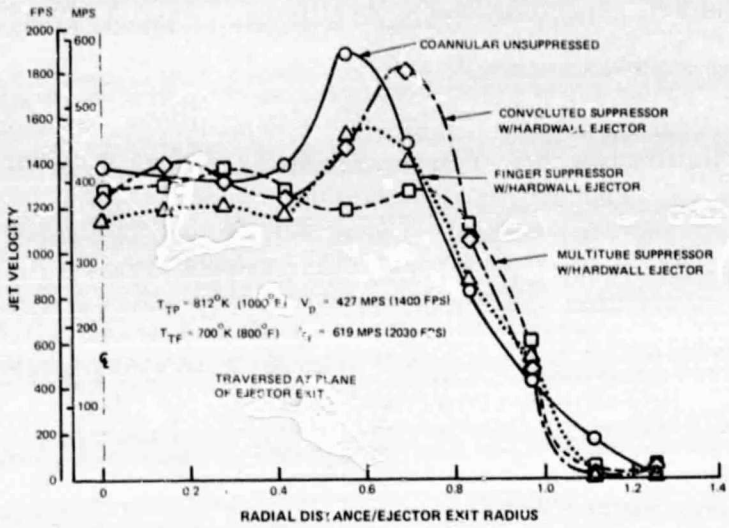

Figure 5.1-61 Exit Velocity Profiles for Various Coannular Nozzle Configurations, 0.75 Area Ratio

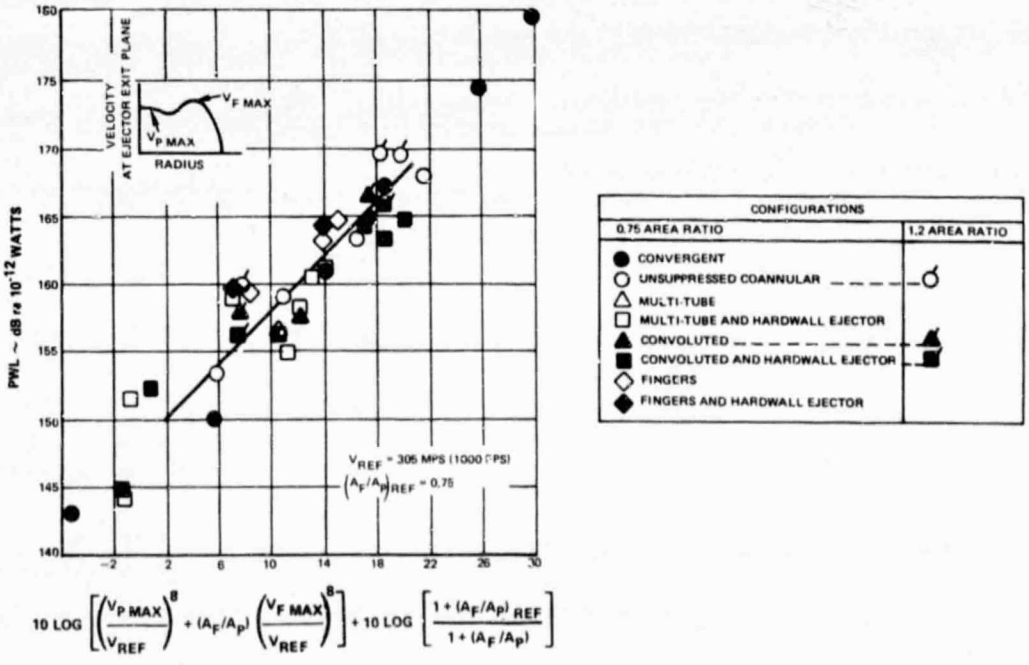

Figure 5.1-62 Correlation of PWL and Velocity Profile Parameter for Coannular Nozzles, 0.75 Area Ratio, Scaled to 1.27 m (50 in.) Equivalent Diameter

5.2 AERODYNAMIC PERFORMANCE

The aerodynamic performance characteristics were obtained simultaneously with the acoustic measurements at each pressure ratio and temperature for all the configurations tested. The aerodynamic performance is defined by the nozzle thrust coefficient, C_V, which is the ratio of actual total thrust generated by the complete exhaust system to the total ideal thrust available. In addition, an array of static pressures on the suppressor configurations was used to aid in diagnosing the flow through the system.

The performance of the various nozzle/suppressor configurations is presented relative to the appropriate unsuppressed coannular nozzle, operating at the same flow conditions. The unsuppressed coannular nozzle is used as a reference configuration since the aerodynamic performance characteristics of a coannular system cannot be directly synthesized from the performance characteristics of a simple convergent nozzle.

The resulting differences between a given test configuration and the unsuppressed coannular nozzle were then compiled, point by point, primarily in terms of fan stream pressure ratio and a smooth mean line carefully established through the data. In some cases, this mean performance level was tempered by cross-correlating with the pressure integrals in the nozzle as well as established differences between other configurations. The large quantity of data on many of the configurations provided a good statistical sampling of the performance levels. All of the data is presented in Volume II of the CDR (Ref. 8). The performance data is used as measured and not adjusted for any full scale effects since the physical full scale exhaust system characteristics have not been established.

The discussion of performance characteristics will cover the following items. The performance of the reference nozzles will be presented first, for both the convergent nozzle which provides a check on the basic facility, and the unsuppressed coannular nozzles which serve as the baselines for all of the suppressor configurations. The characteristics of all the suppressor configurations are then discussed, with the low area ratio ($A_f/A_p = 0.75$) presented first, followed by the larger area ratio ($A_f/A_p = 1.2$) evaluations.

The performance aspects of the ejectors are included in the discussion of the basic nozzle/suppressor rather than in a separate discussion, as in the Acoustic Results (Section 5.1). A brief summary of the flow coefficients for all the models is also included. A special correlation presenting the impact of acoustical treatment is then discussed, prior to a complete summary of the aerodynamic performance relating all the test configurations.

5.2.1 Convergent Nozzle

The convergent nozzle thrust coefficients are shown in Figure 5.2-1 for all the measured points, at temperatures from 395°K to 1090°K. These data do not indicate any discernible trend with variation in temperature, and therefore, a single mean line representing the performance level was established. The level shown is consistent with that generally accepted for a convergent nozzle, when the installation is considered. The installation in this test had a relatively long distance and large amount of internal surface area between the instrumentation station and the nozzle exit. The internal friction losses, therefore, become significant, particularly at the low pressure ratios. This is reflected in the high lapse rate at the low pressure ratios. The losses diminish in importance at the high pressure ratios, where they are small compared to the nozzle thrust.

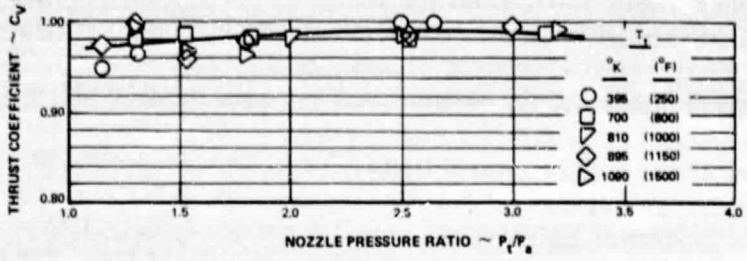

Figure 5.2-1 Aerodynamic Performance of Reference Convergent Nozzle

5.2.2 Unsuppressed Coannular Nozzles

The performance levels of the unsuppressed coannular nozzles are presented in Figure 5.2-2 for all the measured points. As indicated, there was a large amount of data generated with these nozzles, since they were baseline configurations. All of the test conditions simulated with the suppressor configurations were duplicated with the baseline units, plus additional points to ensure a thorough and complete understanding of the baseline configurations. As with the convergent reference nozzle, no significant trend consistent with stream temperature was observed, and therefore, a single smooth mean line was used to represent the baseline performance levels.

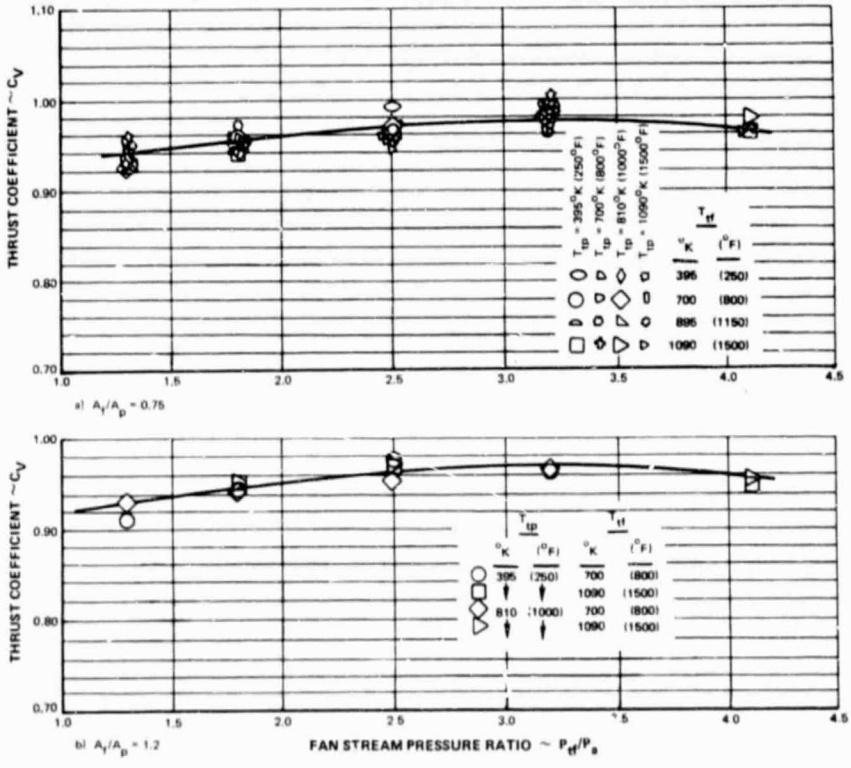

Figure 5.2-2 Aerodynamic Performance of Coannular Unsuppressed Nozzles at a Primary Pressure Ratio of 1.53

The performance of the two unsuppressed coannular nozzles is compared to that of the convergent nozzle in Figure 5.2-3, where the average performance levels of the configurations are illustrated. The performance is presented in terms of mass averaged total pressure ratio so that all the reference nozzles can be meaningfully compared. The difference between the convergent nozzle and the unsuppressed coannular nozzle with an $A_f/A_p = 0.75$ is due to the presence of a convergent-divergent nozzle in the primary stream of the coannular configuration, as well as the increased frictional drag associated with the coannular nozzle. The primary nozzle was selected to reflect requirements of higher design flight speeds associated with a supersonic cruise vehicle. The C-D nozzle ($A/A_{th} = 1.1$) is overexpanded at the low primary pressure ratio (1.53) simulated in this series of tests. The frictional losses are due to the additional wetted areas of the coannular nozzle, downstream of the instrumentation station. As illustrated, when these calculated differences between configurations are accounted for, the performance levels are consistent and acceptable.

Also presented in Figure 5.2-3 is the performance of the higher area ratio ($A_f/A_p = 1.2$) unsuppressed coannular nozzle. As illustrated, it is approximately 0.5% below the 0.75 coannular nozzle. This loss reflects the increased internal duct Mach number associated with increasing the fan stream discharge area with a fixed upstream duct size. The primary stream has an opposite trend, but it is not enough to offset the fan stream losses.

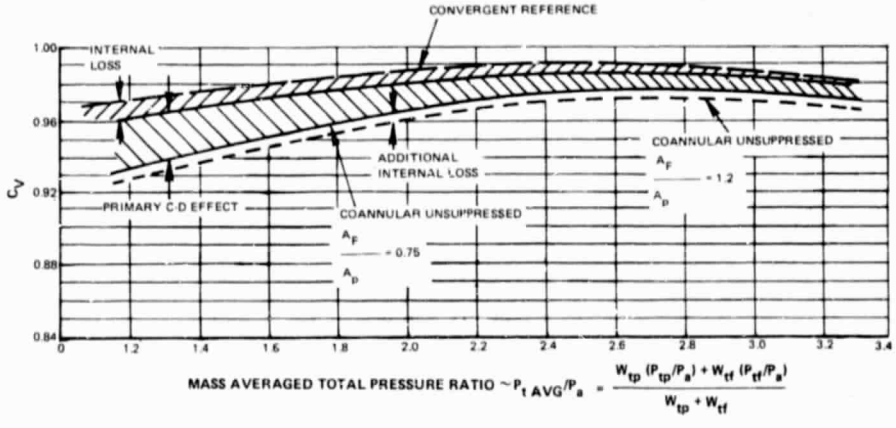

Figure 5.2-3 Comparison of Aerodynamic Performance of Convergent Reference Nozzle, and Coannular Unsuppressed Nozzles at a Primary Pressure Ratio of 1.53

One of the unsuppressed coannular nozzles ($A_f/A_p = 0.75$) was also tested at higher primary pressure ratios to supplement similar tests with suppressor configurations. The performance levels are presented in Figure 5.2-4. The over-all performance level increases slightly when the primary pressure ratio is increased because the primary over-expansion losses, discussed earlier, are reduced. Since the primary overexpansion losses are changing, the data was not included in the comparison of Figure 5.2-3. However, since the data shifts at the higher primary pressure ratios can be entirely attributed to the changes in the overexpansion losses, the data is believed to be consistent with the previous baseline data.

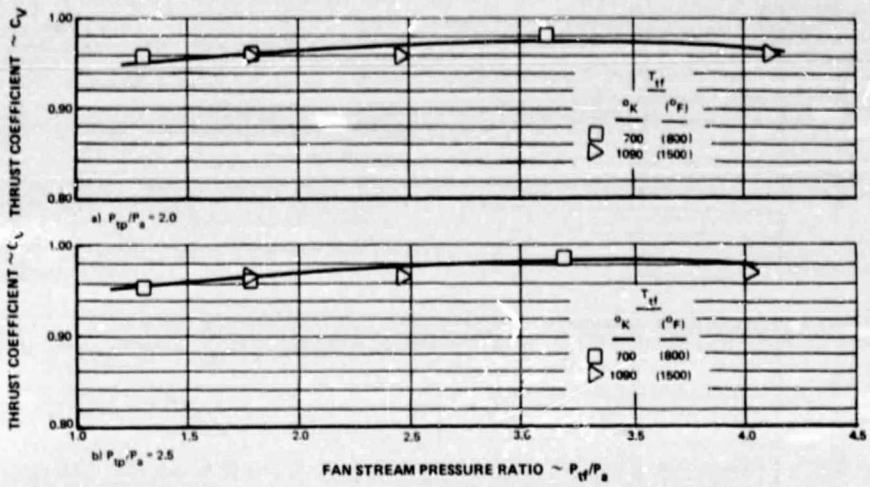

Figure 5.2-4 Aerodynamic Performance of Coannular Unsuppressed Nozzle, 0.75 Area Ratio, at High Primary Pressure Ratios

Since the coannular unsuppressed nozzle demonstrated noise levels well below that which would be predicted using normal methods, the thrust characteristics of this system are of special interest. Mating an ejector to this nozzle would constitute a flight-type exhaust system. The impact of an ejector on the performance characteristics of the unsuppressed coannular nozzle is shown in Figure 5.2-5. At a nominal fan pressure ratio of 2.5 the hardwall ejector provided approximately 1% thrust augmentation to the baseline nozzle. Adding acoustic treatment to the ejector produced a loss of about 0.5%, due primarily to the increased frictional drag. It should be noted that these increments could be improved by slightly altering the relative size and/or position of the ejector. The performance characteristics of both the hardwall and treated ejectors are presented in terms of fan stream jet velocity in Figure 5.2-6. The latter is a transformation from pressure ratio and temperature to jet velocity, and is presented as a convenience to expedite correlation with the corresponding acoustic data.

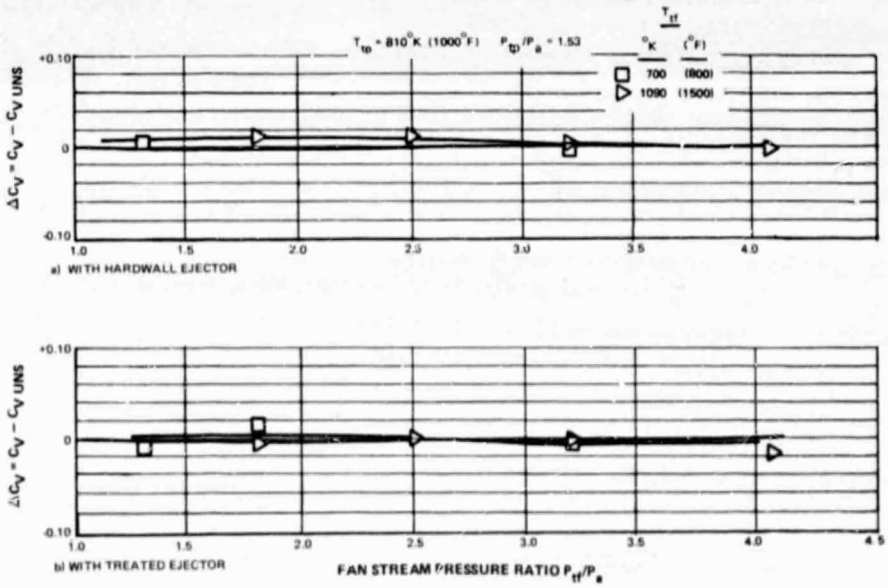

Figure 5.2-5 Effect of Ejectors on Aerodynamic Performance of Coannular Unsuppressed Nozzle, 0.75 Area Ratio

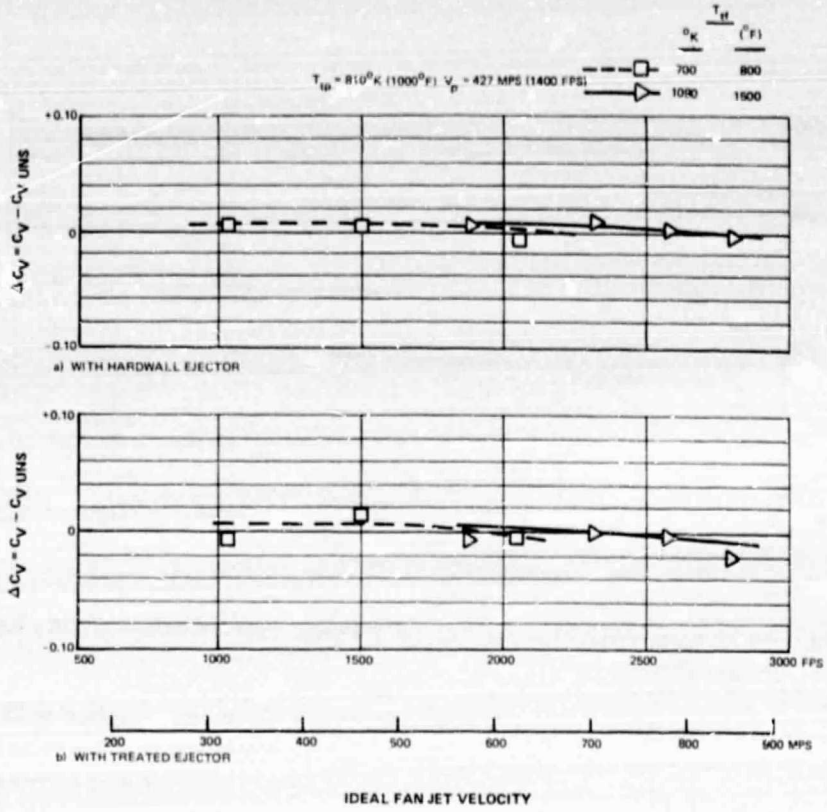

Figure 5.2-6 Correlation of Aerodynamic Performance and Fan Jet Velocity for Coannular Unsuppressed Nozzles, 0.75 Area Ratio

5.2.3 Fan Stream Suppressors

5.2.3.1 Multi-Tube Suppressor

The performance characteristics of the multi-tube suppressor configurations are presented in Figure 5.2-7, relative to the unsuppressed coannular reference nozzle for a typical set of flow conditions. Since fan stream temperature does not appear to significantly affect the performance characteristics, a single line through all of the data establishes the performance change to be a function of the fan stream pressure ratio. The performance loss increases with increasing pressure ratio because the static pressure acting on the base regions of the tube array is decreasing, causing additional drag. At a nominal pressure ratio of 2.5, the basic multi-tube suppressor exhibited a loss of 3.5%. Adding the hardwall ejector reduced the net loss to 2%, reflecting the augmentation gains of the ejector. Adding acoustical treatment to the ejector increases the loss to about 6.5%. This additional loss is due to the increased friction on the internal surface of the ejector, along with an associated change in the ejector pumping characteristics. Since the outer perimeter of the tube array is very close to the inner surface of the ejector (see Figure 3-17, Section 3.2.6), the treatment is being washed by the high velocity discharge from the tubes. The normal frictional loss is magnified by the following factors: the facing sheet of the treatment has a moderately high porosity (30%); and the backing material ("Cerafelt") is penetrable and when subjected

to an axial static pressure gradient, as observed in the ejector, recirculation losses are created in the treated walls of the ejector. The observed overall loss associated with the acoustic treatment could be reduced by: increasing the clearance between the ejector and the tube array, reducing the porosity of the facing sheet, if acceptable from a noise suppressor and exhaust system viewpoint; and compartmentalizing the space behind the facing sheet or adopting a honeycomb backing material tuned to a specific design point. As a convenience, the same performance characteristics are presented in terms of ideal jet velocity in Figure 5.2.8.

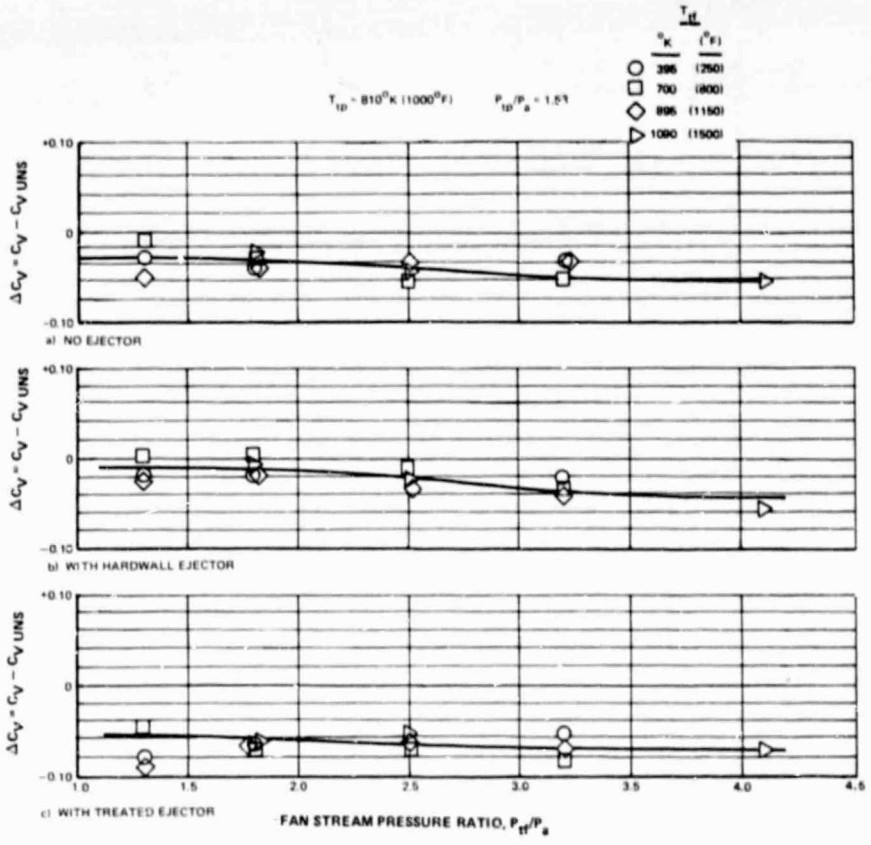

Figure 5.2-7 Aerodynamic Performance of Multi-Tube Suppressor With and Without Hardwall and Treated Ejector Relative to Coannular Unsuppressed Nozzle Without an Ejector, 0.75 Area Ratio

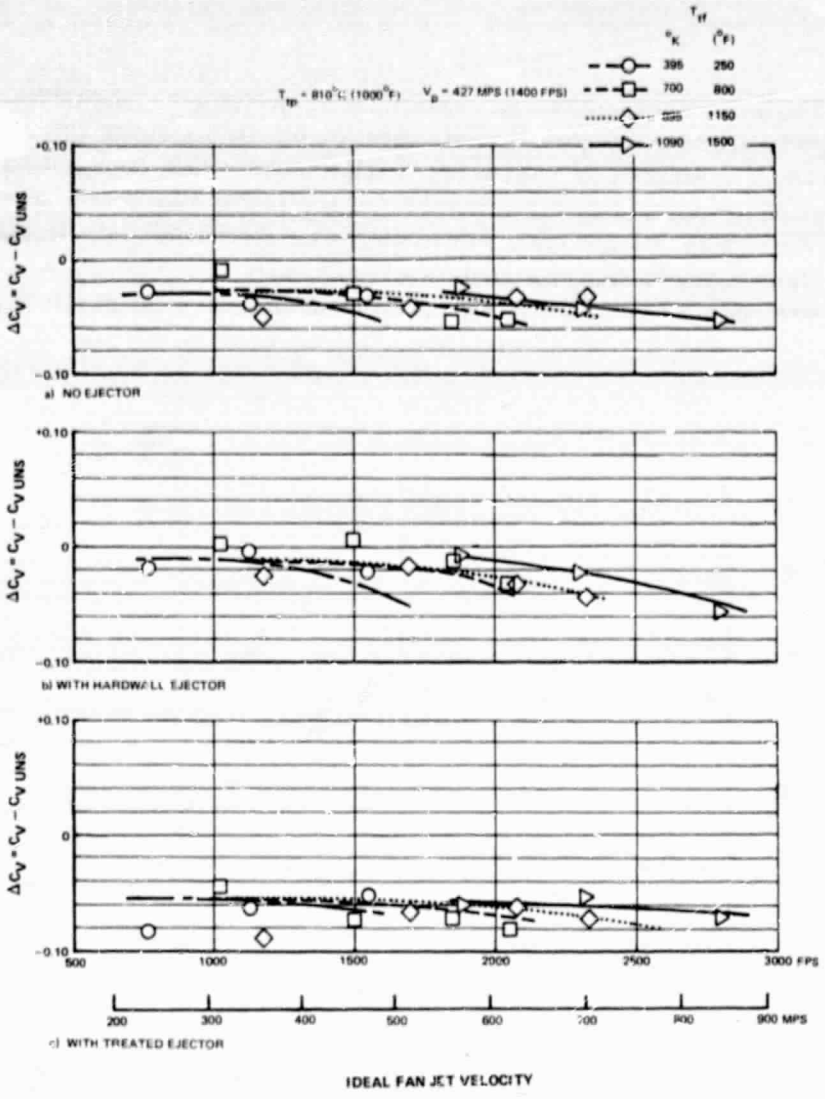

Figure 5.2-8 Correlation of Aerodynamic Performance and Fan Jet Velocity for Multi-Tube Suppressor Relative to Coannular Unsuppressed Nozzle Without Ejector, 0.75 Area Ratio

5.2.3.2 Convoluted Suppressor

The performance characteristics of the convoluted suppressor configurations are illustrated in Figure 5.2-9 relative to the unsuppressed coannular nozzle operating at the same conditions. At a typical fan pressure ratio of 2.5, the basic convoluted suppressor exhibits a loss of almost 1%. The loss is a combination of the internal total pressure losses, associated with a multi-element nozzle, and the base pressure drag generated on the external surface of the convolutions, primarily near the nozzle exit. When the ejector was added, a performance gain of nearly 2% over the unsuppressed nozzle was obtained. This is 3% over the basic convoluted suppressor, representing the ejector augmentation. This augmentation is slightly more

than observed with the multi-tube suppressor. The shift in augmentation between the two suppressor configurations is the result of the changing match between the suppressors and the ejector, which was the same unit in each case. The impact of the ejector on a given suppressor could be altered if the ejector geometry is varied. Adding acoustic treatment to the ejector lowered the performance by approximately 1%, but the resultant convoluted suppressor configuration will still 1% higher than the unsuppressed nozzle. This loss is due to the increased scrubbing drag as well as changes in the ejector pumping characteristics. As illustrated for these three configurations, fan temperature does not appreciably change the performance comparisons; however, increasing fan pressure ratio does cause a slight decay in the performance levels. The same performance characteristics are presented as a function of fan jet velocity in Figure 5.2-10.

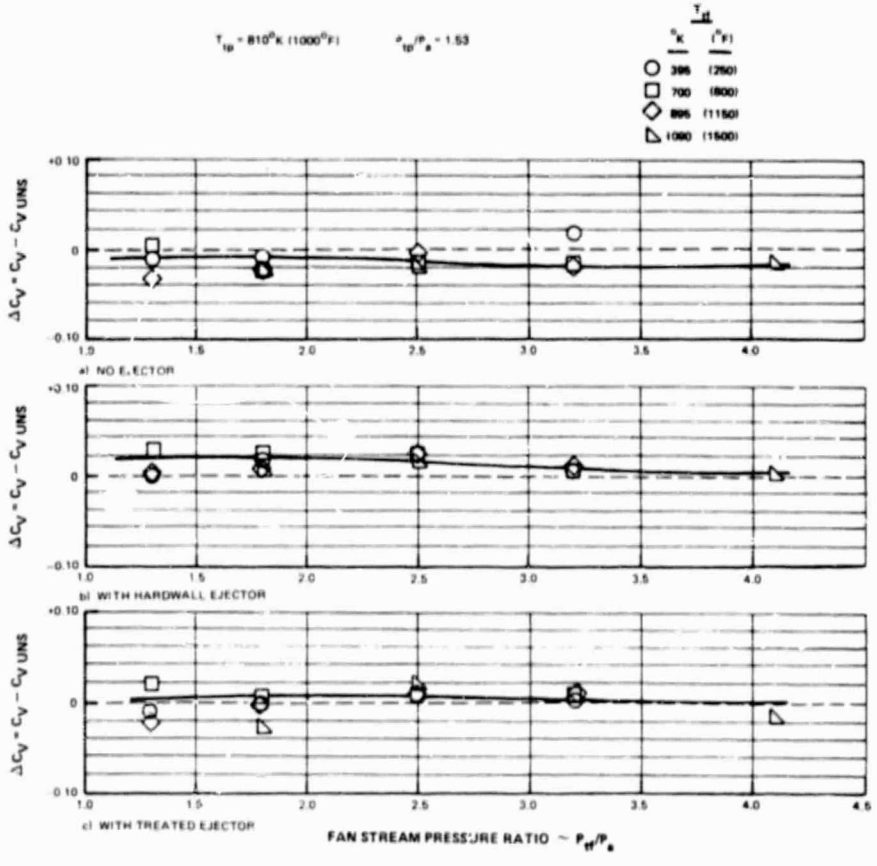

Figure 5.2-9 Aerodynamic Performance of Convoluted Suppressor With and Without Hardwall and Treated Ejector Relative to Coannular Unsuppressed Nozzle Without Ejector; 0.75 Area Ratio

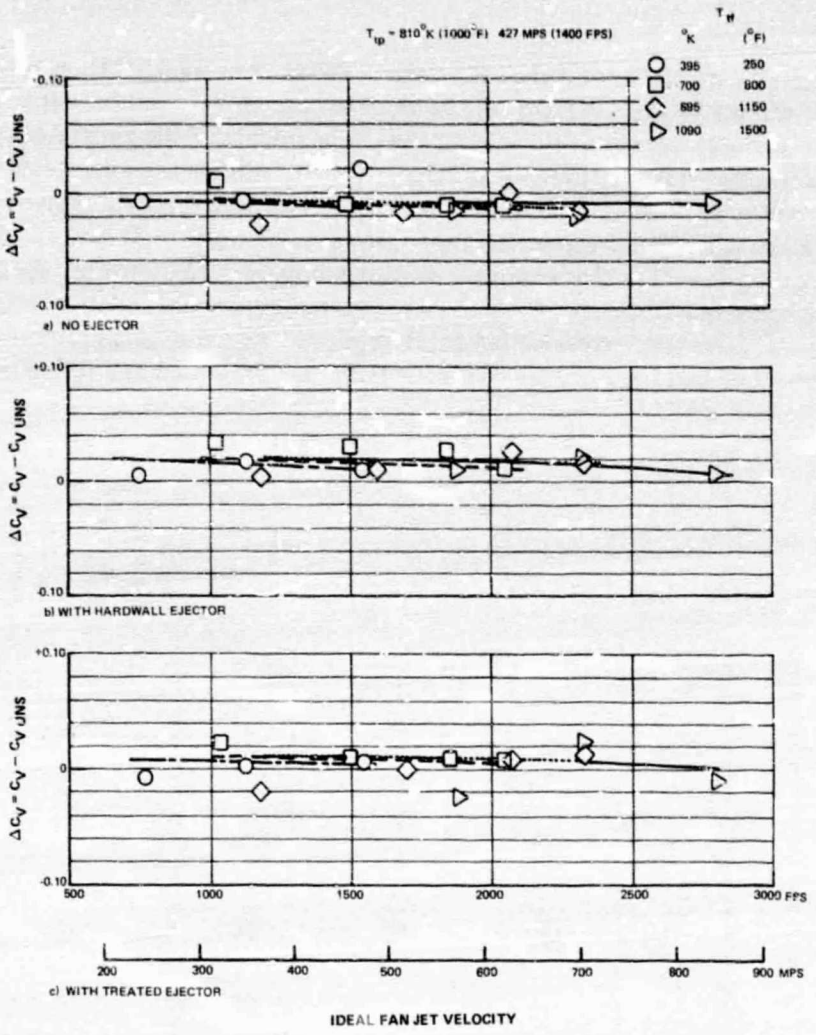

Figure 5.2-10 Correlation of Aerodynamic Performance and Fan Jet Velocity for Convoluted Suppressor Relative to Coannular Unsuppressed Nozzle Without Ejector, 0.75 Area Ratio

Several of the preceeding suppressor configurations were evaluated at higher primary stream pressure ratios, ranging up to 2.5. These configurations were the basic convoluted suppressor and the multi-tube suppressor, with and without an acoustically treated ejector. The resultant performance trends are summarized in Figure 5.2-11, illustrating the decrease in performance loss, relative to the unsuppressed coannular nozzle, when the primary pressure ratio is increased. This is due to the increasing percentage of the total mass flow passing through the relatively loss-free primary nozzle, while the fan stream thrust contribution remains unchanged. The losses in the fan stream suppression device become a smaller percentage of the total thrust produced by the complete nozzle configuration.

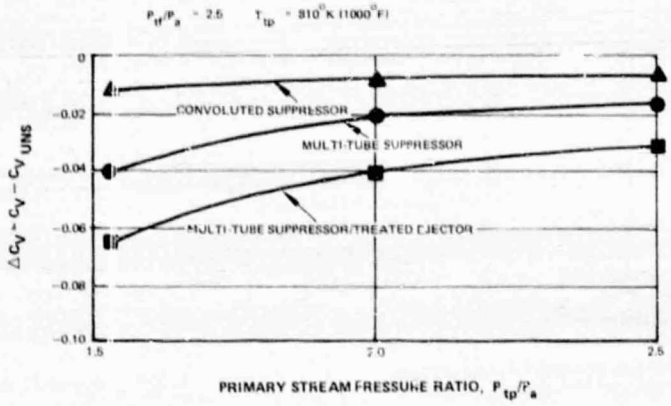

Figure 5.2-11 Effect of Primary Pressure Ratio on Aerodynamic Performance of Several Suppressors Relative to Coannular Unsuppressed Nozzle Without Ejector, 0.75 Area Ratio

The performance characteristics of a convoluted suppressor with an area ratio of 1.2 are shown in Figure 5.2-12, relative to the performance of the comparable unsuppressed coannular nozzle (A_f/A_p = 1.2). The basic convoluted suppressor exhibited a loss of about 1% (ΔCv at a fan pressure ratio of 2.5) relative to the unsuppressed coannular nozzle. Adding the hardwall ejector produced about 3% gain over the basic convoluted suppressor performance level. However, when acoustic treatment was added to the ejector, a loss of about 2% relative to hardwall ejector was noted. The resultant performance of the treated ejector was therefore 1% higher than the basic convoluted suppressor. These performance trends are presented in terms of fan stream jet velocity in Figure 5.2-13.

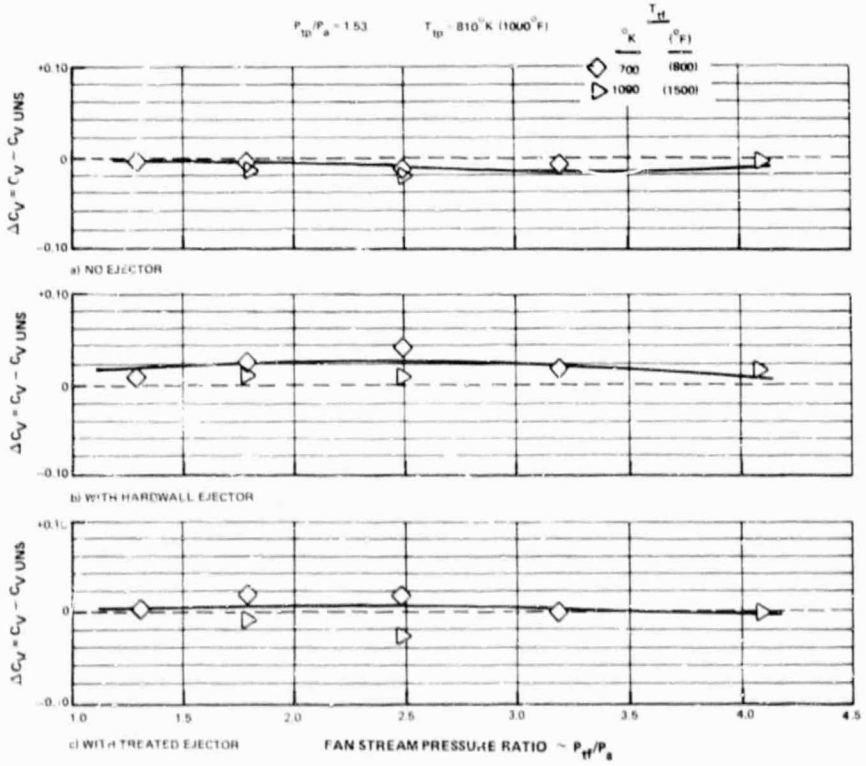

Figure 5.2-12 Aerodynamic Performance of Convoluted Suppressor With and Without Hardwall and Treated Ejector Relative to Coannular Unsuppressed Nozzle Without Ejector, 1.2 Area Ratio

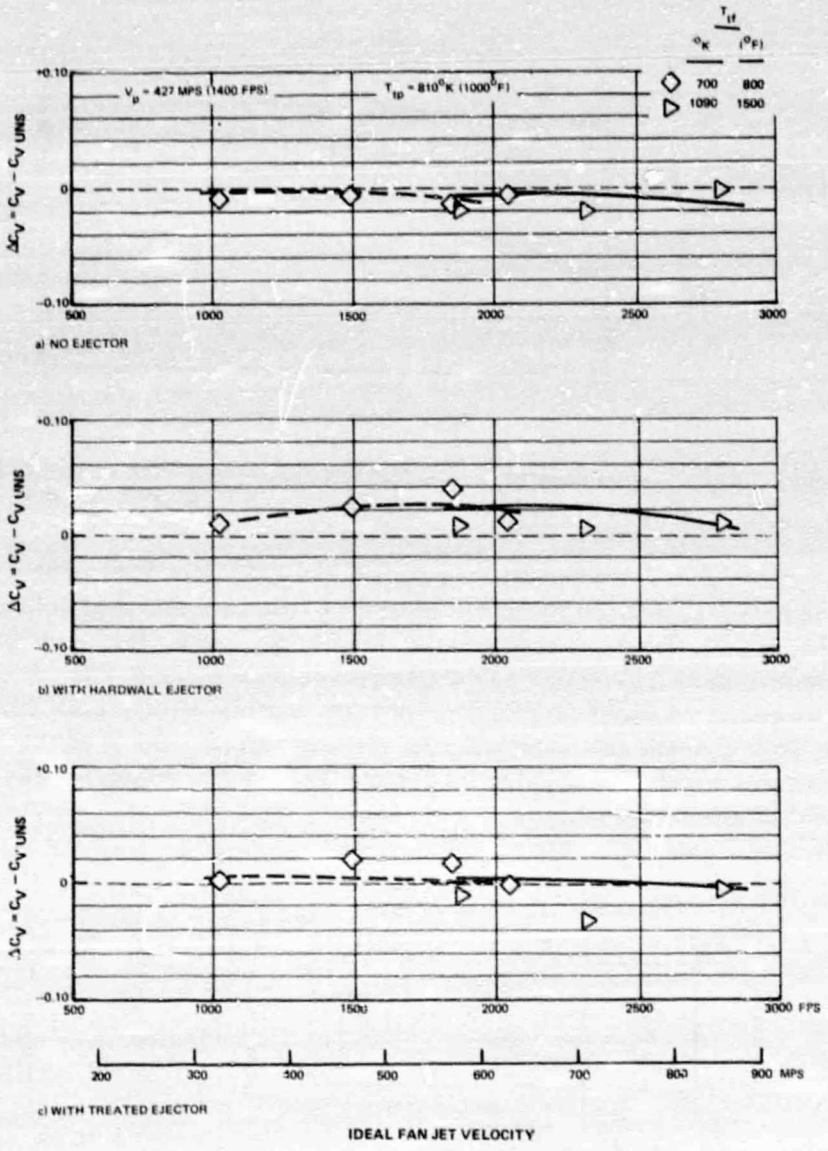

Figure 5.2-13 Correlation of Aerodynamic Performance and Fan Jet Velocity for Convoluted Suppressor Relative to Coannular Unsuppressed Nozzle Without Ejector, 1.2 Area Ratio

These results are quite similar to those obtained with the lower area ratio convoluted nozzle. The performance characteristics for the two configurations are compared in Figure 5.2-14. When the basic suppressor, as well as the suppressor with a hardwall ejector, are considered, the higher area ratio nozzle is only slightly lower in performance level. A higher percentage of the total configuration flow is passing through the loss producing portion (i.e. convolutions) of the nozzle system and therefore total performance is decreasing. When an acoustically treated ejector is added to the suppressor, the impact of nozzle area ratio is magnified and a difference of approximately 1.5% between the configurations is noted.

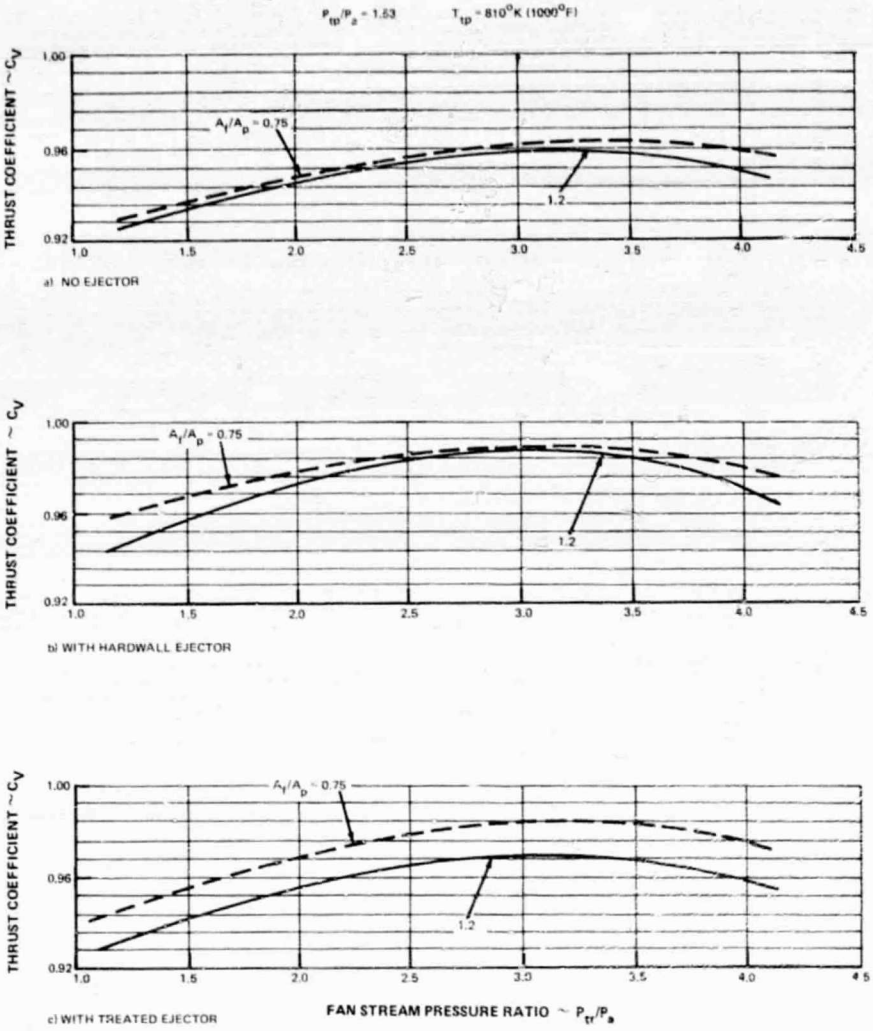

Figure 5.2-14 Effect of Area Ratio on Aerodynamic Performance of Convoluted Suppressors

5.2.3.3 Finger Suppressor

The thrust characteristics of the finger-type suppressor are illustrated in Figure 5.2-15 relative to the unsuppressed coannular nozzle. The finger suppressor by itself, exhibited a performance loss of 2.7% (Δ Cv @ $P_{tf}/P_a = 2.5$) due primarily to the low pressures created on the downstream side of the fingers. When the hardwall ejector was added, the performance loss increased to approximately 4.3%. This performance decay is due to the severe reduction in static pressure on the suppressor as illustrated in Figure 5.2-16. As shown, the average pressure acting on the fingers drops from 95% of ambient to 81%. This is offset somewhat by the low pressure acting on the lip of the ejector, but the dominant force is that acting on the suppressor. This reduction in internal pressures is associated with the induced airflow produced by the ejector.

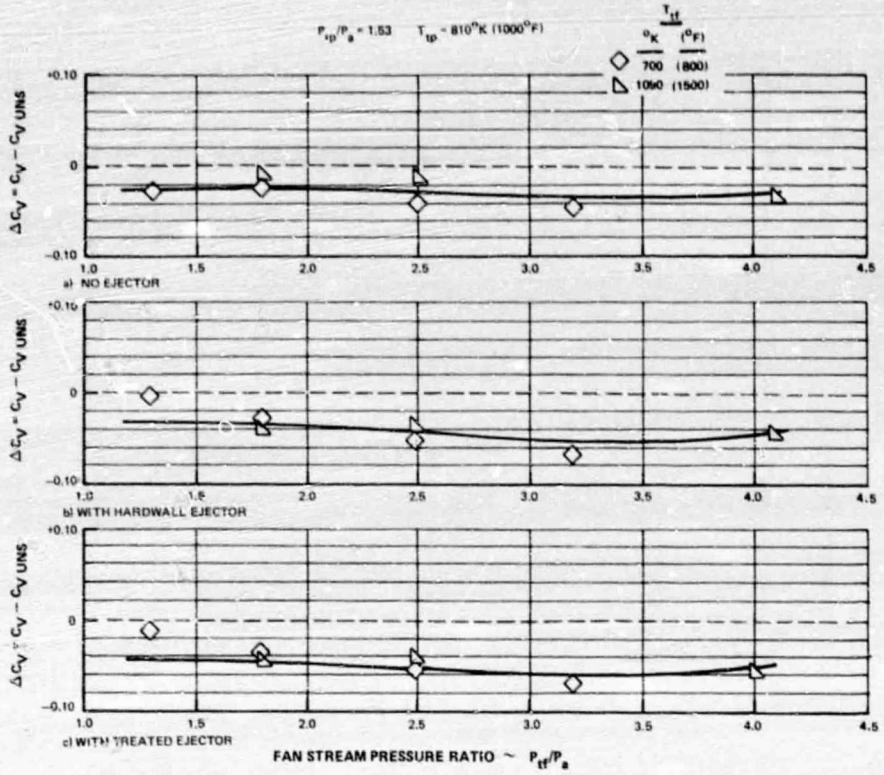

Figure 5.2-15 Aerodynamic Performance of Finger Suppressor With and Without Hardwall and Treated Ejector Relative to Coannular Unsuppressed Nozzle Without Ejector, 0.75 Area Ratio

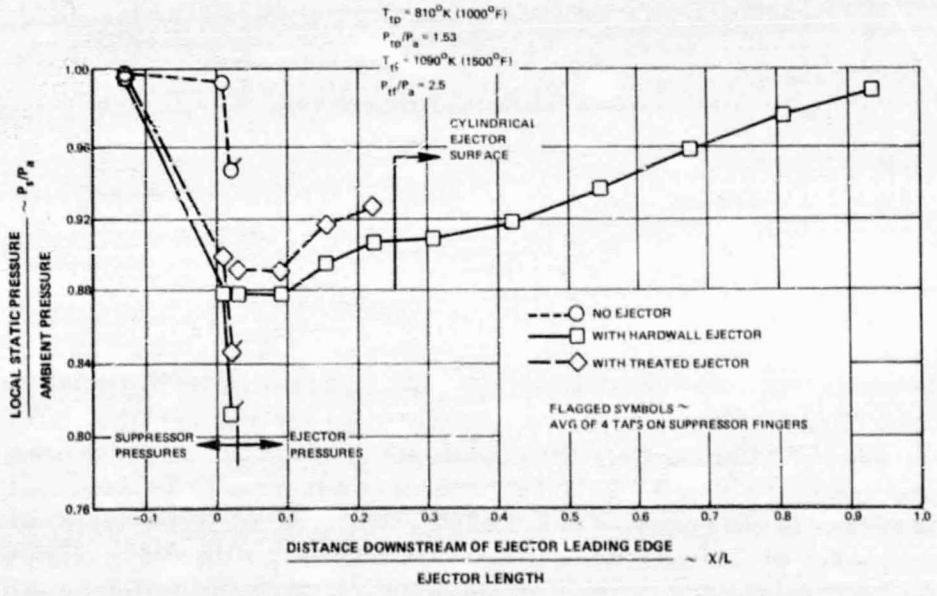

Figure 5.2-16 Static Pressure Distribution on the Finger Suppressor With and Without Hardwall and Treated Ejector, 0.75 Area Ratio

Adding acoustic treatment to the ejector increased the thrust penalty of the system to 5.0%, relative to the unsuppressed coannular nozzle (Figure 5.2-15). Integration of the static pressures, illustrated in Figure 5.2-16, showed that the net force acting on the suppressor and ejector lip was equal to that with the hardwall ejector. The additional performance loss of 0.7% (5.0-4.3) is therefore attributed to the frictional drag of the acoustic treatment. These performance characteristics are presented in terms of fan jet velocity in Figure 5.2-17.

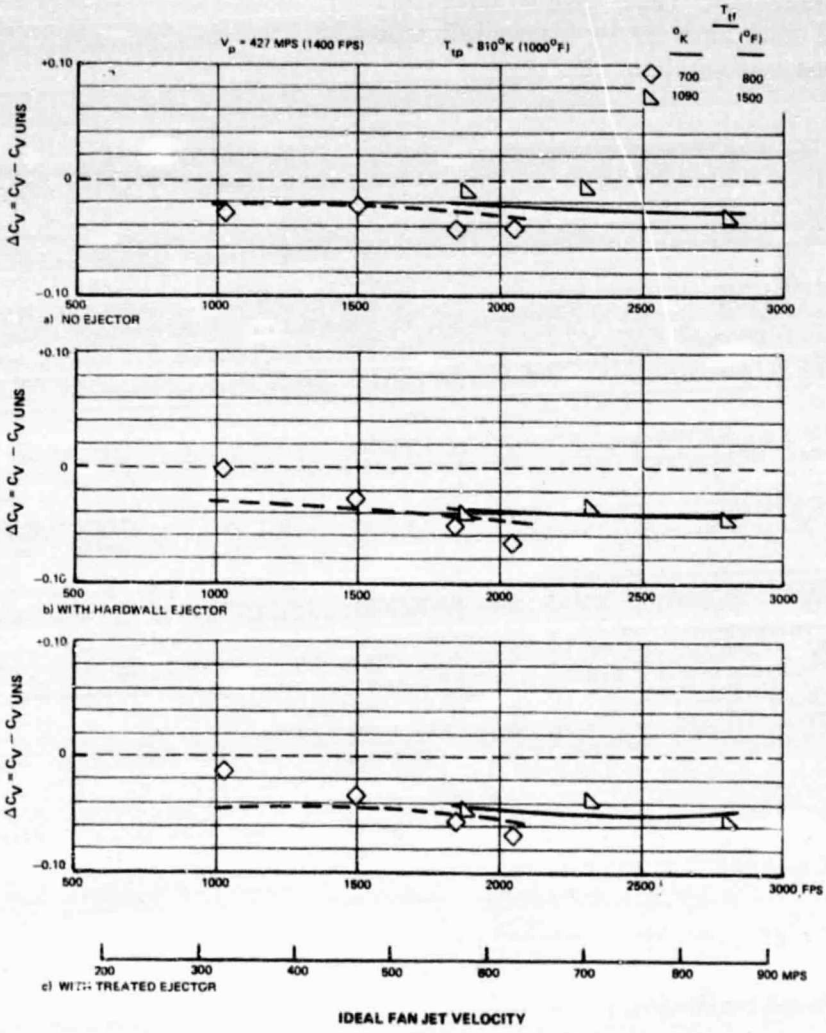

Figure 5.2-17 Correlation of Aerodynamic Performance and Fan Jet Velocity for Finger Suppressor Relative to Coannular Unsuppressed Nozzle Without Ejector, 0.75 Area Ratio

A comparison of the internal pressures for the various suppressor configurations is shown in Figure 5.2-18 for a typical flow condition. The convoluted suppressor, which showed the largest amount of ejector augmentation, had relatively high pressures on the suppressor as a result of proper ventilation. The corresponding pressures in the ejector indicated a moderate amount of lip suction for the convoluted suppressor. Since the ejector is cylindrical for the last 75% of its length, the pressure distribution in this region does not contribute significantly to the overall force. The multi-tube suppressor and the finger-type suppressor both exhibit low pressures on the suppressor, however, the lip suction on the ejector is better for the multi-tube configuration. The integrated forces therefore confirm that the multi-tube suppressor exhibited much more ejector augmentation than did the finger design, but not as much as the convoluted configuration.

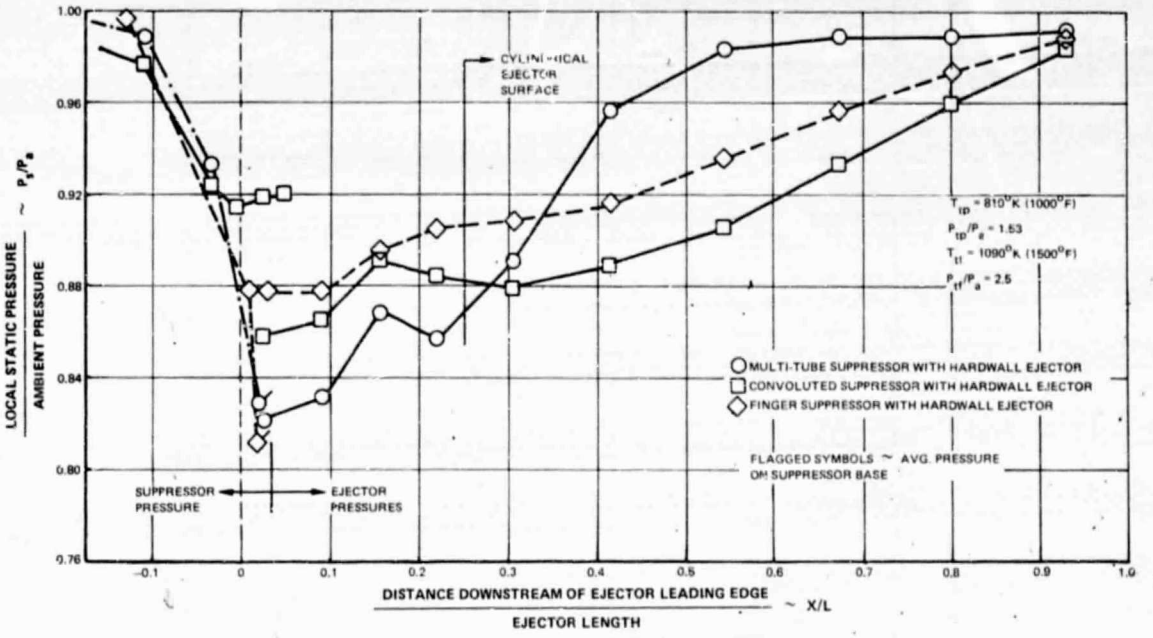

Figure 5.2-18 Comparison of Static Pressure Distribution for Several Suppressors With Hardwall Ejector, 0.75 Area Ratio

5.2.4 Flow Coefficients

The flow coefficients of the primary nozzle for $A_f/A_p = 0.75$ are presented in Figure 5.2-19 for a range of flow conditions. The primary nozzle flow coefficient at a $P_{tp}/P_a = 1.53$ is shown on Figure 5.2-19a. As illustrated, it is not appreciably changed by the type of fan stream nozzle employed (i.e., unsuppressed or suppressed). The thermal growth of the model hardware has been analytically accounted for in the flow calculation and therefore, there is no significant stream temperature effect. A single curve is therefore drawn through all the points. The level is significantly above unity over the range of fan nozzle pressure

ratios. These high values of flow coefficient occur because the primary nozzle is a convergent-divergent design, being aspirated by the surrounding fan stream. The ideal flow of this nozzle is calculated for an indicated pressure ratio of 1.53 (relative to ambient pressure); however, this nozzle is operating with an exit pressure that is lower than ambient and is consequently passing more airflow than defined as ideal. This phenomenon does not occur when the indicated primary pressure ratio exceeds approximately 1.9 since the nozzle becomes choked. The primary flow coefficient at a pressure ratio of 2.5 is illustrated in Figure 5.2-19b where the level is below unity. The general trend of the primary flow coefficient (for both primary nozzle pressure ratios) is to decrease with increasing fan nozzle pressure ratio, due to the suppressive effect of increasing fan pressure ratio. This tends to counteract the high levels of aspiration which the primary nozzle experiences at the lower fan pressure ratios.

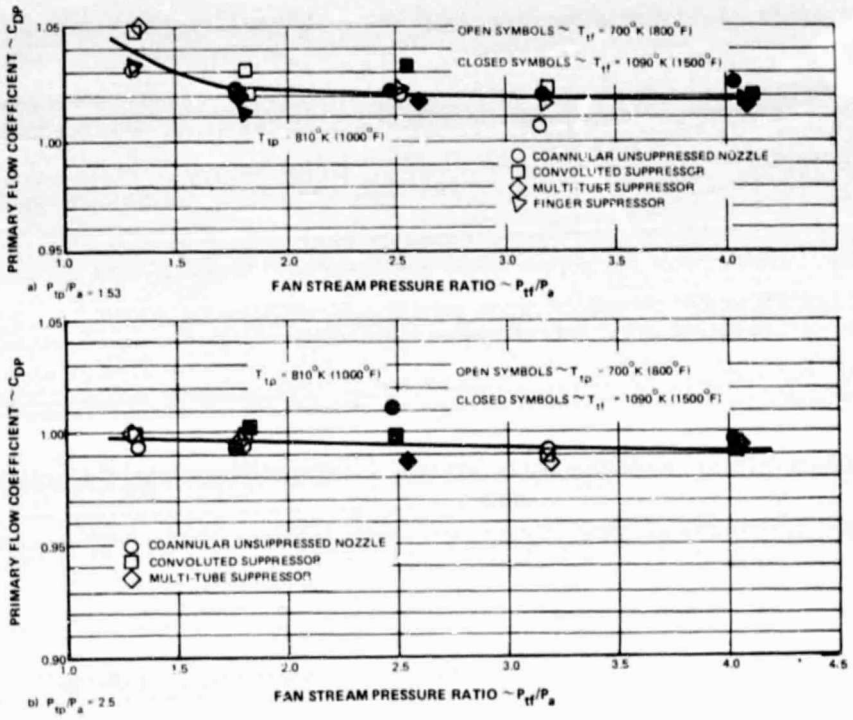

Figure 5.2-19 Typical Primary Flow Coefficients for Several Coannular Nozzles, 0.75 Area Ratio

The flow coefficient of the fan stream for A_f/A_p = 0.75 (shown on Figure 5.2-20) has a more conventional trend, with the peak level varying from 0.95 to 0.98 depending on the configuration. The unsuppressed nozzle and the convoluted suppressor are on the upper end of the band, reflecting the gradual convergence of the fan stream passage. The flow coefficients of the multi-tube and finger suppressors are on the lower end of the band because of the increase in wetted perimeter at the nozzle exit and a more abrupt convergence. Since there is no significant effect of stream temperature on the flow coefficients, single curves represent each of the configurations. The variations in fan flow coefficients are not large enough to create any significant differences in either the relative thrust characteristics or the relative acoustic properties used in the configurational comparisons.

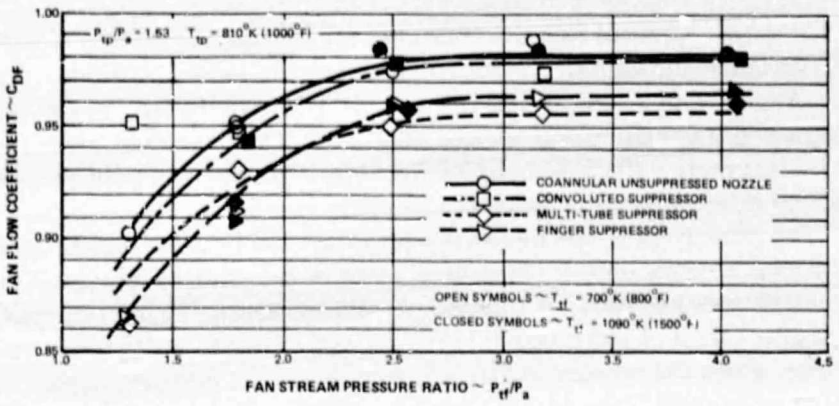

Figure 5.2-20 Typical Fan Flow Coefficients for Several Coannular Nozzles, 0.75 Area Ratio

The configurations having an area ratio, A_f/A_p, of 1.2 are geometrically similar to those having a 0.75 area ratio. The flow coefficients are, therefore, similar, but have slightly different absolute levels. The fan nozzle (A_f/A_p = 1.2) is lower in flow coefficient, as shown in Figure 5.2-21, where the fan flow coefficients of both the unsuppressed nozzles are compared. All of the data taken for each configuration is presented with a mean line indicating the level of flow coefficient for each area ratio. The 1.2 area ratio fan nozzle flow coefficient is lower because the increased fan exit area is associated with a higher fan duct pressure loss due to an increased internal Mach number. This increased loss is equivalent to about 1% decrease in fan nozzle flow coefficient (above the choked pressure ratio) which is the difference between the mean levels of flow coefficient for the two configurations.

The primary stream undergoes the reverse trend when the area ratio is increased from 0.75 to 1.2. However, the resulting change in primary flow coefficient is negligible because the Mach numbers in the primary passage are so low. In other words, the primary flow coefficients presented in Figure 5.2-19 apply to both the 0.75 and 1.2 area ratio nozzles.

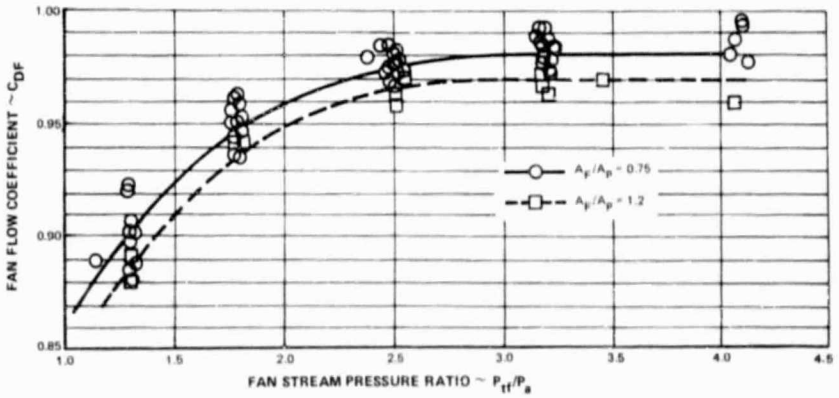

Figure 5.2-21 Effect of Area Ratio on Fan Flow Coefficient of Coannular Unsuppressed Nozzle

5.2.5 Acoustical Treatment

The addition of acoustical treatment to the ejector had a significant impact on the performance of all the suppressor configurations because of the scrubbing drag on the perforated wall liner. The severity of this drag is dependent on the geometry of the suppressor, which will dictate the outer bounds of the fan stream plume. The ratio of the ejector area to the projected area of the suppressor then furnishes a convenient parameter to describe this effect, as illustrated in Figure 5.2-22. Each of the suppressor configurations tested with a treated ejector has been compared to the corresponding hardwall version to establish the thrust decrement. As shown, a distinct trend prevails without regard to the type of suppressor system. As the area ratio is descreased (i.e., when the clearance between the suppressor and the ejector is reduced), the losses increase, especially if the area ratio is below approximately 1.3.

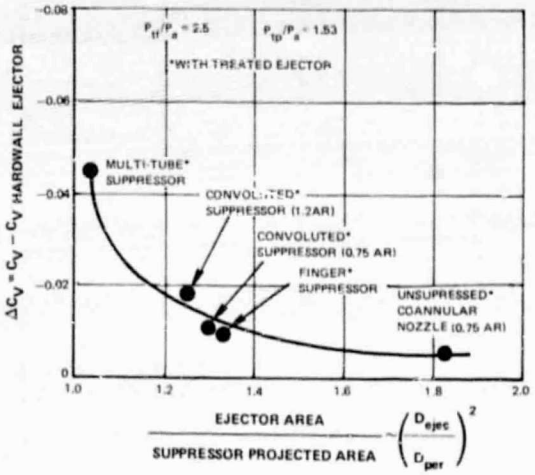

Figure 5.2-22 Correlation of Loss in Aerodynamic Performance Due to Acoustical Treatment With Nozzle Suppressor/Ejector Selection, Relative to Corresponding Nozzle Suppressor with Hardwall Ejector

5.3 IMPLICATIONS FOR CYCLE STUDIES

A cross section of the measured characteristics is presented in Figure 5.3-1, at a typical set of primary and fan stream conditions, representing the current family of engine cycles being evaluated in the Advanced Supersonic Propulsion Study. The amount of noise suppression (relative to noise levels synthesized using modifications to the proposed revision of the SAE jet noise prediction procedures) produced by the various configurations is compared to the associated thrust change, thus providing a measure of the overall system effectiveness. The coannular unsuppressed nozzle, representing a DBTF exhaust system, is 6 PNdB quieter than predicted. Since this is the baseline configuration for the thrust measurements, the thrust change is zero. Adding an ejector to the baseline produced 1 PNdB more suppression and 1% thrust augmentation. Incorporating acoustical treatment in the ejector produced another 1 PNdB suppression, at the expense of 0.5% thrust loss. The net result is that an unsuppressed flight type exhaust system, consisting of a basic nozzle system and a treated

ejector, is 8 PNdB quieter than previously estimated. The characteristics of convoluted, finger and multi-tube suppressors are also shown in Figure 5.3-1. The multi-tube suppressor nearly doubled the coannular baseline noise reduction (up to 15 PNdB), with the other suppressors in between. The hardwall ejector did not appreciably change the noise level (< 1 PNdB) but its thrust impact varied from a gain of 3% to a loss of 1.5%, illustrating the sensitive interaction between the basic suppressor design and the ejector. The introduction of acoustical treatment in the ejector produced from 1.0 to 3.5 PNdB additional reduction but at thrust losses from 0.5 to 4%. These losses indicate that acoustic treatment is a potentially critical factor, requiring careful consideration.

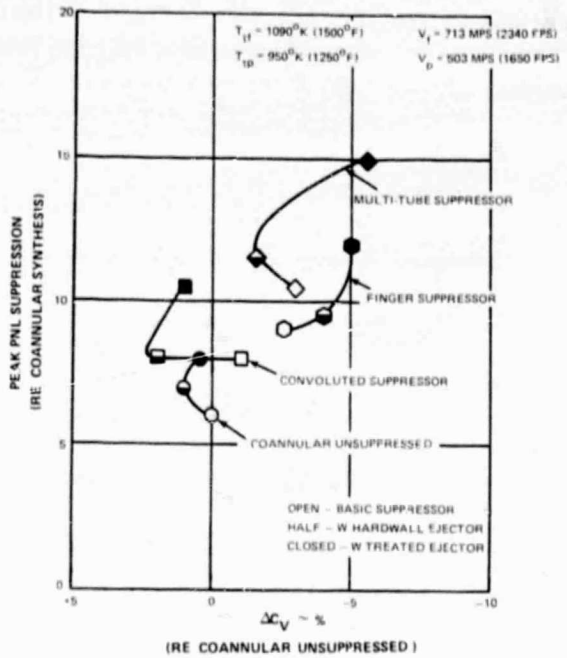

Figure 5.3-1 Exhaust System Effectiveness, 0.75 Area Ratio

Within the range of area ratios considered (0.75 to 1.2), the relative size between the primary and fan streams A_f/A_p, did not appreciably change the jet results.

The results of this program have had a strong influence on the Advanced Supersonic Propulsion Studies being conducted in support of the SCAR program (as summarized in Ref. 18). The inherent suppression characteristics of the coannular exhaust system provide several system advantages. As illustrated in Figure 5.3-2, for a band of study engines, a reduction in vehicle take-off gross weight of approximately 100,000 lbs can be achieved at a given jet noise level by incorporating these new coannular benefits into the previously used prediction techniques. In terms of the noise "footprint" at constant TOGW, the impact is even more dramatic, as shown in Figure 5.3-3. A reduction in footprint size, down to 25% of its original size, is possible because of the coannular benefits. The projected range improvement due to these test results is illustrated in Figure 5.3-4, applied to the evolutionary trend in the

newer variable stream control engines. The range improvements reflect the reduced powerplant weight on a given aircraft, allowing more fuel to be carried, providing increased range. The newly defined exhaust system characteristics intensify the normal engine improvement rate and greatly improve the range pay-offs for the advanced technology engines projected for the future.

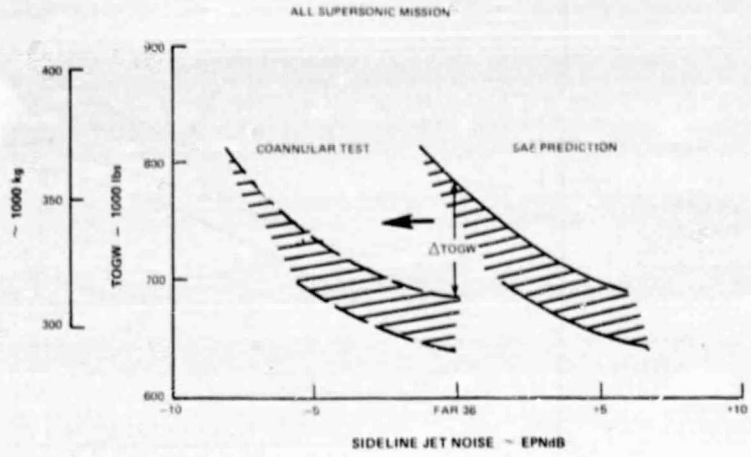

Figure 5.3-2 Impact of Coannular Nozzle Noise Benefit on Aircraft Weight

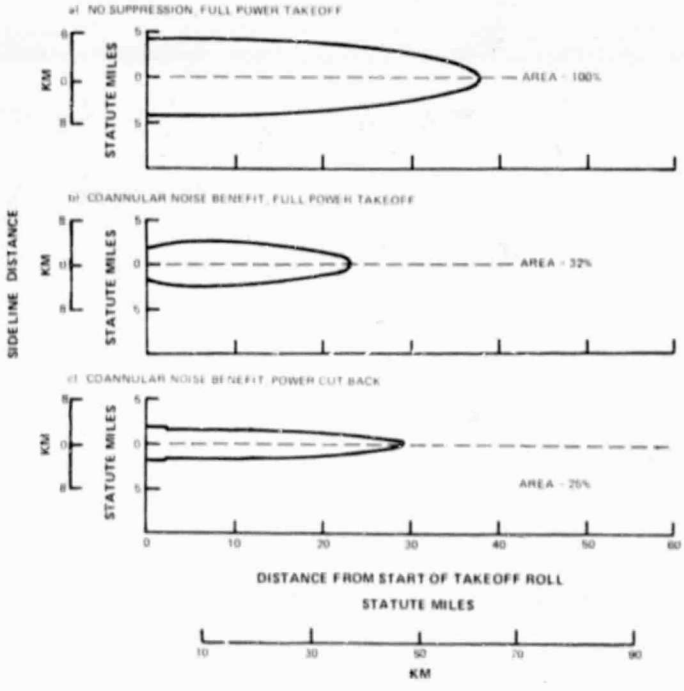

Figure 5.3-3 Impact of Coannular Nozzle Noise Benefit on 90 EPNdB Noise Contours

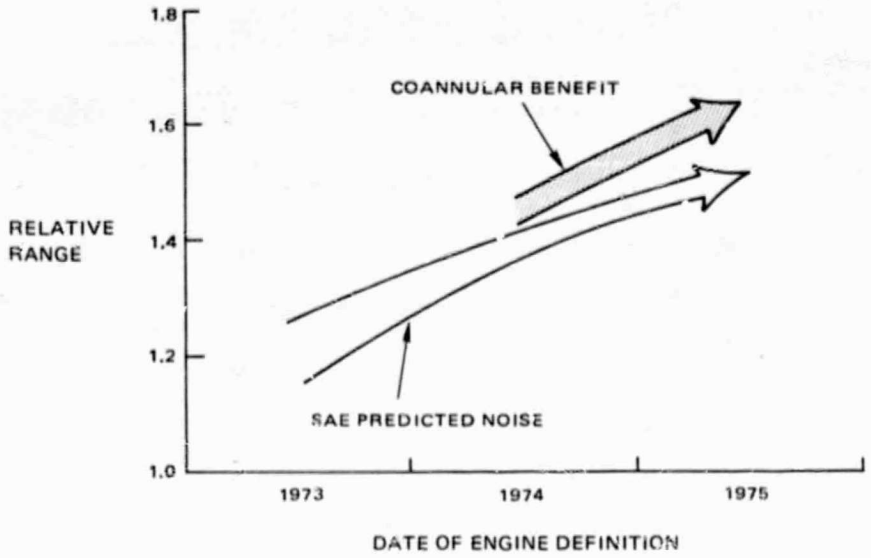

Figure 5.3-4 Impact of Coannular Nozzle Noise Benefit on Evolution of Variable Stream Control Engines

6.0 SUMMARY OF RESULTS

Static acoustic and aerodynamic performance characteristics of typical duct-burning turbofan nozzles were measured during this program using 0.127 m equivalent diameter scale models, approximately 1/10 size. Configurations with and without fan stream jet noise suppressors were evaluated, and the effects of hardwall and treated ejector shrouds were determined.

The nozzles were tested over a large range of operating conditions. Primary stream velocity ranged from 305 mps to 610 mps at temperatures of 395°K to 1090°K. Fan stream velocity varied from 235 mps to 853 mps at temperatures of 395°F to 1090°K. A total of 417 operating points were tested. Radial pressure and temperature profiles were measured at the position of the ejector exit plane at selected conditions. A data bank comprising all of the results obtained during the program has been established and documented in the Comprehensive Data Report, NASA CR-134910. The aerodynamic performance data is presented in terms of non-dimensional coefficients and thus can be applied to any size engine. The acoustic data has been scaled 10X model size to represent the noise characteristics of a 1.27m equivalent diameter nozzle.

6.1 ACOUSTICS RESULTS

The more significant results from the acoustic tests are summarized in this section. First, the coannular unsuppressed nozzle results are presented, followed by the fan stream suppressor nozzle results.

6.1.1 Coannular Unsuppressed Nozzles

- Coannular unsuppressed nozzles were significantly quieter (up to 11 PNdB) than predictions based on a coannular noise synthesis of two unmixed streams. The 0.75 area ratio nozzle produced slightly more noise reduction than did the 1.2 area ratio nozzle. The coannular unsuppressed nozzles were also significantly quieter (up to 7 PNdB) than single stream jets having the same thrust and flow.

- A model of the noise generation process for a coannular jet, based on the measured acoustic spectra and velocity profile data, indicates that the beneficial noise characteristics of the coannular unsuppressed nozzles are due to rapid mixing and velocity decay inherent in an inverted velocity profile jet (i.e., $V_f/V_p > 1$). According to this analytical model, the lowest possible noise level of an inverted profile jet would be the level generated by the primary stream alone.

- The addition of a hardwall ejector to the coannular unsuppressed nozzle produced up to 1 PNdB additional noise reduction. Incorporating acoustical treatment on the inner surface of the ejector produced an additional noise reduction of up to 1 PNdB beyond that obtained with the hardwall ejector.

- The sound power and perceived noise levels produced at all operating conditions where $V_f/V_p > 1$ were normalized for fan stream temperature, fan to primary velocity ratio, and area ratios, and then correlated as a function of fan velocity.

6.1.2 Fan stream Suppressor Nozzles

- The use of three different types of fan stream suppressors with and without hardwall and treated ejectors produced various amounts of noise suppression, up to a maximum of 18 PNdB relative to the synthesized prediction.

- The convoluted suppressor with a 1.2 area ratio produced approximately the same suppression as did the 0.75 area ratio. The noise levels of the various fan suppressor nozzles were shown to correlate with factors relating to both geometry and velocity profile measurements.

- A summary of the noise suppression obtained by each of the suppressors with and without hardwall and treated ejectors is presented in Figure 6-1 for one set of operating conditions representing a typical duct-burning turbofan cycle. (These conditions do not necessarily provide the maximum suppression demonstrated in the test program.) The suppression is defined relative to the synthesized coannular unsuppressed nozzle noise levels and also relative to the measured coannular nozzle noise levels. The multi-tube suppressor clearly provided the most suppression, with and without the hardwall and treated ejectors. The finger and convoluted suppressors provided more modest reductions. For each configuration, the hardwall ejector provided only slight reductions relative to the same configurations without ejectors. The treated ejector provided a significant reduction relative to the hardwall ejector.

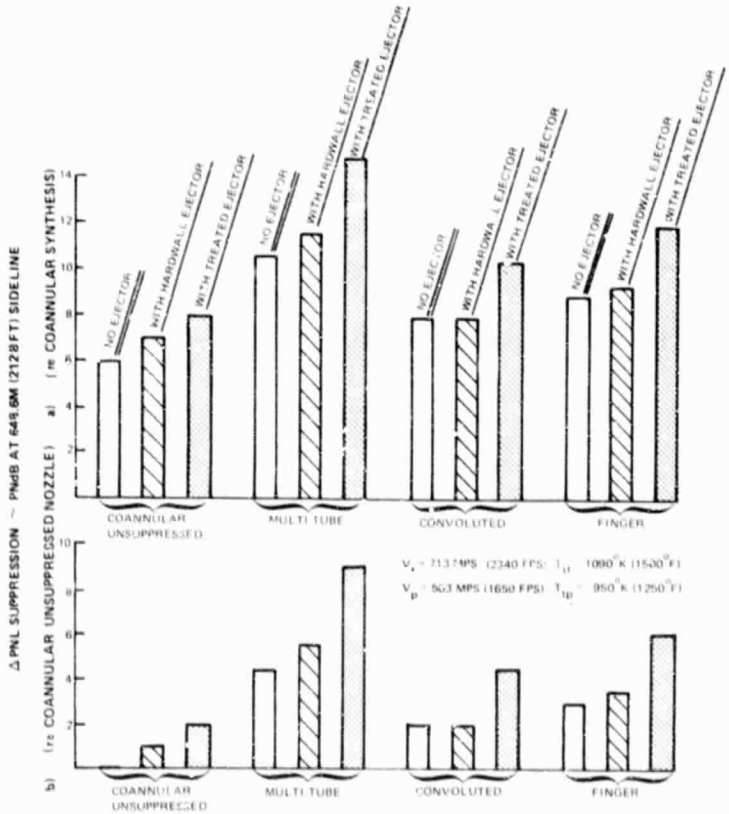

Figure 6-1 Jet Noise Suppression Summary for One Set of Typical DBTF Cycle Conditions, $A_j/A_p = 0.75$

6.2 AERODYNAMIC PERFORMANCE

The relative aerodynamic performance of all the 0.75 area ratio coannular nozzles is summarized in Figure 6.2. This comparison is based on the same flow conditions used for the acoustic summary presented in Figure 6.1. It serves to illustrate the basic performance characteristics established in the program. Similar trends were observed with the 1.2 area ratio configurations, and at other operating conditions. The more significant results are:

- The more intricate suppressors, such as the multi-tube and finger types, with blunt regions between the elements exhibit significant performance losses of as much as 3% relative to the unsuppressed baseline. The convoluted design, which provides a well ventilated multi-element fan stream exit, is clearly better from an aerodynamic point of view.

- The hardwall ejector used in this program improved the performance of the unsuppressed baseline, the multi-tube suppressor and the convoluted suppressor, in varying degrees up to 3% (ΔC_V). It was, however, detrimental to the finger suppressor, creating an additional performance loss of 1.5% (ΔC_V). Ejector augmentation is a complex interaction of many factors. The flow characteristics of the suppressor itself, along with the size, location and particular contours of the ejector, influence system performance. This points out the need for matching the ejector to the particular nozzle for best performance.

- Adding acoustical treatment to the ejector resulted in a performance loss ranging from 0.5% (ΔC_V) with the unsuppressed baseline to 4.5% (ΔC_V) with the multi-tube suppressor. These losses may be reduced somewhat by modifying the design of the acoustical treatment. In general, the more elaborate suppressors, providing high levels of jet noise suppression, result in a closely packaged exhaust system, tending to aggravate this problem. The optimization of the exhaust system characteristics will require careful tailoring of the major components to achieve maximum benefits.

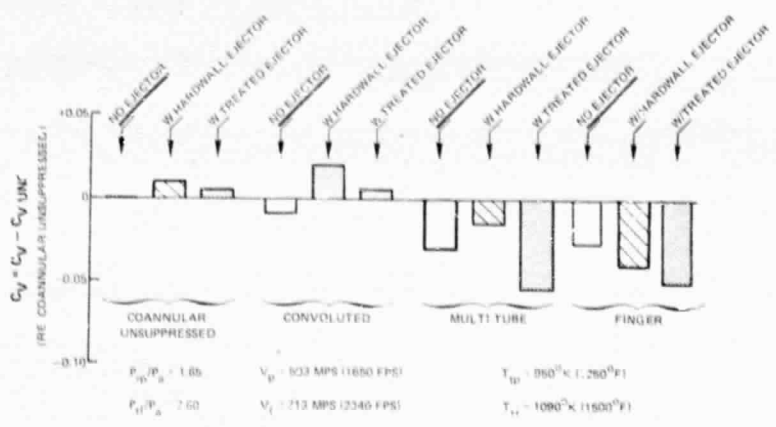

Figure 6-2 Aerodynamic Performance Summary for One Set of Typical DBTF Cycle Conditions, A_f/A_p = 0.75

APPENDIX I

ACOUSTIC POWER AND PERCEIVED NOISE LEVEL DIRECTIVITY DATA

Scaled (10.λ) to 1.27 m (50 in.) Equivalent Diameter Size, Representative of a Full Size AST Powerplant

Run #	P_t/P_a	T_t (°K)	V (mps)	OAPWL	PNL at 648.6 m S.L. θ = 60°	75°	90°	105°	120°	130°	140°	150°	165°
0.75 Area Ratio Convergent Nozzle													
4.01	2.64	414.9	450	170.0	102.1	106.2	107.7	105.6	105.9	100.6	103.7	101.8	91.8
4.02	2.42	426.3	437.4	167.8	100.6	98.1	103.6	102.5	102.0	100.5	102.3	101.7	89.2
4.03	1.80	413.2	357.8	153.6	82.5	83.9	86.2	88.1	89.2	86.9	82.9	–	74.2
4.04	1.54	403.4	305.7	147.4	76.1	76.7	80.4	82.2	82.4	80.4	80.6	78.3	64.0
4.05	1.31	396.1	244.4	141.6	69.0	69.8	72.5	75.3	74.6	72.0	70.8	–	53.5
4.06	1.15	388.7	173.7	130.7	63.1	61.3	65.1	67.0	63.9	59.5	59.9	56.5	43.6
20.02	3.15	719.7	640.1	178.6	106.9	–	111.0	110.3	111.8	113.4	117.0	114.0	99.2
20.03	2.54	702.2	577.6	172.9	101.8	–	104.4	103.8	105.3	106.5	110.6	109.2	95.9
20.04	1.82	705.5	474.9	163.8	86.8	–	92.1	94.7	97.3	98.0	98.3	98.1	88.9
20.05	1.53	699.7	401.7	157.2	82.3	–	87.4	89.7	91.7	92.0	91.1	88.9	79.5
21.01	2.52	825.0	624.8	173.9	100.5	–	103.4	104.0	106.3	108.4	113.3	108.8	94.6
21.02	2.01	816.7	547.1	169.2	90.0	–	95.4	98.4	101.5	102.8	105.5	104.8	95.3
21.03	1.53	813.3	433.4	159.4	83.6	–	89.0	91.5	93.7	94.0	93.4	91.8	82.9
22.01	3.05	884.4	702.3	179.7	110.2	–	110.7	111.1	113.0	116.0	118.2	1 5.2	100.7
22.02	2.53	896.1	652.9	174.3	100.4	–	103.8	104.9	107.3	106.9	114.2	108.3	93.9
22.03	1.80	901.7	531.9	166.8	88.5	–	94.2	97.0	99.8	100.9	102.5	102.1	91.1
22.04	1.54	894.4	456.6	160.9	84.4	–	90.0	92.6	94.9	95.2	95.2	93.9	84.6
22.05	1.16	915.0	274.0	142.8	71.8	73.6	75.7	77.1	77.4	76.4	73.6	68.2	53.7
23.01	3.21	1060.6	816.3	179.7	106.8	110.3	112.1	111.5	114.0	116.6	117.5	113.4	96.8
23.02	2.50	1061.7	707.7	174.9	99.7	101.4	103.6	105.6	108.5	112.4	114.3	107.5	91.1
23.03	1.80	1073.3	580.0	168.2	89.9	92.5	95.6	98.6	101.5	102.8	105.4	103.4	87.9
23.04	1.53	1087.2	502.9	163.0	86.7	89.0	92.0	94.6	96.8	97.4	97.9	97.0	84.4
23.05	1.29	1092.2	395.0	154.5	80.6	–	85.7	87.7	88.8	89.0	87.5	84.9	71.8
24.01	1.30	886.1	361.2	152.1	78.7	–	83.8	85.6	86.8	86.8	84.3	81.6	68.3
25.01	1.30	696.4	316.4	147.6	75.9	–	80.3	81.8	82.6	82.4	80.3	75.6	61.1

Run #	P_{tp}/P_a	T_{tp} (°K)	V_p (mps)	P_{tf}/P_a	T_{tf} (°K)	V_f (mps)	OAPWL	PNL at 648.6 m S. L. θ = 60°	75°	90°	105°	120°	130°	140°	150°	165°
0.75 Area Ratio Unsuppressed Coannular Nozzle																
5.01	1.53	382.1	296.6	2.48	380.1	418.2	159.0	95.8	96.5	98.9	96.6	98.6	94.7	–	88.4	75.0
5.02*	1.52	381.6	293.6	1.78	377.9	340.2	148.2	77.0	80.8	82.5	83.7	84.3	83.8	–	77.1	65.4
5.03*	1.54	381.1	297.5	1.15	370.2	168.0	142.3	70.8	73.9	75.6	76.9	77.5	75.7	–	70.9	59.4
5.04	1.53	395.6	301.8	3.23	390.0	473.0	164.0	101.8	98.7	101.1	103.5	101.1	98.8	100.7	97.6	80.4
6.01	1.53	701.1	401.7	3.19	394.4	473.4	165.3	100.0	97.1	101.7	102.9	103.3	102.1	101.4	97.7	91.0
6.02	1.54	708.9	409.0	2.51	400.0	431.3	141.5	99.5	91.2	98.8	98.1	100.0	95.6	95.5	91.5	76.7
6.03	1.54	696.1	402.6	1.80	393.3	349.6	155.3	78.0	78.6	84.8	88.0	89.9	88.6	85.6	87.3	72.3
6.04	1.54	692.8	402.9	1.31	386.1	238.7	152.6	74.5	74.9	81.3	84.6	86.3	84.7	86.3	84.1	70.3
7.01	1.54	256.1	437.7	3.21	398.9	477.3	166.3	100.2	94.6	101.0	105.5	102.3	100.9	104.0	101.0	91.3
7.02	1.52	811.1	431.6	2.50	401.1	431.6	161.5	85.1	99.2	98.6	100.3	99.1	96.2	96.9	93.0	63.5
7.03	1.54	821.1	440.1	1.81	396.1	353.0	157.1	79.4	77.3	85.9	89.2	91.4	89.5	91.3	89.4	74.7
7.04	1.56	811.1	441.7	1.32	388.9	243.8	155.8	77.3	75.8	83.8	87.1	89.4	87.1	89.7	88.1	75.6
8.01	1.52	1058.9	492.6	3.21	397.8	477.0	166.1	99.2	92.7	101.5	102.4	102.9	99.9	102.3	101.5	84.2
8.02	1.52	1053.3	490.7	2.51	401.7	432.2	162.5	96.2	83.3	98.1	99.2	99.2	96.9	97.8	95.2	80.8

TEST CONDITIONS							ACOUSTIC DATA									
								PNL at 648.6 m S.L.								
Run #	P_{tp}/P_a	T_{tp} (°K)	V_p (mps)	P_{tf}/P_a	T_{tf} (°K)	V_f (mps)	OAPWL	$\theta = 60°$	75°	90°	105°	120°	130°	140°	150°	165°
8.03	1.53	1053.9	495.9	1.79	396.1	349.0	160.4	81.7	70.5	88.1	91.6	94.1	91.6	95.1	93.4	78.4
26.01	1.53	400.1	303.8	3.22	703.0	637.6	166.8	98.0	101.6	101.5	103.3	103.6	104.5	105.1	101.8	85.7
26.02	1.52	404.1	302.8	2.48	706.4	573.0	161.3	92.0	95.9	95.7	98.1	98.9	99.3	97.9	93.9	74.6
26.03	1.52	387.5	296.7	1.80	705.4	468.8	153.3	82.4	84.8	87.4	89.9	91.8	90.9	88.3	83.3	66.6
26.04*	1.53	384.9	297.5	1.29	688.7	310.3	145.1	75.1	77.0	79.1	80.5	81.2	80.4	78.1	73.3	56.3
27.01	1.53	401.1	303.6	3.16	893.9	716.3	167.3	98.1	100.9	101.2	102.4	104.9	105.7	104.9	101.3	85.6
27.02	1.52	408.2	304.4	2.51	892.8	648.9	163.3	91.6	94.7	95.8	98.3	101.7	102.1	100.2	96.5	79.7
27.03	1.52	402.2	301.9	1.78	885.6	521.5	155.3	83.7	86.4	89.2	91.7	93.8	93.2	91.0	86.0	70.0
28.01	1.53	423.2	311.8	4.08	1090.6	864.1	170.8	101.0	103.6	104.0	105.9	108.8	109.1	108.6	105.0	85.8
28.02	1.53	413.6	309.7	3.21	1077.2	793.1	168.2	97.3	100.0	101.3	103.3	106.3	106.7	106.0	102.1	82.7
28.03	1.54	414.1	310.0	2.49	1066.1	708.4	164.2	90.9	95.0	97.0	99.8	103.2	102.8	100.7	97.0	80.1
28.04	1.53	407.8	306.6	1.80	1077.2	582.5	157.2	84.7	88.1	91.0	93.5	96.1	95.3	93.1	88.0	70.2
29.02	1.53	705.2	402.6	3.17	705.9	635.2	167.1	99.2	101.6	101.3	101.5	103.1	104.1	104.6	102.5	83.9
29.03	1.53	696.3	400.8	2.50	704.9	573.9	162.6	93.5	96.4	96.4	97.5	99.2	99.3	99.2	96.9	79.3
29.04	1.52	695.1	396.2	1.78	704.2	464.2	156.4	83.3	85.7	88.9	91.0	93.0	93.0	91.0	87.3	72.3
30.01	1.53	705.0	402.6	3.19	901.7	721.8	168.3	97.9	100.7	101.4	102.3	104.8	105.7	106.1	103.6	81.7
30.02	1.53	699.7	402.3	2.49	898.9	648.6	163.8	92.2	95.3	96.4	98.6	101.1	101.2	100.6	97.9	78.2
31.01*	1.52	389.9	297.2	1.29	903.9	359.4	146.1	76.7	78.7	81.0	82.3	83.9	82.4	79.5	73.9	–
32.01	1.53	693.7	399.9	1.29	905.0	358.1	152.3	80.4	82.4	85.1	86.3	88.2	88.2	86.6	83.5	–
32.02	1.51	703.6	397.5	1.78	898.9	534.0	157.1	85.2	87.8	90.8	92.9	95.4	94.7	92.4	89.2	–
33.01	1.52	697.2	399.3	1.29	683.5	312.7	152.1	79.6	81.6	84.1	85.6	87.5	87.9	86.5	83.7	–
34.01	1.51	713.7	400.2	4.11	1101.1	870.5	171.9	101.7	104.4	104.3	105.8	108.6	109.8	109.8	106.4	90.3
34.03	1.52	701.5	399.9	2.55	1094.4	725.1	165.0	90.6	95.1	96.5	99.1	102.3	102.6	102.0	99.2	79.5
34.04	1.55	697.1	406.9	1.80	1082.8	582.8	159.3	85.9	88.8	91.9	94.1	96.7	96.1	94.3	91.7	73.3
35.01	1.52	812.8	429.8	3.15	703.6	632.8	167.8	101.0	102.3	101.4	102.3	101.0	105.3	106.4	103.7	87.6
35.02	1.52	803.2	429.5	2.49	695.8	573.0	163.7	94.3	98.9	96.3	98.6	99.9	100.1	99.2	97.4	83.2
35.03	1.52	803.5	429.8	1.79	706.1	465.7	158.9	84.7	87.3	90.2	73.1	94.5	94.7	93.2	90.9	77.3
35.04	1.53	806.7	431.0	1.30	698.9	329.6	156.4	81.4	83.7	86.1	88.8	89.8	91.0	89.9	88.3	75.6
36.01	1.52	811.1	428.2	3.17	899.4	724.5	169.3	98.4	101.1	101.5	103.4	105.1	106.4	106.9	104.6	88.9
36.02	1.52	810.4	431.3	2.49	897.2	653.2	165.2	93.1	96.1	96.6	100.1	101.8	102.0	101.9	99.6	84.9
36.03	1.54	791.4	429.2	1.78	898.3	534.0	159.7	85.6	88.2	91.2	94.2	95.8	95.7	94.2	92.1	77.7
36.05	1.54	809.9	431.0	1.29	890.0	357.2	156.1	–	83.3	86.4	88.3	90.0	90.7	89.9	87.7	72.4
37.01	1.51	819.4	428.5	4.03	1089.4	860.5	172.7	–	105.2	104.4	108.4	108.9	110.7	110.8	107.4	90.4
37.02	1.52	809.2	431.0	3.18	1097.8	797.4	169.7	–	100.7	101.8	103.5	106.2	107.0	107.4	104.8	89.1
37.03	1.52	805.7	429.8	2.46	1095.0	713.8	165.3	–	95.3	96.9	100.2	102.4	102.3	102.0	99.5	82.1
37.04	1.53	809.0	433.1	1.78	1089.4	579.7	160.1	–	89.0	92.6	94.8	96.9	96.4	95.1	93.0	76.6
38.01	2.01	811.7	545.9	3.12	705.9	631.5	170.9	–	98.	99.0	101.6	104.5	105.8	108.1	107.1	91.3
38.02	2.02	809.9	547.7	1.80	705.7	468.8	166.5	–	89.6	93.2	95.8	98.8	100.4	102.3	101.6	87.4
38.03	2.01	808.1	543.5	1.31	708.6	323.4	165.5	95.6	87.8	91.6	94.7	97.2	99.5	101.4	100.7	86.3
39.01	2.01	789.6	538.0	4.12	1093.3	867.8	174.9	108.5	108.4	104.4	107.4	109.7	111.5	112.6	109.6	92.8
39.02	1.99	810.4	541.6	2.47	1085.6	711.4	170.2	51.4	96.8	99.1	102.2	104.6	105.7	107.3	105.7	90.1
39.03	2.02	808.9	546.5	1.79	1086.7	582.5	167.6	96.6	91.9	95.3	98.5	100.7	101.9	103.8	103.0	85.4
40.01	2.50	821.1	628.9	3.19	708.4	637.9	174.1	88.0	101.2	103.1	104.8	107.0	109.4	113.1	108.8	91.8
40.02	2.50	809.2	616.3	1.80	701.8	467.6	172.0	63.8	100.4	101.2	102.5	104.4	106.8	111.5	106.1	89.9
40.03	2.50	805.9	614.2	1.31	694.5	320.6	171.6	63.8	100.5	101.2	102.3	104.3	106.8	110.2	106.7	90.7
41.01	2.50	830.0	624.2	4.04	1100.0	865.3	176.3	108.3	104.3	106.0	108.6	110.3	112.8	114.9	109.9	92.9
41.02	2.45	812.2	610.8	2.48	1093.3	715.7	173.6	106.8	102.0	103.4	105.3	106.8	108.7	112.1	107.9	90.9
41.03	2.48	809.1	613.0	1.78	1084.4	578.2	171.7	104.8	100.2	101.2	102.5	104.2	106.2	110.3	105.8	88.5

	TEST CONDITIONS						ACOUSTIC DATA									
								PNL at 648.5 m S.L.								
Run #	P_{tp}/P_a	T_{tp}(°K)	V_p (mps)	P_{tf}/P_a	T_{tf} (°K)	V_f (mps)	OAPWL	$\theta = 60°$	75°	90°	105°	120°	130°	140°	150°	165°
42.01	1.53	1087.8	503.2	3.23	720.1	646.5	170.9	107.3	102.4	102.3	104.0	105.0	106.0	108.6	107.1	86.5
42.02	1.54	1096.7	506.6	2.50	691.4	568.1	166.6	100.8	98.0	97.0	99.3	101.3	101.8	102.1	101.1	82.6
42.03	1.52	1095.0	499.9	1.81	706.8	472.1	162.6	92.4	88.8	91.6	94.8	97.0	97.9	94.5	95.6	75.8
42.04	1.53	1093.9	502.6	1.29	692.4	312.7	160.5	88.4	86.2	88.5	91.6	93.7	95.3	95.4	93.7	78.3
43.01	1.51	1088.9	494.7	3.13	930.0	727.9	170.5	102.4	100.7	100.9	103.4	105.3	106.5	107.8	105.5	87.4
43.02	1.54	1095.0	508.4	2.53	905.0	655.9	167.8	100.3	98.4	97.8	101.1	102.9	103.4	103.9	102.2	82.8
43.03	1.55	1087.2	507.5	1.79	880.0	523.3	163.5	93.8	90.2	92.7	96.1	98.1	98.7	98.5	97.1	81.0
43.04	1.52	1086.7	499.6	1.30	900.0	361.2	160.4	88.8	86.6	88.8	91.6	93.8	95.0	95.0	93.1	74.7
44.01	1.53	1095.9	504.4	4.09	1108.9	872.0	173.8	107.1	103.9	104.1	107.0	108.8	110.6	111.5	108.6	91.0
44.02	1.54	1077.2	504.1	3.19	1082.8	792.8	170.9	101.9	100.0	101.0	103.9	105.7	106.9	108.0	105.8	90.1
44.03	1.54	1100.0	508.1	2.53	1133.3	735.8	168.6	99.5	98.3	98.2	102.0	103.7	104.4	104.9	102.8	82.8
44.04	1.53	1083.9	502.6	1.80	1081.1	583.4	163.4	94.3	91.0	93.1	96.4	98.1	98.5	98.3	96.8	81.6
48.01	1.55	1078.9	499.3	1.29	390.8	235.9	160.2	87.2	86.3	88.7	91.7	93.6	94.8	94.9	93.7	81.0
404.01	2.72	694.8	592.2	0.05	516.1	623.9	175.0	102.3	106.0	106.6	108.1	107.4	110.6	113.2	112.4	97.8
404.02	2.72	701.9	595.6	1.95	372.5	361.5	173.8	102.0	104.5	104.3	106.0	106.5	107.5	115.5	110.9	96.4
404.03	2.72	699.3	594.7	1.44	701.6	372.5	174.3	101.8	105.0	104.8	106.3	107.5	109.4	111.7	110.4	95.6
404.04	2.71	703.5	595.9	1.30	899.4	363.9	175.6	104.3	106.0	106.9	107.6	107.1	109.2	114.2	113.5	98.7
404.05	2.71	700.7	594.1	1.26	1092.8	377.6	175.5	106.6	105.6	108.6	106.7	107.5	109.7	114.7	113.1	98.7
404.06	1.16	390.8	179.3	1.26	1095.6	275.2	145.2	75.9	78.6	80.4	83.2	83.5	81.6	78.3	73.5	58.2
404.07	1.14	360.7	164.9	1.94	357.8	351.7	147.8	78.7	81.6	82.1	85.0	85.1	84.4	83.2	79.4	64.7
0.75 Area Ratio Multi-tube Suppressor																
49.01	1.53	385.0	298.0	3.18	380.1	467.6	157.1	91.5	95.9	94.5	95.5	94.3	93.5	91.4	86.4	69.3
49.02	1.53	402.7	303.5	1.80	390.7	347.8	148.3	78.7	84.3	84.8	86.0	86.2	84.6	81.8	76.9	60.6
49.03*	1.54	396.8	304.7	1.30	380.6	235.3	142.1	51.6	75.6	76.8	77.8	77.6	76.8	74.8	70.9	57.9
50.01	1.53	409.2	306.0	3.18	699.2	633.1	161.7	90.5	99.7	97.4	99.2	99.5	98.8	96.4	91.0	72.7
50.02	1.53	407.5	306.0	2.49	699.9	571.5	158.2	51.6	93.4	93.7	96.4	96.9	95.9	93.5	87.9	69.3
50.03	1.53	401.9	304.6	1.79	699.3	466.6	152.8	51.6	88.0	88.9	91.4	91.7	90.0	87.5	81.9	62.7
50.04*	1.52	392.8	298.7	1.30	698.4	320.6	143.8	51.6	78.5	79.0	81.0	81.3	81.2	76.8	70.7	56.5
51.01	1.52	419.3	308.5	3.18	904.4	722.1	162.7	28.3	100.0	98.2	100.8	101.3	100.1	97.5	92.0	72.9
51.02	1.52	418.5	309.1	2.48	893.3	645.3	159.4	28.3	93.8	94.6	97.9	98.5	97.7	94.8	88.5	68.3
51.03	1.53	419.9	306.6	1.79	897.8	528.2	154.4	51.6	88.9	90.1	92.7	93.9	92.2	89.2	83.4	63.6
51.04*	1.54	396.9	305.1	1.30	894.4	360.6	145.4	51.6	80.0	81.1	83.0	83.5	81.4	78.4	72.5	57.5
52.01	1.53	444.3	321.0	4.11	1103.9	871.1	166.2	63.9	102.5	101.0	103.2	104.2	104.2	102.0	98.0	82.2
52.02	1.54	404.0	306.3	2.51	1090.0	718.4	54.1	51.6	95.4	95.5	99.3	99.9	98.9	95.4	89.4	67.5
52.03	1.53	419.1	310.0	1.81	1090.0	588.3	155.5	51.6	89.4	90.8	94.1	95.1	93.9	90.9	83.7	62.6
53.01	1.52	822.2	432.5	3.19	392.5	465.7	161.0	28.3	100.0	97.3	97.5	96.1	95.9	94.5	91.5	76.7
53.03	1.54	721.9	428.5	1.78	375.7	338.9	154.3	82.4	84.6	86.8	88.6	88.6	89.0	88.6	86.5	73.2
53.04	1.53	805.2	433.1	1.30	374.1	233.4	152.4	79.3	83.3	84.0	86.3	87.3	87.8	87.0	85.7	74.1
54.01	1.53	825.6	437.1	3.19	703.8	635.8	162.9	90.4	98.4	97.8	99.3	99.7	99.5	97.4	93.8	78.4
54.02	1.54	810.0	434.9	2.50	684.4	565.4	160.7	89.7	91.8	94.4	96.8	97.2	97.4	95.4	92.0	76.8
54.03	1.52	808.3	430.1	1.80	685.4	463.0	156.5	85.4	87.9	90.0	91.9	92.7	92.8	90.6	88.1	73.3
54.04	1.54	791.9	430.1	1.30	699.3	317.3	153.5	80.7	83.7	85.1	87.4	87.2	87.8	87.2	85.5	73.0
55.01	1.52	821.1	432.5	3.20	895.0	719.9	164.0	90.8	98.7	98.5	100.8	101.0	101.9	98.7	95.0	79.8
55.02	1.53	817.8	435.3	2.48	907.8	1.2	161.5	90.4	92.2	95.5	98.2	98.8	98.9	96.5	92.7	77.3
55.03	1.55	807.9	–	1.80	907.2	532.5	158.0	86.9	89.2	91.5	94.0	94.4	94.7	92.8	89.5	74.2

	TEST CONDITIONS						ACOUSTIC DATA									
								PNL at 648.6 m S.L.								
Run #	P_{tp}/P_a	T_{tp} (°K)	V_p (mps)	P_{tf}/P_a	T_{tf} (°K)	V_f (mps)	OAPWL	$\theta = 60°$	75°	90°	105°	120°	130°	140°	150°	165°
55.04	1.53	805.8	431.6	1.31	893.9	364.8	155.6	81.1	84.3	91.5	87.0	87.8	88.1	87.6	89.0	76.6
56.01	1.52	811.7	428.5	4.09	1091.1	865.0	167.5	98.3	100.7	101.0	103.3	104.2	104.4	102.8	100.6	87.4
56.02	1.55	812.2	439.5	2.49	1087.8	715.4	161.9	86.2	94.5	96.1	98.9	99.6	99.4	96.8	92.7	76.4
56.03	1.53	805.1	430.4	1.78	1093.3	581.6	158.3	87.5	89.2	92.4	94.8	95.7	95.9	93.6	89.2	74.0
204.01	1.99	394.3	544.1	3.18	712.4	638.9	166.6	96.4	100.0	97.7	100.5	100.7	101.4	102.4	100.2	86.2
204.02	1.99	806.8	541 0	1.80	704.6	469.7	163.0	86.1	90.1	91.1	94.5	96.0	97.3	99.3	97.0	82.2
204.03	1.99	805.0	540.4	1.30	693.9	317.6	162.6	84.2	86.4	88.9	92.5	94.8	96.2	98.7	97.3	82.7
205.01	1.99	806.4	540.7	4.06	1108.9	870.5	170.3	98.7	102.1	100.7	103.9	104.8	105.5	105.9	105.0	91.0
205.02	2.00	798.3	539.8	2.50	1093.3	718.1	165.6	91.6	96.2	96.4	100.1	100.7	101.0	101.4	99.2	84.5
205.03	2.00	784.6	534.9	1.78	1068.3	575.8	163.6	88.0	92.8	93.3	97.0	97.8	98.4	99.7	97.5	82.3
206.01	2.48	810.6	614.2	3.20	713.4	641.0	170.0	98.0	101.5	99.5	101.9	102.5	104.9	107.4	103.6	88.1
206.02	2.51	804.3	615.1	1.80	707.4	470.3	168.7	96.7	97.9	98.7	100.3	101.3	103.6	106.7	102.2	87.1
206.03	2.49	805.9	613 6	1.29	704.2	314.2	168.9	97.3	98.0	98.5	100.1	101.6	103.7	107.7	102.7	87.2
207.01	2.49	808.6	614.5	4.09	1094.4	865.9	172.8	100.0	103.6	102.1	104.7	105.9	107.6	110.2	106.8	91.1
207.02	2.53	802.1	616.3	2.55	1089.4	723.6	169.8	98.4	100.1	100.5	102.5	103.0	104.7	107.3	103.2	86.7
207.03	2.50	802.2	613.3	1.79	1083.9	580.3	168.0	96.3	97.4	97.9	99.8	100.5	102.6	105.9	101.2	85.5
0.75 Area Ratio Multi-Tube Suppressor With Hardwall Ejector																
57.01	1.54	400.7	304.8	2.50	698.4	571.2	156.7	86.5	92.0	92.6	95.6	97.0	91.8	85.6	80.1	64.8
58.01	1.53	413.8	306.6	2.50	903.9	657.1	157.5	86.4	92.0	93.3	97.5	98.2	92.7	87.7	82.5	66.3
60.01	1.54	418.4	312.7	2.50	1095.0	718.7	157.9	86.8	92.5	94.1	98.6	97.9	93.2	89.1	83.8	67.5
60.02	1.55	394.6	304.8	1.80	1097.2	587.0	153.4	83.1	87.4	89.3	93.2	94.8	88.5	83.1	76.8	63.1
61.01	1.54	804.4	433.7	2.50	704.0	573.6	158.2	85.7	91.3	92.4	95.8	97.1	91.7	90.4	88.2	75.5
62.01*	1.54	376.7	296.3	1.80	368.3	338.6	146.4	78 2	82.2	82.5	84.6	84.3	83.9	77.3	73.8	61.2
62.02*	1.54	375.6	296.3	1.30	363.3	229.2	141.8	71.7	75.5	75.4	77.4	77.0	76.7	73.8	70.8	57.8
63.01	1.53	394.4	301.2	1.80	700.0	467.8	151.3	80.9	85.4	86.9	90.4	92.5	87.6	80.4	75.3	61.3
64.01*	1.54	396.1	303.6	1.80	906.1	533.4	152.9	82.0	86.9	88.5	92.8	94.4	88.4	81.9	76.8	62.7
64.02*	1.53	385.6	298.1	1.30	898.3	363.9	145.1	75.8	79.1	80.0	83.4	83.8	80.6	75.8	72.6	59.0
65.01*	1.54	377.8	297.5	1.31	697.8	322.5	144.4	74.8	78.0	79.1	81.8	82.4	80.6	75.5	72.5	59.2
66 01	1.53	816.7	435.6	1.30	678.3	313.9	152.4	79.5	82.4	83.5	85.7	86.8	87.2	86.2	83.9	73.0
67.01	1.53	808.9	433.1	1.31	889.4	363.3	152.6	79.8	81.9	83.9	86.6	87.2	87.2	86.0	84.0	73.0
68.01	1.53	821.7	437.1	1.80	703.9	469.4	154.8	81.7	85.9	87.8	91.5	93.1	89.1	87.7	85.8	73.6
69.01	1.54	812.2	436.5	1.80	912.2	535.5	155.7	82.9	87.5	89.0	93.6	94.9	89.3	87.8	85.8	73.1
70.01	1.53	798.3	430.7	1.80	1088.9	585.2	156.0	83.2	87.9	89.7	94.2	95.3	89.3	87.8	85.9	73.3
72.01	1.53	819.4	427.9	3.20	398.9	467.3	158.2	87.1	92.8	92.9	95.3	94.6	92.2	91.1	89.3	75.5
72.02	1.53	803.8	432.2	1.82	386.4	349.0	152.6	79.4	83.1	84.1	87.1	87.6	87.6	86.1	84.0	72.3
72.03	1.54	799.2	431.6	1.30	382.2	235.7	152.3	78.1	80.8	82.7	85.5	86.5	87.1	86.1	83.7	73.0
73.01	1.54	808.9	436.2	3.20	713.9	641.0	160.6	90.2	97.0	96.7	98.9	97.6	94.3	92.8	90.6	74.3
75.01	1.54	809.0	430.4	3.19	906.7	720.2	161.3	90.5	96.6	97.0	99.7	97.0	95.9	94.1	91.8	78.8
75.02	1.54	805.0	433.4	2.51	902.8	652.3	158.5	86.3	91.4	93.2	97.6	96.5	92.4	90.5	88.1	74.5
77.01	1.54	444.7	316.7	4.09	1095.0	866.2	164.4	94.6	99.1	99.2	102.6	101.9	102.3	99.5	95.5	79.9
78.01	1.53	406.8	293.5	3.19	405.7	463.6	155.5	88.4	93.6	93.0	95.0	93.7	90.8	86.6	81.4	66.2
79.01	1.55	418.2	313.6	3.22	697.2	634.6	159.0	90.3	96.9	96.4	98.6	97.8	93.3	90.0	84.7	68.4

TEST CONDITIONS							ACOUSTIC DATA									
								PNL at 648.6 m S.L.								
Run #	P_{tp}/P_a	T_{tp}(°K)	V_p (mps)	P_{tf}/P_a	T_{tf} (°K)	V_f (mps)	OAPWL	θ = 60°	75°	90°	105°	120°	130°	140°	150°	165°
80.01	1.53	432.8	315.8	3.18	902.2	721.2	159.6	90.4	96.7	96.6	99.3	98.0	94.5	91.5	86.5	69.7
82.01	1.53	804.4	430.1	4.05	1083.3	859.2	165.2	93.6	98.2	98.2	101.6	101.9	102.3	100.3	97.4	81.4
82.02	1.53	693.5	431.3	2.49	1092.8	717.5	158.4	85.8	91.3	93.8	98.3	97.4	92.2	89.7	86.5	71.8
0.75 Area Ratio		Multi-Tube Suppressor With Treated Ejector														
83.01	1.53	399.6	301.1	3.21	399.4	473.7	152.3	83.0	86.6	87.7	91.2	90.9	88.3	85.1	80.5	65.7
83.02	1.53	398.2	302.6	1.80	392.3	349.6	144.2	77.2	79.1	78.9	80.6	81.5	79.7	75.9	71.2	60.4
83.03*	1.52	390.4	302.6	1.30	381.3	232.6	140.8	71.0	72.6	73.0	74.5	75.0	75.1	72.8	68.5	57.2
84.01	1.54	411.0	304.8	3.20	707.8	641.6	157.0	86.1	92.3	93.8	95.8	95.3	92.5	90.5	85.0	69.6
84.02	1.53	405.1	303.9	2.50	701.4	576.4	153.4	83.1	87.4	88.7	92.4	93.4	83.8	84.9	79.9	64.9
84.03	1.52	398.9	303.9	1.79	697.7	469.7	147.9	79.5	81.9	82.8	86.9	87.9	83.7	78.0	72.1	59.5
84.04*	1.52	387.5	299.0	1.31	689.9	321.0	142.2	73.7	75.9	75.2	79.0	78.9	77.8	73.7	68.9	57.3
85.01	1.53	406.7	306.3	3.19	907.8	723.9	158.0	86.1	92.0	93.6	96.7	96.4	94.2	91.7	87.4	71.9
85.02	1.52	415.7	304.2	2.50	900.6	647.1	154.9	83.6	88.0	89.8	94.2	94.5	90.1	86.7	81.8	66.5
85.03	1.54	400.4	303.3	1.80	876.7	529.1	149.8	80.6	83.5	84.5	88.9	89.8	85.3	80.3	74.3	62.6
85.04*	1.54	387.8	299.0	1.31	907.2	352.7	144.6	75.8	77.9	77.6	81.8	81.7	79.9	76.2	71.9	60.6
86.01	1.53	434.1	310.0	4.10	1098.3	868.4	163.7	90.3	95.7	96.6	100.5	100.8	101.4	99.7	96.0	82.6
86.02	1.53	425.6	310.6	2.51	1092.2	721.5	155.7	84.2	88.9	90.8	95.3	95.1	91.5	88.5	83.7	68.4
86.03	1.53	414.2	307.5	1.80	1085.6	583.1	150.8	81.7	84.8	85.6	90.0	91.1	85.7	81.2	75.2	62.2
88.01	1.52	816.1	432.8	3.17	373.7	472.4	156.4	85.6	84.8	86.8	89.9	90.8	90.6	90.4	88.2	74.7
88.02	1.54	806.3	430.7	1.80	371.6	347.5	152.1	81.2	80.4	28.3	84.0	80.9	86.2	86.2	84.2	72.0
88.03	1.53	823.9	428.9	1.31	365.3	232.8	152.4	80.5	79.0	81.4	84.3	81.3	86.5	86.3	84.2	72.9
89.01	1.52	809.9	430.7	3.16	703.8	638.3	159.1	87.5	90.1	92.3	95.0	94.8	93.5	93.0	90.3	77.5
89.02	1.52	808.5	428.5	2.49	698.1	571.5	156.0	85.6	86.3	87.9	91.8	92.5	89.9	89.1	86.7	73 3
89.03	1.52	802.6	431.3	1.79	698.6	473.0	153.5	83.6	83.0	83.8	87.6	88.7	87.3	85.8	84.7	71.6
89.04	1.54	807.6	427.9	1.32	699.9	317.3	152.6	81.7	80.5	82.0	84.7	85.8	86.5	86.3	83.9	72.7
90.01	1.53	804.8	427.6	3.17	903.3	726.9	160.1	90.1	91.7	93.7	97.0	96.4	95.1	94.2	90.5	79.3
90.02	1.54	810.0	426.4	2.49	892.8	650.4	157.9	88.4	88.5	90.5	94.6	93.9	92.1	91.2	88.7	77.0
90.03	1.52	806.3	428.2	1.78	895.0	531.0	154.0	84.7	84.3	85.3	89.4	89.4	87.9	87.4	84.6	72,1
90.04	1.50	804.4	430.4	1.29	893.3	362.4	152.4	81.9	80.6	82.1	84.8	85.6	86.4	86.2	83.8	72.1
91.01	1.52	811.1	427.0	4.07	1102.2	859.0	164.5	92.4	94.5	96.1	100.0	100.3	100.6	99.8	96.8	85.0
91.02	1.51	807.1	427.0	2.50	1085.0	719.0	156.9	86.9	88.1	90.1	94.5	89.3	91.8	90.8	87.9	74.7
91.03	1.55	811.7	428.2	1.80	1079.4	581.3	155.5	82.8	86.1	87.0	91.6	91.6	89.5	88.3	86.2	72.3
92.01	1.98	806.6	539.2	3.20	702.6	635.8	164.6	87.7	93.7	94.3	97.7	97.0	97.8	99.0	97.9	83.2
92.02	1.97	810.7	538.9	1.79	706.7	467.3	162.0	84.0	87.8	88.6	91.8	93.8	95.5	98.1	96.2	80.6
92.03	1.99	805.4	539.8	1.31	690.1	318.8	162.8	84.4	88.3	89.6	92.5	94.6	96.3	99.2	97.6	81.9
93.01	1.97	820.6	542.2	4.10	1084.4	862.9	169.0	93.1	98.4	98.8	101.9	102.2	89.5	104.2	103.2	85.8
93.02	1.99	805.7	539.8	2.49	1081.1	712.3	163.3	87.0	91.2	93.1	96.9	96.1	96.3	98.0	96.5	80.4
93.03	1.97	807.3	537.1	1.77	1090.6	577.3	161.5	84.7	88.7	89.7	93.3	94.0	94.7	96.6	95.2	79.9
94.01	2.45	812.2	611.7	3.17	704.3	634.3	168.6	93.4	96.4	99.1	99.6	100.4	102.6	105.3	102.2	86.9
94.02	2.47	816.7	615.4	1.78	703.4	465.4	167.4	95.7	97.3	99.3	99.2	100.1	102.3	105.3	100.0	83.5
94.03	2.49	802.6	611.7	1.30	686.7	317.9	168.6	98.0	99.2	100.6	100.6	101.4	103.3	107.2	101.8	84.7
95.01	2.49	812.8	616.3	4.09	1102.8	869.9	172.1	97.7	99.8	28.3	103.8	104.2	106.0	109.1	105.8	87.8

Run #	TEST CONDITIONS P_{tp}/P_a	T_{tp}(°K)	V_p (mps)	P_{tf}/P_a	T_{tf}(°K)	V_f (mps)	OAPWL	ACOUSTIC DATA PNL at 648.6 m S. L. $\theta = 60°$	75°	90°	105°	120°	130°	140°	150°	165°
95.02	2.50	804.9	614.5	2.48	1090.6	715.1	167.6	94.6	96.5	28.3	99.7	99.8	88.2	104.9	101.5	85.3
95.03	2.46	808.3	610.5	1.78	1096.1	582.2	167.0	95.2	96.7	98.1	99.0	99.1	87.8	104.9	100.6	83.6
0.75 Area Ratio Convoluted Suppressor																
9.01	1.53	401.6	299.6	3.18	401.7	470.3	160.3	96.4	–	99.4	99.0	96.9	95.7	94.0	89.7	74.0
9.02*	1.54	403.2	300.5	1.79	398.3	344.1	148.0	78.2	–	82.6	84.1	84.5	84.0	82.0	77.8	62.5
9.03*	1.54	394.3	303.2	1.31	386.8	238.8	144.2	70.3	–	76.8	77.8	77.5	76.6	75.3	76.7	58.2
10.01	1.53	824.4	431.6	3.22	396.9	472.6	162.3	95.8	–	99.7	99.7	98.0	97.1	96.4	94.0	81.1
10.02	1.53	813.3	433.4	1.78	396.2	347.5	155.8	78.8	–	85.5	88.1	89.4	89.6	89.9	87.7	74.2
10.03	1.54	815.0	437.7	1.30	386.7	237.5	153.8	76.8	–	83.8	86.6	87.8	87.4	87.4	85.4	72.7
11.02	1.53	408.8	307.5	3.23	907.8	727.9	165.7	92.9	–	101.0	101.9	103.8	104.3	102.2	98.7	82.9
11.03	1.53	413.2	308.5	2.50	898.9	649.8	161.5	92.7	–	95.6	98.2	100.4	100.2	97.3	92.7	75.3
11.04*	1.53	405.7	306.0	1.79	896.1	526.7	156.8	82.4	–	93.9	93.9	96.5	94.4	90.6	85.5	67.4
11.05*	1.54	396.3	303.5	1.33	930.6	383.1	149.5	82.6	–	86.3	87.9	87.8	85.0	81.3	76.5	61.5
12.01	1.54	414.8	310.9	4.01	1100.0	863.2	170.3	98.1	102.7	102.9	104.9	107.7	109.9	107.6	103.9	89.9
12.02	1.53	407.2	306.9	2.52	1085.6	718.7	163.3	93.0	94.0	96.7	99.8	102.1	102.9	99.3	94.2	78.1
12.03*	1.54	396.8	303.5	1.82	1091.1	590.!	158.5	86.9	89.5	92.9	95.7	97.7	98.0	93.4	87.2	70.0
13.01	1.53	397.1	301.3	3.21	708.7	639.2	163.9	97.3	99.3	99.8	99.9	100.9	102.7	99.8	95.7	81.1
13.02	1.53	398.6	302.8	2.51	702.3	574.2	159.7	92.2	88.4	94.7	95.9	97.5	99.4	95.8	90.5	73.6
13.03*	1.54	393.4	302.3	1.84	703.9	476.7	153.3	82.7	86.1	88.2	90.3	91.6	91.9	88.6	83.3	66.4
13.04*	1.54	385.7	300.7	1.34	707.3	339.9	147.8	81.1	80.8	84.4	85.3	85.4	85.2	80.7	75.4	61.0
14.01	1.53	844.4	440.4	2.50	893.9	648.0	163.2	92.6	87.1	95.9	98.5	100.3	102.1	98.5	95.3	82.3
14.02*	1.54	800.6	432.5	1.82	882.2	530.0	158.7	85.8	–	91.6	94.1	95.3	96.7	93.3	90.1	76.3
14.03*	1.53	813.3	439.5	1.31	901.1	368.8	154.0	82.5	–	86.8	88.4	88.8	89.3	87.8	85.3	72.6
15.01	1.53	826.1	437.4	2.49	716.2	577.3	161.6	92.6	78.4	94.8	96.3	97.8	100.0	96.9	93.7	80.5
16.01	1.54	796.6	431.9	4.10	1101.7	869.9	171.9	98.5	–	102.9	106.2	107.8	109.0	109.6	106.8	92.1
16.02	1.55	795.4	435.3	2.53	1111.7	728.8	164.4	93.1	–	97.0	101.0	102.4	101.8	99.8	96.9	84.3
16.03	1.56	802.4	439.5	1.81	1103.3	592.5	161.3	89.5	–	96.5	98.7	100.4	99.2	95.5	91.9	77.9
18.01	1.53	816.7	434.0	3.19	701.2	634.9	165.2	96.2	–	100.1	100.7	101.8	102.2	100.8	98.8	84.6
18.02	1.55	817.2	440.1	1.80	707.8	470.6	157.5	83.3	–	89.6	91.9	93.2	93.3	92.3	89.4	72.3
18.03	1.52	804.0	427.3	1.31	705.4	323.7	152.9	83.2	–	88.5	89.5	89.5	88.7	60.9	84.2	67.9
19.01	1.53	814.4	434.0	3.21	902.2	723.9	163.4	96.2	–	100.3	101.5	103.5	103.5	–	100.6	85.5
208.01	1.99	803.9	540.1	3.21	709.4	639.8	168.9	95.7	99.7	99.9	101.8	102.2	103.8	105.0	103.9	88.9
208.02	1.98	805.0	538.6	1.78	695.6	462.7	164.3	86.6	89.6	92.0	94.9	96.9	98.9	100.4	98.0	82.5
208.03	2.00	808.3	542.2	1.30	700.6	319.1	162.7	85.4	87.6	90.7	93.3	93.3	96.9	99.1	96.6	81.0
209.01	1.98	805.0	538.3	4.07	1104.4	869.3	173.7	97.9	101.4	102.9	106.2	108.3	110.6	111.9	108.3	88.7
209.02	2.00	799.4	539.2	2.51	1097.2	721.2	167.9	92.7	96.8	97.2	100.7	102.5	103.3	104.2	102.5	85.4
209.03	2.00	800.6	540.1	1.80	1084.4	584.3	165.0	89.1	93.1	95.5	97.6	100.0	100.1	100.9	98.4	81.6
210.01	2.48	802.8	611.1	3.17	710.0	637.3	171.8	98.8	100.8	101.6	102.8	104.4	106.6	109.7	106.1	88.6
210.02	2.50	803.9	613.9	1.80	703.3	469.1	169.2	97.4	98.2	99.2	100.3	101.8	104.3	107.0	101.9	85.7
210.03	2.48	798.9	610.2	1.29	719.4	317.3	168.2	97.9	98.3	99.3	100.2	101.4	103.6	106.4	100.4	81.8
211.01	2.50	807.2	614.5	4.06	1098.9	866.5	175.3	101.9	103.6	105.9	107.8	109.2	112.1	114.3	108.2	87.5
211.02	2.50	802.2	613.6	2.49	1105.0	720.5	171.1	98.3	100.0	101.2	103.0	104.4	106.4	109.3	104.5	84.5

	TEST CONDITIONS						ACOUSTIC DATA									
											PNL at 648.6 m S. L.					
Run #	P_{tp}/P_a	T_{tp} (°K)	V_p (mps)	P_{tf}/P_a	T_{tf} (°K)	V_f (mps)	OAPWL	$\theta = 60°$	75°	90°	105°	120°	130°	140°	150°	165°
211.03	2.51	795.6	611.4	1.81	1086.1	586.7	169.3	97.8	99.3	100.2	101.2	102.5	104.7	106.9	101.8	83.5
0.75 Area Ratio Convolated Suppressor With Hardwall Ejector																
105.01	1.52	385.1	296.2	3.17	381.7	464.5	156.4	87.9	91.3	91.4	92.4	93.1	93.2	91.1	87.0	71.4
105.02	1.52	397.3	301.1	1.80	387.6	346.9	148.5	80.1	84.5	83.7	84.3	83.8	83.9	80.4	75.8	62.0
105.03	1.53	391.9	300.7	1.30	378.2	233.4	143.7	73.4	78.8	77.2	78.8	78.9	78.1	75.4	71.8	57.4
106.01	1.52	404.3	303.5	3.20	708.4	638.6	163.2	95.1	102.0	100.3	101.0	101.0	99.8	96.7	92.6	74.7
106.02	1.53	389.2	298.5	2.50	672.3	560.2	158.4	91.2	85.6	95.4	97.8	97.9	96.7	91.7	86.1	69.7
106.03	1.53	391.7	300.3	1.79	696.7	463.9	152.1	82.3	28.3	87.0	90.7	91.9	90.7	83.9	78.3	62.6
106.04	1.52	391.4	298.9	1.30	698.9	318.8	144.9	76.0	78.4	79.1	81.6	81.7	81.5	76.2	72.2	57.6
107.01	1.53	407.7	306.0	3.17	896.7	718.1	164.6	95.2	99.7	99.4	102.5	103.3	102.2	99.7	95.4	79.2
107.02	1.52	407.3	303.3	2.48	89[illegible]	644.3	160.9	90.7	96.5	96.4	100.1	99.7	98.7	93.6	88.3	70.8
107.03	1.52	397.1	300.5	1.79	8[illegible]	524.0	154.5	83.9	88.0	89.9	93.8	93.6	92.7	85.8	79.7	63.5
107.04	1.53	384.6	295.5	1.29	896.1	357.2	146.3	77.1	79.5	80.5	83.4	84.8	83.0	76.6	71.9	56.8
108.01	1.53	426.4	313.0	4.08	1077.2	858.6	169.4	97.7	102.4	102.7	105.9	107.9	108.2	105.9	101.2	84.6
108.02	1.52	419.9	307.8	2.47	1069.4	706.5	162.3	91.2	96.9	97.9	101.9	103.5	99.3	94.0	88.8	71.0
108.03	1.52	396.7	300.5	1.78	1073.3	587.0	156.8	85.2	89.3	91.2	95.9	98.4	93.7	86.8	80.4	63.9
109.01	1.52	818.3	432.2	3.20	702.1	635.5	164.6	95.8	99.9	98.8	101.3	101.7	100.8	99.0	96.1	81.6
109.02	1.51	807.4	424.3	2.51	699.2	572.7	161.3	91.0	96.8	95.6	98.4	99.1	97.0	94.2	91.1	76.0
109.03	1.52	810.0	429.8	1.80	692.8	464.5	156.3	83.4	86.7	88.0	91.5	93.3	91.7	89.8	86.7	71.5
109.04	1.53	804.3	429.8	1.30	676.6	314.6	153.2	80.4	83.0	83.7	86.8	87.8	87.7	87.2	84.3	69.3
110.01	1.52	811.7	4303.8	3.19	897.8	720.2	165.6	95.5	99.9	99.8	102.6	103.6	102.3	100.5	97.2	80.0
110.02	1.52	813.3	421.6	2.49	893.9	647.1	162.0	91.1	96.3	96.4	100.2	101.4	98.1	94.9	92.0	76.3
110.03	1.52	812.2	428.5	1.79	891.7	526.7	157.5	84.9	88.5	90.2	94.4	96.6	93.2	90.2	87.0	72.3
110.04	1.53	810.8	433.4	1.30	896.1	361.8	153.7	81.1	83.5	84.7	87.5	88.5	88.3	87.4	84.7	69.9
111.01	1.52	815.6	429.5	4.05	1087.8	861.1	171.5	97.2	101.2	102.0	106.0	107.7	108.9	109.0	105.9	89.8
111.02	1.53	804.6	432.2	2.50	1078.9	714.1	163.3	91.7	97.1	98.0	102.3	101.6	98.9	97.2	94.2	80.1
111.03	1.52	810.6	425.5	1.78	1087.8	583.7	158.4	84.8	89.3	91.4	96.5	97.4	92.8	90.1	88.1	72.3
112.01	1.53	815.0	434.0	3.18	393.2	472.1	161.6	91.8	96.4	95.0	97.0	96.2	96.1	95.2	93.1	78.9
112.02	1.52	807.5	427.6	1.80	386.1	345.9	154.1	80.8	83.0	84.2	86.8	87.5	87.9	87.3	85.4	71.1
112.03	1.52	807.6	430.1	1.29	376.6	231.4	152.6	78.8	82.9	82.7	86.4	86.3	86.7	86.2	83.9	68.9
0.75 Area Ratio Convolated Suppressor With Treated Ejector																
96.01	1.52	400.6	301.8	3.19	393.2	472.7	156.6	89.7	91.0	91.9	93.4	93.4	92.8	91.1	87.3	72.3
96.02	1.53	392.7	301.2	1.79	383.3	343.8	147.4	80.0	80.6	82.1	83.0	82.4	82.0	79.4	75.7	61.3
96.03	1.52	386.6	296.6	1.29	373.5	229.5	153.6	72.9	74.5	74.9	76.5	76.4	76.1	96.4	71.5	57.1
97.01	1.52	399.2	301.6	3.19	702.8	634.9	161.8	95.1	98.5	98.0	100.0	99.7	98.7	96.5	92.5	75.5
97.02	1.52	395.8	294.7	2.50	702.2	571.5	157.1	89.6	93.1	93.1	95.1	95.8	93.4	90.1	85.4	71.1
97.03	1.53	390.4	300.1	1.79	699.5	466.0	150.2	81.9	83.3	85.6	87.5	88.7	86.9	81.9	77.5	62.2
97.04	1.53	381.9	296.5	1.29	687.1	312.7	144.0	75.0	77.1	77.8	79.5	79.7	78.6	75.5	71.5	48.5
99.01	1.52	394.0	298.5	2.50	904.4	651.4	158.6	90.1	92.9	93.9	96.7	98.5	95.6	90.9	87.2	70.3

Run #	TEST CONDITIONS P_{tp}/P_a	T_{tp} (°K)	V_p (mps)	P_{tf}/P_a	T_{tf} (°K)	V_f (mps)	ACOUSTIC DATA OAPWL	PNL at 648.6 m S. L. θ = 60°	75°	90°	105°	120°	130°	140°	150°	165°
99.02	1.53	388.6	298.7	1.79	907.8	532.2	152.3	83.9	85.1	87.4	90.1	92.3	88.4	83.7	78.0	64.8
99.03	1.53	374.4	292.7	1.30	887.8	360.0	144.4	76.2	77.0	78.5	80.7	81.8	80.5	75.4	70.1	56.4
99.04	1.53	393.9	300.3	3.20	903.9	723.3	163.2	95.6	98.8	98.8	101.2	102.2	101.1	98.9	94.5	–
100.01	1.53	421.7	311.2	4.01	1076.1	853.7	168.8	96.9	100.6	102.3	105.0	107.5	108.3	106.4	101.7	–
100.02	1.53	405.6	304.8	2.51	1102.8	722.4	160.3	90.4	92.8	95.0	98.3	100.2	96.7	93.4	88.8	71.0
100.03	1.52	397.8	300.5	1.79	1058.3	574.5	153.9	83.6	85.7	88.4	91.5	93.8	90.8	84.3	79.4	63.5
101.01	1.53	805.0	429.8	3.22	710.6	641.0	164.1	94.8	97.2	98.3	99.8	100.1	99.7	98.7	96.2	80.2
101.02	1.52	808.3	427.6	2.51	704.4	575.2	160.0	89.1	91.3	93.0	95.0	95.8	95.3	93.4	91.0	74.6
101.03	1.51	802.2	424.6	1.78	697.2	463.0	155.6	83.2	84.8	86.5	88.6	89.5	91.2	87.7	85.5	71.4
101.04	1.53	821.7	436.8	1.29	704.4	317.3	154.2	80.6	82.5	83.4	85.9	86.5	90.4	86.8	84.8	69.5
102.01	1.52	811.1	430.4	3.18	897.2	719.3	165.4	95.2	97.5	98.8	100.9	101.7	102.0	100.2	97.4	80.8
102.02	1.53	803.9	431.6	2.49	902.2	650.1	161.4	89.7	95.1	94.8	96.9	98.3	96.9	94.9	92.3	77.3
102.03	1.51	801.7	425.2	1.80	898.9	530.7	156.2	83.5	87.7	88.6	90.7	92.0	90.5	89.1	86.4	69.1
102.04	1.53	807.8	432.8	1.31	901.7	366.4	153.4	80.4	84.3	84.2	86.0	86.8	87.8	86.8	84.3	66.3
103.01	1.53	810.0	431.3	4.07	1067.2	854.0	171.3	96.6	102.7	103.2	105.3	108.1	109.8	108.7	104.5	83.1
103.02	1.52	806.7	429.5	2.51	1104.4	723.0	162.0	90.7	95.7	95.8	98.1	99.5	97.8	95.6	92.5	77.2
103.03	1.50	812.2	425.2	1.77	1091.7	577.9	156.6	84.3	88.7	89.6	91.8	93.3	91.0	89.1	86.3	70.7
104.01	1.51	827.8	432.2	3.16	381.1	463.3	161.0	89.6	93.6	92.9	94.0	95.2	95.9	95.5	93.0	79.1
104.02	1.51	808.9	425.2	1.78	378.3	339.9	154.4	80.6	84.6	84.7	85.9	87.0	88.5	88.1	85.8	71.5
104.03	1.53	813.3	434.9	1.31	373.9	235.0	153.4	79.0	83.1	83.5	85.3	86.7	88.0	87.3	85.2	72.1
0.75 Area Ratio Unsuppressed Coannular Nozzle With Hardwall Ejector																
200.03	1.52	805.2	428.2	3.18	706.6	636.1	166.2	97.9	99.5	100.8	103.0	102.8	102.7	101.3	98.8	86.5
200.07	1.52	794.1	426.7	1.81	694.7	467.0	159.4	90.3	93.9	91.1	94.7	94.4	94.5	95.3	96.0	87.0
200.09	1.53	803.7	430.7	1.29	694.1	314.2	155.8	82.1	84.3	85.6	88.1	89.2	89.7	88.8	86.9	74.6
201.01	1.52	804.3	427.9	4.07	1101.1	867.8	172.4	102.5	105.0	105.0	107.4	109.0	110.4	109.1	105.7	91.8
201.02	1.52	801.7	425.5	3.19	1091.7	796.7	168.6	97.2	101.4	101.9	104.9	105.6	106.1	104.8	101.5	87.6
201.03	1.52	803.7	429.2	2.49	1090.0	716.6	165.5	93.6	97.3	98.6	102.2	102.8	102.2	100.3	97.4	84.8
201.04	1.53	804.6	431.0	1.80	1083.9	582.8	162.0	89.2	91.7	93.6	96.3	97.0	96.0	94.9	94.0	83.4
0.75 Area Ratio Unsuppressed Coannular Nozzle With Treated Ejector																
202.01	1.52	806.7	428.5	3.22	708.7	640.1	166.2	98.1	100.9	100.5	101.9	102.0	102.4	101.4	99.0	87.2
202.02	1.52	801.9	428.5	1.79	703.9	466.6	161.3	88.0	90.4	90.0	92.3	92.5	93.5	93.2	93.2	83.5
202.03	1.52	809.2	428.5	1.30	705.3	320.0	155.2	81.6	83.1	84.9	87.1	88.3	89.2	88.2	86.9	73.9
203.01	1.51	810.4	425.5	4.07	1105.0	869.6	172.0	103.0	105.3	105.2	107.2	28.3	110.7	109.2	105.8	91.3
203.02	1.52	803.3	429.2	3.18	1100.6	798.6	168.6	97.1	100.7	101.3	104.1	105.3	106.3	105.1	101.7	87.6
203.03	1.52	797.4	426.4	2.49	1086.7	715.1	164.8	92.9	95.6	97.7	100.7	101.7	101.7	100.1	97.0	84.3
203.04	1.53	801.2	428.9	1.81	1080.6	584.9	160.2	88.3	90.4	92.5	94.9	95.4	95.0	93.4	91.5	79.0
0.75 Area Ratio Finger Suppressor																
405.01	1.53	397.3	301.7	3.18	712.9	639.5	163.2	97.0	99.5	100.6	99.4	100.7	99.6	98.2	94.3	78.6
405.02	1.53	399.1	302.7	2.49	702.8	572.1	159.1	90.1	93.5	96.4	96.7	96.8	95.6	93.7	88.8	71.3

TEST CONDITIONS							ACOUSTIC DATA									
								PNL at 648.6 m S. L.								
Run #	P_{tp}/P_a	T_{tp} (°K)	V_p (mps)	P_{tf}/P_a	T_{tf} (°K)	V_f (mps)	OAPWL	$\theta = 60°$	75°	90°	105°	120°	130°	140°	150°	165°
405.03	1.52	395.7	300.4	1.80	698.9	4[illegible]7.9	152.7	82.4	86.3	90.2	90.4	91.1	89.0	87.5	82.8	64.4
405.04	1.53	387.6	298.8	1.30	702.0	319.1	145.8	76.0	79.6	82.8	82.4	82.3	80.3	78.8	74.6	58.3
406.01	1.53	436.4	317.3	4.11	1080.0	861.7	169.5	99.3	102.9	105.1	105.4	106.5	107.4	106.4	103.4	88.0
406.02	1.53	421.7	312.7	2.52	1088.3	719.3	161.8	91.8	95.3	99.3	99.9	100.3	98.8	96.6	91.8	73.4
406.03	1.54	411.5	309.7	1.80	1091.7	585.8	156.4	86.1	90.2	94.2	94.9	95.0	93.4	91.1	85.6	66.3
407.01	1.52	799.2	428.2	4.09	1100.0	869.0	171.3	98.8	102.0	102.9	105.6	107.9	108.1	108.7	105.7	90.8
408.01	1.53	814.4	434.9	2.51	1082.8	715.7	163.7	92.5	94.8	97.3	100.6	100.8	99.5	98.7	96.0	83.1
408.02	1.55	810.9	440.7	1.81	1082.8	584.6	160.4	87.5	90.8	93.3	96.2	96.4	95.4	95.0	92.3	79.2
409.01	1.53	815.6	434.3	3.18	701.3	633.4	164.7	97.3	98.5	98.5	99.8	100.7	100.2	99.7	97.4	85.2
409.02	1.54	804.9	434.6	2.52	700.2	574.2	162.1	91.2	93.4	95.0	97.7	98.2	97.4	97.0	94.2	81.9
409.03	1.55	815.0	438.6	1.82	708.4	475.2	159.3	85.1	88.3	90.4	93.0	94.2	94.0	94.0	91.6	79.1
409.04	1.53	794.8	429.8	1.30	701.1	320.0	155.1	81.6	84.2	85.7	88.3	89.6	89.8	84.4	87.6	75.0
0.75 Area Ratio Finger Suppressor With Hardwall Ejector																
410.01	1.52	831.1	433.4	4.13	1100.6	901.6	170.2	98.8	101.3	103.5	105.2	107.1	107.7	106.5	103.4	90.1
410.02	1.55	818.9	440.4	2.50	1097.8	719.9	162.7	93.3	96.3	98.8	100.0	99.2	97.5	96.2	93.9	82.1
411.01	1.53	813.3	433.7	1.80	1087.8	585.2	159.6	90.3	93.3	94.5	96.2	95.2	92.9	91.8	90.4	79.6
412.01	1.54	812.2	435.3	3.20	697.1	633.7	164.2	95.1	97.5	100.9	100.4	100.4	99.3	98.4	95.6	84.8
412.02	1.54	803.9	434.0	2.52	702.0	574.9	161.4	92.8	96.0	97.3	97.6	97.5	96.0	94.9	92.4	82.2
412.03	1.54	804.2	434.9	1.79	693.2	463.6	159.5	87.9	89.8	92.1	92.9	92.8	92.4	93.1	90.4	81.5
412.04	1.54	811.1	435.6	1.28	697.7	310.3	157.0	83.9	87.1	16.5	87.9	83.4	88.8	89.1	86.6	75.7
0.75 Area Ratio Finger Suppressor With Treated Ejector																
413.01	1.53	811.1	434.0	3.20	698.6	634.0	163.9	94.9	98.1	99.6	98.8	98.9	99.1	98.3	96.5	84.7
413.02	1.53	808.8	433.1	2.49	702.4	572.4	161.0	92.1	94.8	95.8	95.3	94.9	95.2	94.4	93.3	82.8
413.03	1.53	812.2	434.0	1.81	703.2	470.0	159.3	86.7	88.2	91.3	90.4	90.4	91.6	92.5	90.8	80.9
413.04	1.53	811.1	433.4	1.30	701.4	318.5	157.0	82.1	85.6	86.3	86.8	87.3	89.0	88.8	87.6	75.6
414.01	1.52	812.2	4312.9	4.08	1111.7	872.6	170.2	99.0	101.8	104.0	104.7	106.3	107.8	106.7	103.7	89.6
414.02	1.52	815.0	431.3	2.49	1088.9	715.4	161.8	92.6	95.1	97.2	97.3	97.0	97.0	95.8	92.6	81.6
414.03	1.53	813.9	434.6	1.80	1083.3	584.0	159.5	89.7	91.8	93.0	93.0	91.8	95.4	91.4	90.9	79.2
415.01	1.54	445.3	323.1	4.12	1098.3	869.9	168.6	98.4	101.2	103.7	104.6	105.6	106.7	105.3	101.5	85.9
415.02	1.53	420.4	311.2	2.51	1082.8	716.0	159.0	92.4	94.9	97.3	97.5	96.1	95.2	93.0	89.1	73.3
415.03	1.53	604.4	305.4	1.81	1083.9	585.8	153.9	89.4	92.1	93.6	93.1	91.0	88.4	85.8	81.5	66.4
416.01	1.54	402.9	305.7	3.21	709.9	640.1	161.1	94.4	98.2	99.9	99.2	96.7	97.2	95.7	91.9	77.4
416.02	1.54	397.1	303.4	2.51	700.1	573.0	156.8	90.9	94.2	95.7	95.0	92.4	92.4	90.6	86.4	71.9
416.03	1.53	388.1	299.6	1.80	702.0	468.5	151.5	84.2	87.1	89.0	89.2	86.2	85.4	83.9	79.6	65.9
416.04	1.54	371.8	294.1	1.31	693.4	319.7	150.7	78.4	82.7	83.3	82.9	80.3	79.3	78.2	75.7	62.6

Run #	TEST CONDITIONS P_{tp}/P_a	T_{tp} (°K)	V_p (mps)	P_{tf}/P_a	T_{tf} (°K)	V_f (mps)	ACOUSTIC DATA OAPWL	PNL at 648.6 m S. L. θ = 60°	75°	90°	105°	120°	130°	140°	150°	165°
1.2 Area Ratio Unsuppressed Coannular Nozzle																
417.01	1.54	807.4	434.0	2.49	1088.9	716.4	167.9	93.3	97.9	101.3	103.0	104.5	104.3	104.8	102.6	87.9
417.02	1.53	808.2	431.0	1.81	1082.2	587.3	162.0	88.7	92.9	95.8	97.5	98.8	98.2	96.9	94.7	80.4
418.01	1.53	810.9	434.0	3.19	701.9	634.9	169.6	101.7	104.3	105.4	104.7	104.5	105.3	106.1	105.1	89.8
418.02	1.53	809.2	432.8	2.50	701.2	573.0	165.3	94.4	97.7	99.7	99.9	100.7	101.0	101.1	100.1	84.9
418.03	1.54	813.3	435.9	1.81	698.8	470.6	159.9	85.8	89.8	92.5	94.1	95.1	95.5	94.8	92.2	78.2
418.04	1.53	807.1	432.5	1.30	708.4	323.4	155.9	80.7	84.2	87.0	88.3	89.2	90.5	90.0	87.4	73.2
420.01	1.52	448.9	319.7	3.45	1094.4	820.8	172.0	102.2	105.3	106.7	107.9	109.4	109.5	109.1	106.2	91.7
420.02	1.54	420.9	312.4	2.50	1088.9	716.9	166.6	93.1	97.9	100.6	103.0	104.8	104.4	102.9	100.3	85.1
420.03	1.53	397.8	303.0	1.81	1085.0	586.1	159.6	87.6	91.7	94.6	96.9	98.5	97.0	94.8	90.6	74.7
428.01	1.52	398.9	298.4	2.46	704.4	570.3	163.1	95.6	94.9	99.0	99.8	100.3	101.1	99.7	94.6	87.5
428.02	1.52	396.7	301.1	1.80	702.2	468.8	155.9	85.9	86.7	91.0	92.8	93.8	93.6	90.3	86.0	70.5
428.03	1.53	389.4	299.0	1.30	702.2	318.8	147.6	78.1	78.7	82.3	83.3	83.5	83.0	80.3	76.0	61.6
429.01	1.53	843.9	441.4	4.06	1080.6	858.9	174.6	106.0	104.8	108.5	110.1	107.9	110.2	112.1	109.7	94.6
431.01	1.53	414.7	308.8	3.18	707.5	637.0	169.4	103.4	103.6	105.7	106.3	105.0	105.5	106.5	106.1	92.3
1.2 Area Ratio Convoluted Suppressor																
433.01	1.53	814.4	433.1	3.18	704.4	635.2	166.8	99.3	–	102.6	100.2	102.8	103.7	101.4	100.5	87.2
433.02	1.53	806.1	433.1	2.52	698.3	573.0	162.9	95.2	–	97.9	96.1	99.7	99.9	97.2	95.5	80.4
433.03	1.54	811.1	434.9	1.80	695.6	466.0	157.9	86.2	–	90.8	90.8	94.1	94.5	92.1	90.1	73.7
433.04	1.53	811.1	433.1	1.31	702.8	323.4	153.5	81.5	–	85.4	84.5	87.9	88.0	86.7	84.6	69.9
434.01	1.53	825.0	437.1	4.05	1099.4	865.9	174.1	100.7	–	105.4	105.0	109.6	111.5	111.1	108.6	98.1
434.02	1.55	802.9	437.4	2.52	1091.7	721.2	165.9	96.1	–	99.7	100.0	103.8	103.6	100.6	99.1	81.6
434.03	1.54	806.7	434.0	1.79	1091.1	582.2	160.8	89.5	–	94.9	95.4	99.2	98.9	94.8	92.3	75.1
435.01	1.52	394.4	299.3	3.16	703.9	634.0	165.1	99.2	–	102.3	99.9	102.3	102.8	100.1	97.5	80.6
436.01	1.53	394.4	301.2	4.05	1088.9	864.3	172.0	100.8	–	105.4	105.0	109.4	110.8	108.8	106.3	87.2
436.02	1.53	441.7	319.1	2.49	1093.3	716.9	164.9	95.7	95.6	99.3	102.3	103.8	103.4	99.8	96.1	79.2
436.03	1.53	420.6	310.6	1.79	1093.3	583.1	159.5	88.8	90.2	94.7	97.5	99.0	98.5	93.4	88.9	69.8
437.01	1.52	388.9	297.5	1.30	695.0	316.1	146.0	78.1	78.9	81.9	83.4	83.7	82.2	78.4	74.0	58.5
437.2	1.53	390.6	299.3	1.79	700.0	466.3	155.0	85.2	86.1	90.1	92.5	93.6	93.6	89.6	85.5	67.7
437.3	1.53	396.7	302.7	2.49	703.3	572.4	161.4	95.2	94.6	97.7	98.6	99.3	99.7	96.2	92.6	75.6
1.2 Area Ratio Convoluted Suppressor With Hardwall Ejector																
442.01	1.53	383.4	296.4	1.31	698.2	322.2	144.3	77.6	75.7	80.0	81.8	81.6	79.4	74.7	71.8	57.5
442.02	1.54	386.0	299.5	1.80	702.8	468.2	152.7	84.8	83.9	89.7	92.1	92.4	88.1	83.5	79.5	64.0
442.03	1.53	392.1	299.5	2.49	705.1	572.7	160.3	95.1	93.7	99.5	100.2	99.7	96.2	92.3	88.5	72.8
442.04	1.54	396.8	304.3	3.18	700.8	634.0	164.0	99.3	97.4	102.3	102.9	99.3	101.0	98.5	95.7	79.9
443.01	1.54	403.1	306.3	1.81	1088.3	587.3	157.3	88.5	87.7	94.5	97.7	98.3	92.4	–	83.1	67.5
443.02	1.54	409.6	308.5	2.49	1093.6	717.2	162.9	94.8	94.1	100.7	103.3	102.4	99.0	95.6	92.0	76.0
443.03	1.53	439.3	317.9	4.06	1094.4	864.4	171.5	100.8	99.9	105.4	107.4	108.5	109.9	107.9	105.4	91.9
444.01	1.53	807.8	432.2	4.07	1092.2	864.4	173.5	100.8	99.9	105.4	107.4	108.6	110.4	109.8	108.2	94.2
444.02	1.53	807.1	431.3	2.51	1086.7	717.5	164.5	94.7	94.1	100.5	103.5	102.5	99.8	97.4	95.8	83.5

Run #	TEST CONDITIONS P_{tp}/P_a	T_{tp} (°K)	V_p (mps)	P_{tf}/P_a	T_{tf} (°K)	V_f (mps)	ACOUSTIC DATA OAPWL	PNL at 648.6 m S. L. $\theta = 60°$	75°	90°	105°	120°	130°	140°	150°	165°
444.03	1.53	811.1	434.3	1.79	1087.2	582.8	158.6	87.7	88.4	93.6	96.1	97.5	92.7	90.2	88.3	75.8
445.01	1.54	816.7	437.1	1.30	706.0	319.7	151.8	80.7	80.7	83.4	84.4	86.0	85.8	84.6	82.8	70.7
445.02	1.53	817.2	435.9	1.78	700.3	464.2	155.8	84.9	85.3	89.3	90.8	92.9	90.3	88.3	86.3	72.8
445.03	1.53	809.9	433.1	2.50	699.6	571.8	161.8	93.9	93.9	98.6	98.6	99.9	97.1	94.8	92.9	81.1
445.04	1.54	810.4	434.9	3.18	701.6	634.3	165.9	98.3	97.9	101.6	101.6	102.5	102.1	100.1	98.3	87.1
1.2 Area Ratio Convoluted Suppressor With Treated Ejector																
438.01	1.53	372.8	292.6	1.30	708.9	321.0	143.6	75.9	75.9	78.1	79.7	79.9	78.7	74.5	71.2	57.6
438.02	1.54	381.7	295.7	1.80	707.2	470.6	151.8	84.2	84.6	87.5	89.5	90.3	88.1	83.5	79.7	65.2
438.04	1.53	411.7	307.8	3.16	706.3	634.9	163.8	97.9	97.1	100.4	101.8	101.4	101.0	98.3	95.2	80.3
439.01	1.54	420.6	312.7	1.81	1087.2	588.0	155.3	86.8	87.2	91.1	93.3	95.4	93.9	86.9	82.3	68.7
439.02	1.52	434.4	314.2	2.49	1096.1	717.2	161.8	92.7	93.3	97.3	99.9	100.9	98.9	95.7	91.8	79.2
439.03	1.53	464.0	326.1	4.06	1099.4	866.2	171.7	100.2	100.3	104.4	106.7	108.8	110.3	108.2	105.1	93.8
440.01	1.52	806.1	430.4	4.08	1092.8	865.0	173.6	100.8	100.7	104.6	106.9	108.9	110.9	110.1	108.0	96.0
440.02	1.53	810.0	433.4	2.47	1086.1	711.1	163.3	92.5	93.3	97.1	99.4	100.3	99.0	96.9	94.5	85.3
440.03	1.53	805.6	431.0	1.80	1084.4	583.1	157.9	86.9	87.2	91.1	93.3	94.5	91.9	90.1	87.8	78.2
441.01	1.53	808.9	432.2	1.30	693.3	315.8	151.8	76.0	79.3	82.0	83.8	84.8	85.4	84.7	82.3	72.9
441.02	1.52	812.2	431.3	1.80	702.2	468.2	156.2	84.5	84.7	88.3	90.5	91.3	90.2	88.8	86.6	76.9
441.03	1.53	815.6	433.7	2.48	700.6	570.0	162.0	101.8	91.9	95.9	96.5	97.7	96.6	94.6	92.3	82.4
441.04	1.52	814.4	432.2	3.17	707.2	635.8	166.0	97.4	96.6	100.3	101.3	102.0	102.1	100.3	98.2	89.5

* Runs having extraneous facility produced discrete tone. This tone has been analytically removed from the data.
– Data not reliable.

LIST OF ABBREVIATIONS

NOMENCLATURE (The following symbols are used throughout the report unless otherwise defined in the text.)

A	–	Area
C	–	Speed of Sound
C_D	–	Flow Coefficient (Actual Weight Flow/Ideal Weight Flow)
C_V	–	Thrust Coefficient (Actual Thrust/Ideal Thrust)
D	–	Diameter
F	–	Thrust
g_c	–	Gravitational Constant
L	–	Length
M	–	Mach Number
OASPL	–	Overall Sound Pressure Level - dB re 20×10^{-6} Newtons/M^2
P	–	Pressure
PNL	–	Perceived Noise Level
PWL	–	Power Level – dB re 10^{-12} Watts
$\mathcal{R}$	–	Gas Constant
r, R	–	Radius
Ref.	–	Reference
SL	–	Sideline
SPL	–	Sound Pressure Level - dB re 20×10^{-6} Newtons/M^2
Synthesis	–	Synthesized Noise Levels of Coannular Reference Nozzle (As Described in Text)
U	–	Velocity Measured in Plume Traverse
V	–	Jet Velocity (Ideally Expanded to Ambient Conditions)
X	–	Distance
W	–	Mass Flow
γ	–	Specific Heat Ratio
Δ	–	Delta (Difference) in Noise or Thrust Levels
θ	–	Angle From Inlet Centerline
ρ	–	Density

SUBSCRIPTS (The subscripts are used in either lower case or upper case form.)

a	–	Ambient
avg	–	Average
ejec	–	Ejector
eq	–	Equivalent
f	–	Fan
i	–	Ideal
in	–	Inlet Condition
m	–	Mixed
max	–	Maximum
o	–	Initial Conditions
p	–	Primary
Per	–	Perimeter
ref	–	Reference
s	–	Static
t	–	Total
th	–	Throat Condition
uns	–	Unsuppressed

REFERENCES

1. Williams, T.J., M.R.M. Ali, and J.S. Anderson: Noise and Flow Characteristics of Co-axial Jets, Journal of Mech. Engr. Sc., Vol. 11, No. 2, April 1969, pp. 133-142.

2. Eldred, K.: Far Field Noise Generation by Coaxial Flow Jet Exhausts, Vol. I; Detailed Discussion, FAA-RD-71-101-Vol. 1, 1971, Wyle Laboratories, Inc., El Segundo, Calif.

3. Olsen, W. and R. Friedman: Jet Noise from Co-axial Nozzles over a Wide Range of Geometric and Flow Parameters, NASA TM X-71503, 1972, or AIAA Paper No. 74-43, 1974.

4. Bielak, G.W.: Coaxial Flow Jet Noise, D6E-10041-1, 1972, Boeing/Aeritalia Co., Seattle, Wash.

5. Stone, J.R.: Interim Prediction Method for Jet Noise, NASA TMX-71618, 1975.

6. Dosanjh, Darshan S., Yu, James C., Abdelhamid, Amr N.: Reduction of Noise from Supersonic Jet Flows. AIAA J., vol. 9, no. 12, Dec. 1971.

7. Kozlowski, H.: Program to Conduct Acoustic Tests of Duct Burning Turbofan Jet Noise Simulation – Concept Screening and Model Design Report, FWA Report, 14 December 1973.

8. Kozlowski, H. and Packman, A.B.: Aero-Acoustic Tests of Duct-Burning Turbofan Exhaust Nozzles, Comprehensive Data Report, NASA CR-134910, December 1975.

9. Society of Automotive Engineers: Aerospace Recommended Practice, ARP 866A, March 15, 1975.

10. Society of Automotive Engineers: Proposed ARP 876, Gas Turbine Jet Exhaust Noise Prediction, 1 April 1975.

11. Society of Automotive Engineers: Jet Noise Prediction, SAE AIR 876 (1965).

12. Boeing Company: A summary of the SST Noise Suppression Test Program, FAA-SS-72-41, 1972

13. J. F. Brausch: Flight Velocity Influence on Jet Noise of Conical Ejector, Annular Plug, and Segmented Suppressor Nozzles, NASA CR-120960, Aug., 1972

14. A.B. Packman, K.W. Ng, and R.W. Paterson: Effect of Simulated Forward Flight on Subsonic Jet Exhaust Noise, AIAA paper No. 75-869, June, 1975

15. J. Atvars et al.: Development of Acoustically Lined Ejector Technology For Multitube Jet Noise Suppressor Nozzles By Model and Engine Tests Over a Wide Range of Jet Pressure Ratios and Tempeatures, NASA CR-2382, April, 1974.

REFERENCES (Cont'd)

16. G.S. Schairer, J.V. O'Keefe, and P.E. Johnson: Perspective of SST Aircraft Noise Problem, I: Acoustic Design Considerations, J. Aircraft, Jan. 1971.

17. C.Y. Chen: Calculations of Far-Field and Near-Field Jet Noise, AIAA paper No. 75-93, 1975.

18. R.A. Howlett, J. Sabatella, J. Johnson, G. Aronstamm: Advanced Supersonic Propulsion Study – Phase II Final Report, NASA CR-134904, September 1975.